Analysis of the role of *Arabidopsis* extra-large G protein 2 in *cerk1*-4-dependent cell death signalling

Dissertation

zur Erlangung des mathematisch-naturwissenschaftlichen Doktorgrades

"Doctor rerum naturalium"

der Georg-August-Universität Göttingen

im Promotionsprogramm „Biologie“

der Georg-August University School of Science (GAUSS)

vorgelegt von

Julia Anders

aus Hannover

Göttingen, 2021

Betreuungsausschuss

1. BetreuerIn: **Prof. Dr. Volker Lipka**
Zellbiologie der Pflanze
Albrecht-von-Haller Institut für Pflanzenwissenschaften

2. BetreuerIn: **PD. Dr. Thomas Teichmann**
Zellbiologie der Pflanze
Albrecht-von-Haller Institut für Pflanzenwissenschaften

3. AnleiterIn: **Dr. Elena K. Petutschnig**
Zellbiologie der Pflanze
Albrecht-von-Haller Institut für Pflanzenwissenschaften

Mitglieder der Prüfungskommission

ReferentIn: **Prof. Dr. Volker Lipka**
Zellbiologie der Pflanze
Albrecht-von-Haller Institut für Pflanzenwissenschaften

KorreferentIn: **PD. Dr. Marcel Wiermer**
Molekularbiologie der Pflanze-Mikroben Interaktionen
Albrecht-von-Haller Institut für Pflanzenwissenschaften

Weitere Mitglieder der Prüfungskommission

PD. Dr. Thomas Teichmann
Zellbiologie der Pflanze
Albrecht-von-Haller Institut für Pflanzenwissenschaften

Prof. Dr. Ivo Feußner
Biochemie der Pflanze,
Albrecht-von-Haller Institut für Pflanzenwissenschaften

Prof. Dr. Andrea Polle
Forstbotanik und Baumphysiologie,
Fakultät für Forstwissenschaften und Waldökologie

PD Dr. Till Ischebeck
Biochemie der Pflanze
Albrecht-von-Haller-Institut für Pflanzenwissenschaften

Tag der mündlichen Prüfung: 29.04.2021

Table of contents

List of figures

List of supplemental figures

List of abbreviations

A. tumefaciens	*Agrobacterium tumefaciens*
ACD6	Accelerated cell death 6
ADR1	Activated disease resistance 1
AGB1	*Arabidopsis* G-protein beta-subunit 1
AGG1/2/3	*Arabidopsis* G-protein gamma-subunit 1
AP	Appressorium
Arabidopsis	*Arabidopsis thaliana*
BAK1	BRI1 associated kinase 1
Bgh	*Blumeria graminis f. sp. hodrei*
BIK1	Botrytis-induced kinase 1
BIR1	BAK1-interacting receptor-like kinase 1
CERK1	Chitin elicitor receptor kinase 1
CLSM	Confocal laser scanning microscopy
CNL	Coiled coil (CC) domain NLR
Col-0	Columbia-0
Col-3 *gl*1	Columbia-3 *glabra* 1
CPK	Calcium-dependent protein kinase
CRK	Cysteine-rich receptor-like kinase
DAMP	Damage-associated molecular pattern
DCD	Development and cell death
E. pisi	*Erysiphe pisi*
Ec	*Erysiphe cruciferarum*
EDS1	Enhanced disease susceptibility 1
EHC	Extrahaustorial encasement
EHM	Extrahaustorial membrane
EHMx	Extrahaustorial matrix
ER	Endoplasmic reticulum
ESCRT	endosomal sorting complex required for transport
ESCRT	Endosomal sorting complex required for transport
ETI	Effector-triggered immunity
FG	Phenylalanine-glycine
flg22	Flagellin
FLS2	Flagellin sensing 2
GDP	Guaninediphosphate
GEF	Guanine nucleotide exchange factor

GlcNAc	N-acetyl-D-glucosamine
GPCR	G protein-coupled receptor
GTP	Guaninetriphosphosphate
HP	Haustorial periphery
HP	Haustorial periphery
HR	hypersensitive response
LMM	Lesion-mimic mutants
LRR	Leucine-rich repeat
LYK	LysM receptor kinase
LysM	Lysin-motif
MAMP	Microbe-associated molecular pattern
MAPK	Mitogen-activated protein kinase
MBP1	Myrosinase-binding protein 1
MLO	Mildew resistance locus O
MTI	MAMP-triggered immunity
MVB	Multivesicular bodies
NDR1	Non-race specific disease resistance 1
NES	Nuclear export signals
NHR	Non-host resistance
nlp20	Necrosis and ethylene-inducing peptide 1-like proteins
NLR	Nucleotide-binding ARC domain (NB) and LRR superfamily receptor protein
NLS	Nuclear localization signal
NPC	Nuclear pore complex
NRG1	N-requirement gene 1
NTR	Nuclear transport receptor
NUP	Nucleoporin
PAD4	Phytoalexin deficient 4
PCD	Programmed cell death
PCR	Polymerase Chain Reaction
PCS1	Phytochelatin synthase 1
PEN	Penetration
PGN	Peptidoglycan
PLCs	Phosphoinositide-dependent phospholipase C
PLD	Phosphodiesterase phospholipase D
PM	Plasma membrane
RACK	Receptor for activated c-kinase

RGS1	Regulator of G protein signalling 1
RLCK	Receptor-like cytosolic kinase
RLK	Receptor-like kinases
RLP	Receptor-like proteins
RNL	Resistance to powdery mildew 8 (RPW8) domain NLR
ROS	Reactive oxygen species
SAG101	Senescence associated gene 101
SINC	SA-induced NPR1 condensate
SNAP33	Synaptosomal-associated protein 33
SNARE	Soluble N-ethylmaleimide-sensitive factor attachment receptor
SNC1	Non-expresser of PR genes 1 (NPR1)-1 constitutive 1
SOBIR1	Suppressor of BIR1-1
SYP121	SNARE protein PEN1
TNL	Toll/ interleukin-1 receptor (TIR) domain NLR
UPR	Unfolded protein response
UTR	Untranslated region
VAMP	Vesicle-associated membrane protein
XLG1/2/3	Extra-large G protein 1/ 2/ 3
ZAR1	HOPZ-activated resistance 1

I. Abstract

Plants perceive microbe-associated molecular patterns (MAMPs) via so called pattern-recognition receptors (PRRs) at the plasma membrane, which activates an immune response. Heterotrimeric G proteins are intracellular signal transducers, which consist of a Gα subunit and a Gβγ-dimer. Heterotrimeric G proteins typically form a complex at the plasma membrane and are known to play roles in almost all aspects of plant life. In plants, receptor-like kinases (RLKs) and receptor-like cytosolic kinases (RLCKs) were found to interact with heterotrimeric G proteins in a MAMP-responsive way, which activates cell death and defense against pathogens. Besides one classical Gα subunit, *Arabidopsis* has three extra-large G proteins (XLG1-3), of which XLG2/3 are involved in immunity. The Gβ subunit AGB1 and Gγ subunits AGG1/2 are also involved in defense signalling. Plants perceive fungal pathogens via the chitin-elicitor receptor kinase 1 (CERK1). The *cerk1*-4 mutation is known to cause a phenotype with exaggerated cell death upon pathogen inoculation, early senescence, and higher resistance against biotrophic powdery mildews. Mutations that suppress the *cerk1*-4 cell death phenotype were identified via a suppressor screen, including two mutations within the XLG2 gene: *xlg2*-2 (knock-out) and *xlg2*-3 (E293K).

This study focused on the analysis of the role of XLG2 in *cerk1*-4-dependent cell death signalling. Venus-labeled XLG2 variants were generated and analyzed *in planta* via confocal laser scanning microscopy (CLSM) with focus on plasma membrane and nuclear localization. The functionality of XLG2 variants in *cerk1*-4 cell death signalling was analyzed using complementation studies. These studies revealed that the plasma membrane localization is important for functionality of XLG2 in *cerk1*-4 cell death signalling. The nuclear localization was found to be dispensable for this cell death promoting function of XLG2. Pathogen inoculation using *Erysiphe cruciferarum* (*Ec*) caused an increase in abundance of XLG2 and xlg2 variants. In unchallenged *Arabidopsis* plants, XLG2 localized mainly to the cell periphery (plasma membrane as well as cytosolic signal at the periphery), while in *Ec* infected pavement cells XLG2 also accumulated in the nucleus. Several XLG2 mutant variants were analyzed, which showed mainly nuclear localization and lost functionality in *cerk1*-4 cell death signalling. Further, these mainly nuclear localizing XLG2 variants showed a difference in the apparent molecular mass compared to wildtype XLG2 in Western Blots. The relevance of the XLG2 Gα activity for *cerk1*-4 cell death signalling and subcellular localization of XLG2 was analyzed. Two xlg2 varaints, one with impaired nucleotide binding (potentially nucleotide-free) and the other potentially GTPase-dead (likely constitutively bound to GTP), did not cause changes in the localization of XLG2 or functionality in *cerk1*-4 cell death signalling. In contrast to the canonical Gα subunit GPA1, XLGs have a plant-specific N-terminal elongation with a

highly conserved cysteine-rich region. XLG2 cysteine-rich region mutant variants with cysteines exchanged for alanine (C-A), showed mainly nuclear localization, a lower apparent molecular mass in Western Blots, and lost functionality in *cerk1*-4 cell death signalling. Accordingly, the cysteine-rich region seems to be important for correct localization of XLG2 and functionality in this cell death signalling pathway. XLG2 is known to bind the AGB1-AGG1/2-dimer at the plasma membrane. In order to analyze the subcellular localization of XLG2 in the absence of the Gβγ-dimer, G protein mutant *Arabidopsis* were transiently transformed via particle bombardment for expression of Venus-XLG2. The Gβγ-dimer was found to have a weak effect on plasma membrane association of XLG2. In the absence of the Gβγ-dimer, Venus-XLG2 was found to accumulate less to the cell periphery and more inside the nucleus.

At late *Ec* infection time-points, XLG2 was found to associate with haustoria, which are fungal feeding structures formed during compatible plant-microbe interactions. Different XLG2 variants with changed localization were included in the analysis of this co-localization. XLG2 variants with wildtype-like or without a nuclear XLG2 pool co-localized with the haustorial periphery, while for mainly nuclear localizing xlg2 variants significantly less labeled *Ec* haustoria were observed. Propidium iodide staining and bright field images revealed that XLG2 accumulates in the plant-derived encasement, which typically surrounds fully developed haustoria.

II. Zusammenfassung

Pflanzen nehmen Mikroben-assoziierte molekulare Muster (MAMPs) mit Hilfe von sogenannten Muster-erkennenden Rezeptoren (PRRs) an der Zellmembran wahr, wodurch eine Immunantwort ausgelöst wird. Heterotrimere G-Proteine sind an der intrazellulären Signaltransduktion beteiligt und sind aus einer Gα-Untereinheit und einer Gβγ-Untereinheit zusammengesetzt. Heterotrimere G-Proteine formen typischerweise einen Komplex an der Zellmembran und sind dafür bekannt in fast allen Bereichen des pflanzlichen Lebens eine Rolle zu spielen. In Pflanzen interagieren heterotrimere G-Proteine mit Rezeptor-ähnlichen Kinasen (RLK) und Rezeptor-ähnlichen zytosolischen Kinasen (RLCK) in Abhängigkeit zur MAMP-Wahrnehmung, was sowohl den Zelltod als auch die Abwehr von Pathogenen aktiviert. Neben der klassischen Gα-Untereinheit lassen sich in *Arabidopsis* drei extra-große G-Proteine (XLG1-3) finden, von welchen XLG2-3 an der Immunität beteiligt sind. Die Gβ-Untereinheit AGB1 und die Gγ-Untereinheiten AGG1/2 sind ebenfalls an der Abwehr-Signalgebung beteiligt. Pflanzen nehmen pilzliche Pathogene mit Hilfe eines Chitin-erkennenden Rezeptors (CERK1) wahr. Die *cerk1*-4 Mutation ist dafür bekannt einen Phänotyp mit erhöhtem Zelltod als Reaktion auf Pathogen-Inokulation zu verursachen, sowie eine früher einsetzende Seneszenz and erhöhte Resistenz gegen den biotrophen Mehltau. Mutationen, welche den *cerk1*-4-bedingten Zelltod-Phänotyp supprimieren, wurden mit Hilfe eines Suppressor-Screening-Verfahrens identifiziert, einschließlich zweier Mutationen innerhalb des XLG2-Gens: *xlg2*-2 (knock-out) und *xlg2*-3 (E293K).

Im Fokus dieser Studie stand die Analyse von XLG2 in der *cerk1*-4-vermittelten Zelltod-Signalgebung. Venus-markierte XLG2 Varianten wurden generiert und mit Hilfe von konfokaler Laser-Scanning Mikroskopie (CLSM) *in planta* untersucht, wobei der Fokus vor allem auf der Lokalisierung an der Zellmembran und im Zellkern lag. Die Funktionalität der XLG2 Varianten in der *cerk1*-4-vermittelten Zelltod-Signalgebung wurde durch Komplementation-Untersuchungen geprüft. Diese Untersuchungen zeigten, dass die Zellmembran-Lokalisierung für die Funktion von XLG2 in der *cerk1*-4-vermittelten Zelltod-Signalgebung wichtig ist. Die Zellkern-Lokalisierung war dagegen entbehrlich für die Zelltod-fördernde Funktion von XLG2. Pathogen-Inokulation mit *Erysiphe cruciferarum* (*Ec*) verursachte eine Erhöhung der Abundanz von XLG2 Varianten. In ungestressten *Arabidopsis*-Pflanzen lokalisierte XLG2 hauptsächlich an der Zellperipherie (Zellmembran und zytosolisches Signal an der Peripherie eingeschlossen), während in *Ec*-infizierten Epidermiszellen XLG2 ebenfalls im Zellkern akkumulierte. Es wurden verschiedene XLG2 Mutanten analysiert, die hauptsächlich im Zellkern lokalisierten und gleichzeitig ihre Funktion in der *cerk1*-4-vermittelten Zelltod-Signalgebung verloren haben. Des Weiteren zeigten diese vorwiegend Zellkern-lokalisierenden XLG2 Varianten eine veränderte

scheinbare Molekularmasse in Western Blots im Vergleich zum Wildtyp-XLG2. Die Relevanz der XLG2 Gα-Aktivität für die *cerk1*-4-vermittelte Zelltod-Signalgebung und die subzelluläre Lokalisierung wurden ebenfalls analysiert. Zwei XLG2 Varianten, eine mit eingeschränkter Nucleotid-Bindefähigkeit (wahrscheinlich Nucleotid-frei) und die andere mit potenziell defekter GTPase-Aktivität (wahrscheinlich konstitutiv an GTP gebunden), veränderten weder die Lokalisierung von XLG2 noch die Funktionalität in der *cerk1*-4-vermittelten Zelltod-Signalgebung. Im Gegensatz zu der klassischen Gα-Untereinheit GPA1 haben XLGs eine Pflanzen-spezifische N-terminale Verlängerung mit einer Cystein-reichen Region. XLG2 Mutanten betreffend der Cystein-reichen Region, mit durch Alanin ausgetauschten Cysteinen (C-A), zeigten hauptsächlich Zellkern Lokalisierung, eine niedrigere scheinbare Molekularmasse in Western Blots und verloren die Funktionalität in der *cerk1*-4-vermittelten Zelltod-Signalgebung. Entsprechend ist die Cystein-reiche Region wahrscheinlich wichtig für die Lokalisierung von XLG2 und die Funktion in der Zelltod-Signalgebung. XLG2 ist dafür bekannt die AGB1-AGG1/2-Untereinheiten an der Zellmembran zu binden. Um die subzelluläre Lokalisierung von XLG2 in Abwesenheit der Gβγ-Untereinheit zu untersuchen, wurden G-Protein Mutanten *Arabidopsis* mit Hilfe des Teilchen-Bombardements transient transformiert und exprimierten daraufhin Venus-XLG2. Es wurde beobachtet, dass die Gβγ-Untereinheit einen schwachen Effekt auf die Zellmembran-Assoziation von XLG2 hat. In Abwesenheit der Gβγ-Untereinheit akkumulierte Venus-XLG2 weniger an der Zellperipherie und mehr innerhalb des Zellkerns.

Zu späten *Ec*-Infektionszeitpunkten wurde beobachtet, dass XLG2 mit Haustorien assoziiert. Haustorien sind pilzliche Versorgungsstrukturen, die sich während kompatiblen Pflanzen-Mikroben-Interaktionen ausbilden. Verschiedene XLG2 Varianten mit veränderter Lokalisierung wurden daraufhin bezüglich dieser Kolokalisierung untersucht. XLG2 Varianten mit Wildtyp-ähnlicher Lokalisierung, und ohne den im Zellkern-akkumulierten Anteil, kolokalisierten mit der Haustorien-Peripherie, während hauptsächlich Zellkern-akkumulierende XLG2 Varianten signifikant weniger häufig mit *Ec* Haustorien kolokalisierten. Propidiumiodid-Färbung und Hellfeld Bilder zeigten, dass XLG2 in der pflanzen-abgeleiteten Umhüllung akkumulierte, welche typischerweise voll ausgebildete Haustorien umgibt.

1 Introduction

1.1 Plant immune signalling

Plant cells are surrounded by cell walls and have developed an immense monitoring system that is able to distinguish between self ligands (damage-associated molecular patterns, DAMPs) and non-self ligands (Bacete et al. 2018). When pathogens attack, plants can perceive such non-self microbe-associated molecular patterns (MAMPs) using pattern recognition receptors (PRRs), which are located at the plasma membrane (PM) beyond the cell wall (Nürnberger et al. 2004). This perception results in generation of reactive oxygen species (ROS) and activation of mitogen-activated as well as calcium-dependent protein kinases (MAPKs and CPKs) (Monaghan and Zipfel 2012). Known recognized patterns are usually conserved microbial glycans (fungal chitin and bacterial peptidoglycan = PGN), proteins, peptides (bacterial flagellin = flg22, microbial necrosis and ethylene-inducing peptide 1-like proteins = nlp20) or effectors, which are sensed in the apoplastic space (Thomma et al. 2011; Gijzen and Nürnberger 2006). Perception of these extracellular ligands results in immune signalling and is conceptionally described as extracellular or MAMP-triggered immunity (MTI) (Jones and Dangl 2006; Thomma et al. 2011). A more adapted plant-microbe interaction can result in the necessity of intracellular signal perception, which is referred to as effector-triggered immunity (ETI) (Jones and Dangl 2006). The concepts of MTI and ETI can be extended by the accumulated evidence that they share signalling components, ligands as well as transcriptional activation of similar defense genes (Ngou et al. 2020; Yuan et al. 2020). A mechanistic overview of extracellular ligand perception and downstream PRR-triggered immune signalling is depicted in Fig. 1. Extracellular ligands bind to specific ectodomains of receptor-like kinases (RLKs) and receptor-like proteins (RLPs), which are usually conserved among different plant species similar to their corresponding ligands (Thomma et al. 2011; Albert et al. 2015). RLKs have a single transmembrane domain and intracellular kinase domain (Shiu and Bleecker 2001). RLPs lack the intracellular kinase domain and, therefore, depend on interaction with RLKs for signal transduction (Liebrand et al. 2014). One well-studied RLK and major chitin-perceiving component is lysin-motif (LysM)-RLK chitin elicitor receptor kinase 1 (CERK1) (Petutschnig et al. 2010). Upon chitin binding CERK1 dimerizes and auto-phosphorylates which is needed for downstream activation of MAPKs (Liu et al. 2012; Suzuki et al. 2016). Other chitin perceiving and partially redundant LysM-RLKs are LYK4 and LYK5 (Wan et al. 2012; Cao et al. 2014) which are known to be kinase-dead (Petutschnig et al. 2010). CERK1 forms a functional complex with LYK4 (Xue et al. 2019) and LYK5, which is needed for full chitin-dependent immune signalling (Cao et al. 2014). CERK1 was also shown to bind β1-3 glucans derived from plants and fungi (Mélida et al. 2018). As already

mentioned, RLPs are involved in recognition of patterns in association with RLKs. The LysM-RLPs LYM1 and LYM3 perceive the bacterial PGN with the involvement of CERK1 for intracellular signal transduction, while it is still unknown whether CERK1 directly associates with LYM1 and LYM3 (Willmann et al. 2011). Another example is the LysM-RLP LYM2, which was shown to perceive chitin without involvement in classical chitin-dependent downstream signalling (Shinya et al. 2012). LYM2 was shown to be responsible for LYK4 and LYK5-dependent but CERK1-independent plasmodesmata closure in response to chitin (Faulkner et al. 2013; Cheval et al. 2020).

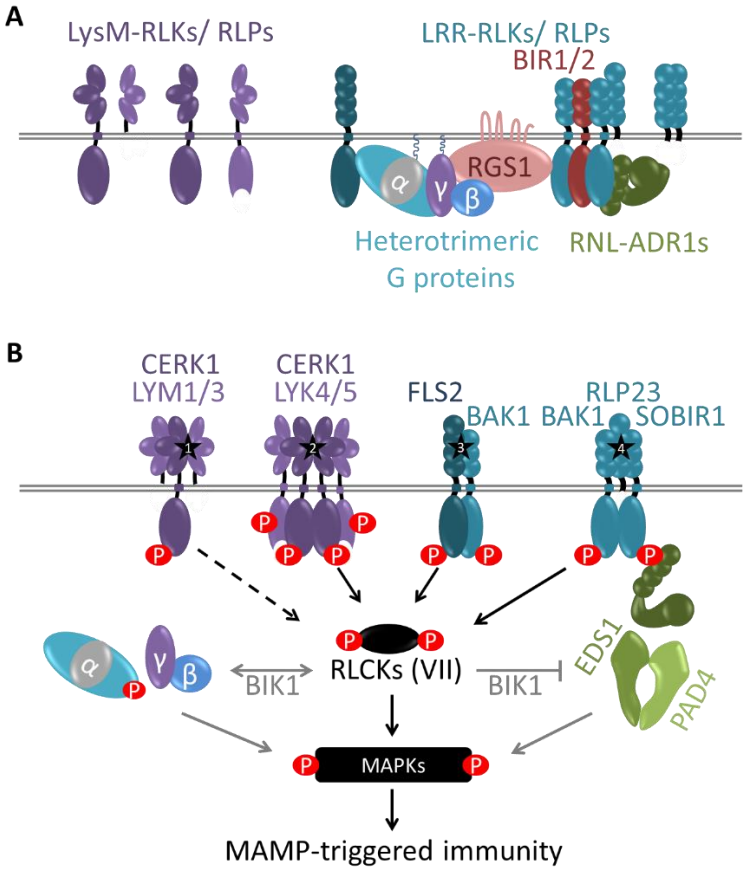

Fig. 1: Extracellular PRR-triggered immunity in plants.

(A) BIR1/2 inactivate plasma membrane-localized LysM-RLKs/ RLPs and LRR-RLKs/ RLPs via BAK1 interaction. Heterotrimeric G proteins (Gα: GPA1 and XLG2, Gβγ: AGB1-AGG1/2) are suggested to be stabilized in the resting state by RGS1. Inactive LRR-RLPs form homodimers or heteromers with SOBIR1. ADR1s (RPW8-NLR, RNL) were found to constitutively interact with SOBIR1. **(B)** Upon ligand binding (black stars: 1. peptidoglycan, 2. chitin, 3. flg22, 4. nlp20), BAK1 is released and activates other RLKs. LysM-/ LRR-RLKs form hetero-/ homodimers, which results in phosphorylation of RLKs and downstream RLCKs (mostly from class VII). In contrast to the other RLKs, LYK4/5 are kinase dead. Other components are activated during MAMP-triggered immune signalling: MAPKs, EDS1-PAD4, and heterotrimeric G proteins (Gα and Gβγ likely dissociate after release of RGS1). Image information was mainly taken from the review Couto and Zipfel 2016. Additional information was taken from Ma et al. 2017, Liang et al. 2018, Xue et al. 2019, Wan et al. 2019b, and Pruitt et al. 2020.

LYM2 can associate with LYK4 as well as LYK5 (Cheval et al. 2020) but LYK5 is not present in plasmodesmata (Erwig 2016; Cheval et al. 2020). In contrast, in *Oryza* the LYM homologue LysM-RLP

CEBiP is the main chitin perceiving component and was shown to dimerize upon chitin perception and then likely forms a complex with CERK1 (Shimizu et al. 2010; Hayafune et al. 2014). The best studied leucine-rich repeat (LRR)-RLK is flagellin sensing 2 (FLS2), which perceives flg22 and activates MAPKs (Asai et al. 2002; Chinchilla et al. 2006). Heterodimer formation of FLS2 and the LRR-RLK brassinosteroid insensitive 1-associated receptor kinase 1 (BAK1) is required for defense signalling (Koller 2014). BAK1 is known to act as co-receptor of many other RLKs and is, therefore, a major point of regulation (Liang and Zhou 2018). Key negative regulators of MTI and cell death are BAK1 interacting receptor kinases 1/2 (BIR1/2) (Halter et al. 2014; Liu et al. 2016). BIR1 interacts with and, thereby, likely restrains BAK1 as well as LRR-RLK suppressor of BIR1 1 (SOBIR1) from immune and cell death signalling (Liu et al. 2016). SOBIR1 is an LRR-RLK that can form a complex with several LRR-RLPs. In *Solanum* two well studied SOBIR1-ineracting LRR-RLPs are Cf-4 and Cf-9, which were originally identified as resistance (R)-genes against the pathogen *C. fulvum* (Liebrand et al. 2013). SOBIR1 as well as BAK1 kinase activity was found to be needed for this LRR-RLK/ RLP-dependent immune signalling pathway (van der Burgh et al. 2019). In *Arabidopsis* several LRR-RLPs were identified as ligand perceiving interactors of SOBIR1 including RLP23, which recognizes the microbial peptide nlp20 (Bi et al. 2014; Albert et al. 2015; Pruitt et al. 2020). Upon activation of PRRs at the PM, intracellular receptor-like cytoplasmic kinases (RLCKs) transmit between RLKs/ RLPs and MAPKs, CPKs, and heterotrimeric G proteins (Couto and Zipfel 2016). Botrytis-induced kinase 1 (BIK1) is a RLCK that is known to interact with many different RLKs and it is phosphorylated by BAK1 among others (Liang and Zhou 2018; Lin et al. 2014). BIK1 is involved in the activation of NADPH-oxidase RbohD, which promotes the formation of ROS (Kadota et al. 2014). Further, BIK1 is stabilized by heterotrimeric G proteins in the resting state, while degradation upon ligand binding is promoted by CPK28 (Wang et al. 2018). Remarkably, BIK1 positively regulates LysM/PRR-RLK-dependent immune signalling, while negatively regulating LRR-RLP-SOBIR1-dependent signalling via EDS1-PAD4 (Wan et al. 2019b). The phosphorylation pattern of BIK1 was found to strikingly differ after flg22-treatment in comparison to nlg20-treatment (Wan et al. 2019b). The negative regulator of G protein signalling RGS1, BIR1 and BAK1 were found to interact at the plasma membrane (Tunc-Ozdemir and Jones 2017; Ma et al. 2017). It is conceivable, that a repertoire of signalling components form a PM-localized inactive complex in the absence of stimuli. The role of G proteins in plant immunity will be further discussed in chapter 1.2.

Intracellular stimuli, such as rapidly evolving effectors or modifications of host components, can be recognized or guarded by intracellular receptors of the nucleotide-binding ARC domain (NB) and LRR superfamily (NLRs) (Jones and Dangl 2006; Jones et al. 2016). NLRs typically trigger local cell death known as the hypersensitive response (HR) in order to hinder pathogens from spreading (Jones and Dangl 2006; Jones et al. 2016). Three groups of well-known NLRs can be distinguished according to their N-terminal domain: coiled-coil (CC) domain (CNLs), Toll/ interleukin-1 receptor (TIR) domain

(TNLs) and resistance to powdery mildew 8 (RPW8) domain (RNLs) (Shao et al. 2016; Jones et al. 2016). The highly diversified sensor NLRs sense effectors either directly or indirectly via host targets of effectors, while conserved and mostly redundant helper NLRs are needed for downstream activation of HR (Bonardi et al. 2011; Collier et al. 2011; Adachi et al. 2019). The two RNL groups activated disease resistance 1 (ADR1s) and N-requirement gene 1 (NRG1s) are the two main groups of helper NLRs found downstream of many sensor NLRs (Jubic et al. 2019). RNLs are present in *rosids* while *asterids* have a network of NLR- required for cell death (NRC)-type helper NLRs instead (Wu et al. 2017). The sensor CNL HOPZ-activated resistance 1 (ZAR1) was shown to form a resistosome pentamer with the pseudokinase RKS1 and uridylated protein kinase PBL2 (Wang et al. 2019). Cell death execution was suggested to be directly triggered by PM association of the pore-forming complex after ligand-binding and ATPase-activity (Wang et al. 2019).

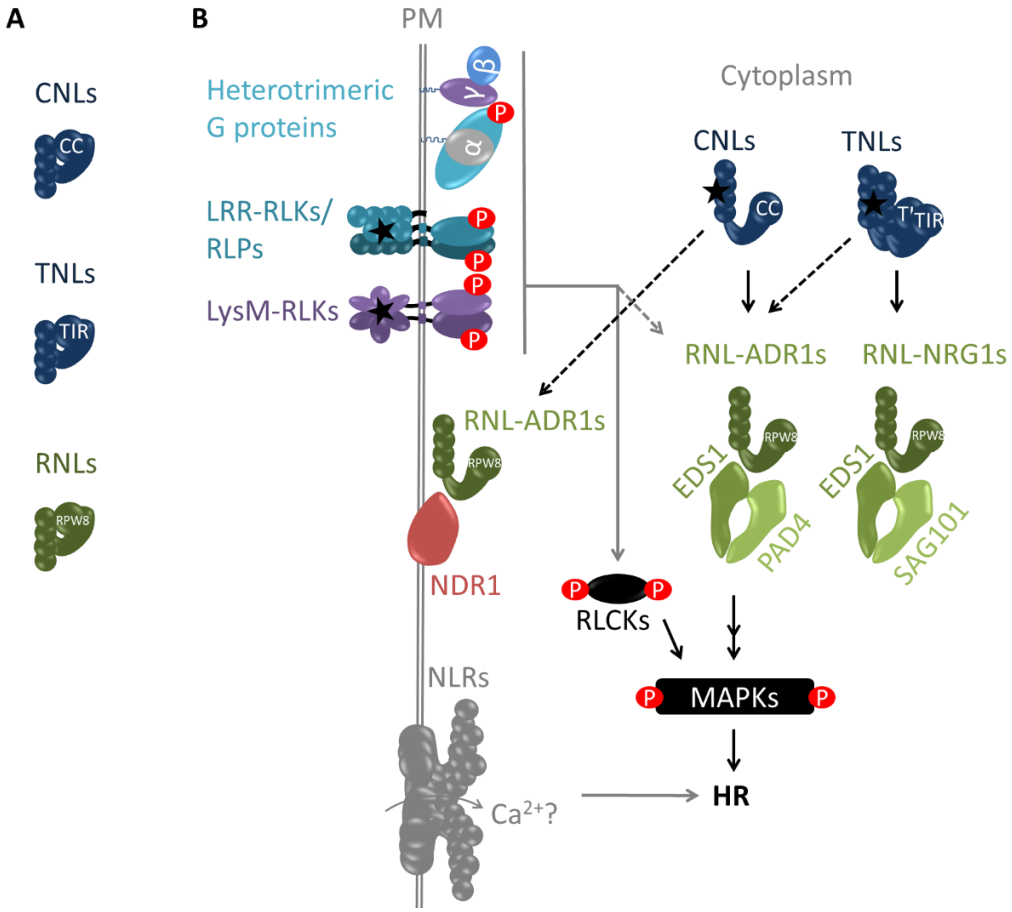

Fig. 2: Intracellular NLR-triggered immunity.

Inactive NLRs **(A)** change their conformation upon ligand perception and ATP-dependent activation **(B)**. CC-NLRs (CNLs) and TIR-NLRs (TNLs) interact with helper RNLs (RPW8-NLRs), which then commonly activate signalling via NDR1, EDS1-PAD4 or EDS1-SAG101. PM-localized PRRs, RLCKs and heterotrimeric G proteins are also involved in intracellular receptor immune signalling (or ETI). NLRs can form oligomeric pore-forming complexes which potentially induce cell death. MAPKs, especially MPK3 and MPK6, are also needed for ETI-induced HR. PM = plasma membrane, HR = hypersensitive response, RLCK = receptor-like cytosolic kinase. Image information was mainly taken from the reviews Jubic et al. 2019 and van Wersch et al. 2020. Additional information was taken from Liang et al. 2018, Pruitt et al. 2020, Yuan et al. 2020, and Ngou et al. 2020.

The pore-forming complex could directly cause cell death by disturbing PM integrity or ion homeostasis and additionally by mediating stress-induced defense gene activation including activation of the SA-pathway (Wang et al. 2020). RNLs were proposed to oligomerize comparable to mammalian NLR proteins but in a plant-specific variant due to strong structural differences (Wang et al. 2020). It was further proposed that RNLs are likely capable of forming pores similar to ZAR1 upon oligomerization (Jubic et al. 2019). For TNLs homomerization was found to be important for activation (Zhang et al. 2017). One well-known TNL is suppressor of non-expresser of PR genes 1 (NPR1)-1 constitutive 1 (SNC1) (Zhang et al. 2003). NADase activity of TNLs is needed for their activation (Wan et al. 2019a). It was suggested that TNLs potentially recruit RNLs for oligomerization (Jubic et al. 2019). However, attempts to find potential homodimers or oligomers of NRG1s failed so far (Wu et al. 2019). While TNLs need helper NLRs mainly from the NRG1 group but were also connected to the ADR1 group, CNLs were only connected to ADR1s (Wu et al. 2019). Downstream of sensor NLRs and the respective helper NLRs activation of the integrin-like protein non-race specific disease resistance 1 (NDR1) or lipase-like proteins such as enhanced disease susceptibility 1 (EDS1) and phytoalexin deficient 4 (PAD4) as well as senescence associated gene 101 (SAG101) is essential for resistance and HR (van Wersch et al. 2020). CNLs mostly require NDR1, while TNLs preferentially trigger HR via EDS1 (Aarts et al. 1998). Helper RNL-ADR1s are mainly involved in EDS1-PAD4 heterodimer-mediated pathogen restriction, while helper RNL-NRG1s contribute primarily to a EDS1-SAG101 complex-dependent cell death response (Feys et al. 2001; Lapin et al. 2019). NDR1 was found to contribute to ETI as well as MTI, as it is required for full MAPK activation (Knepper et al. 2011). MTI and ETI work synergistically: ETI positively regulates MTI signalling components and MTI enhances ETI-induced HR with MAPKs and NADPH oxidases (Ngou et al. 2020; Yuan et al. 2020). PTI-associated signalling components, such as XLG2, AGB1, AGG2, BAK1, BIK1 and MPK3, were transcriptionally induced upon D36E treatment and the same genes were even stronger induced in ETI upon D36E (*avrRpt2*) treatment (Yuan et al. 2020; Liang et al. 2016). It was further shown that SOBIR1 constitutively associates with ADR1 and, in addition, the RLCK PBL31 is required for the nls20-induced and LRR-RLP23-mediated immune signalling pathway (Pruitt et al. 2020). Accordingly, complex formation of LRR-RLPs/ RLKs and RLCKs as well as ADR1-EDS1-PAD4 at the inner side of the PM is likely involved in basal immune signalling showing that ETI components can be required for MTI (Pruitt et al. 2020). PRRs were also shown to be essential for NLR-mediated immune signalling (Yuan et al. 2020). A SA-independent role of EDS1-PAD4 in basal immunity is well-established (Straus et al. 2010) while EDS1-SAG101-mediated signalling is exclusive for ETI (Rustérucci et al. 2001; Pruitt et al. 2020).

1.2 Heterotrimeric G proteins in plants

1.2.1 Repertoire of heterotrimeric G proteins and domain functions

Heterotrimeric G proteins are molecular switches universal to most organisms (New and Wong 1998). Plant heterotrimeric G proteins consist of three subunits (Gα, Gβ and Gγ) and are involved in many different aspects of plant life. They play a crucial role during plant development, cell proliferation, ion channel activities, water and nitrogen use efficiency, plant hormone signalling and immunity as recently reviewed (Trusov and Botella 2016; Pandey 2020). *Arabidopsis* has one classical Gα subunit GPA1 which is in contrast to animal Gα subunits self-activating due to important differences in the helical domain that cause a pronounced intrinsic disorder (Jones et al. 2011; Johnston et al. 2007). Self-activation refers to the ability of GPA1 to bind GTP very fast while hydrolysis of GTP to GDP (GTPase activity) was found to be very slow (Johnston et al. 2007). This repertoire of Gα subunits is expanded by plant-specific extra-large Gα subunits (XLG1, XLG2 and XLG3) (Lee and Assmann 1999; Chakravorty et al. 2015) which were shown to bind and hydrolyse GTP *in vitro* (Lee and Assmann 1999; Heo et al. 2012) but are unlikely bound to GTP or GDP *in vivo* due to (Lou et al. 2019). Further, one classical Gβ subunit (AGB1) and two classical Gγ subunits (AGG1 and AGG2) are present and were shown to form a Gβγ-dimer as well as a heterotrimer with GPA1 (Chen et al. 2006). XLG are also known to form a heterotrimer with the Gβγ subunits at the PM *in vivo* (Zhu et al. 2009; Maruta et al. 2015; Chakravorty et al. 2015). Closely related homologues of AGB1 in terms of domain structure could function as non-canonical or decoy Gβ subunits (Miller et al. 2015) and DRW2 was found to localize to the PM and interact with GPA1 as well as AGG1/ AGG2 (Miller et al. 2019). Further, *Arabidopsis* has one plant-specific Gγ subunit (AGG3) with a C-terminal cys-rich region extension and a transmembrane (TM)-like sequence which were both needed for PM localization (Chakravorty et al. 2011). Classical G protein-coupled receptors (GPCRs) are known to activate mammalian heterotrimeric G proteins upon ligand binding and with help of their guanine nucleotide exchange factor (GEF) activity that accelerates GDP for GTP exchange which activates mammalian Gα subunits (Wettschureck and Offermanns 2005). However, GPCRs are mostly absent in plants (Taddese et al. 2014). Only one GPCR-like seven transmembrane protein was identified to have the typical GPCR-fold prediction, namely GCR1, and was also found to interact with GPA1 (Pandey and Assmann 2004; Taddese et al. 2014). After revelation of the GPA1 self-activation capacity it was debated whether plant heterotrimeric G proteins need GPCRs at all (Urano et al. 2013). The susceptibility requirements for adapted pathogens mildew resistance locus O (MLO) was found to contain several members that partially fulfil the requirements of potential GPCRs including the GPCR fold prediction with a heptahelical scaffold (Consonni et al. 2006; Taddese et al. 2014). The attempted connection of other non-GPCR-like MLOs (2, 6 and 12) to the G protein components GPA1-AGB1-AGG1/ 2 showed that MLO2 acts independently from AGB1 but

together with AGG1/2 in powdery mildew resistance (Lorek et al. 2013). Recently, a transcriptomic analysis showed that GCR1 and GPA1 not only interact with each other but also share many functional pathways while also having distinct roles (Chakraborty et al. 2019). How GCR1 potentially influence the activation status of GPA1 is not known while other GPA1-interacting membrane proteins were shown to fulfil a regulatory role. One such protein is regulator of G protein signalling 1 (RGS1) which is absent in most monocots and has a plant-specific 7 transmembrane expansion (Chen and Jones 2004; Hackenberg et al. 2017). RGS1 was shown to regulate GPA1 signalling by acting as a GTPase accelerating protein (GAP) (Johnston et al. 2007). There are 12 RGS-like phospholipase genes in *Arabidopsis* including PLDα1 which potentially have GAP activity. The PLDα1 was connected to G protein signalling via its interaction with GPA1 and the PLDα1 GAP activity was shown to accelerate GTP-hydrolysis of GPA1 similar to RGS1 (Zhao and Wang 2004; Choudhury and Pandey 2016). Interestingly, PLDα1 and RGS1 are thought to have inhibitory effects in a bidirectional manner (Choudhury et al. 2020). The non-canonical Gα XLG2 showed full interaction capacity with RGS1 independent from nucleotide binding (Lou et al. 2019). Information about the detailed domain organization of heterotrimeric *Arabidopsis* Gαβγ subunits is summarized in Fig. 3. Known phosphorylation sites in *Arabidopsis* heterotrimeric G proteins were recently reviewed (Chakravorty and Assmann 2018) and are indicated in Fig. 3. The Gα domain of GPA1 is self-activating, with spontaneous GTP-binding and low rate GTP-hydrolysis (Johnston et al. 2007) which functionally requires the helical domain (Jones et al. 2011). Further, GPA1 has two lipidation motifs including a covalent N-myristoylation (attached via a amide bond, N) and a reversible S-palmitoylation (attached via a thioester bond, S) site at the N-terminus (Adjobo-Hermans et al. 2006; Li and Qi 2017). Both lipidations were shown to be important for PM localization (Adjobo-Hermans et al. 2006). In contrast, XLG2 was described as atypical Gα subunit with highly reduced GTP-binding/ -hydrolysis activity due to the lack of functionally important residues in the Gα-like domain (Maruta et al. 2019). The plant-specific N-terminal extension harbors a cysteine-rich (cys-rich) region which is annotated as degenerate zinc finger domain with a highly conserved cys spacing pattern that resembles RING/ FYVE domains containing eight cysteines (Lee and Assmann 1999). Most RING zinc finger proteins typically act as E3 ligases, DNA-binding transcription factors or demethylases, while FYVE zinc finger proteins can typically act as lipid-protein scaffolds (Wywial and Singh 2010; Sun et al. 2019; Miura et al. 2009). Two JUMONJI domain containing proteins JMJ24 and JMJ25 with RING-C2 domains resemble the XLG eight cysteine spacing pattern and were shown to function either as DNA demethylase (JMJ25) or E3 ligase (JMJ24) (Miura et al. 2009; Kabelitz et al. 2016). The FYVE domain protein required for endosomal sorting 1 (FREE1) is an ESCRT component and was shown to specifically interact with

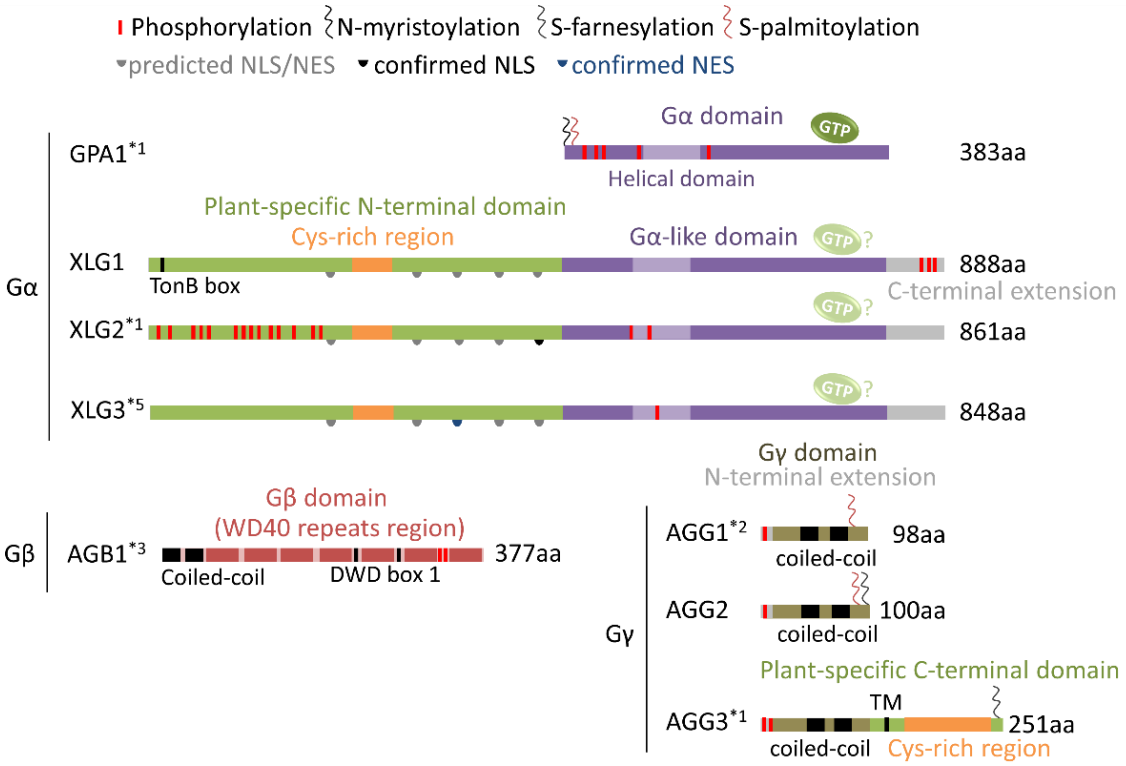

Fig. 3: The domain organization of *Arabidopsis* G protein subunits.

Positions of predicted and confirmed XLG nuclear localization (NLS) or nuclear export signals (NES) and known post-translational modifications as well as domain specifications are annotated. Asterisks indicate numbers of TAIR-listed additional splicing variants which represent potentially expressed isoforms. Image information was collected from uniprot, Chakravorty et al. 2015, Liang et al. 2016, Urano et al. 2016, Urano et al. 2013, Ding et al. 2008, Maruta et al. 2019, Wolfenstetter et al. 2015, Chakravorty and Assmann 2018.

phosphatidylinositol 3-phosphate (PI3P), which is characteristic for FYVE domain proteins (Jensen et al. 2001; Gao et al. 2014). GPA1 has two highly conserved phosphorylation sites at position S49 and Y166 (Chakravorty and Assmann 2018). Interestingly, the GPA1 phosphomimetic mutation Y166E increases RGS1 and GDP-binding affinity of GPA1, probably due to conformational changes within the switch region (Li et al. 2018). XLG2 was found to be phosphorylated in multiple N-terminal positions, including Ser148 and Ser150, which were found to be targeted by BIK1 (Liang et al. 2016). XLG1 is the only plant-specific XLG protein that happens to have an N-terminal TonB box, which is known to be involved in metal scavenging processes in bacteria (Postle 2007). Recently, a TonB-based metal-scavenging mechanism was proposed to occur also in plants, due to the presence of metal incorporating siderophores, several TonB-box containing proteins as well as potential TonB-dependent transporters and their upregulation under heavy metal stress (Theriault and Nkongolo 2017). AGB1 mainly contains a seven bladed propeller-like structure made of WD40-repeats, which is characteristic for Gβ subunits and receptor for activated c-kinase (RACK) proteins (Miller et al. 2015). Two identified phosphorylation sites shortly before the last WD40 region of AGB1 are conserved positions in canonical

Gβ subunits and flank the Gα contact site (Chakravorty and Assmann 2018). WDR-domains are known to be involved in scaffolding DNA-/ protein-protein interactions (Miller et al. 2015). Further, WD40 proteins containing a DWD-box can act as substrate receptors for certain E3 ligases (Lee et al. 2008). *Arabidopsis* contains over 200 WDR-proteins that potentially act as Gβ-like or decoy proteins (Miller et al. 2019). *Arabidopsis* has two classical Gγ subunits AGG1 and AGG2, which likely have the typical coiled-coil structure needed for interaction with other heterotrimeric G proteins (Mason and Botella 2000). Dual lipidation of AGG2, with a covalent S-farnesylation and a reversible S-palmitoylation, was shown to be important for PM tethering (Adjobo-Hermans et al. 2006; Zeng et al. 2007). The plant-specific C-terminal domain of AGG3 has a cys-rich region which was shown to be needed for PM localization together with a short TM-like domain (Wolfenstetter et al. 2015).

1.2.2 Heterotrimeric G protein signalling mechanism

In the classical model for heterotrimeric G protein signalling, mammalian G proteins form a membrane-bound heterotrimeric complex and interact with GPCRs that bind ligands and activate Gα subunits with their GEF-activity, which accelerates the GDP to GTP exchange and dissociation (Wettschureck and Offermanns 2005). In metazoans, a large repertoire of G protein subunits exists with e.g. 16 Gα, 5 Gβ, 12 Gγ known subunits (splicing variants excluded) and over 150 GPCRs as well as 21 RGS1 found to be involved in G protein signalling in humans (Jones and Assmann 2004). The GTP-bound state triggers dissociation of the Gα subunit from the Gβγ-dimer due to conformational changes and involvement of both, the Gα subunit as well as the Gβγ-dimer, in downstream signalling (Jones and Assmann 2004). Effectors of G protein signalling are usually the phosphoinositide-dependent phospholipase Cs (PLCs), phosphodiesterase phospholipase Ds (PLDs) and protein kinase Cs (PKCs) (Jones and Assmann 2004). The Gα subunits are usually switched off via GAP-acting interactors such as RGS proteins (Wettschureck and Offermanns 2005). As soon as the Gα subunit hydrolyses GTP to GDP the heterotrimeric complex can re-assemble with GPCRs in the resting state (Wettschureck and Offermanns 2005). Active heterotrimeric G proteins are typically involved in downstream signalling via ion channels, phospholipases or MAPKs (Wettschureck and Offermanns 2005; Chakravorty and Assmann 2018).

In plants, the repertoire of G proteins is comparably low and due to the self-activation of the single classical Gα subunit GPA1 a GEF-acting GPCR is not needed (Urano et al. 2013). Further, plants have plant-specific subunits such as XLGs, AGG3 and the seven transmembrane RGS1 with GAP activity (Chakravorty and Assmann 2018). Interestingly, XLGs might not depend on nucleotide binding at all (Lou et al. 2019). GCR1 is the only example for a classical GPCR which was shown to interact with GPA1 (Pandey and Assmann 2004). Plant RLKs likely act as main receptors in plant heterotrimeric G protein signalling via a phosphorylation-dependent regulation mechanism involved in activation (Pandey 2020;

Zhang and Zeng 2020). A model of *Arabidopsis*-specific heterotrimeric G protein signalling is depicted in Fig. 4. With G proteins being able to couple to a repertoire of 610 RLKs and 178 candidate RLPs in *Arabidopsis* the plant system finally resembles the perception diversity enabled by the large number of ~1000 mammalian GPCRs (Shiu and Bleecker 2003; Wettschureck and Offermanns 2005). Interestingly, identified phosphorylations within GPA1 and AGB1 represent conserved positions in canonical G proteins, while XLG and AGG phosphorylation sites were found mainly within plant-specific regions (Chakravorty and Assmann 2018). Accordingly, activation of the Gβγ-dimer might occur in a classical way simply due to dissociation of the Gα subunit (Chakravorty and Assmann 2018). In contrast, plant Gα and Gβγ were initially not found to dissociate upon GTP binding (Adjobo-Hermans et al. 2006) but localize to different compartments including the PM and the nucleus (Liang et al. 2017; Chakravorty et al. 2015; Maruta et al. 2015). AGB1 was found to be highly instable without an interacting Gγ subunit (Adjobo-Hermans et al. 2006). For GPA1 as well as XLG2 dissociation from the Gβγ-dimer was found to occur in dependency to further regulatory control such as phosphorylation (Adjobo-Hermans et al. 2006; Liang et al. 2018; Xue et al. 2020).

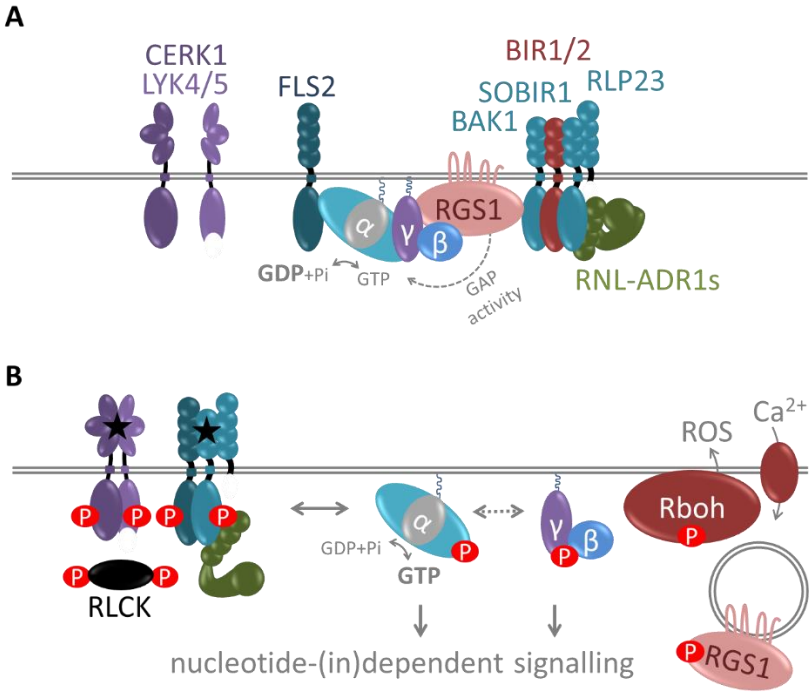

Fig. 4: Heterotrimeric G protein signalling in *Arabidopsis*.

(A) A PM-localized inactive complex of PRRs and heterotrimeric G proteins is partially stabilized by GAP-acting proteins (RGS1) within the receptor complex. **(B)** MAMP-perception activates a phosphorylation cascade in which BAK1 and BIK1 phosphorylate downstream targets such as GPA1 (by BAK1), XLG2, AGB1-AGG1/2, and RGS1. Further, phosphorylation of GAP-acting proteins (RGS1) likely promotes de-repression of heterotrimeric G proteins. Activation of G proteins promotes ROS formation and calcium influx. Image information was mainly collected from Zhong et al. 2019. Additional information was taken from Chakravorty and Assmann 2018, Wang et al. 2018a, Maruta et al. 2019, Lou et al. 2019, and Xue et al. 2020.

Due to the autoactivation of GPA1 and the nucleotide-independent activities of plant Gαs, plant G protein signalling was also described as a de-repression-based mechanism were a GAP is necessary to hold the heterotrimer in the inactive state (Urano et al. 2016; Lou et al. 2019). RGS1 was indeed found to function as such and its phosphorylation was suggested to induce endocytosis resulting in de-repression of Gαs (Urano et al. 2012). Stimulus-dependent release of a repressing component (e.g. RGS1/ PLDα1) activates signalling, while upon removal of the activated receptor the activation is sustained (Urano et al. 2012; Ghusinga et al. 2020). Plant G proteins were found to be stimulated by RLKs and their activity is likely regulated by phosphorylation (Chakravorty and Assmann 2018). Accordingly, a de-repression mechanism is certainly accompanied by a phospho-dependent activation mechanism which can be referred to as concerted switch also known from yeast heterotrimeric G proteins (Ghusinga et al. 2020). One detailed example for G protein signalling in plants is the interaction between XLG2 and the FLS2-BAK1-BIK1-RGS1 receptor complex. Upon ligand-binding and subsequent activation of the FLS2-BAK1-BIK1 receptor complex, BIK1 phosphorylates XLG2 and RGS1, which promotes dissociation of XLG2 from AGB1-AGG1/2 and the receptor complex (Liang et al. 2016; Liang et al. 2018). XLG2 was found to be phosphorylated by BIK1 during MTI at S23 and S169 (Liang et al. 2016) and the same phospho-sites were identified during ETI (Kadota et al. 2019). A similar relation was also found between GPA1 and the same receptor complex (Tunc-Ozdemir et al. 2016), in which BAK1 phosphorylates GPA1 during immune signalling at multiple sites (Xue et al. 2020). The GPA1 phosphorylation site T19 was found to be especially interesting as a phosphonull mutation T19A as well as the phosphomimic mutation T19D abolished all other flg22-induced phosphorylations (Xue et al. 2020). Other post-translational modifications as well as differential expression, turn-over and subcellular localization of G proteins and their interacting partners could be involved in fine tuning G protein signalling (Pandey 2020; Zheng et al. 2019). Recently, S-acylation was shown to be relevant for FLS2 and CERK1 signalling in correctly formed nanodomains (Zheng et al. 2019; Chen et al. 2019) and dynamic S-acylation of G proteins represents an effective way to enable subcellular trafficking of G proteins (Zheng et al. 2019; Adjobo-Hermans et al. 2006). GPA1 and XLG2 could act cooperatively or independently in immune signalling (Liang et al. 2018; Xue et al. 2020). A pool of heterotrimeric G proteins likely remains, inactive and/ or activated, at the PM perhaps due to S-acylations or other interactions according to the results found concerning XLG2 and AGB1 interaction (Zhu et al. 2009; Liang et al. 2016). XLG2 can form a heterotrimeric complex with the other subunits (Maruta et al. 2015; Chakravorty et al. 2015) and dissociation likely depends on phosphorylation of XLG2 (Liang et al. 2016). Zhu et al. pulled down XLG2 with AGB1 from *Pst avrRpm1*-inoculated leaves of stable transgenic lines and failed to pull down XLG2 from uninfected material likely due to typical low abundance of XLG2. Liang et al. found that XLG2 interaction with AGB1 decreased after flg22 treatment based on split-luciferase complementation assays in *Nicotiana benthamiana* with a remaining level of interaction.

Further, they show evidence that flg22-treatment induces phosphorylation of the XLG2 N-terminus in protoplasts (Liang et al. 2016). How these results can be transferred to the full-length XLG2-AGB1 interaction in *Arabidopsis* remains to be further studied.

1.2.3 Heterotrimeric G proteins in plant immunity

The major Gαβγ heterotrimer involved in biotrophic/ hemibiotrophic and necrotrophic pathogen interactions is XLG2-AGB1-AGG1/ AGG2 (Trusov et al. 2006; Maruta et al. 2015; Miller et al. 2015). An overview of heterotrimeric G protein functions in immunity discussed in this chapter can be found in Fig. 5. Expression of heterotrimeric G proteins including GPA1, AGB1, AGG1/ AGG2 as well as XLG2 and XLG3 but not XLG1 and AGG3 were induced upon (non-) host inoculation or elicitor treatment and are, therefore, involved in basal immune responses (Lee et al. 2013; Zhu et al. 2009; Liang et al. 2016). While GPA1 is explicitly not involved in necrotrophic pathogen interactions (Trusov et al. 2006). AGB1 and XLG2 were identified as positive regulators of SA-inducing pathogen interactions (Zhu et al. 2009; Maruta et al. 2015) and found to mostly but not always act cooperatively together during immunity (Desaki et al. 2019a; Liang et al. 2016). Further, AGB1 can also act as negative regulator of SA and JA during viral infections (Brenya et al. 2016). This indicates that heterotrimeric G proteins can respond to diverse pathogens in a highly differentiated manner. GPA1 regulates stomatal movements together with AGB1 which is also important for plant immunity (Zhang et al. 2008a; Yu et al. 2018). GPA1 was suggested to regulate RbohF-dependent ROS formation in guard cells in dependence to abscisic acid (ABA) (Zhang et al. 2011; Qi et al. 2018). Further, phosphorylation of XLG2 and association with RbohD was described to positively regulate RbohD-dependent ROS generation during immune signalling (Liang et al. 2016; Liang and Zhou 2018). A positive role of AGB1 and AGG1/2 downstream of RLKs/ RLPs in ROS burst was repeatedly confirmed, as *agg1 agg2* or *agb1* mutants showed significantly impaired ROS production (Lorek et al. 2013; Liang et al. 2016; Wan et al. 2019b). Contradictory results were found for the *xlg2* mutant with either significantly impaired ROS burst almost similar to *agb1* (Liang et al. 2016) or no significant ROS reduction at all (Wan et al. 2019b). Rather redundant functions of XLG1-3 in ROS formation can be suggested according to the repeatedly observed reduced ROS burst in *xlg2 xlg3* double and *xlg1 xlg2 xlg3* triple mutants (Maruta et al. 2015; Liang et al. 2018). Further, AGB1 together with RGS1 plays a central role in calcium spiking (Tunc-Ozdemir and Jones 2017; Jeon et al. 2019). Heterotrimeric G proteins directly couple to MAPK-components with AGB1 and GPA1 being attached to MPK6 without impact on activation (Cheng et al. 2015) and AGB1 was found to interact with MKK4/5 (Yuan et al. 2017) as well as the scaffold proteins RACK1A-C (Cheng et al. 2015). In addition, AGG1/2 can interact with RACK1A and nudix hydrolase homologue 7 (NUDT7) which regulates the NPR1-EDS1-PAD4 salicylic acid pathway (Olejnik et al. 2011). RACK1 scaffolds were found to be important for the bacterial protease PrpL/ ArgC-triggered but not flg22-induced immunity (Meng

et al. 2015). Whether XLG2 potentially interacts with RACKs remains to be shown. In contrast to AGB1, potential non-canonical Gβ proteins DRW1 and DRW2 were found to play a negative role in plant immunity (Miller et al. 2019). In addition to phosphorylation-dependent regulation, immune signalling is also regulated by single-/ poly-ubiquitination (Zhang and Zeng 2020). Redundantly acting U-box E3 ligases including PUB25/26 and PUB12/13 are known to negatively regulate PRR signalling including CERK1, LYK5, FLS2 and BAK1, which was recently reviewed (Zhang and Zeng 2020).

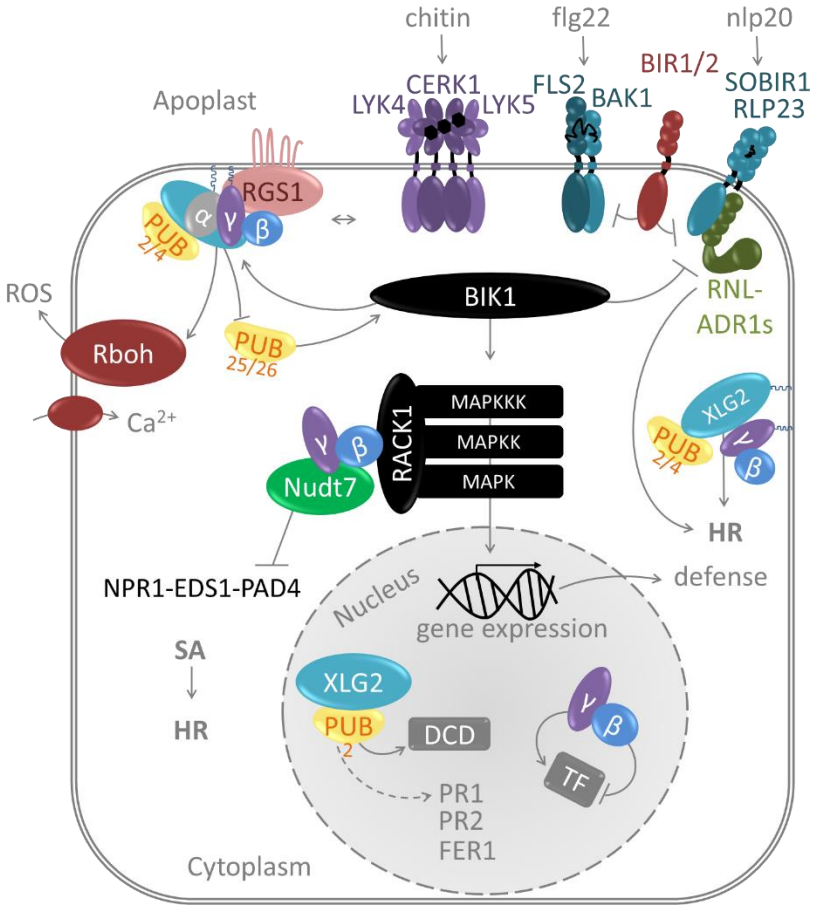

Fig. 5: Subcellular trafficking of heterotrimeric G proteins during immune signalling.

Gα subunits (GPA1 in grey and XLG2 in blue) and the Gβγ-dimers (AGB1-AGG1/2) form a complex at the PM, while XLG2 and AGB1-AGG1/2 are also found in the nucleus (Maruta et al. 2015, Chakravorty et al. 2015). XLG2 likely interacts with a DCD protein in the nucleus (Liang et al. 2017). Heterotrimeric G proteins positively regulate ROS formation and Ca^{2+} influx (Zhang et al. 2011; Maruta et al. 2015). XLG2 and PUB2/4 constitutively interact (Wang et al. 2017) and stabilize BIK1 (Liang et al. 2016; Derkacheva et al. 2020; Wang et al. 2018). Defense gene expression is regulated by G proteins (Zhu et al. 2009; Delgado-Cerezo et al. 2012). XLG2 and AGB1 are involved in cell death signalling, in the absence of BIR1 (Maruta et al. 2015) and in the presence of CERK1-4 (Petutschnig and Stolze, unpublished; Meusel, 2016). AGB1 regulates immunity via RACK1 association (Cheng et al. 2015), while AGG was found to interact with Nudt7 (Olejnik et al. 2011). Additional information was taken from Couto and Zipfel 2016, Pruitt et al. 2020.

Sequential activity of ubiquitin-activating (E1), conjugating (E2) and ligating (E3) enzymes regulate RLK trafficking and stability (Furlan et al. 2012; Hershko and Ciechanover 1998). Reversible ubiquitination can either result in target degradation or changed subcellular localization in a phosphorylation-dependent manner (Zhang and Zeng 2020). Such degradation-controlled processes were suggested to be regulated partially by heterotrimeric G proteins including XLG2, AGB1 and AGG1/2 (Wang et al. 2017; Liang and Zhou 2018). One intensively studied example for degradation-controlled regulation is BIK1. BIK1 was shown to be stabilized by the XLG2-AGB1-AGG1/2 complex in the resting state (Liang et al. 2016), likely via XLG2-dependent inhibition of PUB25/26 (Wang et al. 2018). XLGs were shown to constitutively interact with the U-box E3 ligases PUB2 and PUB4, which positively regulate MTI via stabilization of activated BIK1 downstream of several PRRs (Wang et al. 2017; Liang et al. 2017; Derkacheva et al. 2020). PUB2/4 were shown to contribute to flg22/ GN7-induced ROS and callose deposition and the pub4 mutant was shown to be more resistant against *P. syringae* (Desaki et al. 2019a). Heterotrimeric G proteins were suggested to be potentially stabilized by PUB interactions (Wang et al. 2017). The observation that protein levels of XLG2 are regulated by the proteasome-mediated protein degradation pathway (Zhu et al. 2009) would support this idea. Interestingly, absence of XLG2 results in differential expression of several defense genes including downregulation of PR1 and PR2 while several copper superoxide dismutases (CSDs) and one myrosinase-binding protein 1 (MBP1) among others were found to be upregulated (Zhu et al. 2009). Upregulation of MBP1 in *xlg2 xlg3* as well as *agg1 agg2* mutants was confirmed (Maruta et al. 2015) indicating that the heterotrimer is involved in this outcome. G proteins are also involved in cell death signalling (Wang et al. 2007; Liu et al. 2013). AGB1 together with AGG1/2 was found to be involved in cell death associated with a unfolded protein response (UPR) in the endoplasmic reticulum (ER) independent from GPA1 (Wang et al. 2007). Further, the *xlg2 xlg3* double mutant showed decreased UPR marker gene BIP3 expression levels which were found to be increased in the *rgs1* mutant background (Liang et al. 2018). Interestingly, AGB1 was also found to be involved in one essential UPR pathway (Chen and Brandizzi 2012). Further, a development and cell death (DCD) domain containing protein was shown to interact with XLG1/3 (and XLG2 in Y2H) in the cytosol and the nucleus in BiFC (Liang et al. 2017). XLG2 together with AGB1-AGG1/2 were also identified as positive regulators of cell death downstream of BIR1 (Liu et al. 2013) which will be discussed in more detail in chapter 1.5. Phospholipases were also identified to play a role in MAMP-triggered immunity, including PLDδ (Pinosa et al. 2013; Xing et al. 2019) and PLC2 in ROS burst (D'Ambrosio et al. 2017). The connection between XLG2/3 as main contributors to immunity and these phospholipases has not been analysed yet. Similarly to heterotrimeric G proteins, phospholipases are involved in almost all aspects of plant life including development and immunity and can be regulated via phosphorylation and Ca^{2+} (Takáč et al. 2019).

1.3 Nucleo-cytoplasmic transport

The nuclear envelope consists of an outer and inner nuclear membrane and represents a barrier which can be only passed via the nuclear pore complex (NPC) (Ma et al. 2012). The NPC is a multi-protein complex with high homology between plants and other eukaryotes (Wiermer et al. 2010; Raices and D'Angelo 2012). The NPC represents a large complex composed of around 30 nucleoporins (NUPs) which form a ring structure with their natively unfolded cytoplasmic phenylalanine-glycine (FG) repeats, followed by a central channel and the intranuclear basket structure (Raices and D'Angelo 2012; Suntharalingam and Wente 2003). Compositional differences can occur within the set of NPCs around the envelope (Raices and D'Angelo 2012). It is important for nucleocytoplasmic transport of proteins and mRNA as well as chromatin remodeling (Raices and D'Angelo 2012; Tamura 2020). The role of the NPC in nucleocytoplasmic transport of larger proteins will be further discussed. Nuclear transport receptors (NTRs) actively facilitate bidirectional trafficking of macromolecules (> 40 - 60 kDa) via interaction with the cargo as well as the NPC, while smaller molecules passively diffuse through the NPC (Ma et al. 2012; Raices and D'Angelo 2012). NPC interacting NTRs such as importin-α and importin-β transport cargos into the nucleus, while exportins reach the cytoplasm with their cargos and directionality is facilitated by a small GTPase gradient (Raices and D'Angelo 2012). Importins and exportins can either directly bind their cargo. Importins recognize nuclear localization signals (NLS) typically composed of poly basic amino acid sequences as classical or bipartite NLSs (Kosugi et al. 2009). One of the best characterized example is the classical NLS from the SV40 virus (Dingwall and Laskey 1991). Common nuclear export signals (NES) consist of leucine-rich and mostly hydrophobic residues recognized by exportins such as the highly conserved XPO1 (Xu et al. 2015; Haasen et al. 1999). Interaction of importins as well as exportins with the barrier forming FG-repeat NUPs determines whether cargos can pass the complex (Tamura 2020). NUP mutations were shown to affect several aspects of plant life including defense, symbiosis and hormone signalling (Binder and Parniske 2018). One well-studied autoimmunity gain-of-function mutant is the suppressor of *npr1*-1 constitutive 1 (*snc1*-1), which is a TNL and harbors a single amino acid exchange (E552K) resulting in auto-activation (Zhang et al. 2003). *snc1*-1 *Arabidopsis* constitutively activate defense responses, have a dramatically stunted growth and partially require the SA-pathway for this phenotype (Zhang et al. 2003). Suppressor mutants that did no longer show the characteristics of the *snc1*-1 mutant phenotype were referred to as modifier of *snc1*-1 (*mos*). *mos* mutants including NUP homologues *mos3* and *mos7* showed abolished SA accumulation, PR gene expression and resistance based on R-gene regulation (Zhang and Li 2005; Monaghan et al. 2010). These suppressor mutations revealed that the NPC is highly important for basal and R gene mediated defense responses (van Wersch et al. 2016). MOS6 was shown to be the main responsible importin-α (*imp-α3*) for nuclear import of SNC1, while MOS7 the mammalian NUP88 homologue was shown to be involved in nuclear retention of SNC1 (Lüdke et al. 2020; Wiermer

et al. 2010). XPO1 is involved in recognition and export of SNC1 and EDS1 (García et al. 2010). XPO1-dependent export is inhibited by MOS7 resulting in nuclear retention of SNC1 which is abolished in the *mos7*-1 mutant (Wiermer et al. 2010). Increased export of NPR1 and EDS1 found in *mos7*-1 further underlines that plant defense pathways rely on nucleocytoplasmic transport of involved defense regulators (Wiermer et al. 2010). Several NUPs were specifically identified to be involved in plant defense, including MOS3, SEH1 and NUP160 while others were not involved in defense (Wiermer et al. 2012). Nucleocytoplasmic trafficking was shown to be relevant for the EHM-targeting and cell death induction of the resistance protein RPW8.2 (Huang et al. 2019). This protein harbors several localization signals including EHM-targeting, NLSs and NESs and analysis of mutant variants with changed localization revealed that cytoplasmic accumulation of this protein induces cell death likely due to chloroplast toxicity (Huang et al. 2019). Regarding XLGs, presence of an N-terminal NLS was described (Ding et al. 2008), while one XLG2 NLS and one XLG3 NES were later experimentally shown to be functional in transient systems (Ding et al. 2008; Chakravorty et al. 2015), while their physiological impact was not further analysed. Another example for the importance of nucleocytoplasmic trafficking in plant defense is NPR1. NPR1 is a master regulator of PR1 expression and other defense genes, were upregulation usually results in cell death, and depends on nuclear accumulation of NPR1 (Mou et al. 2003). S-nitrosylation of NPR1 in the presence of SA and subsequent oligomerization due to disulfide formation causes cytoplasmic retention (Tada et al. 2008). SA-induced redox state changes in the plant cell trigger thioredoxin-dependent reduction of NPR1 disulfide bonds and, thus, facilitates NPR1 monomer formation which results also in NLS-recognition and nuclear import (Tada et al. 2008). Recently, cytoplasmic SA-induced NPR1 condensates (SINCs) were described to regulate protein degradation in favor of cell survival (Zavaliev et al. 2020). Accordingly, either cytoplasmic or nuclear localization of NPR1 heavily defines cell fate: direction cell death or survival.

1.4 Interaction between plants and powdery mildews

Powdery mildews are obligate biotrophic *Ascomycetes* of the order *Erysiphales* that invade epidermal cells and can be recognized as white powder on infected plant surfaces above the ground (Hückelhoven 2005). The asexual life cycle of *Erysiphe cruciferarum* (*Ec*) is fulfilled on the host plant *Arabidopsis.* During this compatible interaction the asexual life cycle can be completed with entrance into sexual reproduction and subsequent formation of fruiting bodies that carry endurable ascospores due to the ability of the fungus to overcome basal resistance (Kuhn et al. 2016; Eichmann and Hückelhoven 2008). After germination, a powdery mildew spore differentiates at the tip into a penetration structure called appressorium (AP). The AP enables the fungus to enter the host apoplastic space. Under certain circumstances the fungus is able to develop a haustorium that grows into the host cell without disturbing the PM (Kuhn et al. 2016). The haustorium is a hyphal feeding structure

with bulbous surface enlargement, contains a nucleus and is surrounded by the so called extrahaustorial membrane (EHM) synthesized from plant-derived membrane material (Micali et al. 2011; Kuhn et al. 2016). The extrahaustorial matrix (EHMx) refers to the space between the fungal cell wall and the EHM and is bordered to the apoplast by a haustorial neckband (Micali et al. 2011). *Blumeria graminis f.sp. hordei* (*Bgh*) is known as a barley pathogen and is, therefore, affected by non-host resistance (NHR) in *Arabidopsis* which means that *Bgh* does not proliferate in a visible range on the leaf surface (Lipka et al. 2005). NHR refers to phenomenological aspects of specific pathogen species robustly restricted in growth in certain host species, rather, than to a molecular mechanism (Panstruga and Moscou 2020). Nevertheless, NHR genes can confer broad-spectrum resistance as they are often involved in defense against adapted as well as non-adapted pathogens (Kuhn et al. 2016). NHR can be divided into pre- and post-invasive resistance (Lipka et al. 2005). Gene regulation and post-translational protein modification as well as synthesis, activation and (non-) vesicular secretion of toxic phytoalexins such as camalexin or indolic glucosinolates contributes heavily to pre-invasion resistance against various pathogen classes (Lipka et al. 2010). One identified pre-invasion resistance pathway against non-adapted powdery mildews relies on the cell-autonomously induced and ER-localized P450 monooxygenase CYP81F2 (Fuchs et al. 2016) which was found to synthesize glucosinolate derivatives in epidermal cells (Bednarek et al. 2009). Under attack, *de novo* synthesis of glucosinolate derivatives was observed as well as induced accumulation of another monooxygenase, namely CYP83B1, in support of CYP81F2 (Hunziker et al. 2019). When needed, these glucosinolate derivatives can be activated by the glycoside hydrolyse (myrosinase) PEN2 (Bednarek et al. 2009) which is constitutively expressed and associates with peroxisomes and mitochondria, while association with immobilized mitochondria was shown to solely contribute to NHR (Fuchs et al. 2016). CYP81F2 co-localizes with PEN2 attached to the cytosolic surface of mitochondria at focal accumulation sites (Fuchs et al. 2016). The hydrolyzed aglycon is then actively secreted by PEN3 which is a pleiotropic drug resistance ATP-binding cassette (ABC) transporter contributing to NHR (Stein et al. 2006). PEN3 is recruited to the extracellular space beneath penetration sites which relies on actin filaments and PRRs CERK1 or FLS2 but not on the co-receptor BAK1 (Underwood and Somerville 2013). More precisely, PEN3 was found to be recruited to papillae and during interaction with the adapted powdery mildew *Golovinomyces orontii* to the encasement of haustoria (Meyer et al. 2009). Further, PEN3 requires phosphorylations at S40 and S45 during *Bgh* interaction and phosphorylation at these sites is also induced upon flg22 treatment and during effector *AvrRpt2* expression by Dex treatment (Kadota et al. 2019; Underwood and Somerville 2017). This PEN3 phosphorylation during MTI as well as ETI agrees with its role during interactions with adapted as well as non-adapted powdery mildews. Another pen mutant was identified with reduced extracellular resistance named *pen4* (Hématy et al. 2020; Micali et al. 2008). This *pen4* mutation was mapped to the phytochelatin synthase 1 (PCS1) a heavy metal detoxification

compound. PCS1 might contribute to ITC-glutathione adduct processing, regulation of other enzymes of the pathway, or gene expression control as similarly to *pen2* accumulation of pathogen-inducible indole glucosinolate-derived compounds was measured in the *pen4* mutant (Hemsley et al. 2008). Further, cytoplasmic PEN4 also focally accumulated beneath *Bgh* penetration sites (Hemsley et al. 2008).

The other pre-invasion resistance pathway involves the soluble N-ethylmaleimide-sensitive factor attachment receptor (SNARE) protein PEN1 (SYP121) which is a PM-localized syntaxin and accumulates in PM microdomains at fungal penetration sites upon PRR-dependent recognition (Underwood and Somerville 2013). Further, PEN1 is found in a ternary-complex with the adaptor SNARE synaptosomal-associated protein 33 (SNAP33) and functionally redundant v-SNAREs vesicle-associated membrane proteins VAMP721/722 (Lipka et al. 2010; Kwon et al. 2008). Similarly to PEN3, PEN1 and SNARE33 accumulate at sites of increased callose deposition (papilla/ encasements) (Meyer et al. 2009). A PEN1 homologue was found in barley, the SNARE protein required for MLO-resistance 2 (ROR2), which underlines that conservation of pre-invasive immunity exists in monocots and dicots (Collins et al. 2003; Humphry et al. 2010). The closest homologue of PEN1 is SYP121 and absence of both, *syp121 syp122*, results in constitutive defense activation (autoimmunity) (Zhang et al. 2008b). Cytoskeleton re-organization towards sites of attempted entry often plays a crucial role for recruitment of organelles, such as mitochondria, the nucleus or peroxisomes, and for callose deposition and, therefore, is of high importance for NHR (Takemoto and Hardham 2004; Yun et al. 2003). The recruitment of PEN1 and PEN3 to papilla and encasements was suggested to happen based on an exosome-like formation in which PM-localized defense proteins would end up in intraluminal vesicles (ILVs) within multivesicular bodies (MVBs) which potentially release their content as exosomes upon fusion with the PM (An et al. 2006; Meyer et al. 2009). The usual MVB direction follows the endocytotic pathway towards vacuolar degradation and is protective against cell death (Levine 2002). Recent findings also connect the potential PEN1/ PEN3-dependent exosome pathways to IAOx negative regulation of leaf senescence (Crane et al. 2019). MVBs were found in close proximity to powdery mildew infection sites (An et al. 2006). Further, PEN1 and PEN3 were found in isolated extracellular vesicles from *Arabidopsis* among many other defense-related proteins while the PM marker low temperature-induced 6b (Lti6b) was not found (Rutter and Innes 2017). Their findings underline the equivalence of plant extracellular vesicles, that originate from internalized components crossing the TGN to end up in ILVs of MVBs, to mammalian exosomes (Rutter and Innes 2017; van Niel et al. 2006; Hansen and Nielsen 2017). Bacterial pathogen-induced MVBs were observed in dependence to lyst-interacting protein 5 (LIP5) (Wang et al. 2014). Positive regulation of MVB formation by LIP5 depends on interaction with the endosomal sorting complex required for transport (ESCRT)-III component SKD1, which is a AAA ATPase (Wang et al. 2014). Further, the SKD1-associated deubiquitinase AMSH3 is

guarded by TNLs, required for CNL-dependent immunity (Schultz-Larsen et al. 2018) and needed for intracellular trafficking via ESCRT (Isono et al. 2010). AMSH3 is required for establishment of the *pen1*-1 *syp122*-1 lesion-mimic mutant (LMM) phenotype (Zhang et al. 2007). While PEN1 and PEN3 accumulation at papillae is specific for powdery mildew interactions, the incorporation into encasements can be observed also for other pathogens (Meyer et al. 2009). These observations might indicate distinct roles of this incorporation in pre- and post-invasive resistance. Post-invasive resistance is activated after successful penetration by (non-)adapted powdery mildews and activates EDS1-PAD4/ SAG101 resulting in SA-signalling and HR (Lipka et al. 2005; Stein et al. 2006). The R gene RPW8.2 confers broad-spectrum resistance against powdery mildews (Xiao et al. 2001). RPW8.2 as well as its homologues (HR1-4) were shown to specifically label the *de novo* synthesized EHM of haustoria, while usual PM marker and encasement-localized defense-proteins including PEN1 failed to do so (Berkey et al. 2017). Further, the PEN1 EHC-targeting pathway is not connected or redundant for the RPW8.2 EHM-targeting pathway (Wang et al. 2009). Interestingly, HR4 was found to be hyperinduced in *pen3* mutants (Stein et al. 2006) and promotes NLR-resistosome formation (Li et al. 2020).

MLO genes provide plants with a broad-spectrum penetration resistance against powdery mildew fungi and were first described as negative modulators of PEN1, PEN2 and PEN3 (Consonni et al. 2006; Collins et al. 2003). Later, the observed similarities between the *mlo* resistance phenotypes and those observed for *pen* resistance resulted in the conclusion, that there could be a mechanistic overlap e.g. with *mlo* mutations potentiating the *pen* gene based pre-invasion resistance response making it also sufficient against adapted pathogens (Kuhn et al. 2017). Comparative microarray-based transcriptome analysis and results from infection experiments using adapted powdery mildews revealed that PEN1 as well as PEN2/3-dependent defense pathways are not important for powdery mildew resistance in the *mlo2 mlo6 mlo12* triple mutant (Kuhn et al. 2017). However, *mlo2*-based resistance was shown to depend on the PEN1-SNAP33 trafficking pathway (Consonni et al. 2006). Heterotrimeric G protein signal transducers XLG2 and AGB1 are also known to play a role in pre-invasive resistance against powdery mildews (Humphry et al. 2010; Takahashi et al. 2018). AGB1 was found to act independently from SOBIR1 in pre- and post-penetration resistance of *Arabidopsis* against the non-host *Pyricularia oryzae*, which is a rice pathogen, in the absence of PEN2 (Takahashi et al. 2018). The *pen2*-1 *xlg2*-1 and *pen2*-1 *xlg3*-1 double mutants revealed that XLG2 is a positive regulator of pre-invasive, in this context, while *xlg3* had no additive effect (Takahashi et al. 2018). MLOs were earlier suggested to act as potential GPCRs, which would positively regulate heterotrimeric G protein signalling (Consonni et al. 2006). However, MLO2 was found to not act as positive regulator of GPA1-AGB1 (Lorek et al. 2013). Similarly, MLO4 and MLO11 were not found to act as GPCRs of GPA1-AGB1 (Chen et al. 2009). Interestingly, XLG2 was included in a forward genetic screen to identify suppressors of *mlo2 mlo6*

mlo12 resistance against *G. orontii* and did not suppress the resistance phenotype (Wu 2018). XLG3 was not tested in this context, though a redundant function in this context could be possible. MLO2 was found to act together with AGG1 in pathogen-independent callose deposition. Further, a MLO2-independent differential function of AGG1/2 was observed against adapted *G. orontii* and non-adapted *E. pisi* pathogens (Lorek et al. 2013). Interestingly, potential non-canonical Gβ proteins were recently discovered, DRW1 or DRW2, which were found to play a negative role in plant immunity and interact with GPA1 and AGG1/2 (Miller et al. 2019). The involvement of these non-canonical Gβ proteins in this AGG1/2-dependent function remains speculative.

During powdery mildew interactions, XLG2 was found to be highly co-expressed with cadmium-induced heavy metal stress-responsive genes including PCS1 (Weber 2005) which was later further described as PEN4 resistance gene (Kühnlenz et al. 2015). XLG2 is co-regulated with PEN1, PEN2, PEN3, PEN4, AGB1, CERK1, a AGB1-interacting NRD1-like protein and other defense related genes (Table 5) during NHR (Pajonk 2007; Humphry et al. 2010; Yu et al. 2018). In their study, Humphry et al. distinguished between three independent NHR pathways which were found to share many components but not all: MLO-PEN1-SNAP33, PEN1-SNAP33-VAMP722 and PEN2/ PEN3. XLG2 was co-expressed in all three pathways (Table 5). They also identified over-represented cis-acting elements in 5' untranslated regions (UTRs), 9 of 10 cis element types in XLG2, which indicate stress responsiveness. Importantly, XLG2 was found to play a significant role in entry-control against the non-adapted powdery mildew *E. pisi* (Humphry et al. 2010).

1.5 Plant cell death signalling pathways

1.5.1 Types of programmed cell death

HR is a highly coordinated defense reaction against invading biotrophic or hemibiotrophic pathogens (Jones and Dangl 2006) which need to feed from living plant tissue their whole life cycle or at early stages and can, therefore, be stopped from further growth via the death of an invaded cell (Jones and Dangl 2006; Kuhn et al. 2016). Typical indicators of HR are over-expression of PR1 and PR2 marker genes, SA over-accumulation and increased resistance against these types of pathogens as SA is a main regulator of programmed cell death (PCD) (Alvarez 2000). In contrast, higher susceptibility against necrotrophic pathogens can be observed for so called lesion-mimic mutants (LMM) which are found to have a stronger HR response (Bruggeman et al. 2015). Necrotrophic pathogens have developed a way to trigger unrestrained programmed cell death (PCD) which goes beyond invaded cells as these pathogens can feed from dead plant material (Glazebrook 2005). Autophagy was shown to play a central role in prevention of runaway cell death affecting surrounding cells (Hofius et al. 2011; Liu et al. 2005) and fungal effectors are known to sometimes hijack this system in order to feed from the

spreading cell death event (Leary et al. 2018). SINCs were found to play an important role in cell survival during stress signalling and contribute to systemic acquired resistance and autophagy processes (Zavaliev et al. 2020). Pathogen-triggered variants of PCD stand in contrast to developmentally controlled PCD where differentiation into structural or storage elements depends on the highly controlled death of certain cells within the multicellular organism (Huysmans et al. 2017; van Durme and Nowack 2016). Common features of dPCD include calcium influx, accumulation of ROS and cytoplasmic acidification which results in slow controlled cell death and subsequent corpse clearance for use of remaining structural elements for e.g. water transport (Minina et al. 2014; van Durme and Nowack 2016). While dPCD and pPCD are clearly distinct on the gene regulatory level and molecular outcome there are also similarities such as the calcium control and shared signalling components (Huysmans et al. 2017). Interestingly, G proteins are known as positive regulators of cell death (Takahashi et al. 2018; Liu et al. 2013) with dual roles in development (Ding et al. 2008; Maruta et al. 2019) as well as defense (Liang et al. 2018; Xue et al. 2020; Zhong et al. 2019). Canonical heterotrimeric G proteins showed SA-independent involvement in PCD (Trusov et al. 2009; Liu et al. 2013) while non-canonical *xlg2* was found to show slightly reduced PR1 and PR2 expression levels (Zhu et al. 2009). The SA-signalling potentiation involves parallel acting pathways such as EDS1-PAD4 and MAPKs and is essentially mediated by defense gene expression e.g. via the TF MYB30 (Cui et al. 2017; Raffaele et al. 2006). The membrane localized accelerated cell death 6 (ACD6) is another regulator of SA-responsiveness and it was shown to influence callose deposition as well as abundance of RLKs including FLS2 and CERK1 (Tateda et al. 2015). Chloroplasts are also involved in cell death regulation and/ or execution as chloroplast-localized ACD2 was shown to translocate into mitochondria and inhibit PCD from there (Ambastha et al. 2015). SID2 is another chloroplast-derived protein which is important for SA-synthesis (Nawrath and Métraux 1999). Further, the MAPKs MPK3/6 are engaged in activating chloroplast-derived ROS which is important for induction of HR (Su et al. 2018). The xanthine dehydrogenase (XDH1) and RbohD/F produced ROS (e.g. H_2O_2) with subsequent HR response is triggered by RPW8.2 in haustorial invaded epidermal cells (Wang et al. 2009). Accumulation of the usually constitutively degraded RPW8.2 in the cytoplasm was suggested to result in chloroplast toxicity which again shows how components relevant for one or the other type of PCD are connected (Huang et al. 2019).

1.5.2 Lesion mimic mutants

Around 50 different lesion mimic mutants (LMM) are currently known and studied in order to understand PCD pathways (Bruggeman et al. 2015). Suppressors of such LMMs were mapped and reveal the molecular mechanisms behind such strong phenotypes. LMMs and their suppressors revealed a large variety of involved cellular compartments including chloroplasts, mitochondria and

membrane trafficking with components such as chloroplast-localized (ACD1/2), fatty acid synthesis (FAHs) and vesicular trafficking syntaxins (SYP121/ 122) as well as several RLK mutants (CERK1, BAK1, BIR1) (Bruggeman et al. 2015). This chapter will focus on known RLK LMMs as summarized in Table 1. One well-known example for a RLK with loss-of-function mutation is the knock-out mutant *bir1*-1 which shows spontaneous cell death, constitutive activation of defense responses as well as extremely stunted growth (Gao et al. 2009). Suppressors *o*f *bir1*-1 (*sobir*) partially recover the dwarf phenotype and show reduced PR1 and PR2 expression levels (Gao et al. 2009; Zhang et al. 2015). Absence of BIR1 was shown to result in activation of BAK1 which then constitutively activates defense signalling and revealed BIR1 as major inhibitor of PTI (Gao et al. 2009; van Wersch et al. 2016; Liu et al. 2016). ER-quality control (*erdj3b*-1) was shown to be important for the abundance of SOBIR1, which is needed as positive regulator of cell death in *bir1*-1 (Oliveira et al. 2016). Mutations in XLG2 (*xlg2*-1) and AGB1 (*agb1*-4) were found to suppress the *bir1*-1 LMM phenotype (Maruta et al. 2015) indicating that heterotrimeric G proteins are involved in cell death signalling via this pathway. Recently, SOBIR1 together with RLPs was found to activate EDS1-PAD4 via ADR1, which constitutively binds SOBIR1 (Pruitt et al. 2020). Thus, the SOBIR1-RLP complex can directly activate HR via helper NLRs (Pruitt et al. 2020). While BAK1 is known as positive regulator of immune signalling, it was found to inhibit cell death with redundant involvement of BKK1, the closest homologue (Jeong et al. 2010; He et al. 2007; Oliveira et al. 2016; Kemmerling et al. 2007). BAK1 allelic mutations differ in their outcome on distinct pathways such as brassinosteroid signalling, plant immunity and cell death. *bak1*-3 and *bak1*-4 null mutants show a necrotrophic pathogen-inducible spreading lesion phenotype and early senescence (Kemmerling et al. 2007; Schwessinger et al. 2011) while *bak1*-5 was found to cause reduced MTI due to defects in the kinase domain (Schwessinger et al. 2011). The BAK1 knock-out also results in sensitization of MAMP signalling e.g. via PEPR1/2 RLKs which sense propep peptides in the apoplast (Yamada et al. 2016). The double mutant *bak1*-4 *bkk1* accumulates SA and shows a phenotype reminiscent of constitutive defense signalling (autoimmunity) resulting in stunted growth and enhanced cell death (He et al. 2007). Further genetic analysis revealed the importance of nucleocytoplasmic trafficking via nucleoporin component (*sbb1*-1) and defense-related mRNA export via a DEAD-box RNA helicase (*drh1*) as well as SA dependence of the cell death phenotype (Du et al. 2016). Further, N-glycosylations (*stt3a*-2, *alg3*, *alg12*, *uggt*) and ER-quality control (*erdj3b*-1 and *sdf2*-2) are involved *bak1 bkk1*-mediated cell death, while an unfolded protein response (UPR) and N-glycan modifications in the Golgi were ruled out (Oliveira et al. 2016; Du et al. 2016). Interestingly, 22 of 44 *Arabidopsis* CRK genes were found to be upregulated in *bak1*-4 *bkk1*-1 (Oliveira et al. 2016). The authors claim to provide evidence that CRK4 serves as a client protein for STT3a-dependent N-glycosylation and ER-quality control in *bak1*-4 *bkk1*-1, thus, that N-glycosylation of CRK4 and potentially other redundantly acting CRKs is important for cell death induction.

Table 1: Examples for LMM mutations and their suppressors. *gain of function, ** loss of function, [ ] results were obtained using RNA-silencing

LMM	Required for cell death	Not required for cell death	Mechanism	Reference
bir1-1 **	*bak1*-4, *bak1*-5, *sobir1*-12, *sobir1*-14, *sobir2-1 (agb1-4)*, *xlg2*-1, *stt3a*-2, *sobir6*-1 (*uggt*), *pad4*	[*crt3*-1, *erdj3b*-1, *sdf2*-2, *cgl1*-3, *hgl1*-1, *fucTa fucTb xylT* triple]	BAK1 and SOBIR1 are inhibited by BIR1 and absence of BIR1 results in constitutive defense signalling, SOBIR1 directly activates ADR1-NLR, SA dependent cell death	(Gao et al. 2009; Oliveira et al. 2016; Zhang et al. 2015; Pruitt et al. 2020; Maruta et al. 2015)
bak1-3/4 bkk1-1 **	*sbb1*-1, *stt3a*-2, *alg3*, *alg12*, *uggt*, *pepr1 pepr2*, *adr1* triple, *seh1, erdj3b*-1, *sdf2*-2 [*sid2*]	*sobir1*, [*pad4*, *ndr1*, *crt3*-1, *rsw3*-1, *cgl1*-3, *hgl1*-1, *fucTa fucTb xylT* triple, *ire1a ire1b*, *bzip28 bzip60*]	ADR1s likely guard BAK1 (CNLs?), constitutive defense signalling, SA-dependent cell death	(He et al. 2007; Du et al. 2016; Oliveira et al. 2016; Wu et al. 2020)
bak1-4 *bik1*-1 **	pad4		(TNLs?), constitutive defense signalling, SA-dependent cell death	(Liu et al. 2017)
cerk1-4/5 *	*xlg2*-1, *xlg2*-2 (noce1-4), *xlg2*-3 (noce4-6); *agb1*-2; *agg1*-1c; *crk7, crk43, pad4, eds1, sid2, mos7*	*bak1*-4, *bak1*-5, *sobir1*-12, *sobir1*-14, *gpa1*-3, *xlg1*-2, *xlg3*-4, *rbohd, rbohf*	Unknown (NLRs?), pathogen-induced lesions & early senescence, SA-dependent cell death	(Petutschnig et al. 2014; Stolze, unpublished; Meusel 2016; Trippel, 2020)

This cell death pathway was also found to be SOBIR1-independent (Oliveira et al. 2016). Most importantly, the *bak1*-5 *bkk1*-1 double mutant did not cause autoimmunity indicating that only absence of BAK1 and BKK1 induces cell death (Wu et al. 2020). Several groups of helper NLR-proteins were found to be upregulated in *bak1*-4 *bkk1*-1 and knock-out of ADR1s resulted in remarkably reduced cell death (Wu et al. 2020). The *adr1* triple mutant-dependent reduction of cell death was more effective in comparison to the *pepr1 pepr2*-dependent reduction (Wu et al. 2020). Accordingly, the authors of this finding suggest that BAK1, as a key component in many known immune signalling pathways, is likely guarded by NLRs. Since direct activation of ADR1s was found in dependence to SOBIR1 (Pruitt et al. 2020) while SOBIR1 is not involved in *bak1 bkk1* cell death, the involvement of CNLs remains to be investigated to further evaluate the guardee hypothesis (Wu et al. 2020). The *bik1* mutant, which is a RLCK that crosstalks to many RLKs in MTI and, therefore, is included in this overview, was found to have elevated PR1 and PAD4 expression levels and an aphid-inducible cell death phenotype (Lei et al. 2014). Analysis of this interaction revealed that BIK1 suppresses PAD4 and senescence gene expression and that the observed cell death depends on PAD4. The double mutant *bak1*-4 *bik1*-1 also results in constitutive defense signalling and the authors suggest an independent mechanism compared to *bak1*-4 *bkk1*-1 (Liu et al. 2017) perhaps involving TNLs. Presence of BKK1 in this autoimmunity phenotype would act redundantly to BAK1 as guardee, as suggested by Wu et al.,

and inactivate this cell death pathway. Interestingly, CRKs were found to be upregulated in both autoimmunity mutants *bak1 bkk1* as well as *bak1 bik1* (Liu et al. 2017; Oliveira et al. 2016) indicating that CRKs likely commonly act downstream of RLKs in cell death responses. Interestingly and in contrast to the autoimmunity phenotype, BAK1 over-expression-based cell death depends on SOBIR1 but not BIK1 (Zhou et al. 2019). BIK1 was found to serve as inhibitor of RLP-SOBIR1-induced defense signalling, while positively regulating RLK-mediated defenses (Wan et al. 2019b). Heterotrimeric G proteins, more precisely the XLG2-AGB1-AGG1/2 trimer, were found to positively regulate both defense signalling pathways (Wan et al. 2019b).

In contrast to the loss-of-function LMMs with constitutive autoimmunity signalling, *cerk1*-4 (L124F) was identified as gain-of-function mutation that causes an enhanced cell death and resistance phenotype upon infection with powdery mildews and develops early senescence (Petutschnig et al. 2014). CERK1 undergoes constitutive recycling alongside with constitutive ectodomain shedding (Erwig et al. 2017; Petutschnig et al. 2014). More RLKs were identified to be likely subject to ectodomain shedding including LYK5 (Meusel 2016; Petutschnig et al. 2014). The process of ectodomain shedding is not well characterized in plants but commonly described in animals (Lichtenthaler et al. 2018). The soluble *cerk1*-4 ectodomain is undetectable and, thus, potentially affects apoplastic stability after shedding (Petutschnig et al. 2014). CERK1 ectodomain shedding and the *cerk1*-4 phenotype are uncoupled from chitin-signalling (Petutschnig et al. 2014; Meusel 2016). In contrast, the CERK1 overexpression-dependent cell death depends on kinase activity (Petutschnig, unpublished). Interestingly, BAK1 and CERK1 share ectodomain shedding as well as over-expression induced cell death phenotypes (Domínguez-Ferreras et al. 2015; Yamaguchi et al. 2017; Kim et al. 2017; Petutschnig et al. 2014). Abolishing proteolytic cleavage of BAK1 through mutation of a highly conserved position (D287) was accompanied by multiple effects on almost all aspects of BAK1-dependent signalling (Zhou et al. 2019). Accordingly, ectodomain and cytosolic shedding products likely fulfil different functions which agrees to the described uncoupling of CERK1/-4 ectodomain shedding and chitin signalling (Petutschnig et al. 2014; Meusel 2016). Proteases in general could be involved in proteolytic cleavage of RLKs and there are ~800 predicted proteases in *Arabidopsis* (Hou et al. 2018). Importantly, BAK1 was found to be cleaved by a highly conserved Ca^{2+}-dependent protease (Zhou et al. 2019). Similarly to the described autoimmunity mutants involving *bak1* (Liu et al. 2017; Oliveira et al. 2016) in *cerk1*-4 (upon infection) upregulation of CRK genes was observed (Petutschnig, unpublished; Trippel, 2020). The *cerk1*-4 gain-of-function mutation is distinct from loss-of-function autoimmunity mutants as SA over-accumulation and the cell death phenotype is inducible via pathogen inoculation and not constitutive (Petutschnig et al. 2014). Several suppressors of this phenotype originally named no *cerk1*-4 (noce) were identified including two *xlg2* mutant alleles and several mutations which affect essential components of the SA-pathway. One suppressor mutation *xlg2*-2 results in a premature stop codon

(Stolze, unpublished) while *xlg2*-3 harbors a single amino-acid exchange (E293K) within a highly conserved region (Meusel 2016). *xlg2*-1, a T-DNA insertion line, was crossed with *cerk1*-4 and similarly to *xlg2*-2 and *xlg2*-3 resulted in suppression of the exaggerated cell death phenotype of *cerk1*-4 (Meusel 2016). Two other XLG and canonical G protein mutants known to form a heterotrimeric complex (Maruta et al. 2015; Chakravorty et al. 2015) were crossed with *cerk1*-4. Neither *gpa1* nor *xlg1* or *xlg3* suppressed *cerk1*-4, while *agb1* and *agg1* showed partial suppression of *cerk1*-4 (Petutschnig, unpublished). This indicates that XLG2 is specifically important for *cerk1*-4 cell death signalling and is supported by AGB1 and AGG1, while AGG2 could have a partially redundant function. Further, the nuclear pore complex component mutant *mos7* was shown to suppress development of the *cerk1*-4 deregulated cell death phenotype (Wiermer et al. 2010; Genenncher et al. 2017). MOS7 is essential for SA-signalling (Wiermer et al. 2010; Heidrich et al. 2011; Lapin et al. 2019) and the *cerk1*-4 phenotype depends on SA-signalling (Petutschnig et al. 2014) which explains the connection. Most recently, *crk7* and *crk43* were identified as suppressors of *cerk1*-4 (Trippel 2020). In addition, *bir1*-1 suppressors *bak1*-4/5 as well as *sobir1*-12/14 were tested regarding *cerk1*-4 involvement. Neither *bak1*-4/5, nor *sobir1*-12/14 suppressed *cerk1*-4 and, therefore, *cerk1*-4 cell death signalling underlies a SOBIR1/ BAK1-independent mechanism (Petutschnig, unpublished).

1.6 Aims of this work

This work aimed to characterize the role of XLG2 in *cerk1*-4 cell death signalling. The pathogen-inducible cell death phenotype of *cerk1*-4 renders this mutant resistant to compatible powdery mildews (Petutschnig et al. 2014). *cerk1*-4 was EMS mutagenized and a forward genetic screen was started. Several suppressors of *cerk1*-4 cell death were identified including essential components of the conserved SA-signalling pathway and two suppressor alleles of XLG2 (Stolze, unpublished; Meusel, 2016).

In interest of analyzing the subcellular localization of XLG2, Venus-fusion XLG2/ xlg2 variants with potentially changed localization were generated and analysed via CLSM transiently in *N. benthamiana* as well as in stably transformed *Arabidopsis* plants, with focus on plasma membrane and nuclear localization. Unchallenged as well as *Ec* inoculated *xlg2*-2 and *cerk1*-4 *xlg2*-2 were analysed to characterize the localization of XLG2 in the absence/ presence of a pathogen. Functionality of Venus-XLG2/ xlg2 variants regarding *cerk1*-4 cell death signalling was investigated via phenotypic complementation studies to find out whether plasma membrane and/ or nuclear localization of XLG2 support cell death signalling. In order to gain more information about the relevance of the XLG2 Gα-like domain for *cerk1*-4 cell death signalling and subcellular localization of XLG2, a potentially nucleotide-free (T476N) and potentially GTPase-dead (R673L) xlg2 mutant variant were generated and

characterized using CLSM and complementation studies. In the interest of testing the possibility that the XLG2 N-terminal cysteine-rich region is relevant for XLG2 localization and/ or *cerk1*-4 cell death signalling, cysteine to alanine exchange mutant variants were generated and analysed. XLG2 is known to form a heterotrimeric complex at the plasma membrane (Maruta et al. 2015; Chakravorty et al. 2015). Localization of XLG2 in the absence of the Gβγ-dimer was analysed via a transient approach using particle bombarded heterotrimeric G protein mutants. Further, XLG2 was previously linked to pre-/ post-invasive resistance against powdery mildews (Humphry et al. 2010). The role of XLG2 in post-invasive resistance was addressed, in this work, by analyzing the localization of XLG2 after *Ec* haustoria formation. Different XLG2 variants with changed localization were included in this approach.

2 Materials and Methods

2.1 Materials

2.1.1 Chemicals

Table 2: Companies from which chemicals and other materials were ordered in this study.

Company	Location
Agrisera AB	Vännäs, Sweden
Bio-Rad	Munich, Germany
ChromoTek GmbH	Planegg-Martinsried, Germany
Difco	Heidelberg, Germany
Duchefa	Haarlem, Netherlands
GE Healthcare	Munich, Germany
Intas	Göttingen, Germany
Macherey Nagel	Düren, Germany
Merck	Darmstadt, Germany
New England Labs (NEB)	Frankfurt am Main, Germany
Qiagen	Hilden, Germany
Roche	Mannheim, Germany
Roth	Karlsruhe, Germany
Serva	Heidelberg, Germany
Sigma-Aldrich	Deisenhofen, Germany
Thermo Fisher Scientific™ (Invitrogen)	Waltham, USA
VWR™	Darmstadt, Germany

2.1.2 Buffers

Buffers used in this study (Table 3) were either filtered (pore size 0,2µm) or autoclaved at 121°C for 20min for sterilization before use.

Table 3: Buffers used in this study

Buffers used for nucleic acid methods:	
genomic DNA extraction buffer	
Tris-HCl (pH 7.5)	0,2M
NaCl	1,25M
EDTA	0,025mM
SDS	0.5%
P1 buffer (stored at 4°C)	
Tris-HCl (pH 8.0)	50mM
EDTA (pH 8.0)	10mM
RNase A (DNase free)	100µg/ml
P2 buffer	
NaOH	200mM
SDS	1% (w/v)
P3 buffer	
Potassium acetate	3M
Acetic acid	2M
Homemade *Taq*-buffer (10x, aliquots stored at -20°C)	
TRIS	100mM
KCl	500mM
$MgCl_2x6H_2O$	15mM
Triton-x-100	1%
Adjust to pH 9.0	
DNA loading dye (6x)	
Sucrose	4g
EDTA (0.5M)	2ml
Bromophenol blue	25mg
Add H_2O (ultrapure) to 10ml	
TAE (50x)	
Tris base	2M
Glacial acetic acid	57,1M
EDTA (0.5 M, pH 8.0)	100M
TE buffer	
Tris-HCl (pH 8.0)	10mM
EDTA	1mM

Buffers used for protein methods:

CERK1 extraction buffer (50ml aliquots stored at -20°C)

Sucrose	250mM
HEPES-KOH (pH 7.5)	100mM
Glycerol	5% (v/v)
$Na_4P_2O_7$	50mM
Na_2MoO_4	1mM
NaF	25mM
EDTA	10mM
DTT	1mM
Triton X-100	0.5 % (v/v)

PIC was added prior to use (1:100 diluted)

Protease inhibitor cocktail (PIC, 100x, 2ml aliquots stored at -20°C)

4-(2-aminoethyl)benzenesulfonyl fluoride hydrochloride (AEBSF)	1g
Bestatin hydrochloride	5mg
Pepstatin A	10 mg
Leupeptin hemisulfate	100mg
E-64 (trans-epoxysuccinyl-L-leucylamido-(4-guanidino)butane)	10mg
Phenanthroline (1, 10-phenanthroline monohydrate)	10g

A small amount of DMSO was used to dissolve all components separately. After combining all, the solution was filled up to a total volume of 200ml and 2ml aliquots were store at -20°C.

SDS sample buffer (4x)

Tris-HCl (pH 6.8)	200mM
DTT	400mM
SDS	8%
Glycerol	40%
Bromophenol blue	0.1%

Stacking gel buffer

Tris-HCl (pH 6.8)	150mM
SDS	0.12%

Resolving gel buffer (8%)

Tris-HCl (pH 8.8)	525mM
SDS	0.14%

SDS running buffer (10x)

Tris	30.28g/l
Glycine	144.13g/l
SDS	10g/l

Transfer buffer (20x)	
Tris	1M
Boric acid	1M
Adjust pH to 8.3	
TBS-T (20x)	
NaCl	3M
Tris-HCl (pH 8.0)	200mM
Tween-20	1%
Alkaline phosphatase (AP) buffer	
Tris (pH 9.5)	100mM
NaCl	100mM
$MgCl_2$	50mM
Coomassie staining solution	
EtOH	300ml
H_2O_{dd}	300ml
Acetic acid	100ml
Coomassie Brilliant Blue R250	0.05% (w/v)
Coomassie destaining solution	
EtOH	300ml
H_2O_{dd}	300ml
Acetic acid	100ml
Other buffers used in this study:	
Agrobacterium infiltration medium (pH 5.4)	
$MgCl_2$	10mM
MES	10mM
Acetosyringone	150µM

2.1.3 Media

For sterilization, media (Table 4) were autoclaved at 121°C for 20min. Antibiotics were added after cooling (<60°C) according to the resistance provided by the selected vector. Media were stored at RT (with antibiotics at 4°C).

Table 4: Media used in this study

Bacterial growth media:	
Lysogeny broth/ Luria-Bertani broth (LB) medium (pH 7.0)	
Tryptone	10.0g/l
Yeast extract	5.0g/l
NaCl	10.0g/l

Double yeast tryptone (DYT) medium (pH 7.0)

Tryptone	16.0g/l
Yeast extract	10.0g/l
NaCl	10.0g/l

For solid medium

Agar (bacterial grade)	1.5 % (w/v)

2.1.4 Plasmids used in this study

Table 5: Constructs used in this study

Designation	Relevant characteristics	Reference
pUBQ10-mKate2-Lti6b-T35S (pHG122)	Resistance for Carbenicillin, expression of mKate2-LTI6b-Tnos under the 35S promoter, plant membrane marker	Hassan Ghareeb
p35S-mTQ-N7 (pHG141)	Resistance for Carbenicillin, expression of mturqoise-7-Tnos under the 35S promoter, plant nuclear marker	Hassan Ghareeb
pGreenII-0229	Resistances for Kanamycin (bacteria) and Basta^{R} (plants) binary vector (A. tumefaciens mediated Arabidopsis transformation)	(Hellens et al. 2000)
pGreenII-0229-pXLG2-NLS-Venus-XLG2	Expression of XLG2 (WT) gDNA under the native promoter with N-terminal Venus-NLS fusion	Elena Petutschnig, Christopher Meusel
pGreenII-0229-pXLG2-nls-Venus-XLG2	Expression of XLG2 (WT) gDNA under the native promoter with N-terminal Venus-nls fusion	Elena Petutschnig, Christopher Meusel
pGreenII-0229-pXLG2-NES-Venus-XLG2	Expression of XLG2 (WT) gDNA under the native promoter with N-terminal Venus-NES fusion	Elena Petutschnig, Christopher Meusel
pGreenII-0229-pXLG2-nes-Venus-XLG2	Expression of XLG2 (WT) gDNA under the native promoter with N-terminal Venus-nes fusion	Elena Petutschnig, Christopher Meusel
pGreenII-0229-pXLG2-Venus-XLG2 (WT)	Expression of XLG2 (WT) gDNA under the native promoter with N-terminal Venus-fusion	Elena Petutschnig, Christopher Meusel

pGreenII-0229-pXLG2-Venus-xlg2 (R673L)	Expression of xlg2 (R673L) under the native promoter with N-terminal Venus-fusion	Elena Petutschnig, Christopher Meusel
pGreenII-0229-pXLG2-Venus-xlg2 (T476N)	Expression of xlg2 (T476N) under the native promoter with N-terminal Venus-fusion	Elena Petutschnig, Christopher Meusel
pGreenII-0229-pXLG2-Venus-xlg2 (E293K)	Expression of xlg2 (E293K) under the native promoter with N-terminal Venus-fusion	Elena Petutschnig, Christopher Meusel
pGreenII-0229-pXLG2-Venus-xlg2 (nls204i)	Expression of xlg2 (nls204i) under the native promoter with N-terminal Venus-fusion	This work
pGreenII-0229-pXLG2-Venus-xlg2 (NLS204S)	Expression of xlg2 (NLS204S) under the native promoter with N-terminal Venus-fusion	This work
pGreenII-0229-pXLG2-Venus-xlg2 (nlsKR-AA)	Expression of xlg2 (nlsKR-AA) under the native promoter with N-terminal Venus-fusion	This work
pGreenII-0229-pXLG2-Venus-xlg2 (nlsKR-AA+E293K)	Expression of xlg2 (nlsKR-AA+E293K) under the native promoter with N-terminal Venus-fusion	This work
pGreenII-0229-pXLG2-Venus-xlg2 (nls426)	Expression of xlg2 (nls426) under the native promoter with N-terminal Venus-fusion	This work
pGreenII-0229-pXLG2-Venus-xlg2 (nls387)	Expression of xlg2 (nls387) under the native promoter with N-terminal Venus-fusion	This work
pGreenII-0229-pXLG2-Venus-XLG2-NES	Expression of XLG2 (WT) gDNA under the native promoter with N-terminal Venus-fusion and C-terminal NES-fusion	This work
pGreenII-0229-pXLG2-Venus-XLG2-nes	Expression of XLG2 (WT) gDNA under the native promoter with N-terminal Venus-fusion and C-terminal nes-fusion	This work
pGreenII-0229-pXLG2-Venus-XLG2-NLS	Expression of XLG2 (WT) gDNA under the native promoter with N-terminal Venus-fusion and C-terminal NLS-fusion	This work
pGreenII-0229-pXLG2-Venus-XLG2-nls	Expression of XLG2 (WT) gDNA under the native promoter with N-terminal Venus-fusion and C-terminal nls-fusion	This work

pGreenII-0229-pXLG2-Venus-xlg2 (C214/217A)	Expression of xlg2 (C214/217A) under the native promoter with N-terminal Venus-fusion	This work
pGreenII-0229-pXLG2-Venus-xlg2 (C254/257A)	Expression of xlg2 (C254/257A) under the native promoter with N-terminal Venus-fusion	This work
pGreenII-0229-pXLG2-Venus-xlg2 (C229/232/237/240A)	Expression of xlg2 (C229/232/237/240A) under the native promoter with N-terminal Venus-fusion	This work
pGreenII-0229-pXLG2-Venus-xlg2 (C237/240A)	Expression of xlg2 (C237/240A) under the native promoter with N-terminal Venus-fusion	This work
pGreenII-0229-pXLG2-Venus-xlg2 (C229/232A)	Expression of xlg2 (C229/232A) under the native promoter with N-terminal Venus-fusion	This work
pGreenII-0229-pXLG2-Venus-xlg2 (C296A)	Expression of xlg2 (C296A) under the native promoter with N-terminal Venus-fusion	This work
pGreenII-0229-pXLG2-Venus-xlg2 (C435A)	Expression of xlg2 (C435A) under the native promoter with N-terminal Venus-fusion	This work

2.1.5 Oligonucleotides

Oligonucleotides used in this study (Table 6) were taken from -20°C stocks (designed by UL, Ulrike Lipka; EP, Elena Petutschnig; CM, Christopher Meusel; MW, Marcel Wiermer; MS, Marnie Stolze; JE, Jan Erwig, JF/JA, Julia Anders) or ordered from Invitrogen (Thermo Fisher). Lyophilized oligonucleotides were diluted to stock-concentrations of 100µM. A working solution of 10µM was prepared as aliquots for standard usage and stored at -20°C.

Table 6: Oligonucleotides used in this study

Primer	Sequence 5' to 3'	Use
Oligonucleotides for sequencing		
UL154_for	TCTTCTTCCCCACAGAGCAACGACG	Genotyping of cerk1-4
UL166_rev	TTCCAGGCACATAAACGATTCC	
MS227_for	GCTGCAACGCATAGAGCTGAAAG	Genotyping of xlg2-2
MS226_rev	GGCGCTTGAGCATTCTTGAACAC	

JA74_upstream 5'UTR_for	GGAAGTGGCGCGTGGAGTTCACGCAATG	Genotyping transgenic xlg2-2 expressing XLG2 gDNA
CM74_rev	CCAATAGTGTCCGGGTTTTAGCTTCTTGG	
Oligonucleotides for mutagenesis		
JF7_nls426_for	ttatgcgctgtgttaTCTCTGCCAGTTCCTCCG	Site-directed mutagenesis
JF8_nls426_rev	taattttgttcccgcCTGTAAAAATAATATCCTTCGTTGTCTTTAG	
JF27_nes387_for	gggaggcaagGTTCTTTTGCTTTTCACCTTTG	Site-directed mutagenesis
JF28_nes387_rev	gtaccctctggCTTGGTTATTTCCCGGCC	
JF13_nls204i_for	aggtgcagcaggatcgTGTTACCGGTGCCAGTTG	Site-directed mutagenesis
JF29_nls204i_rev	gccgcttcagctgcATGCGTTGCAGCTATACTTTCTC	
JF23b_NLS204S_for	gaaaaagAAAAGAGGATCGTGTTACCGGTGCCAG	Site-directed mutagenesis
JF24_NLS204S_rev	cttctcctTCTATGCGTTGCAGCTATAC	
JF25_nlsKR-AA_for	cccatctCACGGATTCTGAACTTCG	Site-directed mutagenesis
JF26_nlsKR-AA_rev	ctgcgagcATTCTTGAACACTTTCCGAG	
JF18_introNotI_for	GCATGAAGGGATCCACTAGTTCTAGAGTCCGCAA	Introduce NotI site for C-terminal fusions
JF17_introNotI_rev	TGCGGCCGCAGAGGACGAGCTGGCCTCTATG	
JF19_C_NLS_for	GGCCCCTAAGAAGAAGAGAAAGGTTGGAGGATGAG	C-terminal fusion
JF20_C_NLS_rev	GATCCTCATCCTCCAACCTTTCTCTTCTTCTTAGG	
JF21_C_NES_for	GGCCCTCCAATTACCACCTTTGGAAAGACTAACACTGTGAG	
JF22_C_NES_rev	GATCCTCACAGTGTTAGTCTTTCCAAAGGTGGTAATTGGAG	
JF41_C214/217A_for	cgggccCAGTTGGGGAACCGGTTT	Site-directed mutagenesis
JF42_C214/217A_rev	gtaagcCGATCCTCTTTTACCTTTCCTTTC	
JF45_C229_232A_for	gtcgccGATGCCAAATACTGTTTC	Site-directed mutagenesis
JF46_C229_232A_rev	aatagcGACTTCCTTCTCAGTAAAC	
JF47_C237_240A_for	aacgctGTGCGCAGAGCCATGGGT	Site-directed mutagenesis
JF48_C237_240A_rev	gaaagcGTATTTGGCATCGCAGACAATACAG	
JF49_C229_232_237_240A_for	aaatacgctttcaacgctGTGCGCAGAGCCATGGGT	Site-directed mutagenesis
JF50_C229_232_237_240A_rev	ggcatcggcgacaatagcGACTTCCTTCTCAGTAAACCGGTTC	
JF51_C254_257A_for	gctgccATTGGTTATAGGATTGATGAGTC	Site-directed mutagenesis
JF52_C254_257A_rev	ttgagcCTTTCTTCCTTCGGGCATC	
JF53_C296A_for	CGAGATCACCgccAAGGCGAATC	

JF54_C296A_rev	GCATTCATGACTTGTCGAAG	Site-directed mutagenesis
JF55_C435A_for	AAAAATTGCTgccGCTGTGTTCTC	Site-directed mutagenesis
JF56_C435A_rev	GCTCTCTTCTGTAAAAATAATATC	
Oligonucleotides for control PCR		
EP219_for	CCTAACCCGCGTTGACGGCAAG	Control PCR (1243bp) for pGreen-pXLG2-Venus-NLS/nls/NES/nes-XLG2
MW81_rev	CTTGTACAGCTCGTCCATGC	
EP221_for	CCGGGAAATAACCAAGCCAGAG	Control PCR (643bp) for pGreen-pXLG2-Venus-XLG2/xlg2 (WT/T476N)
CM102_rev	CCAGATAGGTATAGAGATTTGTTTGG	
EP222_for	AGAGATGAGCAATGACCAGTCTTC	Control PCR (1347bp) for pGreen-pXLG2-Venus-xlg2 (R673L)
EP315_rev	AGAGGACGAGCTGGCCTCTATGC	
EP222_for	AGAGATGAGCAATGACCAGTCTTC	Control PCR (511bp) for pGreen-pXLG2-Venus-xlg2 (E293K)
CM74_rev	CCAATAGTGTCCGGGTTTTAGCTTCTTGG	
EP231_for	CACGGATTCTGAACTTCGACAAG	Control PCR (752bp) for pGreen-pXLG2-Venus-xlg2 (nes387)
EP233_rev	AACTGGCAGAGAGAACACAGC	
EP222_for	AGAGATGAGCAATGACCAGTCTTC	Control PCR (1852bp) for pGreen-pXLG2-Venus-XLG2-NLS/nls/NES/nes
CM30_rev	GACAGGTTTCCCGACTGGAAAG	
MS227_for	GCTGCAACGCATAGAGCTGAAAG	Control PCR (414bp) for pGreen-pXLG2-Venus-xlg2 (nlsKR-AA/ nlsKR-AA+E293K)
CM74_rev	CCAATAGTGTCCGGGTTTTAGCTTCTTGG	
EP220_for	AGTTTCGGATGTGGGACCTAGAG	Control PCR (338bp) for pGreen-pXLG2-Venus-xlg2 (nls204i/ NLS204S)
MS226_rev	GGCGCTTGAGCATTCTTGAACAC	
EP221_for	CCGGGAAATAACCAAGCCAGAG	Control PCR (475bp) for pGreen-pXLG2-Venus-xlg2 (nls204i/ NLS204S)
CM79_rev	TTGTTTGTAAATTGTATTGGCGCCACCTTT	
CM95_for	GTACCAACTCATCCGGCTAAATCCGCTAAGCCTTGGTGAAAACTGGAAATTGC	Control PCR (716bp) for pGreen-pXLG2-Venus-XLG2-NotI
EP218_rev	CTATAAGAACCCTAATTCCCTTATCTG	
Oligonucleotides for sequencing		
EP222_for	AGAGATGAGCAATGACCAGTCTTC	Sequencing of pGreen-pXLG2-Venus-XLG2-NES/nes/NLS/nls
CM30_rev	GACAGGTTTCCCGACTGGAAAG	

CM102_rev	CCAGATAGGTATAGAGATTTGTTTGG	Sequencing of pGreen-pXLG2-Venus-XLG2/xlg2 (WT/T476N)
EP156_rev	AGCTTGCCGTAGGTGGCATC	Sequencing of pGreen-pXLG2-Venus-NLS/nls/NES/nes-XLG2
EP315_rev	AGAGGACGAGCTGGCCTCTATGC	Sequencing of pGreen-pXLG2-Venus-xlg2 (R673L)
CM74_rev	CCAATAGTGTCCGGGTTTTAGCTTCTTGG	Sequencing of pGreen-pXLG2-Venus-xlg2 (E293K/ nls204i/ NLS204S, nlsKR-AA, nlsKR-AA+E293K)
EP233_rev	AACTGGCAGAGAGAACACAGC	Sequencing of pGreen-pXLG2-Venus-xlg2 (nes387)
EP218	CTATAAGAACCCTAATTCCCTTATCTG	Sequencing of pGreen-pXLG2-Venus-XLG2-NotI
CM79_rev	TTGTTTGTAAATTGTATTGGCGCCACCTTT	Sequencing of pGreen-pXLG2-Venus-xlg2 (nls426)
CM19_for	TTGAATCCTGTTGCCGGTCTTG	Sequencing pGreen-pXLG2-XLG2/xlg2 vector from left border to right border
EP166_rev	CCAACAGTTGCGCAGCCTGAATG	
EP23_rev	cttcaacgttgcggttctgtcagtt	
EP342_rev	ATAGGGTCAACACCTCCGGTTTTC	
JE23_for	ATGGTGAGCAAGGGCGAGGAGC	
CM94_for	ATGGCTGCAGTTATAAGAAAGTTATTACCTTTC	
EP231_for	CACGGATTCTGAACTTCGACAAG	
EP222_for	AGAGATGAGCAATGACCAGTCTTC	
EP136_rev	CGCTCATGTGTTGAGCATATAAG	
CM30_rev	GACAGGTTTCCCGACTGGAAAG	

2.1.6 Plant material

Table 7: *Arabidopsis* accessions used in this study

Accession	Abbreviation	Reference
Columbia-0	Col-0	J. Dangl, University of North Carolina, USA

Table 8: *Arabidopsis* mutants used in this study

Arabidopsis mutant	Accession	AGI identifier	T-DNA / mutagen	Reference
Col-3 *gl*1	Col-3	AT3G27920		Volker Lipka
cerk1-4	Col-3 *gl*1	AT3G21630	EMS	(Petutschnig et al. 2014)
xlg2-2 (noce1-4/ nole1-1)	Col-3 *gl*1	AT4G34390	EMS	Marnie Stolze
cerk1-4 *xlg2*-2	Col-3 *gl*1	AT3G21630, AT4G34390	EMS	Petutschnig et al. 2014, Marnie Stolze
agb1-2	Col-0	AT4G34460	T-DNA	(Ullah et al. 2003)
agg1-1 *agg2*-1	Col-0	AT3G63420, AT3G22942	T-DNA	(Trusov et al. 2007)
gpa1-3	Col-0	AT2G26300	T-DNA	(Jones et al. 2003)

Table 9: Transgenic *Arabidopsis* used in this study

Accession/ mutant	Construct	Resistance	Reference
Col-3 *gl*1, *xlg2*-2, *cerk1*-4 *xlg2*-2	*pGreenII-0229-pXLG2-Venus-XLG2 (WT)*	Basta^R	This work
Col-3 *gl*1, *xlg2*-2, *cerk1*-4 *xlg2*-2	*pGreenII-0229-pXLG2-Venus-xlg2 (E293K)*	Basta^R	This work
Col-3 *gl*1, *xlg2*-2, *cerk1*-4 *xlg2*-2	*pGreenII-0229-pXLG2-Venus-xlg2 (T476N)*	Basta^R	This work
Col-3 *gl*1, *xlg2*-2, *cerk1*-4 *xlg2*-2	*pGreenII-0229-pXLG2-Venus-xlg2 (R673L)*	Basta^R	This work
Col-3 *gl*1, *xlg2*-2, *cerk1*-4 *xlg2*-2	*pGreenII-0229-pXLG2-Venus-NES-XLG2*	Basta^R	This work
Col-3 *gl*1, *xlg2*-2, *cerk1*-4 *xlg2*-2	*pGreenII-0229-pXLG2-Venus-nes-XLG2*	Basta^R	This work
Col-3 *gl*1, *xlg2*-2, *cerk1*-4 *xlg2*-2	*pGreenII-0229-pXLG2-Venus-NLS-XLG2*	Basta^R	This work
Col-3 *gl*1, *xlg2*-2, *cerk1*-4 *xlg2*-2	*pGreenII-0229-pXLG2-Venus-nls-XLG2*	Basta^R	This work
Col-3 *gl*1, *xlg2*-2, *cerk1*-4 *xlg2*-2	*pGreenII-0229-pXLG2-Venus-XLG2-NES*	Basta^R	This work
Col-3 *gl*1, *xlg2*-2, *cerk1*-4 *xlg2*-2	*pGreenII-0229-pXLG2-Venus-XLG2-nes*	Basta^R	This work
Col-3 *gl*1, *xlg2*-2, *cerk1*-4 *xlg2*-2	*pGreenII-0229-pXLG2-Venus-XLG2-NLS*	Basta^R	This work
Col-3 *gl*1, *xlg2*-2, *cerk1*-4 *xlg2*-2	*pGreenII-0229-pXLG2-Venus-XLG2-nls*	Basta^R	This work
Col-3 *gl*1, *xlg2*-2, *cerk1*-4 *xlg2*-2	*pGreenII-0229-pXLG2-Venus-xlg2 (nes387)*	Basta^R	This work
Col-3 *gl*1, *xlg2*-2, *cerk1*-4 *xlg2*-2	*pGreenII-0229-pXLG2-Venus-xlg2 (nls426)*	Basta^R	This work
Col-3 *gl*1, *xlg2*-2, *cerk1*-4 *xlg2*-2	*pGreenII-0229-pXLG2-Venus-xlg2 (nlsKR-AA)*	Basta^R	This work
Col-3 *gl*1, *xlg2*-2, *cerk1*-4 *xlg2*-2	*pGreenII-0229-pXLG2-Venus-xlg2 (nlsKR-AA+E293K)*	Basta^R	This work
Col-3 *gl*1, *xlg2*-2, *cerk1*-4 *xlg2*-2	*pGreenII-0229-pXLG2-Venus-xlg2 (nls204i)*	Basta^R	This work

Col-3 *gl*1, *xlg2*-2, *cerk1*-4 *xlg2*-2	*pGreenII-0229-pXLG2-Venus-xlg2 (NLS204S)*	Basta^R	This work
Col-3 *gl*1, *xlg2*-2, *cerk1*-4 *xlg2*-2	*pGreenII-0229-pXLG2-Venus-xlg2 (C214/217A)*	Basta^R	This work
Col-3 *gl*1, *xlg2*-2, *cerk1*-4 *xlg2*-2	*pGreenII-0229-pXLG2-Venus-xlg2 (C229/232A)*	Basta^R	This work
Col-3 *gl*1, *xlg2*-2, *cerk1*-4 *xlg2*-2	*pGreenII-0229-pXLG2-Venus-xlg2 (237/240A)*	Basta^R	This work
Col-3 *gl*1, *xlg2*-2, *cerk1*-4 *xlg2*-2	*pGreenII-0229-pXLG2-Venus-xlg2 (C229/232/237/240A)*	Basta^R	This work
Col-3 *gl*1, *xlg2*-2, *cerk1*-4 *xlg2*-2	*pGreenII-0229-pXLG2-Venus-xlg2 (C254/257A)*	Basta^R	This work
Col-3 *gl*1, *xlg2*-2, *cerk1*-4 *xlg2*-2	*pGreenII-0229-pXLG2-Venus-xlg2 (C296A)*	Basta^R	This work
Col-3 *gl*1, *xlg2*-2, *cerk1*-4 *xlg2*-2	*pGreenII-0229-pXLG2-Venus-xlg2 (C435A)*	Basta^R	This work

2.1.7 Antibiotics

Standard antibiotics used for selection of bacterial vectors (Table 10) were prepared with the appropriate solvents. Aliquots were prepared and stored at -20°C. Antibiotics were added to liquid media or agarose containing media (<60°C) for plates according to the resistance provided by the selected vector.

Table 10: Antibiotics used in this study. All antibiotics were diluted 1:1000 to reach final working concentrations.

Antibiotic	Stock concentrations	Solvent
Ampicillin (Amp)	100mg/ml	Ultrapure water
Carbenicillin (Carb)	50mg/ml	Ultrapure water
Gentamycin (Gent)	15mg/ml	Ultrapure water
Kanamycin (Kan)	50mg/ml	Ultrapure water
Rifampicin (Rif)	20mg/ml	Methanol
Spectinomycin (Spec)	100mg/ml	Ultrapure water
Tetracyclin (Tet)	5mg/ml	Ethanol

2.1.8 Antibodies

Antibodies used in this work (Table 11) were aliquoted and stored at -80 °C. Aliquots in use were stored at 4 °C. Secondary antibodies conjugated to alkaline phosphatase (AP) were also stored at 4°C. Due to low expression levels of XLG2 under the native promoter, SuperSignal® Western Blot Enhancer (Thermo Fisher) was used for every XLG2 Western Blot. The primary antibody-containing pre-treatment solution was stored at 4°C and used repeatedly. The anti-XLG2 (α-XLG2) antibody was raised against the XLG2 N-terminal region to avoid co-detection of close homologues.

Table 11: Antibodies used in this study

Primary antibody	Source	Appropriate secondary antibody	Source
α-GFP (1:3000 dilution)	ChromoTek	Goat-α-rat AP-conjugate (1:5000 dilution)	Sigma-Aldrich
α-XLG2 (1:2000 dilution)	Agrisera	Goat-α-mouse AP-conjugate (1:5000 dilution)	Sigma-Aldrich

2.1.9 Enzymes

All enzymes used in this study were stored at -20°C. All enzymes were used according to the manufacturer's manual. RNAse A (Thermo Fisher) was added to the P1 buffer used for plasmid DNA extractions. Pepstatin A (Sigma-Aldrich) was added to the protease inhibitor cocktail, which was used for protein extractions. For genotyping and plasmid control PCRs homemade *Taq* polymerase was used, while for cloning the iProof™ High-Fidelity DNA Polymerase (Bio-Rad) was used. Fast digest restriction endonucleases (Thermo Fisher) were used for cloning, genotyping and plasmid control PCRs. T4 DNA ligase (Thermo Fisher) and shrimp alkaline phosphatase (SAP) (Thermo Fisher) were used for cloning.

2.1.10 Kits

Table 12: Kits used in this study

Application	Kit	Company
Site-directed mutagenesis	Q5 Site-directed Mutagenesis Kit	NEB
DNA purification from agarose gel	QIAquick Gel Extraction Kit	Qiagen

2.2 Methods

2.2.1 Nucleic acid methods

2.2.1.1 Isolation of plasmid DNA from bacteria

E. coli overnight cultures with 1,5 - 5ml (or *A. tumefaciens* with 200µl) were centrifuged at RT with maximum speed for 1min. The supernatant was discarded, and the pellet resuspended in 200µl P1 buffer. 200µl of P2 buffer were added and the solution mixed by carefully inverting (no pipette was used for mixing). The sample incubated for 3 - 5min at RT and the reaction was stopped by adding 200µl P3 buffer. The solution was then mixed by carefully inverting and centrifuged at RT with maximum speed for 5 - 10min. 500µl of clear supernatant was transferred into new Eppendorf tubes. For precipitation of DNA, 1ml 96% ethanol was added and the tube content mixed by inverting carefully before the sample was centrifuged at RT and maximum speed for 5min. The supernatant was discarded, and the pellet washed with 1ml 70% ethanol. After the final centrifugation at RT with

maximum speed for 1min the supernatant was discarded carefully using a pipette. Finally, the dried DNA pellet was resuspended in 30 - 50µl H_2O (ultrapure) and directly used or stored at -20°C.

2.2.1.2 Polymerase chain reaction

All PCRs were prepared on ice. The respective reagents were stored at -20°C and thoroughly thawed and shortly spined down before use as listed in Table 13. The same PCR master mix without template DNA was used as negative control. The standard PCR program is presented inTable 14.

Table 13: Homemade *Taq* polymerase PCR 25µl mix for genotyping and control PCR

Component	Concentration	Comment
10x Taq buffer (homemade)	2,5µl	
dNTPs (25µM)	0,5µl	
Primer for (10µM)	1µl	
Primer rev (10µM)	1µl	
Taq polymerase (homemade, 1kb/min)	0,1µl	added last to the master mix
H_2O (ultrapure)	up to 24µl	
Template DNA (undiluted)	1µl	added directly into the reaction tube

Table 14: Standard PCR program for homemade *Taq* polymerase mix

	Cycle step	Temp	Time
	Initial denaturation	95°C	5min
35 x Repeats	Denaturation	95°C	30s
	Annealing	55°C	30s
	Extension	72°C	1min/kb
	Final extension	72°C	10min
	Cooling	10°C	forever

2.2.1.3 Gel electrophoresis

The agarose gel was prepared using 1xTAE buffer with weighed in agarose (0.8 or 1%) that was subsequently boiled in a microwave and cooled down to 50 - max. 60°C. Either ethidium bromide was added to a final concentration of 1 - 5µg/ml or HDgreen™ (Intas) was added with 5µl per 100ml liquid agarose gel. Agarose gels were either directly poured or kept at 50 – 60°C until use. Gels were poured into a casting chamber and a comb was placed on top. The solid gel was placed in a Sub-Cell GT tank filled with 1x TAE buffer and the pocket spacer removed. Before loading, 2µl 6x DNA loading dye was

added to 10µl PCR product and then loaded into the prepared pockets. As standard, a Generuler™ ladder (Thermo Fisher) was used. The loaded DNA was separated according to the size using a voltage from 90 – 120 V for 20 – 60 minutes. The separation was stopped before the smallest control fragment reached the end of the gel. The gel was either exposed to UV light (ethidium bromide) or blue light (HDgreen^{TM}) to visualize the DNA fragments. Images of the separated DNA fragments were taken using a gel documentation and analysis system (VWR, Lutterworth, UK).

2.2.1.4 Site-directed mutagenesis

The Q5 site-directed mutagenesis kit (NEB) was used with the indicated primers from the primer list according to the manufacturer's manual. Primer were designed using the NEBChanger online tool. After transformation of bacteria at least ten colonies were picked for control PCR and control digest. Three good candidate plasmids were sequenced at the site of mutation. One plasmid was selected for sequencing from left border to right border and finally used for this study.

2.2.1.5 Enzymatic DNA-digest

The restriction enzymes as listed in (Table 15) were used according to the manufacturer's instructions. The reaction mix was incubated at the appropriate temperature for ½ - 4h (FastDigest) and subsequently analysed by agarose gel electrophoresis. Clone Manager was used for vector-specific prediction of enzymatic digest product sizes using the respective vector maps and restriction enzyme recognition sites. Restriction digestion was used for genotyping, plasmid controls and cloning.

Table 15: Restriction digest

Component	Control digest	Cloning
10 x FD buffer	2µl	2µl
FD enzyme A	0,2µl for control digest	0,5µl
(FD enzyme B)	0,2µl	0,5µl
DNA sample	10µl PCR product	1-2µg plasmid
H_2O (ultrapure)	up to 20µl	up to 20µl

2.2.1.6 Preparation of dimer-inserts

For C-terminal viral localization signal insertions, oligonucleotides were designed to form dimers with NotI and BamHI overhangs. NES/nes/NLS/nls-dimers were prepared from 5' phosphorylated oligonucleotides. Accordingly, the vector (pGreen) was digested with NotI and BamHI before T4 DNA ligation. For preparation of the dimers, 15µl were taken from the 10µM stock of the forward and the corresponding reverse oligonucleotide, respectively, and mixed. This 30µl mix was boiled at 96°C for

5min in a thermoblock with the lid on. After shortly spinning down, the mix was put back into the thermoblock with the lid on and the thermoblock was turned off (the plug was also pulled) to slowly cool down. The mix cooled down to RT (around 4h). The prepared dimers were directly used for T4 DNA ligation or stored at -20°C.

2.2.1.7 DNA ligation

The sticky end T4 DNA ligation process was adapted from the manufacturer's instructions (Thermo Fisher). After restriction digest of the vector, SAP (Thermo Fisher) treatment (Table 16) was used to avoid re-cycling of the vector. The T4 DNA ligation mix (Table 17) was prepared and after the indicated incubation time, the T4 DNA ligation mix was either directly used for transformation of bacterial cells or stored at -20°C until use.

Table 16: SAP treatment mix

Component	Volume
Gel purified plasmid	16,5µl
SAP-buffer	2µl
SAP (1U/µl)	1,5µl
Incubation at 37°C for 1/2h and inactivation by incubation at 65°C for 15min	

Table 17: T4 DNA ligation mix

Component	Volume
Dimer mix (3µg/µl working solution)	5µl / 2µl
SAP-treated plasmid mix	5µl
T4 Ligase (5U/µl)	0,7µl
10xbuffer	2µl
H_2O	up to 20µl
Incubation at 16°C overnight	

2.2.2 Bacterial cell cultures

Chemically competent *Escherichia coli* (*E. coli*) TOP10 cells (Thermo Fisher) were used for cloning (Table 18). Electro-competent *Agrobacterium tumefaciens* (*A. tumefaciens*) strain GV3101 (Koncz and Schell 1986) was used for stable transformation of *Arabidopsis* plants (Table 18). GV3101 which is Rif resistant and contains the helper plasmids Ti pMP90 and pSoup, conferring resistances to Gent and Tet (Hellens et al. 2000), was used. Liquid/ solid medium was used with additional antibiotics according to the resistance provided by selected vectors. Solid medium was inoculated with freshly transformed

bacterial cells and incubated at 37°C (*E. coli*) or 28°C (*A. tumefaciens*) in an IPP 500 incubator (Memmert, Schwabach, Germany). Liquid *E. coli* cultures were inoculated from single colonies and grown under shaking (220rpm) in an Innova 4230 incubator (New Brunswick Scientific Co, Enfield, CT, USA). Liquid *A. tumefaciens* cultures were inoculated either from frozen stock cultures or from single colonies and were shaken for up to three days at 180rpm and 28°C in a CERTOMAT^{TM} BS-1 incubator (Sartorius-Stedim Biotech, Göttingen, Germany).

Table 18: Bacterial cells used in this study

Bacterial cells	Growth medium	Growth conditions	Application	Source
Chemically competent *E. coli* TOP10	LB	37°C	Cloning	Thermo Fisher
Electro-competent *A. tumefaciens* GV3101 pMP90 pSoup	DYT + Tet, Rif, Gent	28°C	Stable transformation of *Arabidopsis* or transient transformation of *N. benthamiana*	Koncz and Schell, 1986; Hellens et al., 2000

2.2.2.1 Transformation of bacterial cells

Chemically competent E. coli transformation:

Competent E. coli TOP10 were used from -80°C stocks (prepared by Erwig, 2016). Plasmid DNA (1µl) or ligation products (5-10µl) were added to defrosted E. coli TOP10 cells and incubated for 20min on ice. Cells were incubated for 30 - 45s at 42°C (heat shock). Afterwards, 600µl LB medium was added to the cells and incubated for 60min at 37°C at 650rpm. Next, cells were centrifuged for 1min at 14000rpm in a tabletop centrifuge (Heraeus Pico21, Thermo Fisher) and 300µl of the supernatant were discarded. The remaining supernatant was used to resuspend the pelleted *E. coli* cells, which were then gently spread out on LB plates with the appropriate antibiotics for overnight vector selection at 37°C.

Electro-competent *A. tumefaciens* transformation:

Competent *A. tumefaciens* GV3101 were used from -80°C stocks (prepared by Erwig, 2016). Plasmid DNA (1µl) was added to defrosted *A. tumefaciens* GV3101 cells (on ice) and transferred into a cold electroporation cuvette (0,1cm gap width). The electroporation cuvette was placed in a Micro PulserTM (BioRad, München, Germany) electroporation apparatus (setting: 25µF, 2.5kV and 400Ω) and pulsed. Next, 800µl LB/ DYT medium was added, and the cell mix was transferred into a 1,5ml Eppendorf cup. After incubation at 28°C with shaking at 180rpm for 2-5h, 50µl of the cell mix were spread on a LB plate with the appropriate antibiotics for vector selection. Plates were incubated at 28°C for 2-3 days for bacterial cell growth.

2.2.3 Protein-chemical methods

2.2.3.1 Protein extraction

Standard extraction:

Plant leaf material was collected in a 1,5ml Eppendorf cup and directly frozen in liquid nitrogen. 300µl CERK1 extraction buffer (including PIC) and a small amount of quartz sand (a spatula tip) was added to the cup. A glass pistil was attached to a drill (IKA-Werke GmbH & Co. KG, Staufen, Germany) and used to thoroughly grind the plant material within a 1,5ml Eppendorf cup. Next, 700µl of CERK1 extraction buffer was added by rinsing the glass pistil and the mix centrifuged for 15min at 17000xg and 4°C. The supernatant was transferred to a fresh 1,5ml Eppendorf cup and put on ice. The Bradford method (2.2.3.2) was used for measuring the protein concentration. All samples analyzed within one experiment were extracted in parallel and equalized by adjusting all samples to the sample with the lowest protein concentration using CERK1 extraction buffer. 4 x SDS loading dye was added to all extracted samples, which were then stored at -20°C until use.

SDS-based extraction:

Alternatively, proteins were extracted directly using 2x SDS loading dye. 20 x 4mm leaf discs were collected and frozen using liquid nitrogen. 500µl 2x SDS buffer were added per sample containing 20 x 4mm leaf discs. This defined amount of plant material was thoroughly ground with a glass pistil after adding a spatula of quartz sand. The mix was boiled at 95°C for 10min and centrifuged at 17000xg RT for 10min. The supernatant was transferred to new Eppendorf cup and stored at -20°C until use.

2.2.3.2 Bradford assay

The Bradford assay (Bradford, 1976) was used for determination of protein concentrations. Roti®-Quant Bradford reagent (Roth, Karlsruhe, Germany) was diluted 1:5 in ultrapure H_2O. For calibration curve measurement, 0, 3, 5, 7, 10 and 15µl of a 1mg/ml bovine serum albumin (BSA) solution was pipetted into cuvettes. Next, 3µl of each protein extract was pipetted into cuvettes in duplicates if possible. 1ml of the 1:5 diluted Bradford reagent was added to each cuvette and mixed by vortexing. The cuvettes were incubated for a maximum of 10min at RT. A WPA Biowave II photometer (Biochrom AG, Berlin, Germany) was used to measure the absorption of BSA and the protein extract samples at 595nm. The absorption of the BSA standards was plotted against the protein amount in µg to generate a calibration curve. This calibration curve was used to determine the concentration of each protein extract. All samples within one experimental setup were extracted and equalized in parallel on the same day within one Bradford assay.

2.2.3.3 SDS PAGE

Denaturing sodium dodecyl sulfate polyacrylamide gel electrophoresis (SDS-PAGE) was used to separate extracted proteins according to their molecular mass. The polyacrylamide gels were prepared using glass plates with 1.5mm spacing in a gel stand. 8% resolving gel (Table 19) was prepared and directly poured between the glass plates. Isopropanol was poured on top to remove air bubbles and smoothen the border to the stacking gel. After polymerization and discarding of the isopropanol, the stacking gel (Table 19) was prepared and poured over the resolving gel. A comb was placed on top of the glass plates to prepare pockets for the samples within the gel.

Table 19: SDS gel mixes (for 1,5mm glass plates)

Gel type	Component	Relevant working amounts (for 12 - 14 gels)
Stacking gel	Stacking gel buffer	48,96ml
	Acrylamide (30%)	9,96ml
	APS (10%)	0,3ml
	TEMED	0,003ml
Resolving gel (8%)	Resolving gel buffer (8%)	86,4ml
	Acrylamide (30%)	32,4ml
	APS (10%)	1,2ml
	TEMED	0,072ml

After polymerization the comb was removed. Mini-PROTEAN™ 3 system (BioRad, Munich, Germany) were prepared for SDS-PAGE experiments. For this, gels were placed in the apparatus and the tank was filled with 1 x SDS-running buffer. All SDS protein samples were boiled for 3 - 5min at 95°C and, after cooling down to RT, up to 20µl SDS protein sample volume was loaded in the gel pockets. A PageRuler™ Prestained Plus protein Ladder (Thermo Fisher Scientific, Waltham, USA) was loaded as standard. For each 1.5mm gel, 30mA/gel was applied using a PowerPac™ HC power supply (BioRad, Munich, Germany). The gels ran until the bromophenol blue front ran out of the gel. Next, the gel apparatus was disassembled, and the gels were used for Western blotting.

2.2.3.4 Western blot

After SDS-PAGE separation of extracted proteins according to their molecular weight, immunoblotting was used for detection of protein bands. First, a PVDF membrane with a pore size of 0.45µm (Roth, Karlsruhe, Germany) was labeled and activated with methanol, and then washed with transfer buffer. A TRANS-BLOT® CELL (Bio-Rad, Munich, Germany) apparatus was used to transfer proteins from the SDS gel to the PVDF membrane using electro blotting and assembled according to the manufacturer's instructions. The apparatus was filled with pre-cooled 1x transfer buffer and Western blotting was performed at 100V for 1,5 - 2h at 4°C. The apparatus was disassembled and the PVDF membrane

prepared for the SuperSignal® Western Blot Enhancer (Thermo Fisher) treatment. For this, membranes were washed 3 x for 2min with ultrapure water and incubated for up to 30min in the provided Pre-Treatment Solution. Next, membranes were washed 5 x 2min with ultrapure water. All added solutions fully covered the membranes. The membranes were then blocked for 1h with TBS/T + 3 - 5% milk powder at RT while gently shaking. The membrane was washed 3 x 1min and 2 x 5min using TBS/T (without milk powder) while shaking. The primary antibody was diluted in the provided Primary Antibody Diluent according to Table 11 and the membrane was incubated with the primary antibody overnight at 4°C while gently shaking. Next, the primary antibody diluted in the Primary Antibody Diluent was removed and stored at 4°C to be reused. The membrane was washed with TBS/T + 3 - 5% milk powder 6 x for 15min to remove residual primary antibody. The secondary antibody was diluted in TBS/ T + 3 - 5% milk powder according to Table 11 and the membrane was incubated with the secondary antibody for 2h at RT while gently shaking. Then, membranes were washed 6 x for 15min with TBS/T (without milk powder). Finally, the membrane equilibrated in Alkaline Phosphatase (AP) buffer for at least 5min until 500µl Immun-Star™ AP substrate (BioRad, Munich, Germany) was added to the membrane, which was placed on an opened plastic bag. The bag was closed to evenly distribute the AP substrate on the membrane. The membrane was incubated for 10min in the dark and transferred to a fresh plastic bag for detection of chemiluminescence in a ChemiDoc™ Touch detection device (Bio-Rad, Munich, Germany). The relative protein quantity was quantified using the Image Lab Software (Bio-Rad).

2.2.3.5 Coomassie staining of PVDF membrane

PVDF membranes were stained with a Coomassie staining solution for approximately 10min under shaking until protein bands became clearly visible. For destaining of the background, membranes were placed into destaining solution for 5 - 10min under shaking. The membrane was rinsed with water between the steps and before drying.

2.2.4 *Arabidopsis thaliana* and *Nicotiana benthamiana* methods

2.2.4.1 *Nicotiana benthamiana* cultivation

The standard conditions for cultivation of *N. benthamiana* plants were 65% relative humidity and long-day conditions with 16h photoperiod at 25°C and 8h at 18°C night in a JC-ESC 300 climate chamber (Johnson Controls). *N. benthamiana* seeds originated from T. Romeis (Biochemistry of Plants, Institute of Biology, Freie Universität Berlin) and were sterilized before use. Around four to five-week-old *N. benthamiana* plants were used for *Agrobacterium tumefaciens*-mediated transient transformation for expression of Venus-XLG2/ xlg2 variants and subsequent analysis via confocal laser scanning microscopy (CLSM).

2.2.4.2 *Nicotiana benthamiana* transformation via *Agrobacterium tumefaciens*

First, 5ml LB/ DYT medium containing the appropriate antibiotics were inoculated with transgenic *A. tumefaciens* from tested glycerol stocks and incubated at 28°C 180rpm overnight. Next, 50ml LB/ DYT medium containing the appropriate antibiotics were inoculated with the 5ml overnight culture and continued growth up to two days under the same conditions. Cells were centrifuged at 4000xg RT for 20min and resuspended in 50ml infiltration buffer. The OD_{600} was measured and cells were diluted to an OD_{600} of 0.4 - 2. Diluted cells were left on the bench for several hours before use. Around four to five-week-old *N. benthamiana* plants were infiltrated with the bacterial cells using a 1ml needle-less syringe and areas on the leaves were labeled. Finally, plants were transferred back to the growth chamber, and after 2 – 3 days leaves were analyzed by CLSM.

2.2.4.3 *Arabidopsis* cultivation and selection on soil

The standard conditions for cultivation of *Arabidopsis thaliana* plants were 65% relative humidity, short-day conditions with an 8h photoperiod (150µmol/m²s light intensity) at 22°C and 16h night 18°C in a JC-ESC 300 climate chamber (Johnson Controls). *Arabidopsis* seeds were put three days on -20°C, sterilized and then sown directly on sterilized soil. Two-week-old non-transgenic *Arabidopsis* seedlings without Basta™ resistance were pricked out into single pots. One-week-old stably transformed *Arabidopsis* seedlings with Basta™ resistance were sprayed three times in an 2-3 days interval with a 1:1000 diluted Basta™ solution (200g/l glufosinate ammonium, Bayer CropScience AG). After selection, transgenic *Arabidopsis* seedlings were pricked into single pots. For experiments 4 to 6-week-old plants were used. Plants used for seed propagation were transferred to long-day conditions with a 16h photoperiod at 22°C and 8h at 18°C night.

2.2.4.4 *Arabidopsis thaliana* transformation via *Agrobacterium tumefaciens*

Two-to-three-week-old *Arabidopsis* plants were transferred to long day growth conditions to induce flowering. The plants were prepared by cutting primary flowers for development of secondary growth which resulted in an increased number of flowers and, thus, increased transformation success. *Arabidopsis* plants were transformed via the floral dipping method (Clough and Bent, 1998).

When plants were ready for transformation, 5ml LB or DYT medium containing the appropriate antibiotics were inoculated with transgenic *A. tumefaciens* from tested glycerol stocks and incubated at 28°C 180rpm 1-2 days. Next, 500ml LB or DYT medium containing the appropriate antibiotics were inoculated with the 5ml overnight culture and continued growth for 1-2 days. Cells were centrifuged at 4000rpm RT for 20min (Heraeus multifuge 3 SR+, Thermo Fisher) and resuspended in 1l infiltration medium (water containing 0.5% sucrose). 0,05% Silwet-77 was added shortly before transformation of *Arabidopsis* plants to the cell-sucrose-solution. Plants were dipped upside down 2 x for 30s into a little

plastic tray containing ~300ml bacteria-sucrose-Silwet-solution. Flowers were covered with this solution by gently shaking. Plants were watered and left on the bench overnight with the lid on before they were transferred back to the growth chamber.

2.2.4.5 Transient transformation of *Arabidopsis* via particle bombardment

The instruments used for particle bombardment are listed in Table 20. Preparations for one biolistic shot: 3mg gold microcarriers in 50µl H2O were prepared, washed with 70% ethanol, vortexed for 30s, centrifuged for 1min at 13.000rpm in a tabletop centrifuge (Heraeus Pico21, Thermo Fisher) and the supernatant was discarded. Gold microcarriers were re-diluted in 50µl H2O (vortexed) and either directly used or stored at -20°C. Macrocarriers were washed with 2-propanol and dried (7 per shot). Gold particles were put on ice and 5µg DNA was added (best >1µg/µl concentration) and vortexed. Then, 50µl of 2.5M CaCl2 were added drop by drop and vortexed. Finally, 20µl of 0.1M spermidin (Sigma Aldrich) was added, vortexed and centrifuged at 5000rpm for 5min. Gold microcarriers were washed with 100µl of 70% ethanol and two times with 100µl of 100% ethanol. Finally, gold microcarriers were diluted in 50µl 100% ethanol and left on ice until use. 7µl of prepared gold microcarriers were vortexed loaded on the washed and dried macrocarrier. The Hepta adapter was assembled with the loaded macrocarrier, a stopping screen and a rupture disc and added to the PDS1000/He™ particle delivery system. *Arabidopsis thaliana* plants (4-5week old) were put inside the chamber. A vacuum pump was used to get a pressure of 27In of Hg (Inch of mercury). Fire was pressed until a clicking sound was noted and around 1000psi was measured (1-3s). A burst of high-pressure helium gas then accelerated the gold particles, which were coated with DNA in order to transfect cells. Afterwards, plants were put back into the growth chamber and were analyzed at 1 – 2 days post bombardment.

Table 20: Instruments used for particle bombardment

Component	Company/ source	Accession no.
Biolistic Hepta Adapter for PDS1000/He	BIO-RAD	#1652225
Biolistic rupture disks (900psi)	BIO-RAD	#1652328
Biolistic Macrocarriers	BIO-RAD	#1652335
Gold Microcarriers 1µm	BIO-RAD	#1652263

2.2.4.6 Seed sterilization

All seed material was placed into 2x zip-plastic bags and was stored at -20°C for three days. Seeds were sterilized either with alcohol or chloric gas.

Alcohol-based seed sterilization (low number of seed packages):

Seeds were transferred into 1.5ml Eppendorf cup and washed three times with 1ml ethanol (p.a. 70% including 0.05% Tween20) for 1min. Ethanol p.a. (96%) was used for the final wash and the seeds were poured on a filter paper (labeled). Dried seeds were then sown.

Chloric gas-based seed sterilization (large number of seed packages, under the fume hood):

A little beaker was placed at the bottom of a desiccator filled with 15ml of 5% sodium hypochlorite. Seed packages (without paper clip) were placed around the desiccator ring which was then placed above the beaker inside the desiccator. The sterilization reaction was started by adding 5ml of 37% HCl and the desiccator immediately closed and left for 4h.

2.2.4.7 DNA extraction from *Arabidopsis* leaf material

Arabidopsis leaf material was collected in a 1,5ml Eppendorf cup. The genomic DNA extraction buffer was shortly warmed up in a microwave to resolve precipitates. 300µl extraction buffer was added to the leaf sample. A clean plastic pistil was used for grinding up the sample and which were then incubated at RT while shaking in a thermomixer. After 5min centrifugation at max. speed RT, 240µl supernatant were transferred into a new 1,5ml Eppendorf cup filled with 300µl isopropanol. After another 5min shaking at RT (thermomixer) the sample was centrifuged at max. speed RT for 10min. The supernatant was discarded, and the sample centrifuged again for 1min at max. speed RT. The remaining supernatant was removed with a 200µl pipette and the pellet dried at RT. 50µl ultrapure water was added and the DNA resuspended by shaking for 5min at RT. The extracted genomic DNA was stored at -20°C.

2.2.4.8 Mutant genotyping

xlg2-2 (noce1-4) expressing the complete XLG2 gene including 5'UTR under the native XLG2 promoter was genotyped in two steps. First, 1µl genomic DNA was used as template for PCR using the primers JA74 and CM74, which give a 2306bp product (standard PCR program, 3min extension time). 2µl of a 1/10 dilution of this first PCR product was used as template for a second PCR using the primers MS226 + MS227, which give a 241bp product (standard PCR program). The second PCR product was digested with SaqAI. The presence of the *xlg2*-2 (noce1-4) mutation was confirmed when successful digest was indicated by the presence of two 165 + 76bp products. For non-transgenic plants, the first PCR was not necessary. Instead, genomic DNA was directly used as template for PCR using the MS226/7 primers.

For *cerk1*-4 genotyping, 1µl of genomic DNA was used as template for PCR using the primers UL154 and UL166, which give a 713bp product (standard PCR program). This PCR product was then digested with XapI, which gives two 442 + 271bp products in the presence of *cerk1*-4.

2.2.5 Confocal laser scanning microscopy

For confocal laser scanning microscopy (CLSM) a Leica TCS SP8 Confocal system (Leica Microsystems, Wetzlar, Germany), equipped with a White Light laser (WLL) and HyD hybrid detectors, was used to detect Venus-labeled proteins in living cells. The nuclear marker mTurquoise2-N7 and the plasma

membrane marker mKate2-Lti6b (Hassan Ghareeb) were used for co-localization experiments. Small leaf samples were collected from plants and placed with the adaxial site on top in an ultrapure water droplet on glass object slides and were covered under a glass cover. Excitation and detection details are listed in Table 21.

Table 21: Excitation and detection parameters used in this study.

Fluorophore	Excitation	Detection
Venus	514nm WLL (85%)	525-560nm
mKate2	594nm HeNe laser (20%)	600-641nm
mTurquoise2	458nm Argon (15%)	438-485nm
Fluorescent brightener 28 (FB28)	405nm Diode laser	410-470nm
Propidium iodide (PI)	514nm Argon laser/ WLL	580-630nm

Sequential scan was used for fluorophores with overlapping emission spectra. Images were scanned with a resolution of 512 x 512 pixels at 200Hz and z stacks were recorded 1µm apart. Further, a line average of 3 and a bidirectional scan were used. A WLL light pulse excited the fluorophore and triggered the start time-point of the measurement. Time-gated rejection of chlorophyll autofluorescence allowed clearer fluorescence imaging (gate-on time 0.4 - 6.0ns). The Navigator statistical merge function was used to stitch maximum projections of larger leaf areas. Maximum z projections were exported as TIFFs using LASX LASAF Leica Application Suite X software (LASX) and brightness/ contrast was changed using Adobe Photoshop CS5 software packages (Microsoft). Final figures were prepared using Adobe Illustrator. All images within one figure were processed using the same settings to enable comparability of individual images from one experiment.

2.2.5.1 CLSM after *Ec* inoculation

One day post infection with *Erysiphe cruciferarum* (*Ec*), plants were analysed via CLSM. Fluorescent brightener 28 (FB28) (Sigma-Aldrich Deisenhofen, Germany) was used as a 10µg/ml solution (in ultrapure water) for visualization of fungal structures (spores, appressoria, hyphae) Pavement cells under attack of individual spores were selected for imaging. Invasion of the fungus was indicated in the presence of a formed appressorium (whether a penetration peg was formed was not further analyzed).

For analysis of *Ec* haustoria, a propidium iodide (PI) 10mg/ml stock solution (in ultrapure water) was used to stain fungal structures (spores, hyphae, appressoria, haustoria) as well as plant structures (plasma membrane, stomata, nuclei). 20µl from the PI stock solution were diluted in 10ml ultrapure water and used as PI working solution. The PI working solution was infiltrated into 4mm leaf discs using a 5ml syringe and incubated for 30min. Leaf discs were transferred to ultrapure water in a 2ml Eppendorf cup, inverted several times and incubated another 15min for washing before the sample was used for CLSM.

2.2.5.2 Quantification of CLSM images

The Fiji distribution of ImageJ (open source) was used to measure fluorescence intensities (gray values) of cell compartments (stomata, cell periphery, background, nuclei) and for counting of nuclei.

Quantification of CLSM images in cells transiently transformed by particle bombardment:

Cells were transformed with three constructs in parallel: Venus-XLG2 (wild type or mutant version), the nuclear marker (mTurquoise2-N7) and the plasma membrane marker mKate2-Lti6b. In the Venus channel, nuclei, cell periphery and background were selected using the multi-point tool as indicated in Fig. 6. Maximum gray values per point were measured (Table S 6a) and the average signal intensity of all points was calculated for each compartment. The background signal intensity was subtracted from the cell periphery and nuclear gray value average respectively.

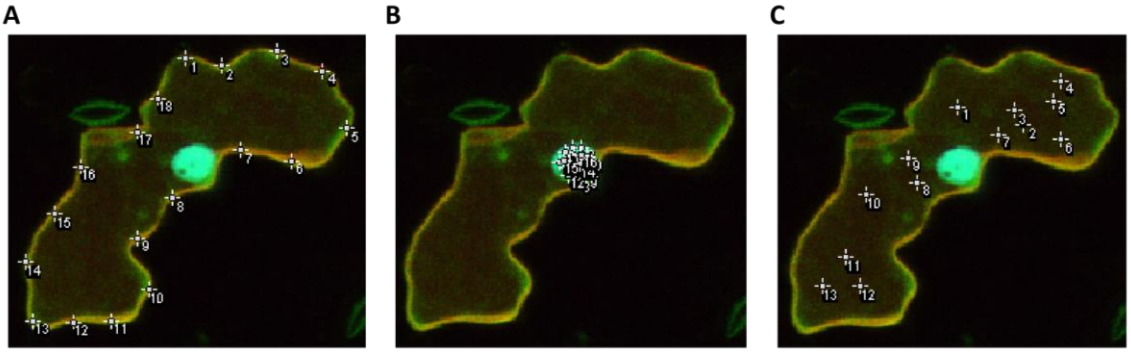

Fig. 6: Quantification of CLSM images (particle bombardment).

Transiently transformed *Arabidopsis* plants expressing Venus-XLG2/ xlg2 after particle bombardment. Cell compartment areas were defined for gray value quantification: plasma membrane (A), nuclei (B), and background (C).

Quantification of CLSM images of unchallenged stable transgenic Arabidopsis plants:

The number of nuclei was counted for an area of 290 x 290µm (0,0841 mm²) using ImageJ ROI manager for labeling positions after counting. For fluorescence intensity quantification, cell periphery, nuclei and stomata were selected using the freehand tool as indicated in Fig. 7. Maximum gray values per ROI were measured (Table S 6b) and average signal intensities of all ROIs were calculated for each compartment.

In addition, cell periphery and nuclear signals were normalized to the consistent stomatal autofluorescence:

$$\text{Normalized signal intensity} = \frac{\text{Average cell periphery signal intensity [gray values]}}{\text{Average stomatal autofluorescence signal intensity [gray values]}}$$

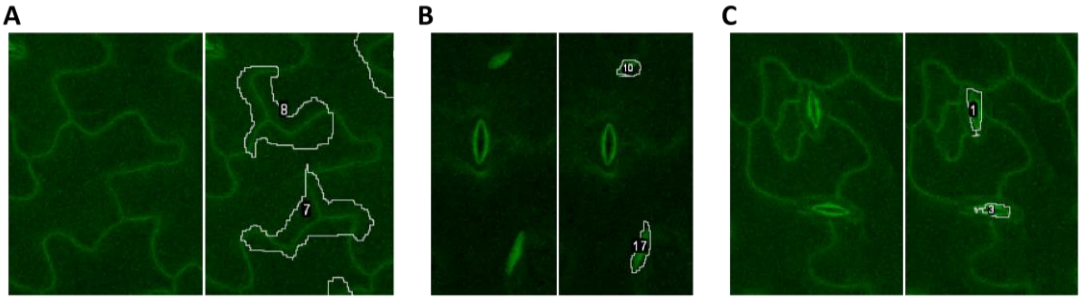

Fig. 7: Quantification of CLSM images (stably transformed *Arabidopsis*).

Stable transgenic *Arabidopsis* plants expressing Venus-XLG2/ xlg2. Cell compartment areas were marked for gray value quantification: cell periphery (A), nuclei (B), and stomata (C).

Quantification of CLSM images of unchallenged vs. infected (1dpi Ec) stable transgenic Arabidopsis plants:

For fluorescence intensity quantification, cell periphery, nuclei (when visible) and background were selected using the line tool at multiple positions. Maximum gray values per ROI were measured (Table S 6c) and the average signal intensity for cell periphery and nucleus was calculated. The non-normalized gray values were compared between unchallenged and infected (1dpi Ec) plants.

2.2.6 Online tools and programs

Table 22: Online tools and programs used in this study

Program	Purpose	Reference
LocNES	NES prediction	(Xu et al. 2015)
cNLS Mapper	NLS prediction	(Kosugi et al. 2009)
ImageJ	CLSM image quantification	(Rueden et al. 2017; Schindelin et al. 2012)
DISULFIND	Disulfide bridge prediction	(Ceroni et al. 2006)
Microsoft office	Text and figures	Microsoft Corporation
Adobe Photoshop CS5	Brightness and contrast	Adobe Inc.
Adobe Illustrator CS5	Figures	Adobe Inc.
LAS X	CLSM processing	Leica Microsystems
Clone Manager	Cloning	Sci-Ed Software
Clustal Omega	Alignments	(Madeira et al. 2019)

2.2.7 Statistical Analysis

For calculating the significance of difference between two samples, a two-tailed, unpaired student's t test in Excel was used. $P < 0,05$ was defined as significant (*), $P < 0,01$ very significant (**), $P < 0,001$ highly significant (***) and $P < 0,0001$ extremely significant (****).

3 Results

3.1 A mutation in the N-terminal domain (E293K) alters the localization of XLG2 and renders it non-functional

Two previously identified *cerk1*-4 suppressor mutations *xlg2*-2 and *xlg2*-3 were mapped to the XLG2 gene (Meusel 2016; M. Stolze, unpublished). The *xlg2*-2 mutation results in an early stop codon within a highly conserved cysteine-rich region at the N-terminus. The second suppressor mutation *xlg2*-3 is a single amino acid exchange of a highly conserved glutamic acid to lysine (E293K) shortly next to the XLG2 cysteine-rich region. This amino acid exchange potentially enhances a predicted nuclear localization signal (NLS) which starts at position 275 (Fig. 8). A fluorescent Venus-tag was fused to the N-terminus of XLG2 in order to analyze subcellular localization of Venus-XLG2/ xlg2 E293K under native promoter expression. The full-length genomic DNA including the five prime untranslated region (UTR), the endogenous XLG2 promoter, all introns and exons were used as transgene.

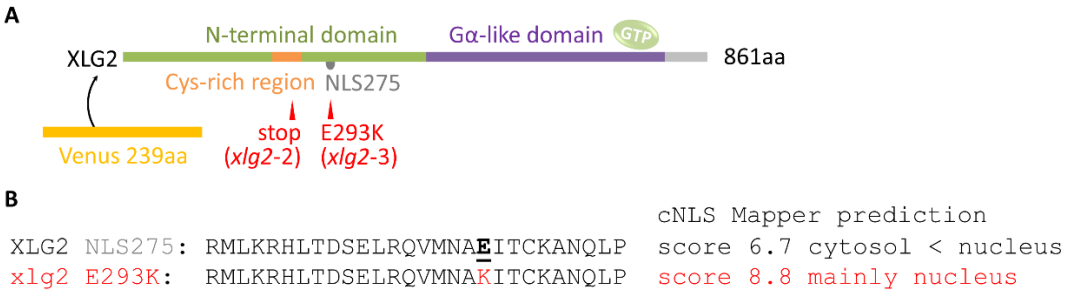

Fig. 8: The *xlg2*-2 and *xlg2*-3 (E293K) mutations.

(A) Two suppressor mutations *xlg2*-2 (early stop codon) and *xlg2*-3 (a conserved glutamic acid at position 293 mutated to a lysine) were identified earlier in a *cerk1*-4 suppressor screen. cNLS Mapper predicted a localization signal NLS275 between the cys-rich region and the Gα-like domain (labeled in grey). The yellow fluorescent protein Venus was fused to the N-terminus of XLG2. **(B)** The E293K mutation is located within a predicted NLS that is potentially enhanced according to cNLS Mapper predictions (Kosugi et al. 2009). NLS Mapper score info: 1 - 2 cytoplasm, 3 - 6 equally localized to nucleus and cytoplasm, 7 - 8 cytoplasm and stronger to nucleus, >9 exclusively nuclear (http://nls-mapper.iab.keio.ac.jp/cgi-bin/NLS_Mapper_help.cgi#appendix).

3.1.1 E293K changes the localization of transiently expressed XLG2

Transient expression was initially used in order to investigate the generated fusion constructs. Transient expression of Venus-XLG2 or Venus-xlg2 E293K in *N. benthamiana* via *Agrobacterium tumefaciens*-mediated transformation was analysed via confocal laser scanning microscopy (CLSM). Venus-XLG2 showed strong cell periphery and nuclear localization, with occasionally visible cytoplasmic strands (Fig. 9). In comparison, Venus-xlg2 E293K showed strongly reduced cell periphery signals.

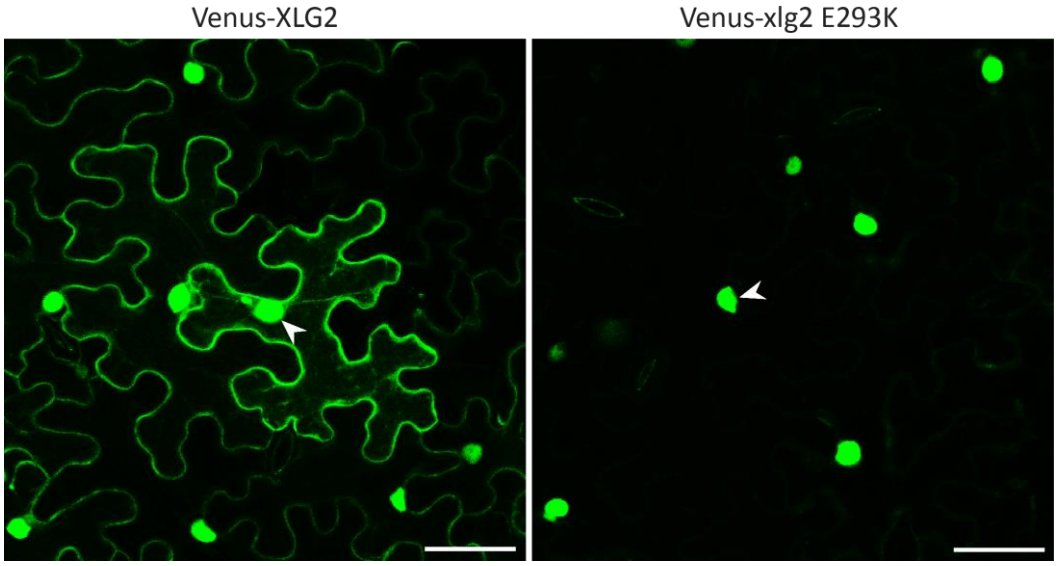

Fig. 9: The E293K mutation abolishes cell periphery but not nuclear localization of XLG2 in *N. benthamiana*.
Venus-XLG2 WT and Venus-xlg2 E292K were transformed into *N. benthamiana* via *A. tumefaciens* infiltration. CLSM was performed 3dpi. Representative images of three independent experiments are maximum projections of 31 focal planes recorded 1µm apart. Example nuclei are marked by arrowheads. Scale bar = 50µm.

Next, the localization pattern was analysed in *xlg2*-2 single mutant *Arabidopsis* plants via particle bombardment. Co-expression of cellular compartment markers for the nucleus (mTurquoise2-N7) and the PM (mKate2-Lti6b) (Hassan Ghareeb) were used to define regions for quantification of Venus-XLG2 WT and Venus-xlg2 E293K signals. Venus-XLG2 localized strongly to the cell periphery and the nucleus, while the mutant variant Venus-xlg2 E293K showed mainly nuclear localization (Fig. 10 A) similar to the observed localization in *N. benthamiana*. The nucleus to cell periphery ratio was significantly higher for Venus-xlg2 E293K compared to Venus-XLG2 WT (Fig. 10 B). Further, Venus-xlg2 E293K showed a significantly reduced cell periphery signal intensity compared to Venus-XLG2 WT (Fig. 10 C), while nuclear signal intensities were similar (Fig. 10 D).

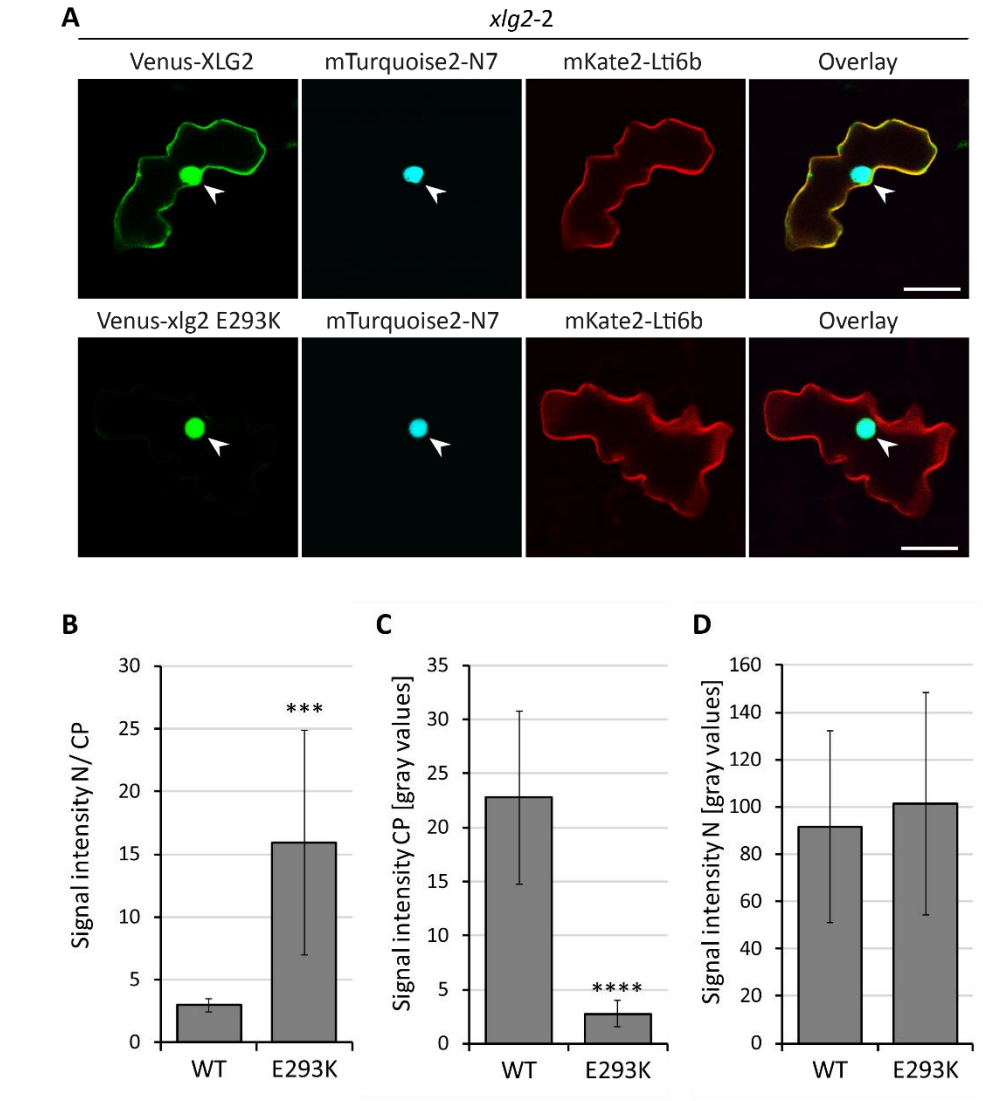

Fig. 10: XLG2 cell periphery localization was abolished by the E293K mutation in bombarded *xlg2*-2.

(A) Venus-XLG2 and Venus-xlg2 E293K were co-transformed with Turquoise2-N7 (nuclear marker) and mKate2-LTI6b (PM marker) in *xlg2*-2. Representative CLSM images show single planes 2d after particle bombardment. This experiment was repeated three times. Nuclei are marked by arrowheads. Scale bar = 50µm.

Quantification of Venus-XLG2 WT and Venus-xlg2 E293K signal intensities: **(B)** signal intensity nucleus (N)/ cell periphery (CP), **(C)** signal intensity CP and **(D)** signal intensity N. Regions were defined by mTurquoise2 (N) and mKate2 (CP) channels. Data are means ± StDev of n = 10 cells. ** P < 0.01, **** P < 0.0001

3.1.1 Stably expressed XLG2 localizes mainly to the cell periphery in unchallenged *Arabidopsis* plants

Homozygous *xlg2*-2 single and *cerk1*-4 *xlg2*-2 double mutant plants were previously generated (M. Stolze, unpublished). These were used in this study in order to generate stable transgenic lines expressing Venus-XLG2 and Venus-xlg2 E293K. Subcellular localization was analysed in both genetic backgrounds in order to get insight whether the *cerk1*-4 mutation has any impact on subcellular dynamics of XLG2. *xlg2*-2 lines expressing Venus-XLG2 (42 independent lines) and *xlg2*-2 expressing

Venus-xlg2 E293K (15 lines) as well as *cerk1*-4 *xlg2*-2 expressing Venus-XLG2 (46 lines) and Venus-xlg2 E293K (21 lines) were generated and analysed via CLSM. Compared to transient expression, lower expression levels of Venus-XLG2/ xlg2 E293K were observed in stably transformed *xlg2*-2 (Fig. 11 A, Fig. S 1, Fig. S 2) and *cerk1*-4 *xlg2*-2 (Fig. 12 A, Fig. S 3, Fig. S 4). Further, Venus-XLG2 was found mainly at the cell periphery in pavement cells of *Arabidopsis* leaves. In contrast, Venus-xlg2 E293K was detected mainly inside the nucleus. No difference in localization was observed for either XLG2 variant between *xlg2*-2 (Fig. 11, Fig. S 1, Fig. S 2) and *cerk1*-4 *xlg2*-2 (Fig. 12 A, Fig. S 3, Fig. S 4). Venus-xlg2 E293K labeled nuclei significantly more often and cell periphery signals were significantly reduced compared to Venus-XLG2 WT in *xlg2*-2 (Fig. 11 B, Fig. S 5) and *cerk1*-4 *xlg2*-2 (Fig. 12 B, Fig. S 6). CLSM analysis of four to seven-week-old transgenic lines in *xlg2*-2 (Fig. 11) and *cerk1*-4 *xlg2*-2 (Fig. 12) (≥ 6 independent lines per construct and genotype) indicated that aging had no effect on subcellular localization of Venus-XLG2/ xlg2 E293K. This developmental study was important due to the observation that *cerk1*-4 mutant *Arabidopsis* develop an early senescence phenotype (Petutschnig et al. 2014).

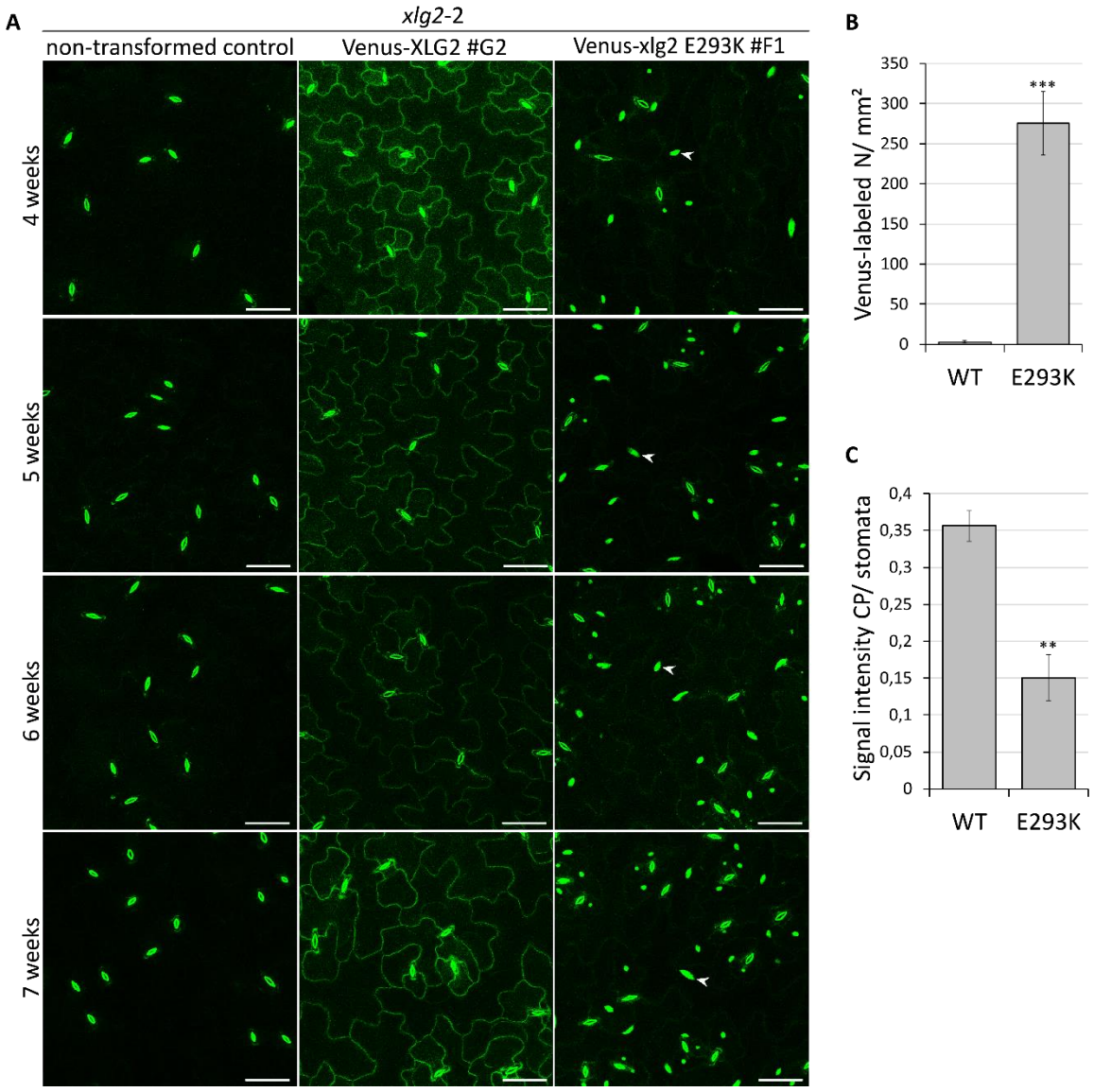

Fig. 11: Cell periphery localized XLG2 WT compared to mainly nuclear localized xlg2 E293K in *xlg2*-2.

(A) CLSM images of representative lines expressing either Venus-XLG2 WT or Venus-xlg2 E293K in *xlg2*-2 plants are maximum projections of z stacks spanning the epidermal cell layer. Scale bar = 50µm.

Quantification of Venus-XLG2 WT and Venus-xlg2 E293K localization/ signal intensities in stably transformed *xlg2*-2:

(B) Venus-labeled N/ mm² and **(C)** signal intensity CP/ stomata autofluorescence. N = nucleus, CP = cell periphery. Data are means ± StDev of three images from three individual plants (≥ 9 images in total per line) of three independent lines**.** ** P < 0.01, *** P < 0.001

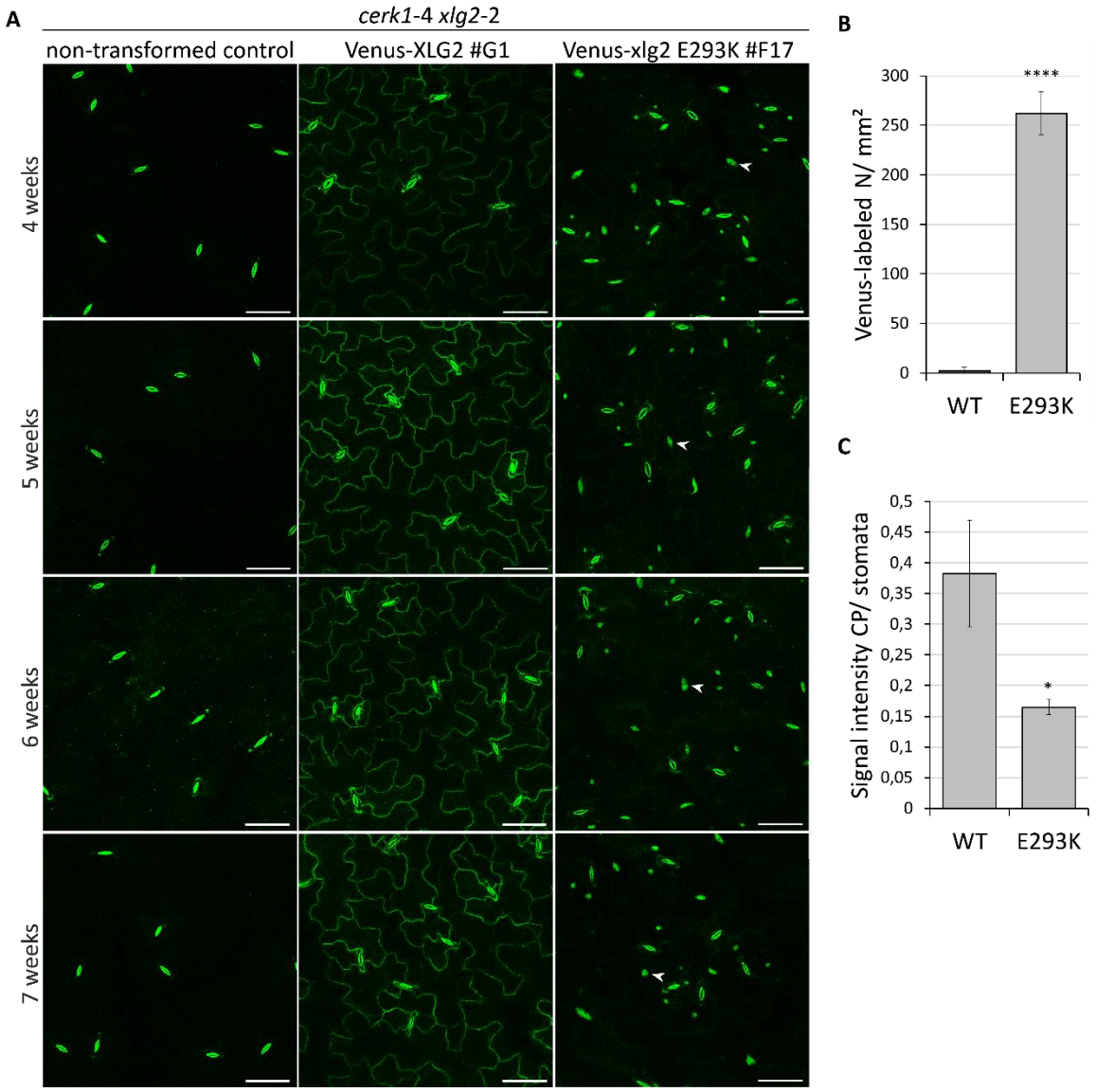

Fig. 12 Cell periphery localized XLG2 WT compared to mainly nuclear localized xlg2 E293K in cerk1-4 xlg2-2.

(A) CLSM images of indicated lines expressing either Venus-XLG2 WT or Venus-xlg2 E293K in *cerk1*-4 *xlg2*-2 plants are maximum projections of z stacks spanning the epidermal cell layer. Scale bar = 50µm.

Quantification of Venus-XLG2 WT and Venus-xlg2 E293K localization/ signal intensities in stably transformed *cerk1*-4 *xlg2*-2: **(B)** Venus-labeled N/ mm² and **(C)** signal intensity CP/ stomata autofluorescence. N = nucleus, CP = cell periphery Data are means ± StDev of three images from three individual plants (≥ 9 images in total per line) of three independent lines**.** * $P < 0.05$, **** $P < 0.0001$

3.1.2 Powdery mildew infection increases XLG2 abundance and nuclear localization

In contrast to transient systems, Venus-XLG2 nuclear signals were rarely observed when stably expressed in *Arabidopsis* plants. Further, Venus-XLG2/ xlg2 E293K showed rather low expression levels in both *xlg2*-2 and *cerk1*-4 *xlg2*-2 as described in the previous chapter. It was previously shown that XLG2 gene expression is stress-responsive (Zhu et al. 2009; Humphry et al. 2010; Meusel 2016). Here, Venus-XLG2/ xlg2 E293K expression upon pathogen challenge using the compatible powdery mildew

Ec was analysed. In order to document immune signalling after invasion compared to the basal expression level and localization, Venus-XLG2/ xlg2 E293K expressing plants (≥ 8 independent lines) were analysed via CLSM before and one day post inoculation with *Ec* (Fig. 13 A). Pavement cells infected by one fungal spore were selected and presence of an appressorium indicated attempted entry of the fungus.

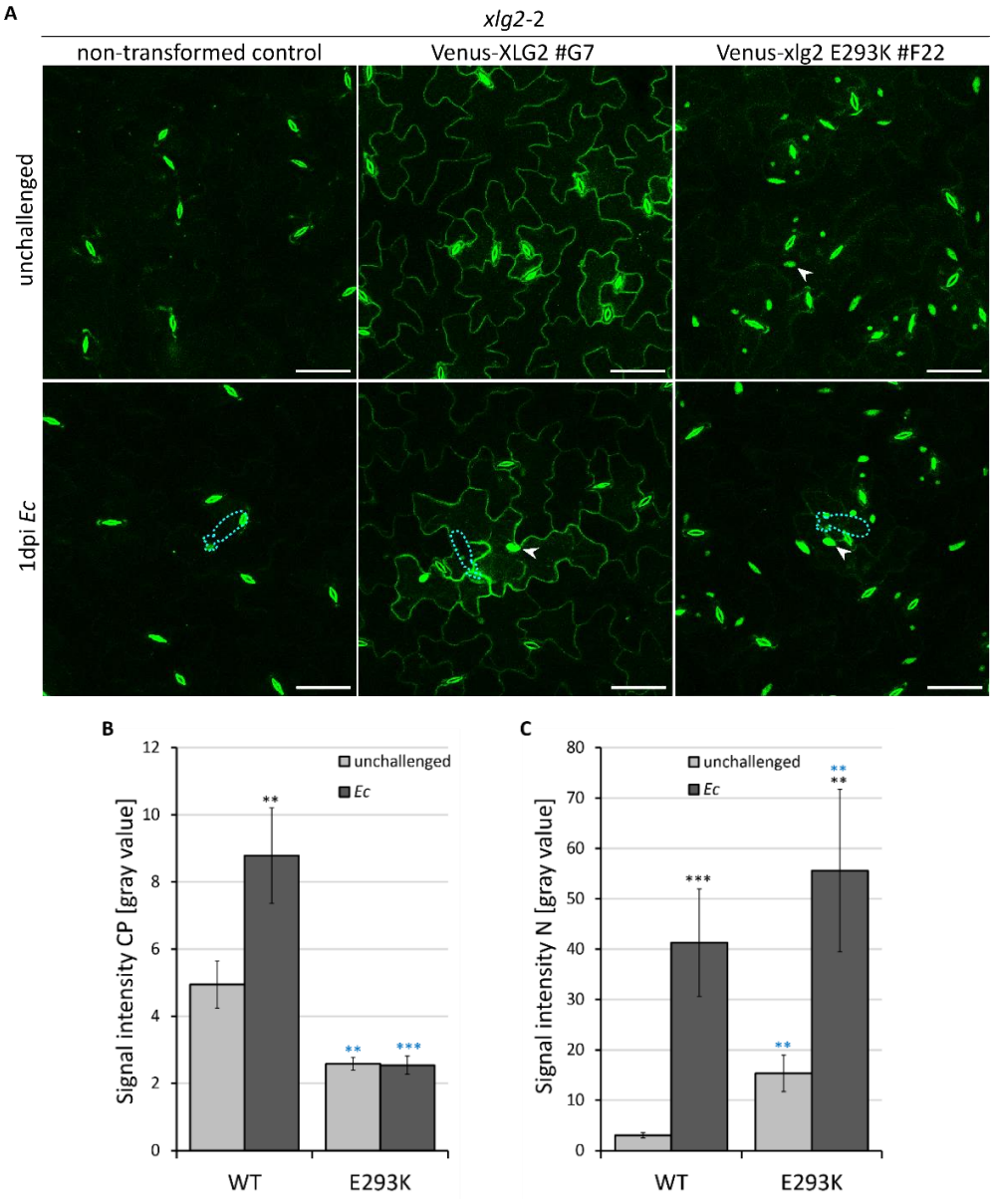

Fig. 13: Powdery mildew attack increases XLG2 and xlg2 E293K nuclear localization in *xlg2*-2.

(A) CLSM images of indicated unchallenged vs. infected (1dpi *Ec*) lines expressing Venus-XLG2 or Venus-xlg2 E293K in *xlg2*-2 are maximum projections of z stacks spanning the epidermal cell layer. Nuclei are marked by arrowheads and the position of fungal spore and appressorium are outlined by dashed blue lines. Scale bar = 50µm. The lines presented in this Figure were analyzed together with the lines in Fig. 47. Therefore, the same images for Venus-xlg2 E293K are shown.

Quantification of CLSM images of *xlg2*-2 expressing Venus-XLG2/ xlg2 E293K. Signal intensities at the cell periphery (CP) **(B)** and inside the nucleus (N) **(C)** of unchallenged and infected (1dpi *Ec*) cells were quantified. Data are means ± StDev of four independent lines (1-5 interaction sites of 1-3 plants were analysed per line). Asterisks indicate significance unchallenged vs infected (black) and compared to WT (blue). ** P < 0.01, *** P < 0.001

In unchallenged *xlg2*-2 Venus-XLG2 localized predominantly to the cell periphery, while Venus-xlg2 E293K accumulated mainly in the nucleus as described before. Signal intensities for Venus-XLG2 WT as well as xlg2 E293K increased upon pathogen inoculation. Venus-XLG2 signal intensity significantly increased at the cell periphery as well as inside the nucleus in attacked cells according to the quantification of CLSM data (Fig. 13 B, C; Fig. S 7). Venus-xlg2 E293K nuclear accumulation also significantly increased upon fungal attack while cell periphery signals were significantly lower compared XLG2 WT. No difference was observed between *xlg2*-2 (Fig. 13 A, Fig. S 8) and *cerk1*-4 *xlg2*-2 (Fig. 14, Fig. S 9) concerning subcellular localization dynamics of Venus-XLG2 and Venus-xlg2 E293K upon infection.

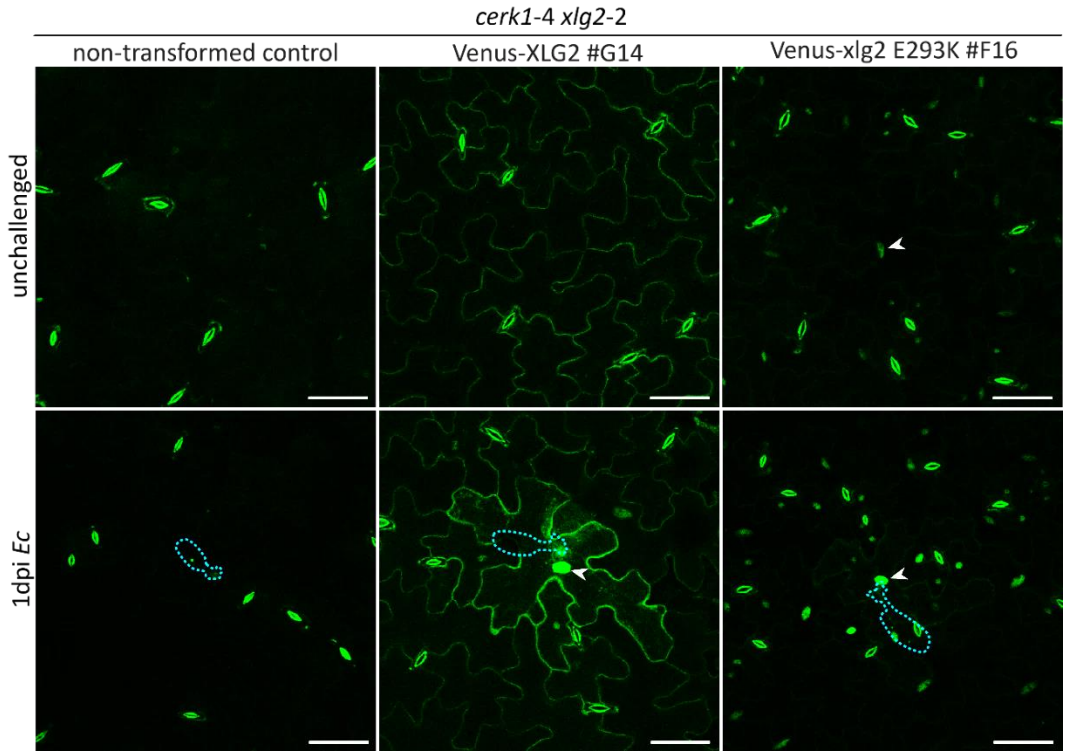

Fig. 14: Powdery mildew attack increases XLG2 and xlg2 E293K nuclear localization in *cerk1*-4 *xlg2*-2.

CLSM images of indicated unchallenged vs. infected (1dpi *Ec*) lines expressing Venus-XLG2 or Venus-xlg2 E293K in *cerk1*-4 *xlg2*-2 are maximum projections of z stacks spanning the epidermal cell layer. Nuclei are marked by arrowheads and the position of fungal spore and appressorium are outlined by dashed blue lines. Scale bar = 50µm.

Next, larger leaf areas of unchallenged vs. infected (1dpi *Ec*) plants were analysed via CLSM. This was done in order to show an overview of the observed pathogen-induced patchy areas with elevated Venus-XLG2 and Venus-xlg2 E293K signals in *xlg2*-2 (Fig. 15 A) and *cerk1*-4 *xlg2*-2 (Fig. 16 A) plants. Areas with elevated Venus-XLG2/ xlg2 E293K signals in patches were covered with fungal spores, but unchallenged areas of the leaf epidermis did not show any increase in Venus-XLG2/ xlg2 E293K signal intensity (Fig. 15 B, Fig. 16 B). Powdery mildew-dependent elevation of XLG2 WT/ xlg2 E293K protein levels was further analysed using Western blotting. Leaf material from Venus-XLG2/ xlg2 E293K

expressing *xlg2*-2 and *cerk1*-4 *xlg2*-2 was collected before and 3 days after *Ec* inoculation. Interestingly, Venus-xlg2 E293K showed a slightly lower apparent molecular mass in Western Blot compared to Venus-XLG2 in *xlg2*-2 (Fig. 17 A) and *cerk1*-4 *xlg2*-2 (Fig. 17 B). One reason could be changed structural elements such as disulfide bridges in the xlg2 mutant. A more likely reason for the observed motility difference could be post-translational modifications that are changed in xlg2 E293K compared to XLG2 WT. A XLG2-specific antibody was ordered and used for native XLG2 detection in non-transgenic Col-3 *gl*1 and *cerk1*-4 (Fig. 17 C). The abundance of Venus-XLG2 and Venus-xlg2 E293K significantly increased upon infection according to the quantification of GFP-specific antibody signals from Western Blots (Fig. 17 D, E). Further, the α-GFP signal intensity of Venus-XLG2 was significantly stronger induced compared to Venus-xlg2 E293K in *xlg2*-2 (Fig. 17 D, Fig. S 10) and *cerk1*-4 *xlg2*-2 (Fig. 17 E, Fig. S 10). This could indicate a potential role of XLG2 in feed forward regulation which is abolished by the E293K mutation. XLG2 abundance drastically increased upon infection in both Col-3 *gl*1 and *cerk1*-4 to similar extend (Fig. 17 F, Fig. S 10). The difference between Venus-XLG2 and xlg2 E293K abundance seemed to be less prominent with the XLG2-specific antibody compared to the GFP-specific antibody (Fig. S 11 A, B). The reasons for this effect are unclear. Venus-XLG2 and xlg2 E293K were more abundant in all analysed *xlg2*-2 and *cerk1*-4 *xlg2*-2 lines than endogenous XLG2 in Col-3 *gl*1 probably due to the selection of transgenic plants via CLSM with focus on good Venus signal detection (Fig. S 11 C, D).

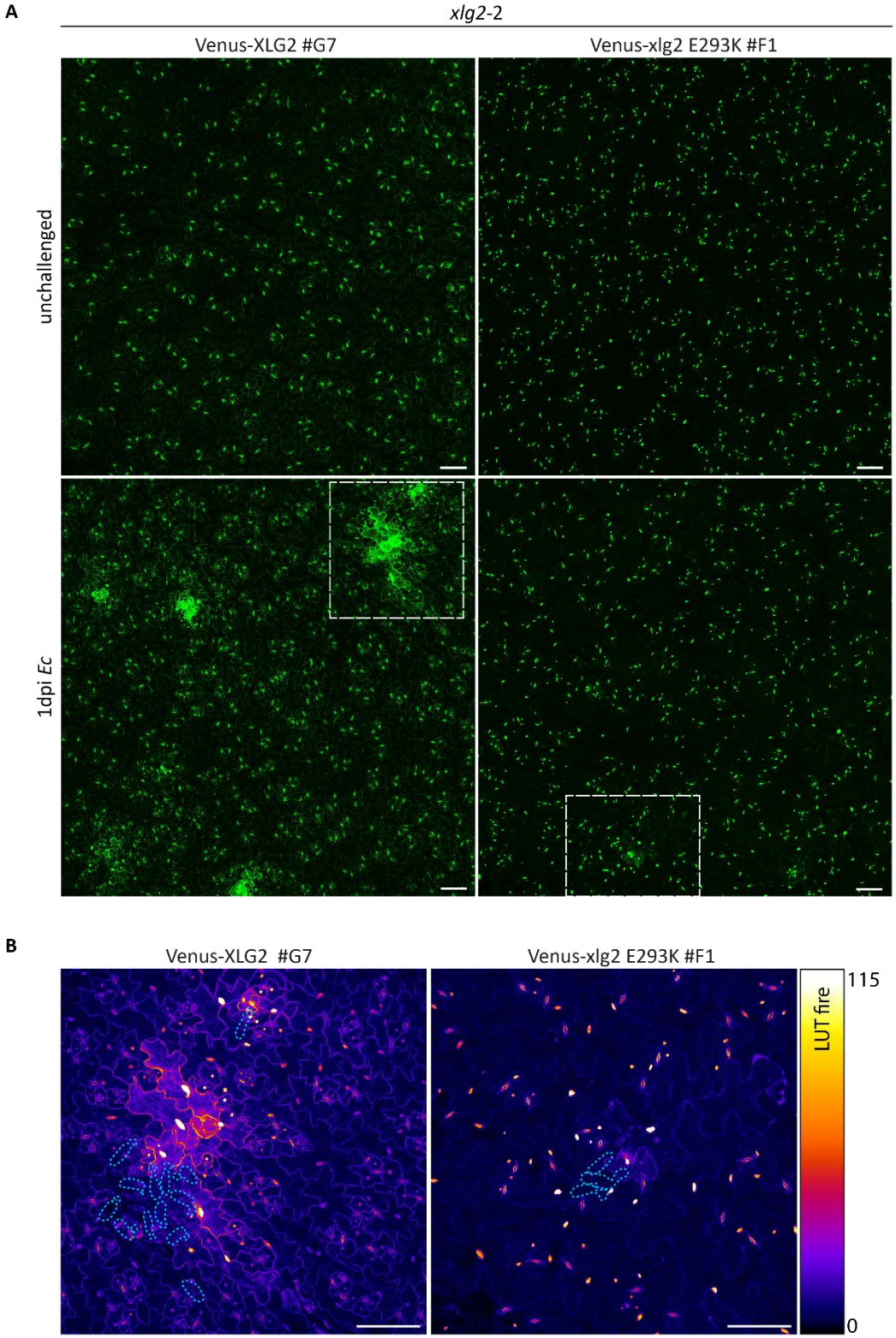

Fig. 15: Basal abundance and pathogen-induced local accumulation of XLG2 (E293K) in xlg2-2.

(A) Low basal abundance levels of Venus-XLG2 and Venus-xlg2 E293K in *xlg2*-2 were detected in unchallenged leaves while locally elevated levels of XLG2 (E293K) were detected upon infection (1dpi *Ec*). Stitched maximum projections of larger leaf areas of 60 focal planes recorded 1.5µm apart. Scale bar = 100µm. **(B)** Enlarged selected area (white dashed box) with fungal spores marked by dashed blue lines. For better visualization of elevated signals, a multicolor LUT was applied (lower panel). Scale bar = 100µm.

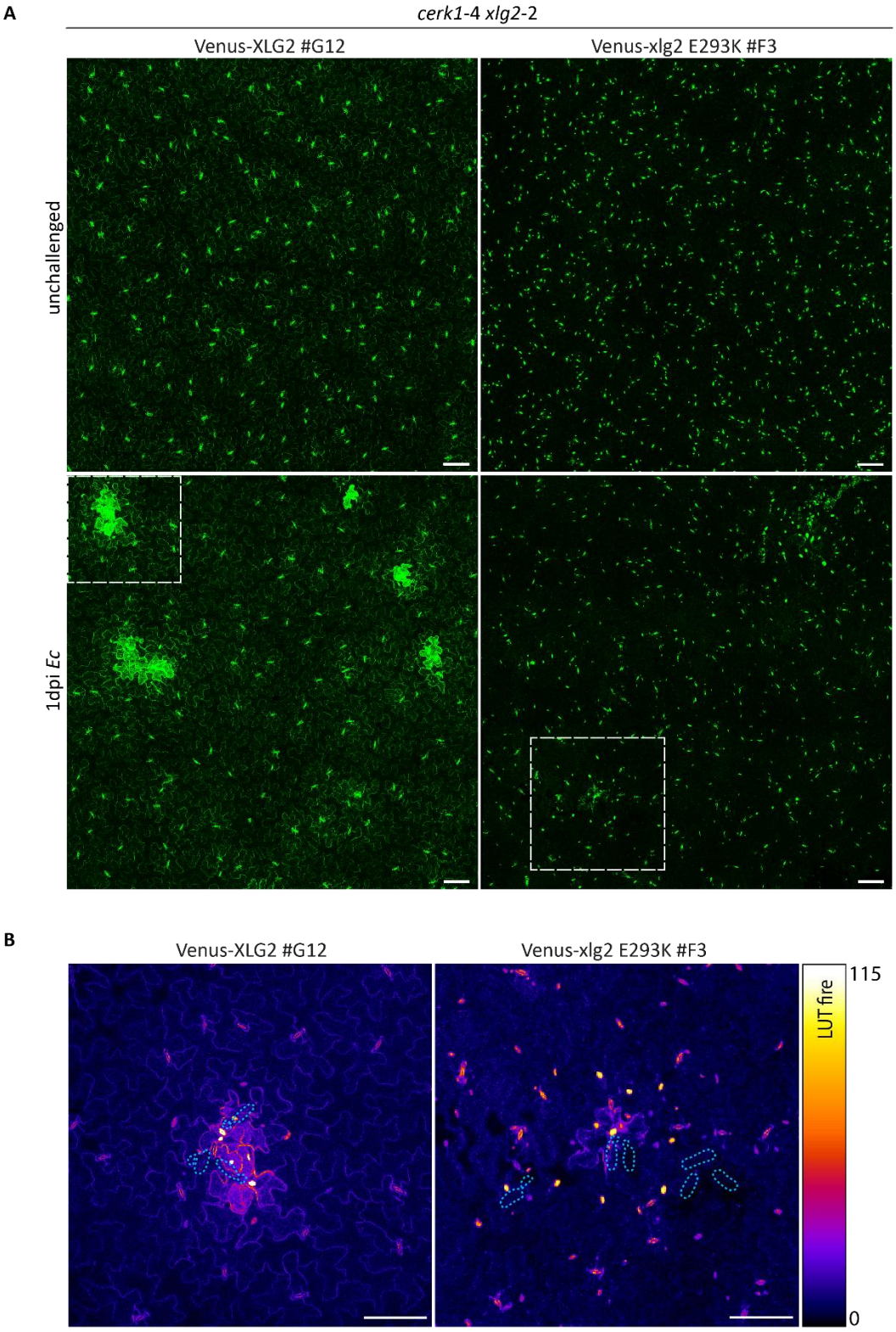

Fig. 16: Basal abundance and pathogen-induced local accumulation of XLG2 (E293K) in *cerk1*-4 *xlg2*-2.

(A) Low basal abundance levels of Venus-XLG2 and Venus-xlg2 E293K in *cerk1*-4 *xlg2*-2 were detected in unchallenged leaves while locally elevated levels of XLG2 (E293K) were detected upon infection (1dpi *Ec*). Stitched maximum projections of larger leaf areas of 60 focal planes recorded 1.5µm apart. Scale bar = 100µm. **(B)** Enlarged selected area (white dashed box) with fungal spores marked by dashed blue lines. For better visualization of elevated signals, a multicolor LUT was applied (lower panel). Scale bar = 100µm.

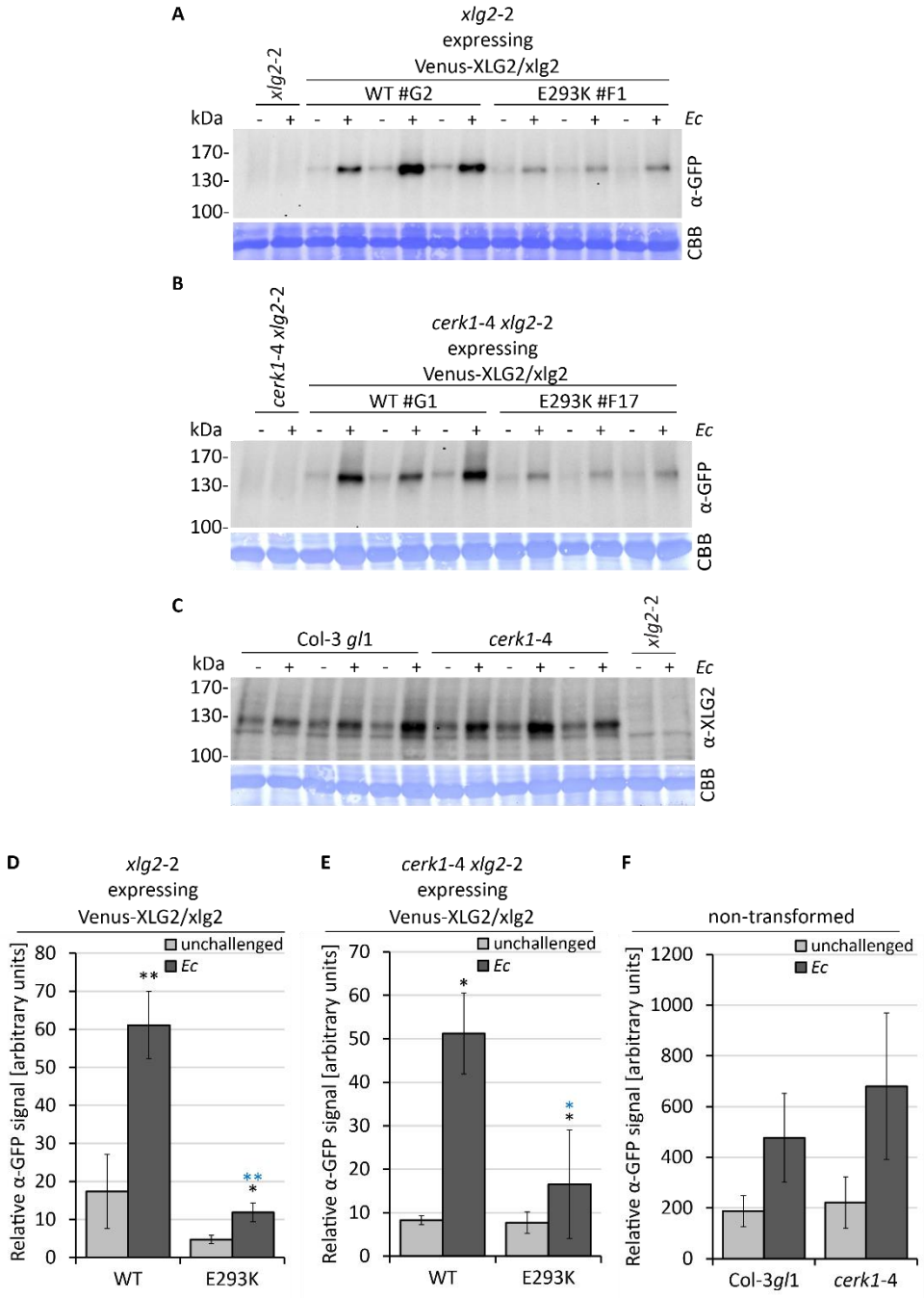

Fig. 17: XLG2 (E293K) protein levels increase upon pathogen attack.

Unchallenged (-) vs. inoculated (3dpi *Ec*, +) transgenic plants expressing Venus-XLG2 WT or Venus-xlg2 E293K in *xlg2*-2 **(A)**/ *cerk1*-4 *xlg2*-2 **(B)** and non-transformed Col-3 *gl*1 and *cerk1*-4 **(C)** were analysed via Western blotting using GFP/ XLG2-specific antibodies. One representative Western blot is shown respectively (experiment was repeated three times). CBB = Coomassie Brilliant Blue stained membrane.

Relative protein quantification of (Venus-)XLG2 WT/ xlg2 E293K via α-GFP in *xlg2*-2 **(D)** and in *cerk1*-4 *xlg2*-2 **(E)** as well as α-XLG2 in non-transformed Col-3 *gl*1/ *cerk1*-4 **(F)**. Data are means ± StDev of 3 plants of three independent lines. Signals were normalized to the background. Asterisks indicate significance - vs *Ec* (black) and compared to WT (blue). * P <0.05 ** P<0.01

3.1.3 The N-terminal E293K mutation renders XLG2 non-functional

cerk1-4 *Arabidopsis* develop a characteristic cell death phenotype upon infection with powdery mildews (Petutschnig et al. 2014). As described previously, xlg2 E293K was identified as suppressor mutation *xlg2*-3 for the *cerk1*-4 cell death phenotype, while Venus-XLG2 WT was already shown to be functional and able to complement *xlg2*-2 (Meusel 2016). To test if fusion proteins cause any phenotypic changes, transgenic *xlg2*-2 plants expressing Venus-XLG2 WT/ xlg2 E293K were inoculated with *Ec* together with non-transgenic control plants Col3-gl1, *cerk1*-4 and *xlg2*-2. Infection phenotypes were documented two weeks after fungal inoculation. No difference in overall rosette shape, cell death or fungal growth was observed between transgenic plants and non-transgenic *xlg2*-2 (Fig. 18 A). Accumulation of the fusion protein in the presented transgenic plants was confirmed (Fig. 18 B). Venus-XLG2 WT signals detected with the α-GFP antibody appeared stronger compared to xlg2 E293K. This observed difference was slightly weaker when using the XLG2-specific antibody, as observed before. While Venus-XLG2 WT ran slightly higher than expected but in the commonly observed range of SDS-gel-dependent variation, Venus-xlg2 E293K ran consistently lower than Venus-XLG2 WT.

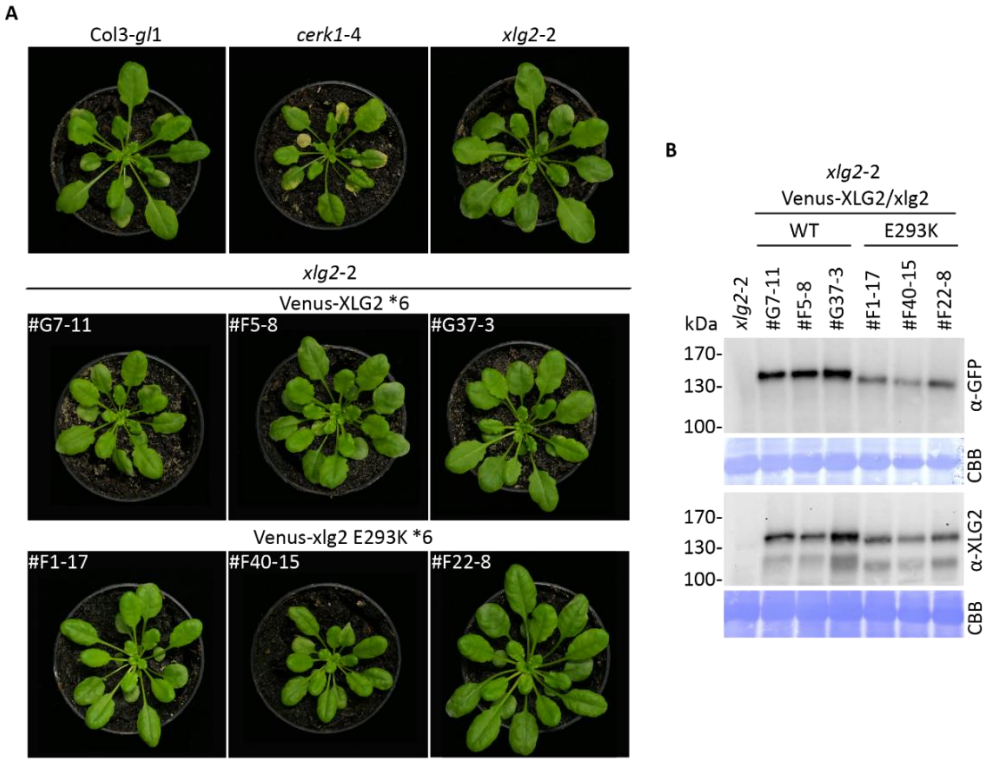

Fig. 18: Expression of Venus-XLG2 or Venus-xlg2 E293K did not affect growth of *xlg2*-2 upon infection.

(A) *xlg2*-2 expressing Venus-XLG2 or Venus-xlg2 E293K and non-transformed controls are shown. Macroscopic cell death and fungal growth was evaluated 2wpi with *Ec*. *Indicated number of independent lines per construct were analysed and three representative lines are shown. The plants presented in this Figure were inoculated with *Ec* together with the lines in Fig. 24, 30, 36, 42 and 49. Therefore, the same images for the controls Col-3 *gl*1, *cerk1*-4, *xlg2*-2 and Venus-XLG2 (WT) lines are shown. **(B)** For the lines presented, accumulation of Venus-XLG2/ xlg2 E293K fusion proteins was confirmed by Western blotting after phenotype documentation (3wpi *Ec*) using GFP/ XLG2-specific antibodies. CBB = Coomassie Brilliant Blue stained membrane.

cerk1-4 *xlg2*-2 plants expressing Venus-XLG2 WT (E293K) were used for functional characterization of fusion proteins and were inoculated with *Ec*. Two weeks after fungal inoculation infection phenotypes were documented (Fig. 19 A, Fig. S 12). Non-transgenic control plants Col3-*gl*1 and *cerk1*-4 *xlg2*-2 appeared with partially visible fungal growth and weak or no cell death. Plants homozygous for *cerk1*-4 developed increased cell death and no growth of fungal mycelium was observed. Expression of Venus-XLG2 WT in *cerk1*-4 *xlg2*-2 resulted in complementation of *xlg2*-2 with development of the *cerk1*-4 specific deregulated cell death phenotype. Venus-xlg2 E293K failed to complement *xlg2*-2. Full length expression of fusion proteins in the presented transgenic plants was confirmed via Western blotting (Fig. 19 B). The motility difference between Venus-XLG2 and xlg2 E293K was also observed in the presented transgenic *cerk1*-4 *xlg2*-2 plants.

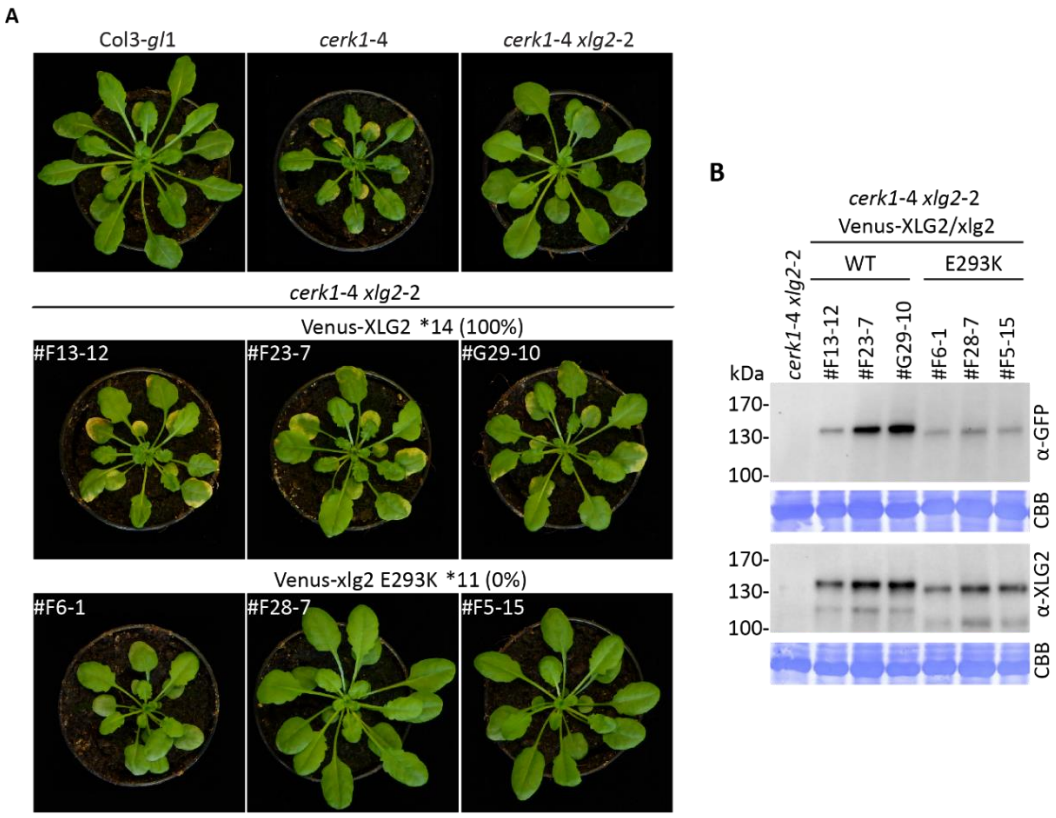

Fig. 19: Venus-xlg2 E293K is non-functional.

(A) *cerk1*-4 *xlg2*-2 expressing Venus-XLG2 or Venus-xlg2 E293K and non-transformed controls are shown. Macroscopic cell death and fungal growth was evaluated 2wpi with *Ec*. *Indicated number of independent lines per construct were analysed (complementation rate) and three representative lines are shown. The plants presented in this Figure were inoculated with *Ec* together with the lines in Fig. 50. Therefore, the same images for the controls Col-3 *gl*1, *cerk1*-4, *xlg2*-2 and Venus-XLG2 (WT) lines are shown. **(B)** For the lines presented, accumulation of Venus-XLG2 (E293K) fusion proteins was confirmed by Western blotting after phenotype documentation (3wpi *Ec*) using GFP/ XLG2-specific antibodies. CBB = Coomassie Brilliant Blue stained membrane.

The studies showed that Venus-xlg2 E293K failed to complement *xlg2*-2 and showed altered subcellular localization with predominantly nuclear signals. To investigate if this is a causal relation, more XLG2 and xlg2 variants with changed subcellular localization were analysed.

3.2 Changing XLG2 localization with viral NES and NLS signals does not impair its functionality

The fact that the Venus-xlg2 E293K variant with mainly nuclear localization was unable to complement *xlg2*-2 suggests that the cell periphery localization of XLG2 is important for *cerk1*-4 cell death signalling. In order to elucidate if the nuclear pool of XLG2 is necessary for development of the *cerk1*-4 cell death phenotype, Venus-XLG2 variants with altered subcellular localization were generated. To do so, two approaches were followed: First, an exportin 1-recognised nuclear export signal from HIV1 (NES) and importin α-recognized SV40 nuclear localization signal (NLS) (Heidrich et al. 2011) were fused to the N-terminus of Venus-XLG2 (NLS-/ NES-Venus-XLG2). To rule out possible side effects from additional sequences, the respective non-functional signal sequence mutant variants (nes/ nls) were used as controls (Heidrich et al. 2011). Unfortunately, the N-terminal fusion proteins nes-/ nls-Venus-XLG2 used as controls were not able to complement *xlg2*-2 when expressed in *cerk1*-4 *xlg2*-2 (data not shown). Due to unknown side effects of the N-terminal fusion, constructs with C-terminally attached -NES/ -nes and -NLS/ -nls sequences were generated as shown in (Fig. 20).

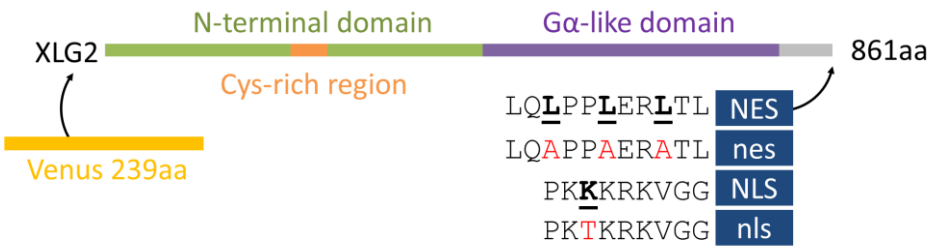

Fig. 20: Localization signal fusion variants XLG2-nes/ -NES/ -nls/ -NLS.

Exportin-recognized NES from HIV1 and importin α-recognized NLS from SV40 (Heidrich et al. 2011) were fused to the C-terminus of XLG2. The known non-functional mutant variants nes and nls were included as controls (Heidrich et al. 2011).

3.2.1 C-terminally fused -NES/ -NLS change the localization of XLG2

In order to investigate if the signal fusions change localization of XLG2, *N. benthamiana* was transformed and analysed via CLSM (Fig. 21). Indeed, Venus-XLG2-NLS showed constantly weaker cell periphery signals compared to Venus-XLG2 WT and the NES fusion drastically reduced nuclear accumulation of XLG2. The control signals -nes/ -nls did not change XLG2 localization.

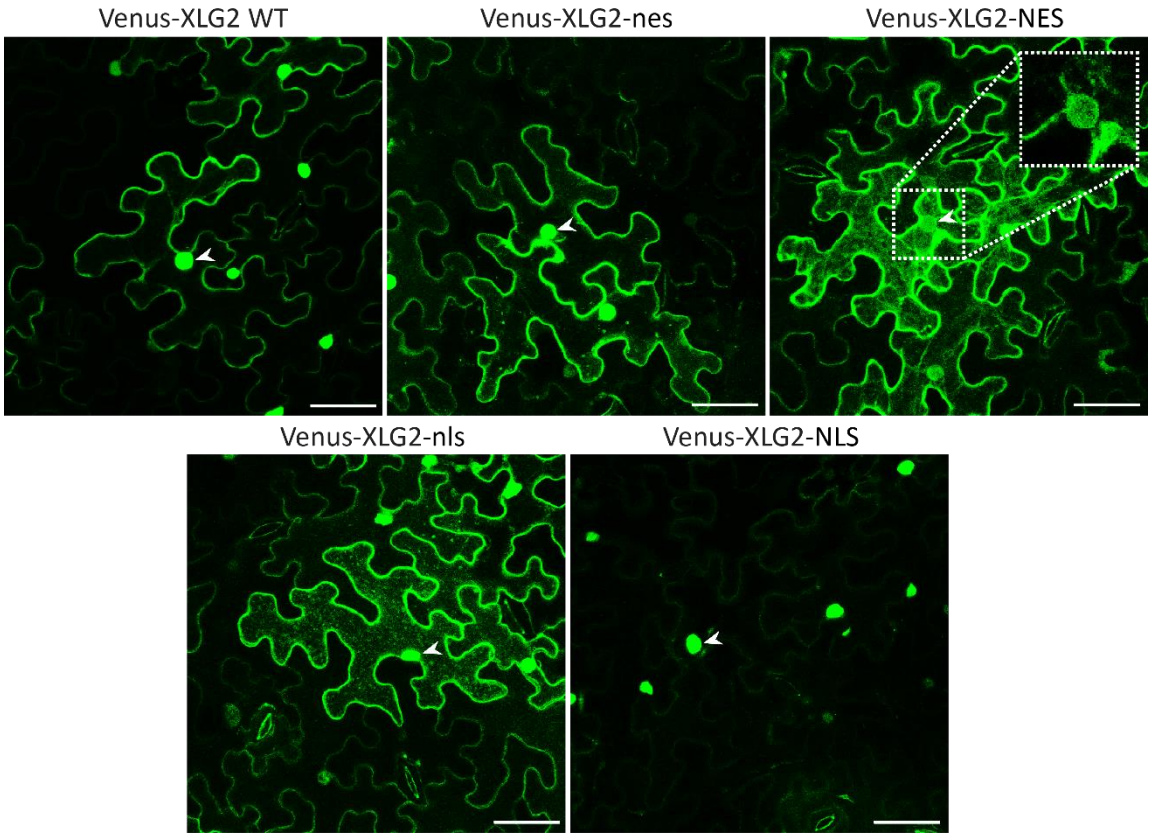

Fig. 21: C-terminally fused -NES/ -NLS change localization of XLG2 in *N. benthamiana*.

Venus-XLG2 WT and Venus-XLG2-NES/ -nes/ -NLS/ -nls were transformed into *N. benthamiana* via *A. tumefaciens* infiltration. CLSM was performed 3dpi. Representative images of three independent experiments are maximum projections of z stacks spanning the epidermal cell layer. For Venus-XLG2-NES an enlarged nucleus is presented as single plane (dashed white box). Example nuclei are marked by arrowheads. Scale bar = 50µm.

In order to further characterize subcellular localization of Venus-XLG2 fusion proteins, *xlg2*-2 and *cerk1*-4 *xlg2*-2 plants stably expressing Venus-XLG2-nes (8 independent *xlg2*-2 lines and 31 *cerk1*-4 *xlg2*-2 lines), Venus-XLG2-NES (10 *xlg2*-2 and 36 *cerk1*-4 *xlg2*-2 lines), Venus-XLG2-nls (12 *xlg2*-2 and 41 *cerk1*-4 *xlg2*-2 lines), and Venus-XLG2-NLS (12 *xlg2*-2 and 27 *cerk1*-4 *xlg2*-2 lines) were analysed via CLSM. Selected lines (≥ 8) were further analysed via CLSM before as well as one day post inoculation with *Ec*. In unchallenged tissue Venus-XLG2-nls/ -nes displayed uniform but relatively weak signals at

the cell periphery while upon infection signals increased for cell periphery and nuclei resembling Venus-XLG2 WT (Fig. 22 A, Fig. S 13). Subcellular localization of Venus-XLG2-NES resembled Venus-XLG2-nes in unchallenged tissue with weak cell periphery signals. In contrast, Venus-XLG2-NES did not accumulate inside the nucleus in *Ec* infected cells with higher fluorescence level. The C-terminal NLS resulted in constitutively labeled nuclei in pavement cells and only slightly reduced cell periphery signals compared to Venus-XLG2 WT. Signal intensities significantly increased upon infection for XLG2-NES at the cell periphery and for XLG2-NLS inside the nucleus (Fig. 22 B, C). In contrast to XLG2 WT, XLG2-NES did not accumulate significantly more to the nucleus and XLG2-NLS did not accumulate significantly more to the cell periphery upon infection. Similarly to the subcellular localization observed in transgenic *xlg2*-2 plants, for Venus-XLG2-NES mainly extranuclear signals were detected with strong cell periphery signals upon infection, while XLG2-NLS accumulated constitutively to the nucleus with retained basal levels of cell periphery localization (Fig. 23, Fig. S 14).

The significant reduction of Venus-XLG2-NES nuclear abundance indicates that the C-terminal viral NES fusion sufficiently drove XLG2 out of the nucleus. Further, Venus-XLG-NLS nuclear signals were observed throughout the leaves and cell periphery signals were significantly reduced after infection. This indicates that the added NLS sequence drove XLG2 successfully into the nucleus but was not sufficient to do so completely. Unknown strong interactions or modifications of XLG2 responsible for PM-attachment might be responsible for the inability of the C-terminal NLS to fully drive XLG2 inside the nucleus. No differences were observed between transgenic *xlg2*-2 (Fig. 22 A, Fig. S 13) and *cerk1*-4 *xlg2*-2 plants (Fig. 23, Fig. S 14).

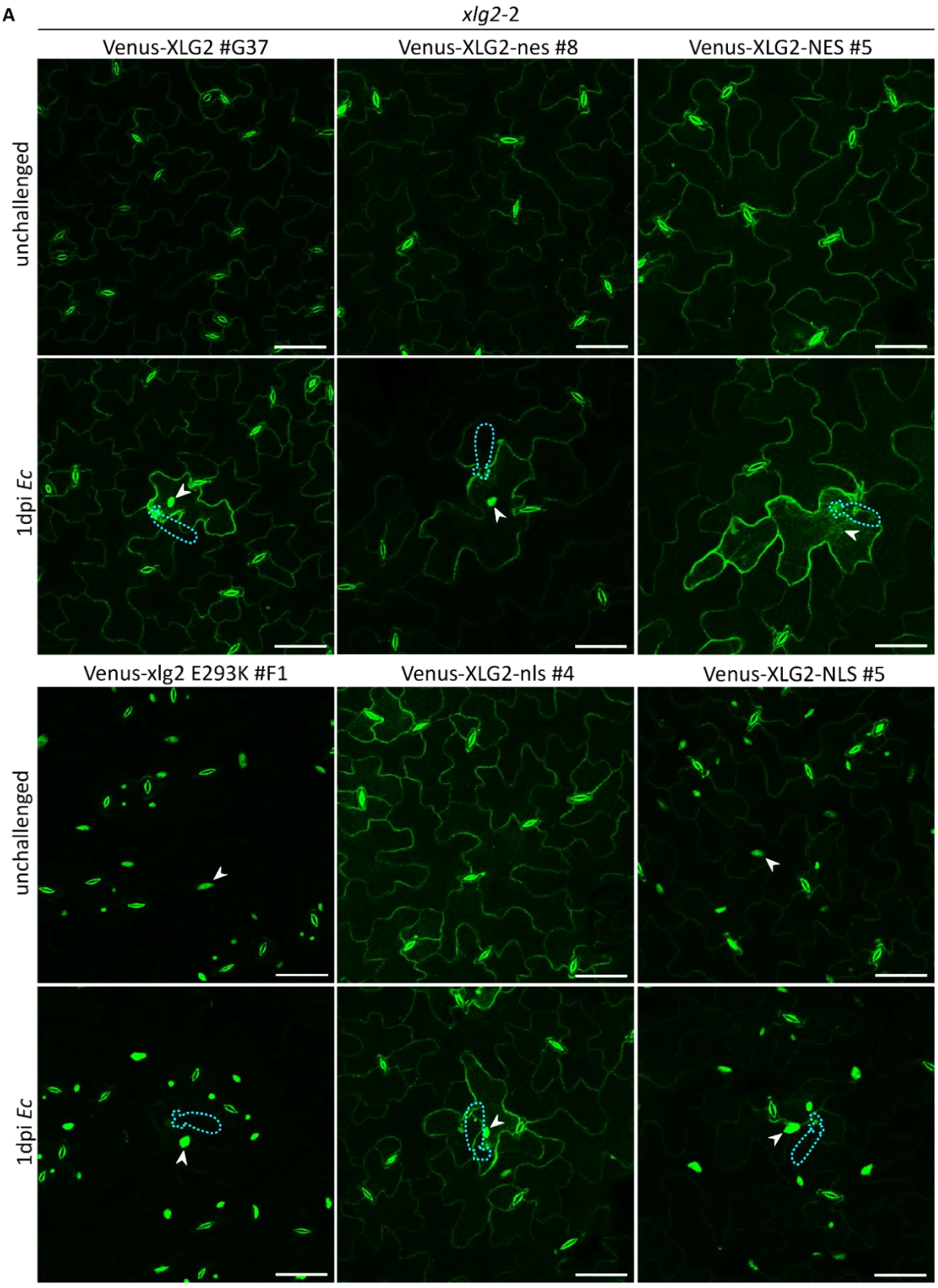
A
xlg2-2
Venus-XLG2 #G37
Venus-XLG2-nes #8
Venus-XLG2-NES #5
unchallenged
1dpi Ec
Venus-xlg2 E293K #F1
Venus-XLG2-nls #4
Venus-XLG2-NLS #5
unchallenged
1dpi Ec

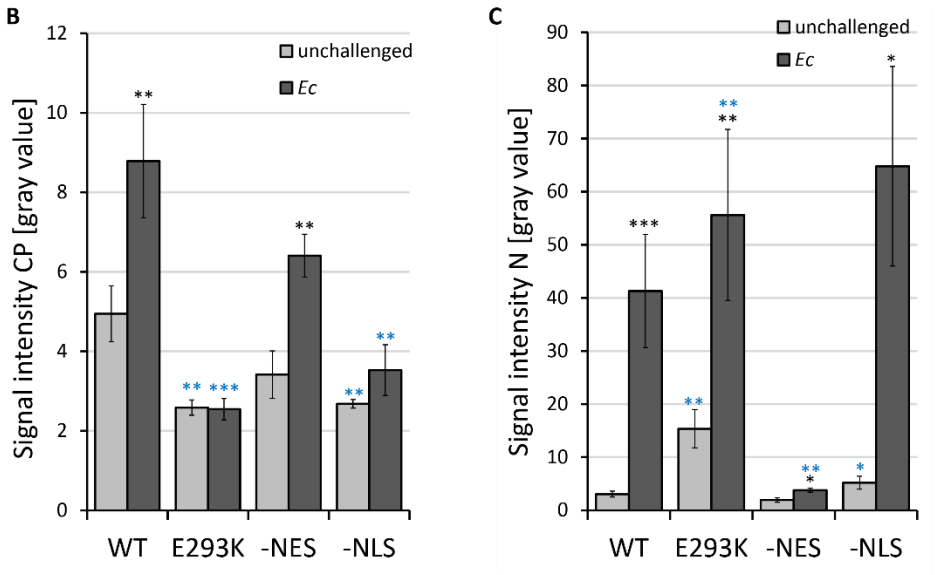

Fig. 22: C-terminally fused -NES/ -NLS change localization of XLG2 in *xlg2*-2.

(A) CLSM images of unchallenged vs. infected (1dpi *Ec*) representative lines expressing Venus-XLG2, Venus-xlg2 E293K and Venus-XLG2-nes/ -NES/ -nls/ -NLS are maximum projections of z stacks spanning the epidermal cell layer. Nuclei are marked by arrowheads and the positions of fungal spores at sites of attempted penetration are outlined by dashed blue lines. Scale bar = 50µm. Quantification of CLSM images of *xlg2*-2 expressing Venus-XLG2/ -NES/ -NLS and xlg2 E293K. Signal intensities at the cell periphery (CP) **(B)** and inside the nucleus (N) **(C)** of unchallenged and infected (1dpi *Ec*) cells were quantified. Data are means ± StDev of three independent lines (1-5 interaction sites of 1-3 plants were analysed per line). Asterisks indicate significance unchallenged vs infected (black) and compared to WT (blue). * P < 0.05, ** P < 0.01, *** P < 0.001

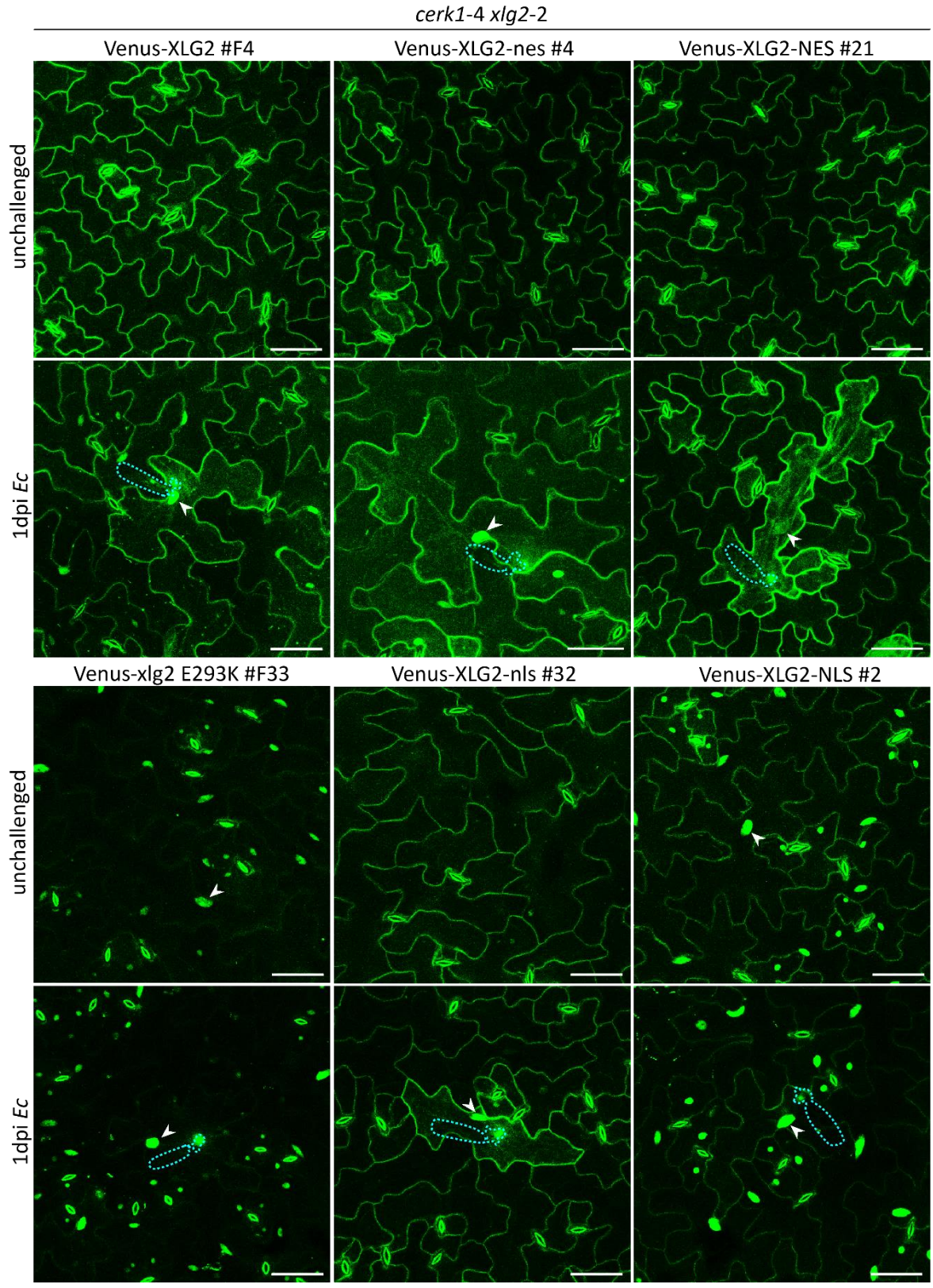

Fig. 23: C-terminally fused -NES/ -NLS change localization of XLG2 in *cerk1*-4 *xlg2*-2.

CLSM images of unchallenged vs. infected (1dpi *Ec*) representative lines expressing Venus-XLG2, Venus-xlg2 E293K or Venus-XLG2-nes / -NES / -nls/ -NLS are maximum projections of z stacks spanning the epidermal cell layer. Nuclei are marked by arrowheads and the positions of fungal spores at sites of attempted penetration are outlined by dashed blue lines. Scale bar = 50µm.

3.2.2 Venus-XLG2-NES/ -NLS fusion proteins complement *xlg2*-2

In order to test phenotypic effects and functionality of the differentially localized Venus-XLG2-NES/ -NLS fusion proteins including their WT-like localizing controls Venus-XLG2-nes/ -nls, transgenic *xlg2*-2 and *cerk1*-4 *xlg2*-2 were infected with Ec and the (complementation) phenotype was documented two weeks after infection. Transgenic *xlg2*-2 lines expressing Venus-XLG2 or Venus-XLG2-nes/ -NES/ -nls/ -NLS resemble the growth phenotype of non-transformed *xlg2*-2 and Col-3 *gl*1 after *Ec* infection (Fig. 24 A). Note the difference between the *cerk1*-4-dependent deregulated cell death phenotype without any fungal growth, in contrast to the occasionally visible weak cell death caused by extensive fungal growth on the other plants. All four Venus-XLG2-nes/ -NES/ -nls/ -NLS fusion proteins were able to confer macroscopically visible cell death to *cerk1*-4 *xlg2*-2 plants and no fungal growth was observed similar to Venus-XLG2 WT expressing plants (Fig. 25 A, Fig. S 15). These complementation phenotypes show that all four fusion constructs are functional regarding *cerk1*-4 cell death signalling. Western blotting confirmed presence of full length transgene and Venus-XLG2-nes/ -NES as well as Venus-XLG2-nls/ -NLS ran slightly higher than Venus-XLG2 due to the C-terminal fusion sequence (Fig. 24 B, Fig. 25 B, Fig. S 15).

These results indicate that the nuclear pool of XLG2 is not necessary for *cerk1*-4-dependent cell death signalling. Unfortunately, Venus-XLG2-NLS retained plasma membrane localization of XLG2. A constitutive nuclear localization variant is nevertheless valuable for analyzing the nuclear function of XLG2 in general. In order to further elucidate whether cell periphery localization of XLG2 is needed for *cerk1*-4 cell death signalling, more xlg2 mutant variants were generated based on bioinformatic prediction tools and experimental data concerning internal XLG NES and NLS sites.

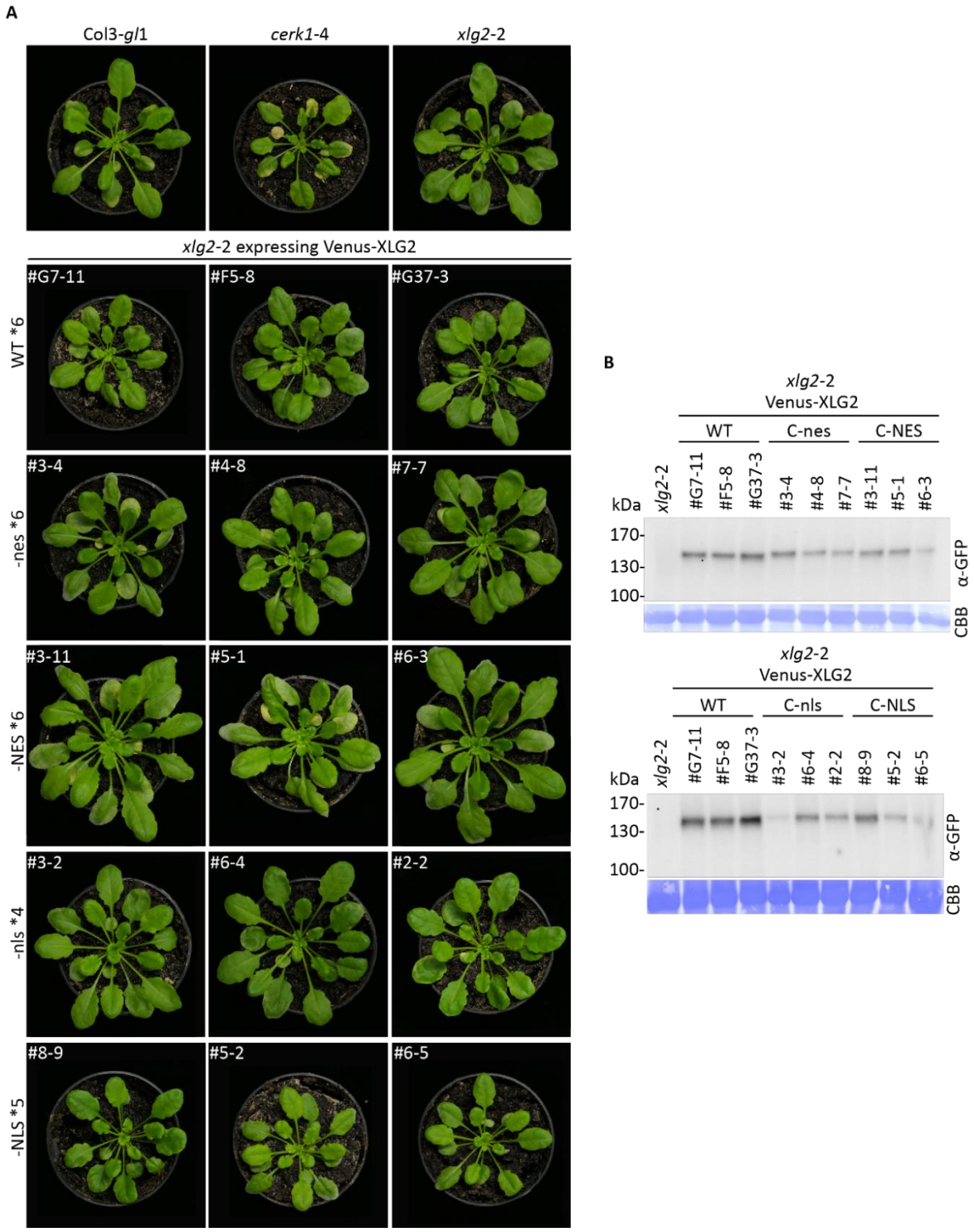

Fig. 24: Expression of Venus-XLG2-NES/ -NLS fusion proteins in *xlg2*-2 did not affect growth upon infection.

(A) *xlg2*-2 expressing Venus-XLG2 WT or Venus-XLG2-nes/ -NES/ -nls/ -NLS and non-transformed controls were evaluated 2wpi with *Ec* for macroscopic cell death and fungal growth. *Indicated number of independent lines per construct were analysed and three representative lines are shown. The plants presented in this Figure were inoculated with *Ec* together with the lines in Fig. 18, 30, 36, 42 and 49. Therefore, the same images for the controls Col-3 *gl*1, *cerk1*-4, *xlg2*-2 and Venus-XLG2 (WT) lines are shown. **(B)** For the lines presented, accumulation of Venus-XLG2 or Venus-XLG2-nes/ -NES/ -nls/ -NLS fusion proteins was confirmed by Western blotting after phenotype documentation (3wpi *Ec*) using GFP/ XLG2-specific antibodies. CBB = Coomassie Brilliant Blue stained membrane.

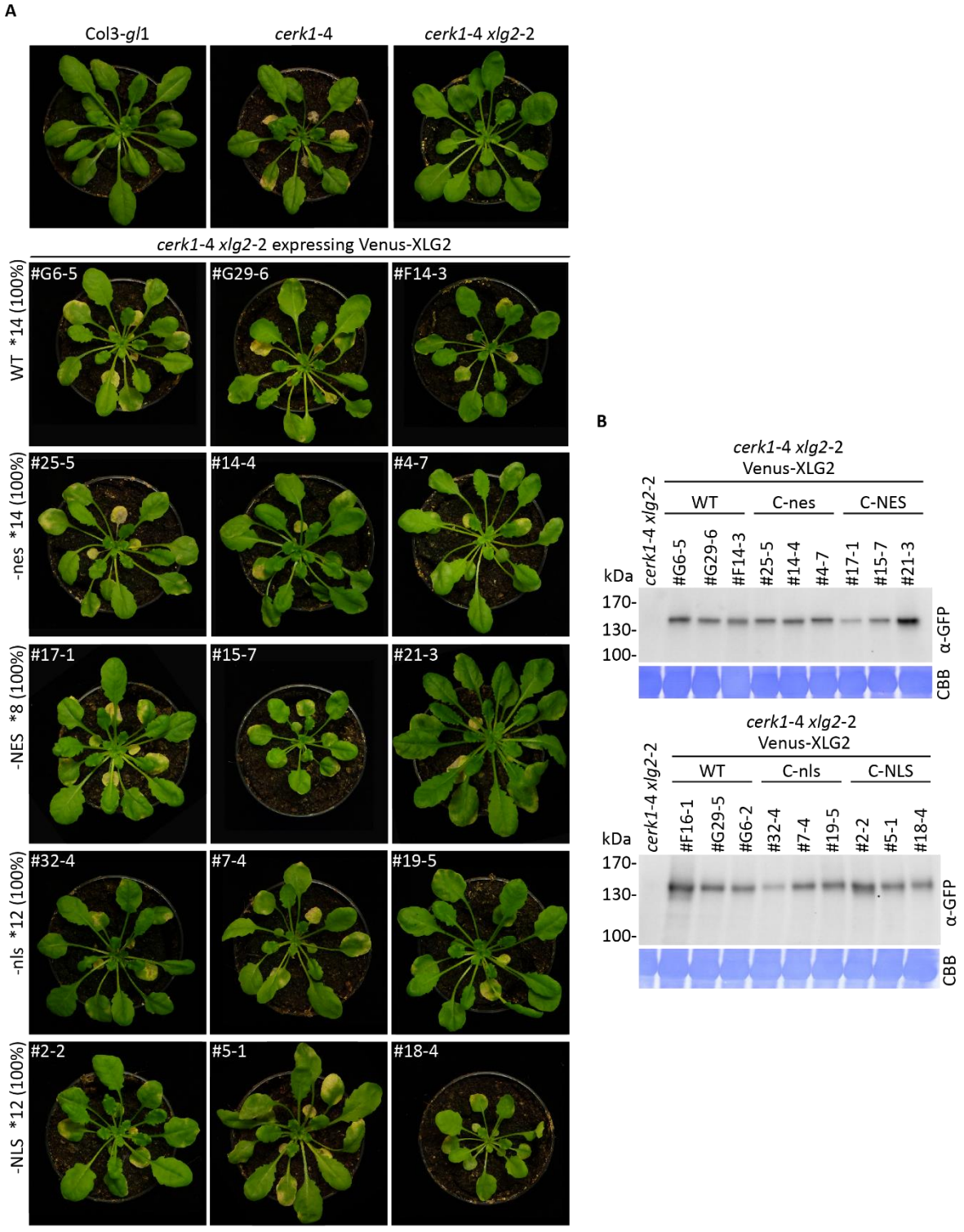

Fig. 25: C-terminal NES/ nes/ NLS/ nls XLG2 fusion proteins complement *cerk1*-4 *xlg2*-2.

(A) *cerk1*-4 *xlg2*-2 expressing Venus-XLG2 WT or Venus-XLG2-nes/ -NES/ -nls/ -NLS and non-transformed controls were evaluated 2wpi with *Ec* for macroscopic cell death and fungal growth. *Indicated number of independent lines per construct were analysed (complementation rate) and three representative lines are shown. The plants presented in this Figure were inoculated with *Ec* together with the lines in Fig. 31 and Fig. 43. Therefore, the same images for the controls Col-3 *gl*1, *cerk1*-4, *xlg2*-2 and Venus-XLG2 (WT) lines are shown. **(B)** For the lines presented, accumulation of Venus-XLG2 or Venus-XLG2-nes/ -NES/ -nls/ -NLS fusion proteins was confirmed by Western blotting after phenotype documentation (3wpi *Ec*) using GFP-specific antibody. CBB = Coomassie Brilliant Blue stained membrane.

3.3 Two localization signal mutations (nes387, nls426) drastically alter the localization of XLG2

Several aspects of the previous results led to the necessity of analyzing more Venus-xlg2 mutant variants. The C-terminally attached NLS did not fully remove XLG2 from the plasma membrane. Accordingly, additional mutant variants with reduced cell periphery localization would help to test the hypothesis, that the cell periphery locallization of XLG2 is needed for *cerk1*-4-dependent cell death signalling. Additional nuclear exclusion variants would help to confirm the conclusion drawn from the Venus-XLG2-NES expressing *Arabidopsis* phenotype data, that the nuclear pool of XLG2 is dispensable for development of the *cerk1*-4 phenotype. Using LocNES (Xu et al. 2015) and cNLS Mapper (Kosugi et al. 2009) prediction tools as well as experimental data information (Chakravorty et al. 2015) that described localization signals found in XLGs, the most promising internal NLS and one NES were chosen for mutagenesis. Localization signals were annotated according to the amino acid number of the predicted starting position. An overview of the localization signal positions within the domain organization of XLG2 and mutated amino acids in either xlg2 nes387 or xlg2 nls426 is presented in Fig. 26. The XLG2 NLS at position 426aa was previously experimentally tested and confirmed to be functional (Chakravorty et al. 2015). Therefore, XLG2 NLS426 was mutated in this study to resemble the XLG1 sequence which has a cNLS Mapper score below 2 and, thus, is considered inactive. In addition, the XLG1 sequence at this homologous position was previously experimentally confirmed to not function as NLS (Chakravorty et al. 2015). A functional NES was identified for XLG3 by the same group and, therefore, the potential NES in XLG2 at the homologous position 387aa was mutated.

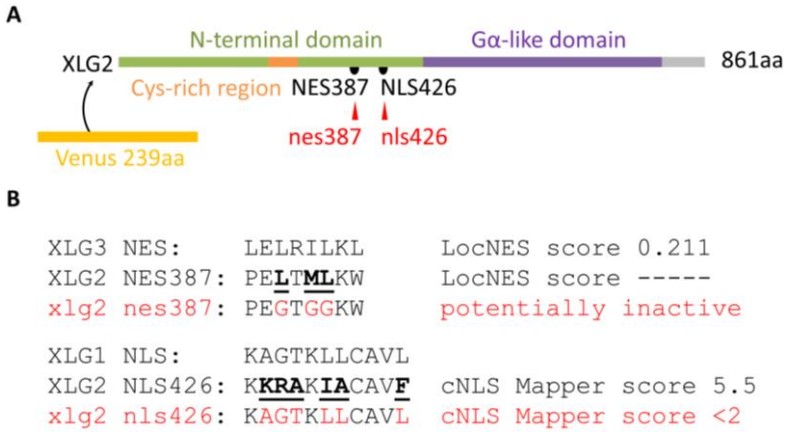

Fig. 26: Translocation signal mutations xlg2 nes387 and xlg2 nls426.

(A) One known XLG2 nuclear localization signal (NLS426) and another potential nuclear export signal (NES387) which are both located between of the cys-rich region and the Gα-like domain are labeled in black and were targeted for mutagenesis. **(B)** xlg2 nes387 and nls426 mutations potentially result in inactive localization signals according to the previously published XLG localization signal mutant information (Chakravorty et al. 2015) and LocNES (Xu et al. 2015)/ cNLS Mapper prediction (Kosugi et al. 2009). NLS Mapper score info: 1 - 2 cytoplasm, 3 - 6 equally localized to nucleus and cytoplasm, 7 - 8 cytoplasm and stronger to nucleus, >9 exclusively nuclear (http://nls-mapper.iab.keio.ac.jp/cgi-bin/NLS_Mapper_help.cgi#appendix).

3.3.1 The localization of XLG2 is changed upon nes387/ nls426 mutations

Transiently expressed Venus-XLG2 WT showed strong cell periphery and nuclear signals and occasionally visible cytoplasmic strands in *N. benthamiana* (Fig. 27). Venus-xlg2 nes387 showed similarly strong labeled nuclei but reduced cell periphery signals and Venus-xlg2 nls426 showed highly reduced nuclear accumulation in this transient assay.

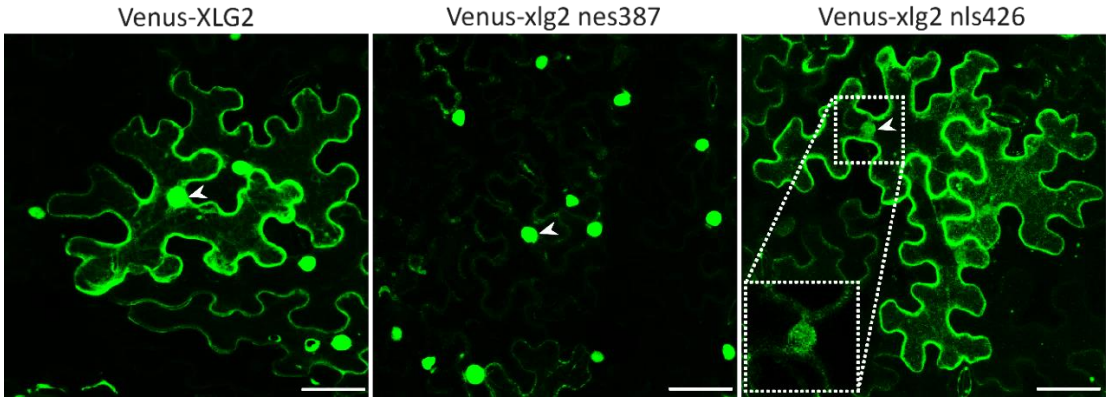

Fig. 27: The nes387 and nls426 mutations change the localization of XLG2 in *N. benthamiana*.
Venus-XLG2 (WT), Venus-xlg2 nes387 and Venus-xlg2 nls426 were transformed into *N. benthamiana* via *A. tumefaciens* infiltration. CLSM was performed 3dpi. Representative images of three independent experiments are maximum projections of z stacks spanning the epidermal cell layer. For Venus-xlg2 nls426 an enlarged nucleus is presented as single plane image (dashed white box). Arrowheads mark example nuclei. Scale bar = 50µm.

These results indicated that the mutations within NES387 and NLS426 indeed caused a change in XLG2 localization. Transgenic plants expressing either Venus-xlg2 nes387 (16 lines in *xlg2*-2 and 54 lines in *cerk1*-4 *xlg2*-2) or Venus-xlg2 nls426 (with 15 and 25 analysed lines in *xlg2*-2 and *cerk1*-4 *xlg2*-2 respectively) were initially analysed via CLSM. A selection of ≥ 8 independent lines was then analysed in more detail before and one day after infection with *Ec*. Venus-xlg2 nes387 cell periphery signals were drastically reduced and nuclear accumulation occurred independently from pathogen challenge while upon infection nuclear signals were elevated in *xlg2*-2 (Fig. 28 A, Fig. S 16) and *cerk1*-4 *xlg2*-2 (Fig. 29, Fig. S 17). Venus-xlg2 nls426 signals were undistinguishable from Venus-XLG2 WT in unchallenged tissue. However, Venus-xlg2 nls426 showed lower nuclear accumulation in infected pavement cells compared to Venus-XLG2 WT in *xlg2*-2 (Fig. 28 A, Fig. S 16) and *cerk1*-4 *xlg2*-2 (Fig. 29, Fig. S 17). The signal intensities increased significantly for Venus-xlg2 nes387 and nls426 upon pathogen challenge (Fig. 28 B, C). The changed localization dynamics of Venus-xlg2 nes387 (with reduced cell periphery localization) and nls426 (reduced nuclear accumulation) were significant compared to XLG2 WT. This study confirms that the analysed internal nuclear export (NES387) and nuclear localization (NLS426) signals are involved in XLG2 nuclear translocation and, therefore, functional localization signals.

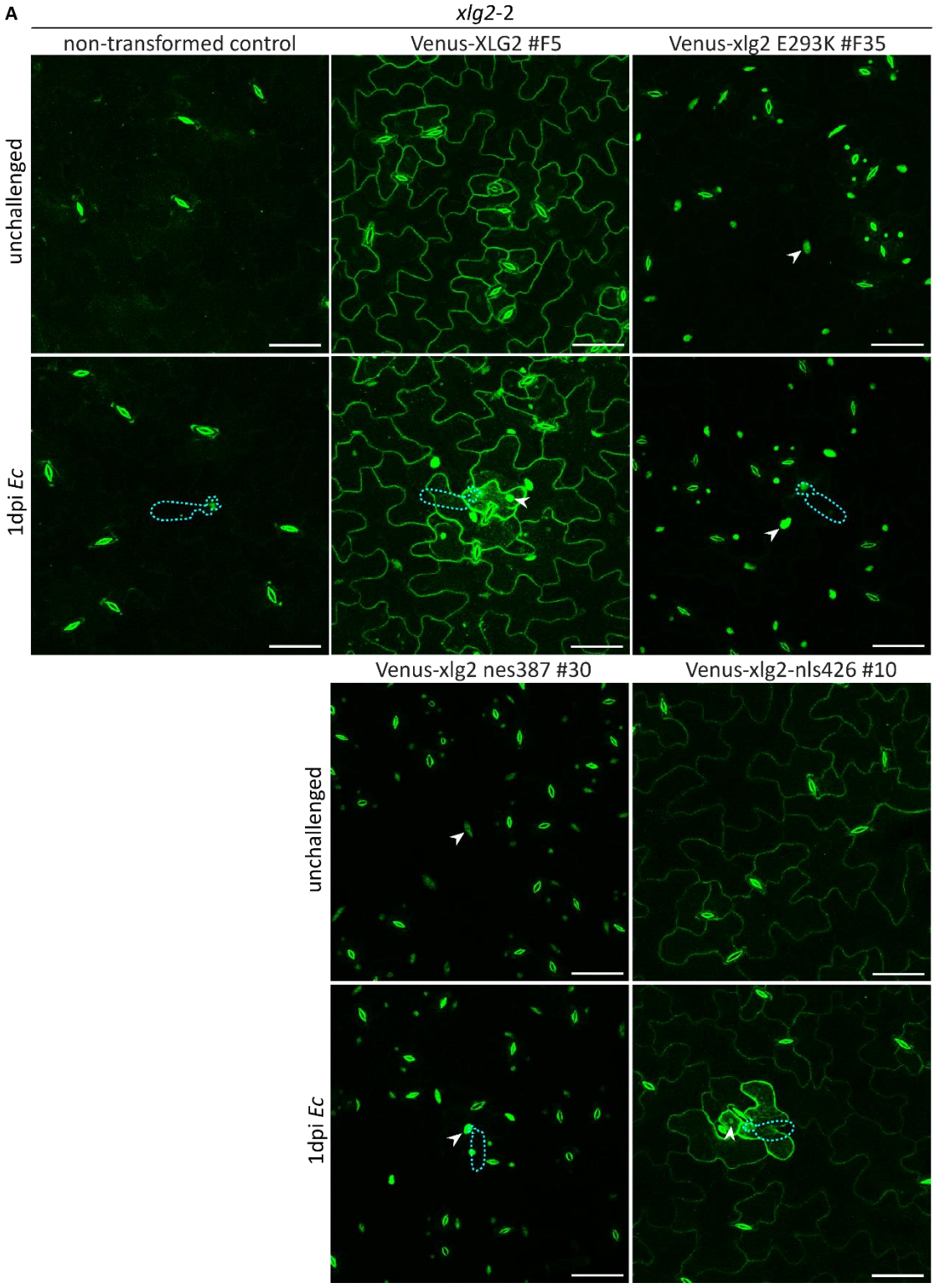
A
xlg2-2
non-transformed control
Venus-XLG2 #F5
Venus-xlg2 E293K #F35
unchallenged
1dpi Ec
Venus-xlg2 nes387 #30
Venus-xlg2-nls426 #10
unchallenged
1dpi Ec

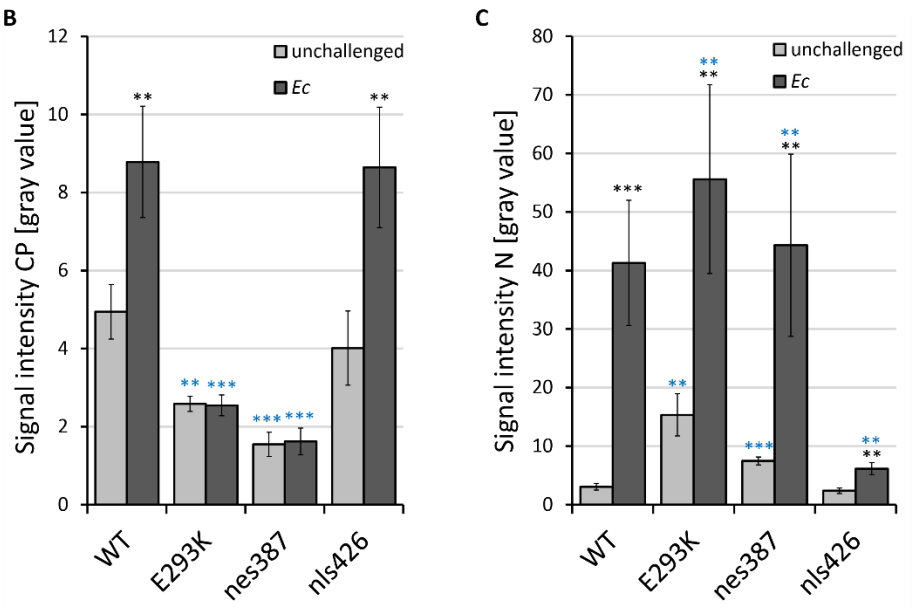

Fig. 28: The nes387 and nls426 mutations change the localization of XLG2 in *xlg2*-2.

(A) CLSM images of unchallenged vs. infected (1dpi *Ec*) representative lines expressing Venus-XLG2, Venus-xlg2 E293K, Venus-xlg2 nes387 and Venus-xlg2 nls426 in *xlg2*-2 are maximum projections of z stacks spanning the epidermal cell layer. Nuclei are marked by arrowheads and the positions of fungal spores with appressorium are outlined. Scale bar = 50µm.

Quantification of CLSM images of *xlg2*-2 expressing Venus-XLG2/ xlg2 E293K/ xlg2 nes387/ xlg2 nls426. Signal intensities at the cell periphery (CP) **(B)** and inside the nucleus (N) **(C)** of unchallenged and infected (1dpi *Ec*) cells were quantified. Data are means ± StDev of four independent lines (1-5 interaction sites of 1-3 plants were analysed per line). Asterisks indicate significance unchallenged vs infected (black) and compared to WT (blue). ** P < 0.01, *** P < 0.001

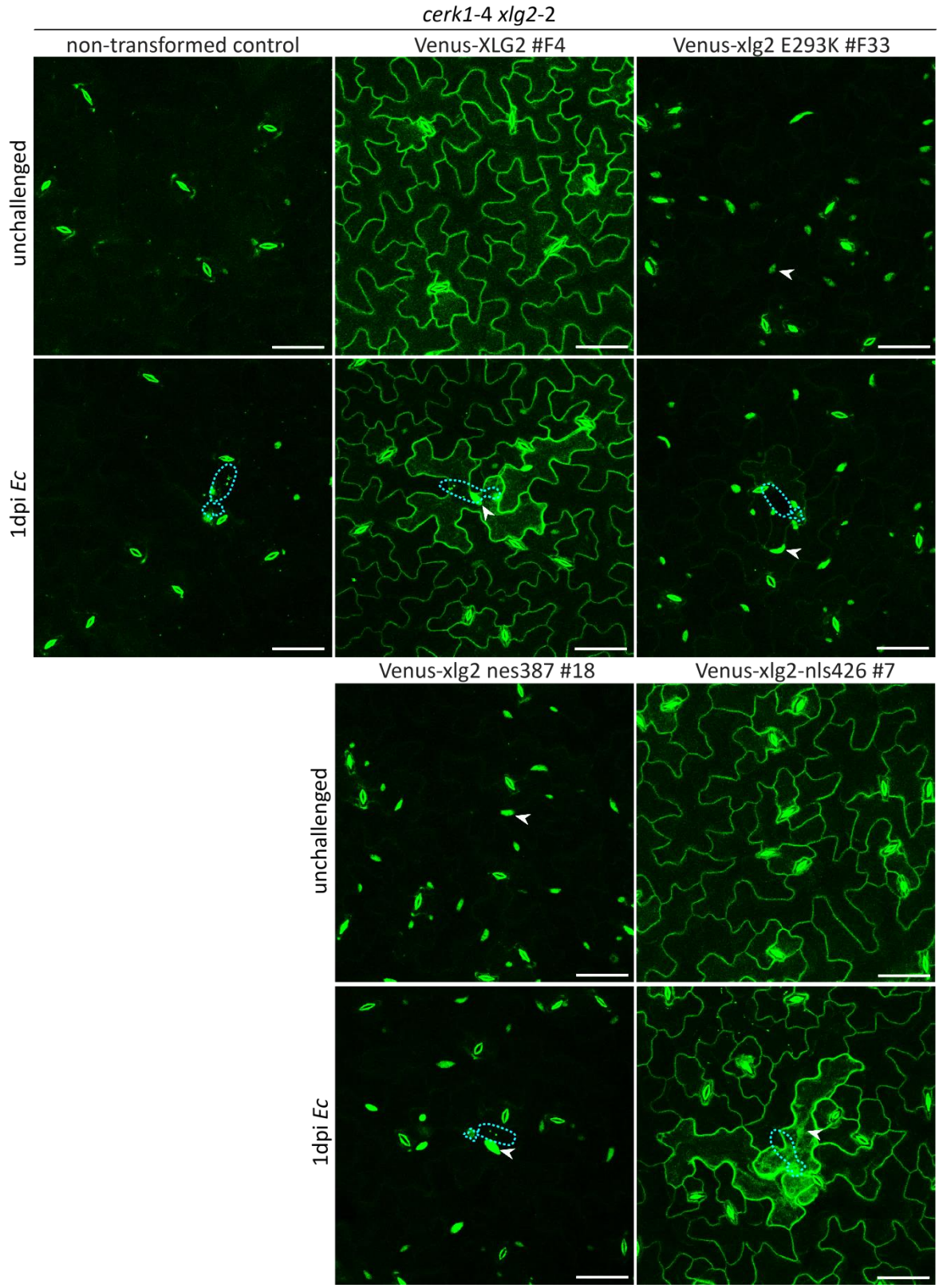

Fig. 29: The nes387 and nls426 mutations change the localization of XLG2 in *cerk1*-4 *xlg2*-2.

CLSM images of unchallenged vs. infected (1dpi *Ec*) representative lines expressing Venus-XLG2, Venus-xlg2 E293K, Venus-xlg2 nes387 and Venus-xlg2 nls426 in *cerk1*-4 *xlg2*-2 are maximum projections of z stacks spanning the epidermal cell layer. Nuclei are marked by arrowheads and the positions of fungal spores with appressorium are outlined. Scale bar = 50µm.

3.3.2 The nes387 mutation renders XLG2 non-functional while the nls426 mutation does not impair *cerk1*-4 cell death signalling of XLG2

In order to test phenotypic effects and functionality of Venus-xlg2 nes387 and Venus-xlg2 nls426 transgenic *xlg2*-2 and *cerk1*-4 *xlg2*-2 were infected with *Ec* and the (complementation) phenotype was documented two weeks after infection. Expression of Venus-xlg2 nes387 and Venus-xlg2 nls426 did not influence the *xlg2*-2 phenotype (Fig. 30 A). A non-functional xlg2 is unable to complement *xlg2*-2. Venus-xlg2 nes387 expressing *cerk1*-4 *xlg2*-2 showed visible fungal growth and no cell death in contrast to the *cerk1*-4 control with absence of fungal growth and increased cell death (Fig. 31 A, Fig. S 12) and accumulation of the full length protein was confirmed (Fig. 30 B). This indicates that Venus-xlg2 nes387 is non-functional in *cerk1*-4 cell death signalling. In contrast, Venus-xlg2 nls426 expression in *cerk1*-4 *xlg2*-2 results in development of the *cerk1*-4 phenotype. The complementation of *xlg2*-2 by XLG2 which harbors the nls426 mutation indicates that this nuclear exclusion xlg2 mutant variant is still functional in *cerk1*-4 cell death signalling. Full length protein expression was confirmed for the analysed transgenic lines (Fig. 31 B, Fig. S 12). Interestingly, Venus-xlg2 nes387 and Venus-xlg2 E293K show the same motility difference in Western Blot in comparison to Venus-XLG2 WT/ xlg2 nls426 (Fig. 30 B, Fig. 31 C, Fig. S 12). The signal intensities for Venus-xlg2 nes387 were weaker compared to Venus-XLG2 WT/ xlg2 nls426 using the α-GFP antibody. This difference was less pronounced, but still present, when using the α-XLG2 antibody.

This study shows that xlg2 E293K and xlg2 nes387 share the drastic loss of cell periphery localization and enhanced nuclear accumulation independent from fungal attack. Further, xlg2 E293K and xlg2 nes387 share the inability to restore the *cerk1*-4 phenotype in *cerk1*-4 *xlg2*-2 and a motility difference in Western Blot compared to XLG2 WT. This and the proximity of these two mutated sites gives rise to the suggestion that the inability to complement *xlg2*-2 and changed localization of xlg2 E293K and xlg2 nes387 likely be connected to the same cause. The cause could be loss of specific protein interactions or post-translational modifications. Conclusive from this study is that nuclear localized XLG2 is dispensable for *cerk1*-4 cell death while loss of plasma membrane localized XLG2 causes loss of *cerk1*-4 cell death signalling.

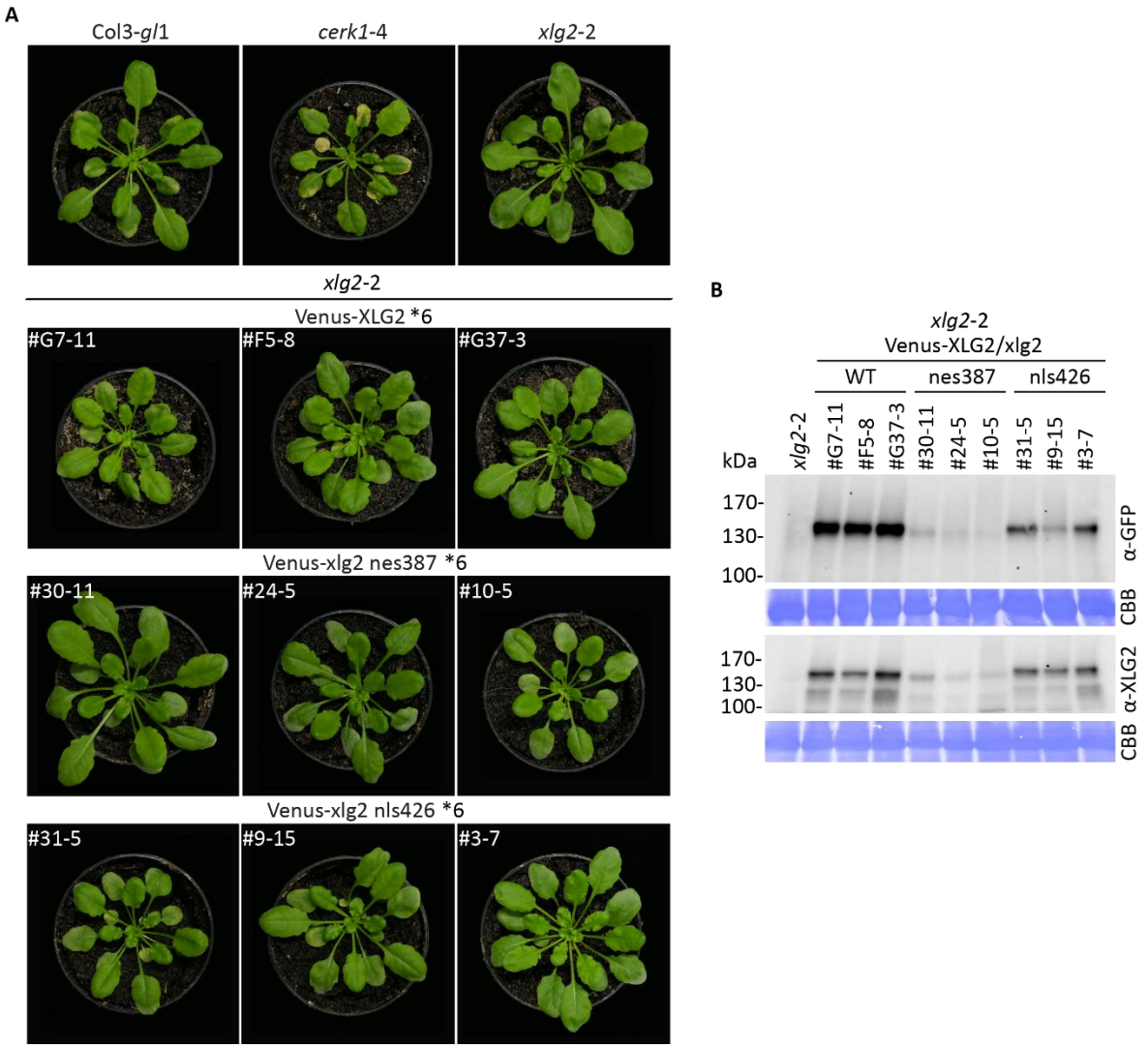

Fig. 30: Expression of Venus-xlg2 nes387/ nls426 in *xlg2*-2 did not affect *xlg2*-2 growth upon infection.

(A) *xlg2*-2 expressing Venus-XLG2, Venus-xlg2 nes387 or Venus-xlg2 nls426 and non-transformed controls are shown. Macroscopic cell death and fungal growth was evaluated 2wpi with *Ec*. *Indicated number of independent lines per construct were analysed and three representative lines are shown. The plants presented in this Figure were inoculated with *Ec* together with the lines in Fig. 18, 24, 36, 42 and 49. Therefore, the same images for the controls Col-3 *gl*1, *cerk1*-4, *xlg2*-2 and Venus-XLG2 (WT) lines are shown. **(B)** For the lines presented accumulation of the Venus-XLG2 and Venus-xlg2 nes387/ nls426 fusion proteins was confirmed by Western blotting after phenotype documentation (3wpi *Ec*) using GFP/ XLG2-specific antibodies. CBB = Coomassie Brilliant Blue stained membrane.

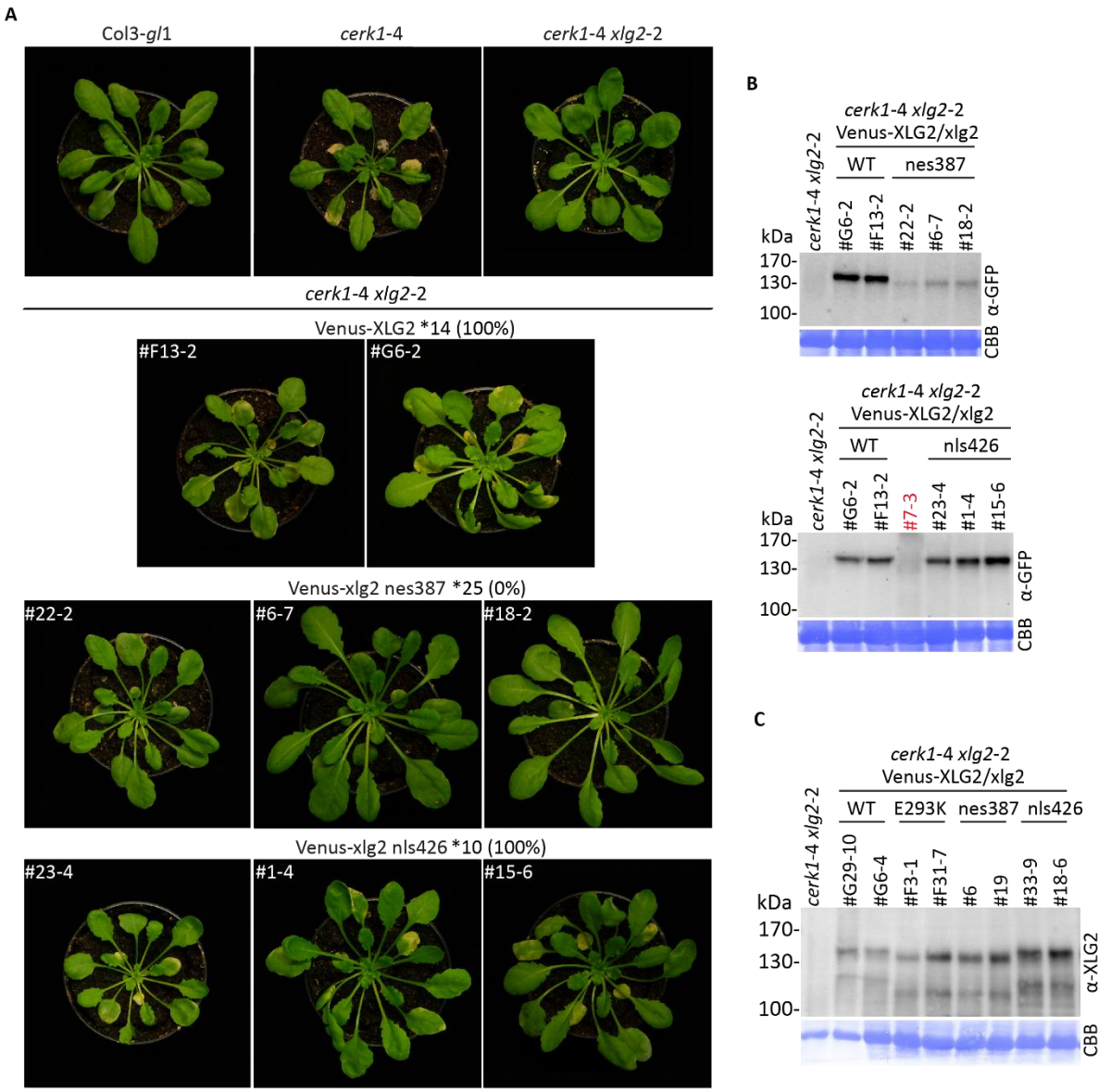

Fig. 31: Venus-xlg2 nls426 complements *cerk1*-4 *xlg2*-2 while Venus-xlg2 nes387 is non-functional.

(A) *cerk1*-4 *xlg2*-2 expressing Venus-XLG2, Venus-xlg2 nes387 or Venus-xlg2 nls426 and non-transformed controls are shown. Macroscopic cell death and fungal growth was evaluated 2wpi with *Ec*. *Indicated number of independent lines per construct were analysed (complementation rate) and three representative lines are shown. The plants presented in this Figure were inoculated with *Ec* together with the lines in Fig. 25 and 43. Therefore, the same images for the controls Col-3 *gl*1, *cerk1*-4 and *xlg2*-2 are shown. **(B)** For the lines presented, accumulation of the Venus-XLG2 or Venus-xlg2 nes387/ nls426 fusion proteins was confirmed by Western blotting after phenotype documentation (3wpi *Ec*) using GFP/ XLG2-specific antibodies. **(C)** Western Blot shows samples for Venus-XLG2 WT, Venus-xlg2 E293K, Venus-xlg2 nes387 and Venus-xlg2 nls426 (3wpi *Ec*) as comparison for the apparent molecular mass. CBB = Coomassie Brilliant Blue stained membrane.

3.4 Another localization signal mutation (NLS275 KR-AA) does not change the localization or functionality of XLG2

Several N-terminal XLG NLSs were predicted or experimentally described before (Chakravorty, *et al*. 2015; Ding *et al*. 2009; cNLS Mapper). The predicted XLG2 NLS275 was found to be perhaps relevant for correct localization of XLG2, due to the observation that the E293K mutation within this sequence resulted in enhanced nuclear localization and an enhanced cNLS Mapper score for the predicted NLS275. However, the causative connection between the E293K mutation and the potentially enhanced NLS275 is not known. Therefore, two basic amino acids were changed into alanine in order to weaken the predicted bipartite NLS at position 275 (K278A, R279A referred to shortly as KR-AA) with a score of 3.3 (not completely inactive, still cytosolic and nuclear distribution) (Fig. 32 C). This mutation was also analysed in combination with the E293K mutation (KR-AA+E293K). The E293K mutation changes the NLS275 score from 6.7 (cytosolic and more nuclear distribution) up to 8.8 (mainly nuclear localization) and reduces to 4.0 (cytosolic and nuclear distribution) in combination with KR-AA according to the cNLS Mapper predictions. The E293K mutation was combined with the KR-AA mutation to test whether the observed localization changes can be reversed.

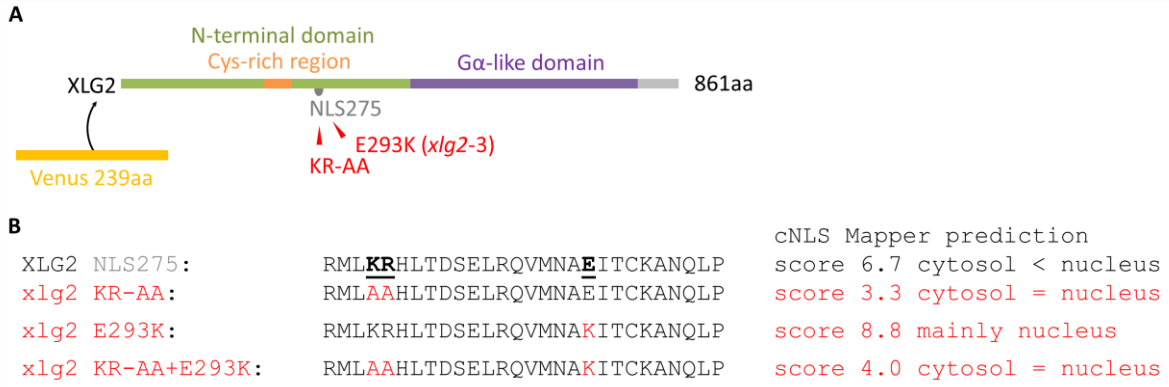

Fig. 32: Mutation of NLS275.

(A) Predicted N-terminal XLG2 nuclear localization signal NLS275 located between the cys-rich region and the Gα-like region (labeled in grey). **(B)** NLS275 was mutated at position K278 and R279 to alanine (KR-AA) to potentially reduce nuclear accumulation of XLG2. This KR-AA mutation was also combined with E293K to test if a compensation is possible. cNLS Mapper prediction (Kosugi et al. 2009).

3.4.1 The KR-AA mutation does not change the localization of XLG2

Transient expression of Venus-xlg2 KR-AA and Venus-xlg2 KR-AA+E293K in *N. benthamiana* was analysed via CLSM (Fig. 33). The KR-AA mutation alone did not have any impact on nuclear accumulation of XLG2. Interestingly, the combined KR-AA+E293K mutation still resembled the single E293K mutation with highly reduced cell periphery signals compared to Venus-XLG2.

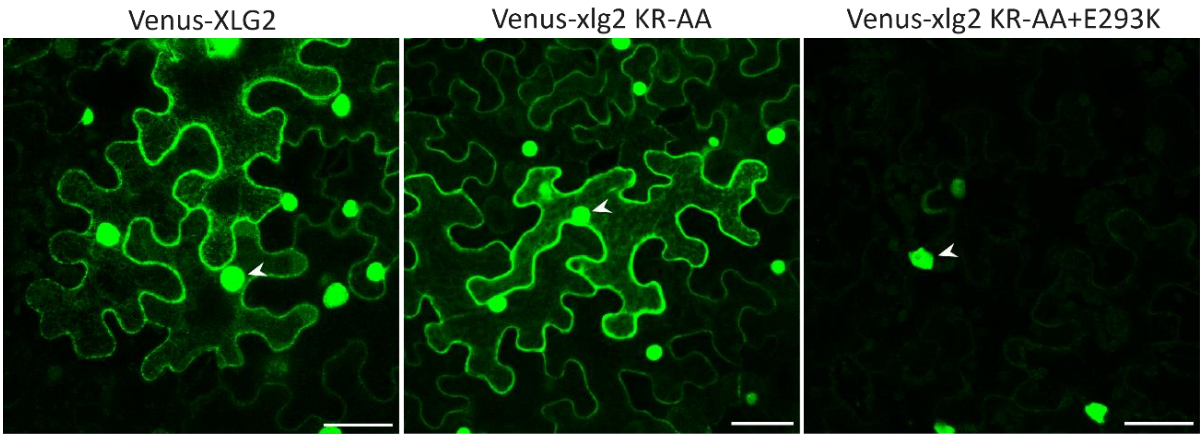

Fig. 33: The KR-AA mutation did not change localization of XLG2 in *N. benthamiana*.

Venus-XLG2 WT and Venus-xlg2 KR-AA (potentially weaker)/ xlg2 KR-AA+E293K (potentially compensated) were transformed into *N. benthamiana* via *A. tumefaciens* infiltration. CLSM was performed 3dpi. Representative images of two independent experiments are maximum projections of z stacks spanning the epidermal cell layer. Example nuclei are marked by arrowheads. Scale bar = 50µm.

Plants expressing Venus-xlg2 KR-AA (8 independent lines in *xlg2*-2 and 16 lines in *cerk1*-4 *xlg2*-2) as well as Venus-xlg2 KR-AA+E293K (10 *xlg2*-2 lines and 13 *cerk1*-4 *xlg2*-2 lines) were analysed next. Venus-xlg2 KR-AA localized to the cell periphery in unchallenged tissue and accumulated within the nucleus upon infection with *Ec* or *Bgh* in *xlg2*-2 (Fig. 34) and *cerk1*-4 *xlg2*-2 (Fig. 35) similar to WT XLG2. In contrast, most analysed Venus-xlg2 KR-AA+E293K expressing lines showed constitutive nuclear signals resembling Venus-xlg2 E293K.

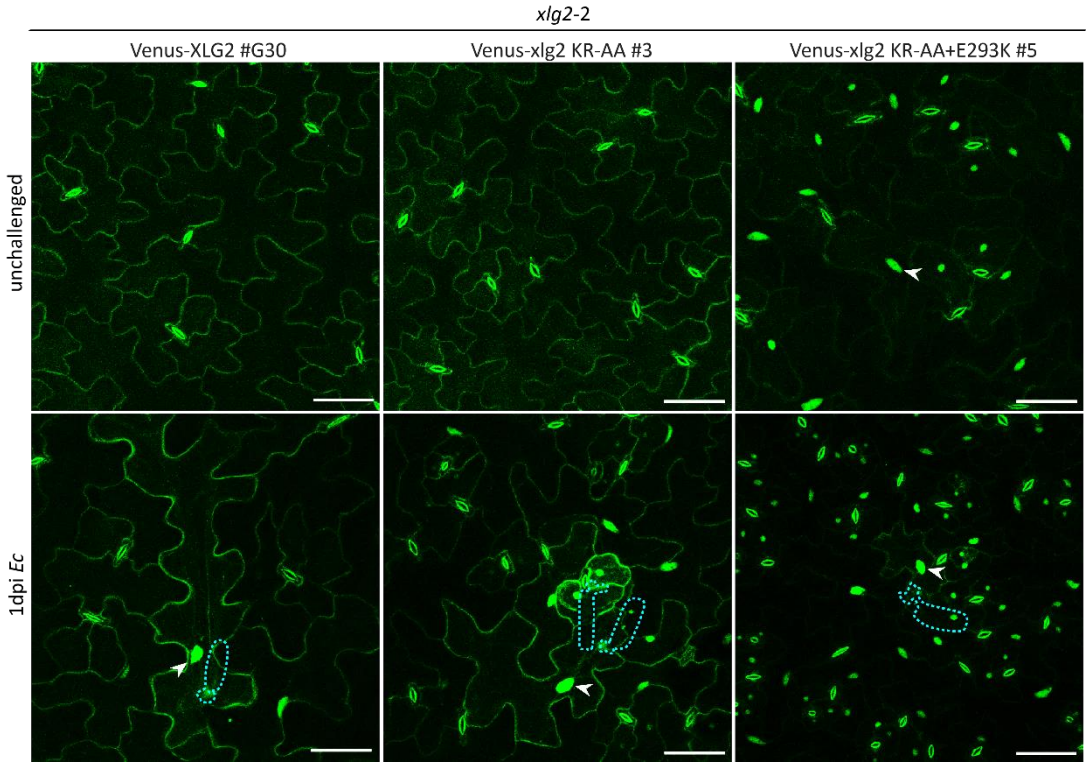

Fig. 34: The KR-AA mutation did not change the constitutive nuclear localization of XLG2 caused by E293K in *xlg2*-2.
CLSM images of unchallenged vs. infected (1dpi *Ec*) representative lines expressing Venus-XLG2, Venus-xlg2 KR-AA or Venus-xlg2 KR-AA+E293K in *xlg2*-2 are maximum projections of 18-22 focal planes recorded 1µm apart. Nuclei are marked by arrowheads and the positions of fungal spores with appressorium are outlined by dashed blue lines. Scale bar = 50µm.

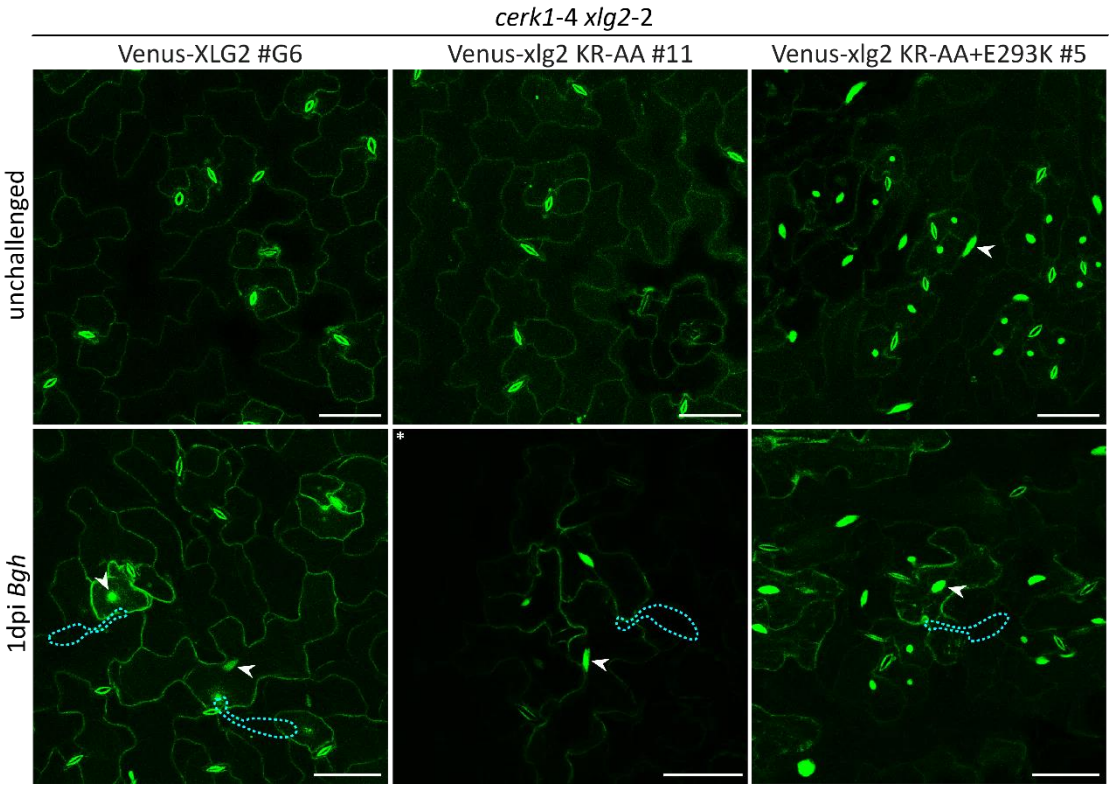

Fig. 35: The KR-AA mutation did not change constitutive nuclear localization of XLG2 caused by E293K in *cerk1*-4 *xlg2*-2.
CLSM images of unchallenged vs. infected (1dpi *Bgh*) representative lines expressing Venus-XLG2, Venus-xlg2 KR-AA or Venus-xlg2 KR-AA+E293K in *cerk1*-4 *xlg2*-2 are maximum projections of 18-22 focal planes recorded 1µm apart. * Venus-xlg2 KR-AA #27 (9 focal planes). Nuclei are marked by arrowheads and the positions of fungal spores with appressorium are outlined by dashed blue lines. Scale bar = 50µm.

3.4.2 The KR-AA mutation does not affect functionality of XLG2 in *cerk1*-4 cell death signalling

Further, *xlg2*-2 as well as *cerk1*-4 *xlg2*-2 expressing Venus-xlg2 KR-AA and Venus-xlg2 KR-AA+E293K were analysed phenotypically after *Ec* infection. Venus-xlg2 KR-AA as well as Venus-xlg2 KR-AA+E293K had no effect on the growth phenotype after *Ec* infection when expressed in *xlg2*-2 (Fig. 36 A). Full length expression of fusion proteins was confirmed via Western blotting (Fig. 36 B). Importantly, a motility difference was observed for KR-AA+E293K as well as KR-AA alone. Venus-xlg2 KR-AA was shown to be functional concerning *cerk1*-4 cell death signalling as it was able to complement *xlg2*-2 (Fig. 37 A). In contrast, Venus-xlg2 KR-AA+E293K did not complement *xlg2*-2. Further, full length expression of fusion proteins was confirmed in the presented lines (Fig. 37 B) and the same motility difference was observed. This was surprising as the KR-AA mutation alone was shown to not render

XLG2 non-functional. The observed motility difference correlated in E293K as well as nes387 (and C-A, will be described in 3.6) with the loss of plasma membrane localization and loss of functionality.

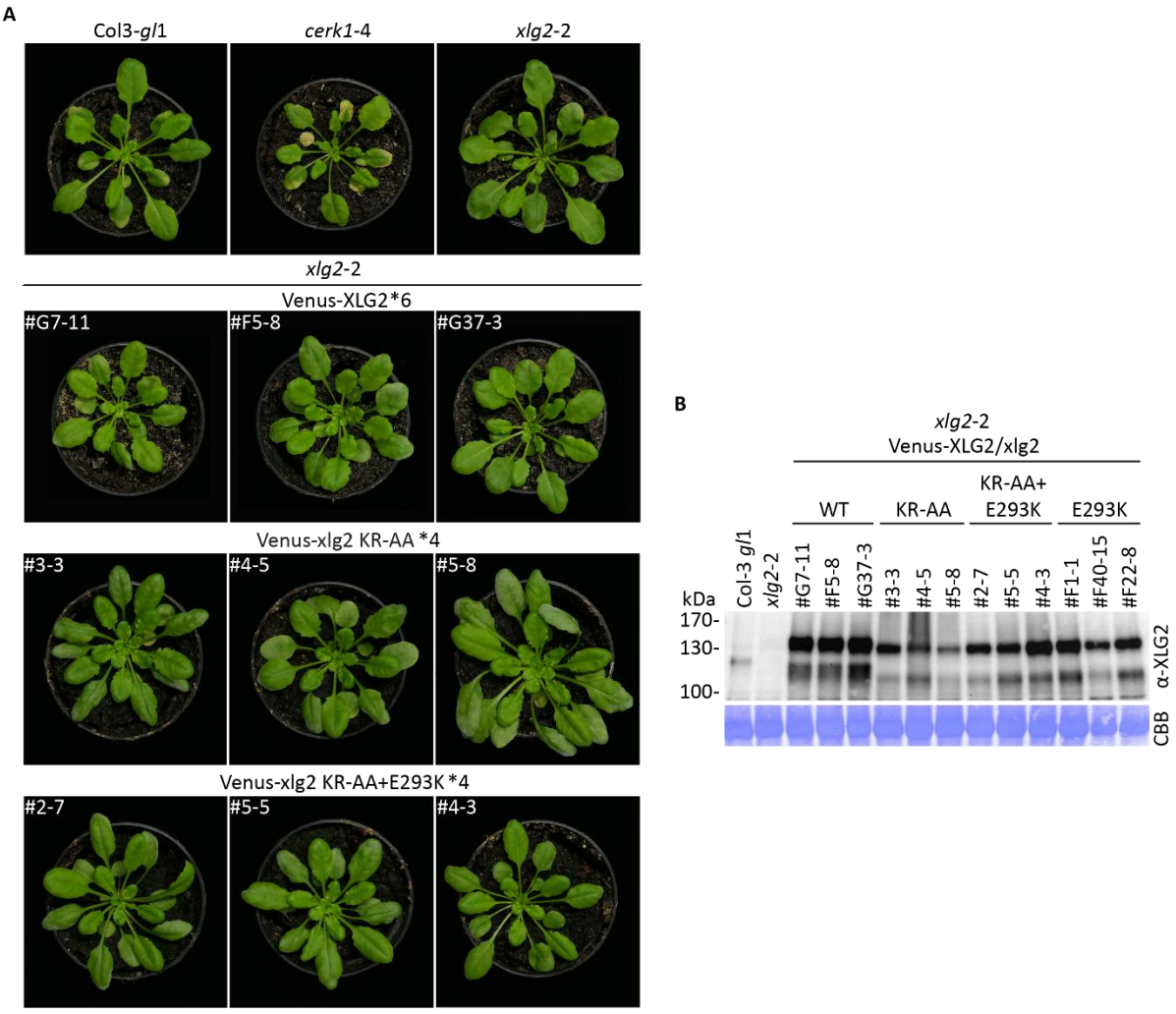

Fig. 36: Expression of Venus-xlg2 KR-AA and Venus-xlg2 KR-AA+E293K does not affect growth of *xlg2*-2 upon infection.
(A) *xlg2*-2 expressing Venus-XLG2, Venus-xlg2 KR-AA or Venus-xlg2 KR-AA+E293K and non-transformed controls are shown. Macroscopic cell death and fungal growth was evaluated 2wpi with *Ec.* *Indicated number of independent lines per construct were analysed and three representative lines are shown. The plants presented in this Figure were inoculated with *Ec* together with the lines in Fig. 18, 24, 30, 42 and 49. Therefore, the same images for the controls Col-3 *gl*1, *cerk1*-4, *xlg2*-2 and Venus-XLG2 (WT) lines are shown. **(B)** For the lines presented, accumulation of the Venus-XLG2 or Venus-xlg2 KR-AA/ KR-AA+E293K fusion proteins was confirmed by Western blotting after phenotype documentation (3wpi *Ec*) using a XLG2-specific antibody. Samples for Venus-xlg2 E293K were included for comparison of the motility difference. CBB = Coomassie Brilliant Blue stained membrane.

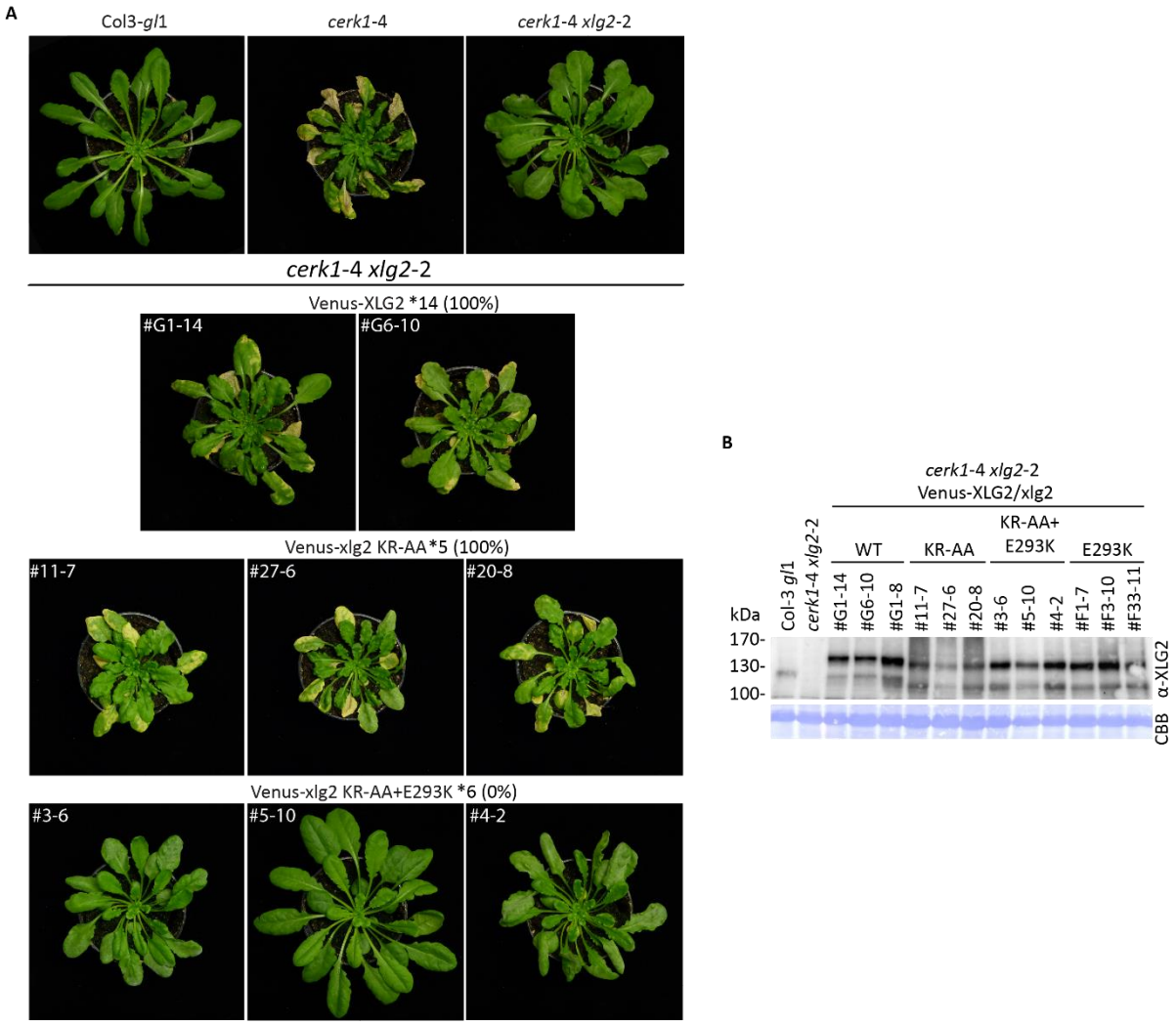

Fig. 37: Venus-xlg2 KR-AA fully complements *cerk1*-4 *xlg2*-2 while KR-AA+E293K still renders XLG2 non-functional.

(A) *cerk1*-4 *xlg2*-2 plants expressing Venus-XLG2, Venus-xlg2 KR-AA or Venus-xlg2 KR-AA+E293K and non-transformed controls are shown. Macroscopic cell death and fungal growth was evaluated 2wpi with *Ec.* *Indicated number of independent lines per construct were analysed (complementation rate) and three representative lines are shown. The plants presented in this Figure were inoculated with *Ec* together with the lines in Fig. S 15, 21. Therefore, the same images for the controls Col-3 *gl*1, *cerk1*-4, *xlg2*-2 and Venus-XLG2 (WT) lines are shown. **(B)** For the lines presented, accumulation of the Venus-XLG2 or Venus-xlg2 KR-AA/ KR-AA+E293K fusion proteins was confirmed by Western blotting after phenotype documentation (3wpi *Ec*) using a XLG2-specific antibody. Samples for Venus-xlg2 E293K were included to compare the motility difference. CBB = Coomassie Brilliant Blue stained membrane.

Conclusive from the KR-AA+E293K mutation data is that there is likely no causative connection between the observed motility difference of xlg2 E293K and the loss of function in *cerk1*-4. Further, this data indicates that the potentially enhanced nuclear localization signal (predicted NLS275) in XLG2 harboring the E293K mutation is not likely causative for the observed constitutive nuclear localization.

3.5 Two mutations (T476N/ R673L) in the XLG2 Gα-like domain do not change localization or *cerk1*-4 cell death signalling

XLG2 was previously shown to bind and hydrolyse GTP *in vitro* in dependency to calcium (Heo et al. 2012). Recently, a scenario in which XLGs would be bound to nucleotides *in vivo* was predicted to be highly unlikely based on bioinformatic studies and in depth comparison of conserved amino acids within Gα-domains (Lou et al. 2019). Another group described nucleotide exchange-dependent as well as nucleotide exchange-independent roles of the Gα protein GPA1 (Maruta et al. 2019). Both studies discuss the use of Gα-domain mutations S52C and Q222L for understanding the role of this domain for GPA1 functions. In XLG2, the T476N mutation was described earlier as likely nucleotide-free (Heo et al. 2012), which resembles the dominant negative gpa1 S52C mutation (Maruta et al. 2019). Based on homology to GPA1, the xlg2 R673L mutation potentially results in constitutive binding to GTP as it resembles the known gpa1 Q222L mutation, which is GTPase dead (Heo et al. 2012; Maruta et al. 2019; Ullah et al. 2003). In order to analyze the potential role of the XLG2 Gα-like domain in *cerk1*-4 cell death signalling these two Gα-like domain mutations (T476N, R673L) were introduced (Fig. 38 A, B).

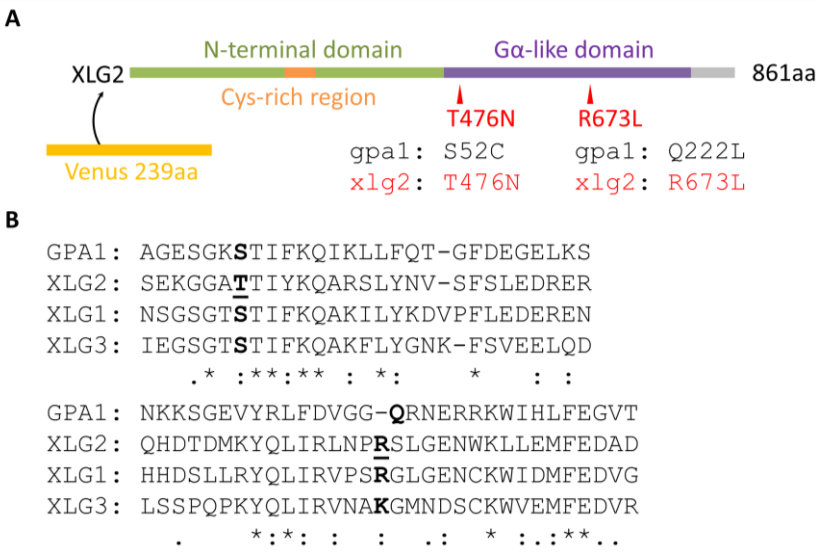

Fig. 38: XLG2 Gα-like domain mutations.

(A) XLG2 Gα-like domain amino acids of potential functional importance were mutated based on previous XLG2 data (Heo et al. 2012) and homology to the canonical *Arabidopsis* Gα subunit GPA1 (Maruta et al. 2019): T476N and R673L. **(B)** Alignments of GPA1 and XLG1-3 show S/T positions of GTP-binding (XLG2 T476 underlined) as well as GTP-hydrolysis related amino acids R/Q (XLG2 R673 underlined).

3.5.1 Two mutations (T476N/ R673L) in the Gα-like domain have no impact on localization of XLG2

Transient expression of Venus-xlg2 T476N (likely nucleotide-free) and Venus-xlg2 R673L (potentially constitutively GTP-bound) in *N. benthamiana* resulted in strong cell periphery and nuclear signals as well as occasionally visible cytoplasmic strands similar to Venus-XLG2 WT (Fig. 39).The similarity

between the xlg2 mutant variants with changed GTP-binding or hydrolysis capacity and XLG2 WT indicates that the Gα-like domain state does not influence subcellular localization of XLG2 in *N. benthamiana*.

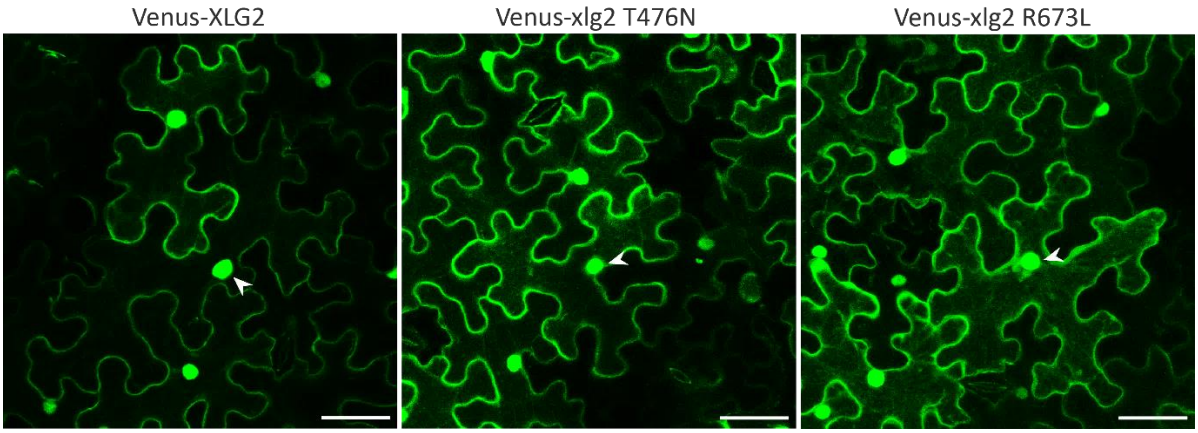

Fig. 39: Gα-like domain mutations T476N and R673L did not affect localization of XLG2 in *N. benthamiana*.
Venus-XLG2 (WT), Venus-xlg2 T476N and Venus-xlg2 R673L were transformed into *N. benthamiana* via *A. tumefaciens* infiltration. CLSM was performed 3dpi. Representative images of three independent experiments are maximum projections of 22 single planes recorded 1µm apart. Example nuclei are marked by arrowheads. Scale bar = 50µm.

Further experiments were done using stable transgenic *Arabidopsis* plants. *xlg2*-2 and *cerk1*-4 *xlg2*-2 expressing Venus-xlg2 T476N (16 and 23 independent lines) and Venus-xlg2 R673L (16 and 24 independent lines) were generated in this study. An initial screen using CLSM for good expressing lines resulted in a selection of ≥ 8 independent lines which were further analysed before and after infection with *Ec*. Both mutant variants showed WT-like weak cell periphery signals in unchallenged tissue while upon infection with *Ec* Venus-xlg2 T476N/ R673L accumulated in the nucleus and signals increased in *xlg2*-2 (Fig. 40, Fig. S 19) and *cerk1*-4 *xlg2*-2 (Fig. 41, Fig. S 20). The Gα-like domain T476N (likely nucleotide-free) and R673L (potentially constitutively GTP-bound) mutations did not influence subcellular localization of XLG2.

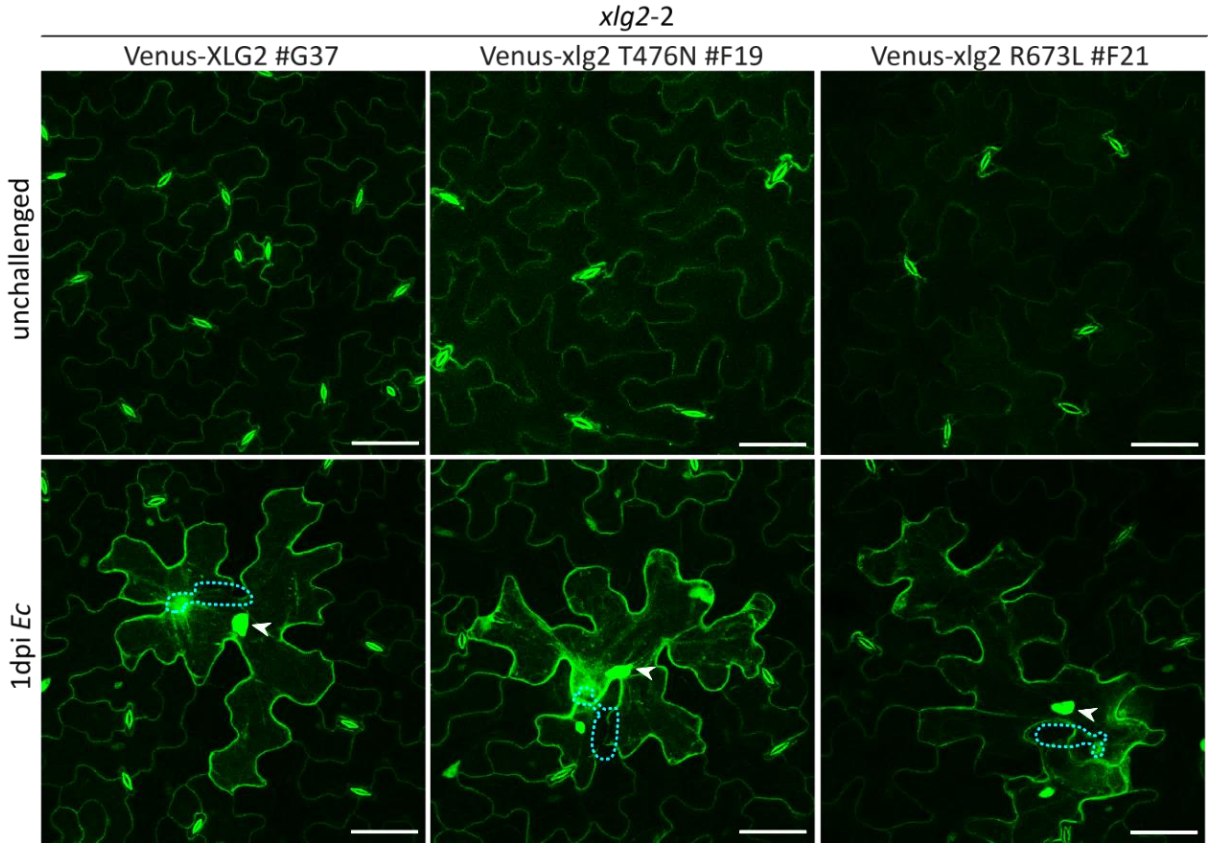

Fig. 40: Gα-like domain mutations T476N and R673L did not affect localization of XLG2 in *xlg2*-2.

CLSM images of unchallenged vs. infected (1dpi *Ec*) representative lines expressing Venus-XLG2, Venus-xlg2 T476N/ R673L in *cerk1*-4 *xlg2*-2 are maximum projections of z stacks spanning the epidermal cell layer. Nuclei are marked by arrowheads and the positions of fungal spores at sites of attempted penetration are outlined by dashed blue lines. Scale bar = 50µm. The lines presented in this Figure were analyzed together with the lines in Fig. 47. Therefore, the same images for Venus-XLG2 WT are shown.

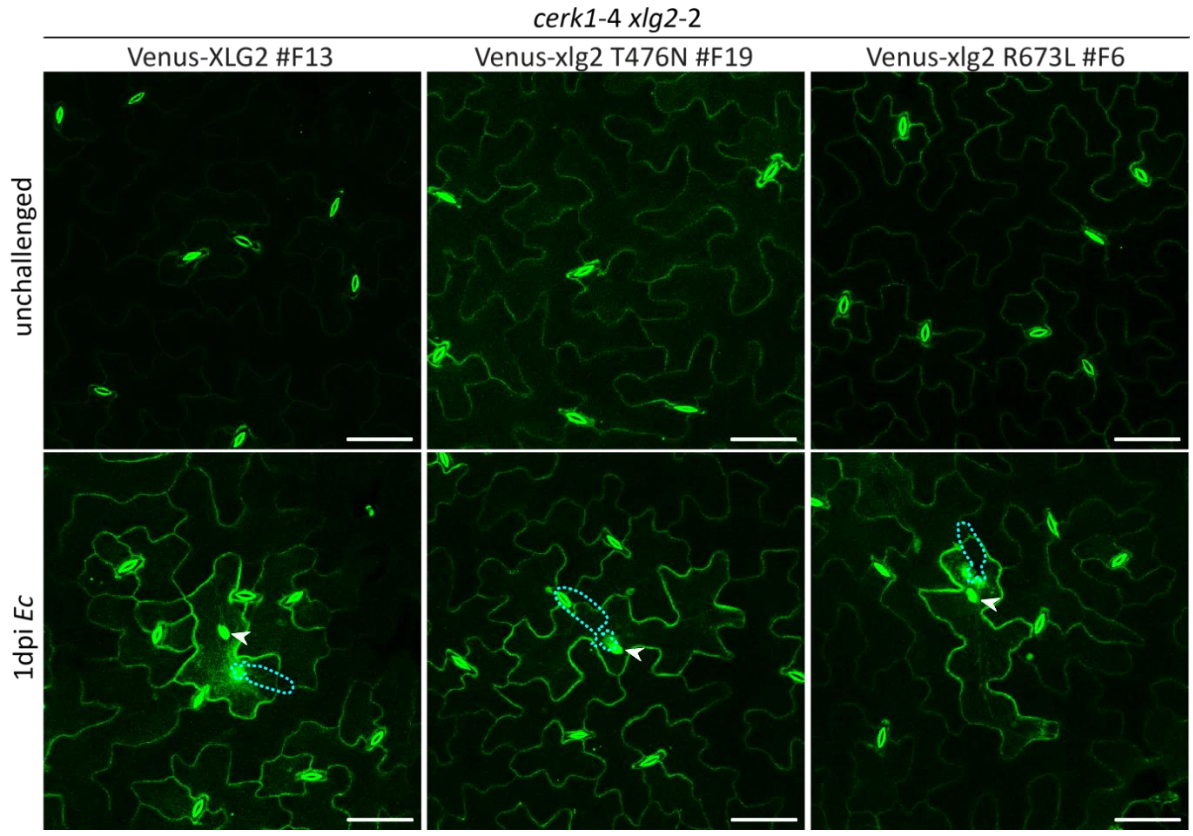

Fig. 41: Gα-like domain mutations T476N and R673L did not affect localization of XLG2 in *cerk1*-4 *xlg2*-2.

CLSM images of unchallenged vs. infected (1dpi *Ec*) representative lines expressing Venus-XLG2, Venus-xlg2 T476N/ R673L in *cerk1*-4 *xlg2*-2 are maximum projections of z stacks spanning the epidermal cell layer. Nuclei are marked by arrowheads and the positions of fungal spores at sites of attempted penetration are outlined by dashed blue lines. Scale bar = 50µm.

3.5.2 Two mutations (T476N/ R673L) in the Gα-like domain do not affect functionality of XLG2 in *cerk1*-4 cell death signalling

In order to test phenotypic effects and functionality of Venus-xlg2 T476N (likely nucleotide-free) and Venus-xlg2 R673L (potentially constitutively GTP-bound) transgenic *xlg2*-2 and *cerk1*-4 *xlg2*-2 were infected with *Ec* and the (complementation) phenotype was documented two weeks after infection. Expression of Venus-xlg2 T476N and Venus-xlg2 R673L did not influence the *xlg2*-2 phenotype (Fig. 42 A). In *cerk1*-4 *xlg2*-2 Venus-xlg2 T476N as well as Venus-xlg2 R673L expression resulted in complementation of *xlg2*-2 which confirmed functionality of these XLG2 mutant variants concerning *cerk1*-4 cell death signalling (Fig. 43 A). Presence of full length fusion protein for analysed transgenic lines was confirmed via Western Blot (Fig. 42 B, Fig. 43 B). This data supports the conclusion that Gα-like domain-dependent nucleotide-exchange is not relevant for XLG2s role in *cerk1*-4 cell death signalling.

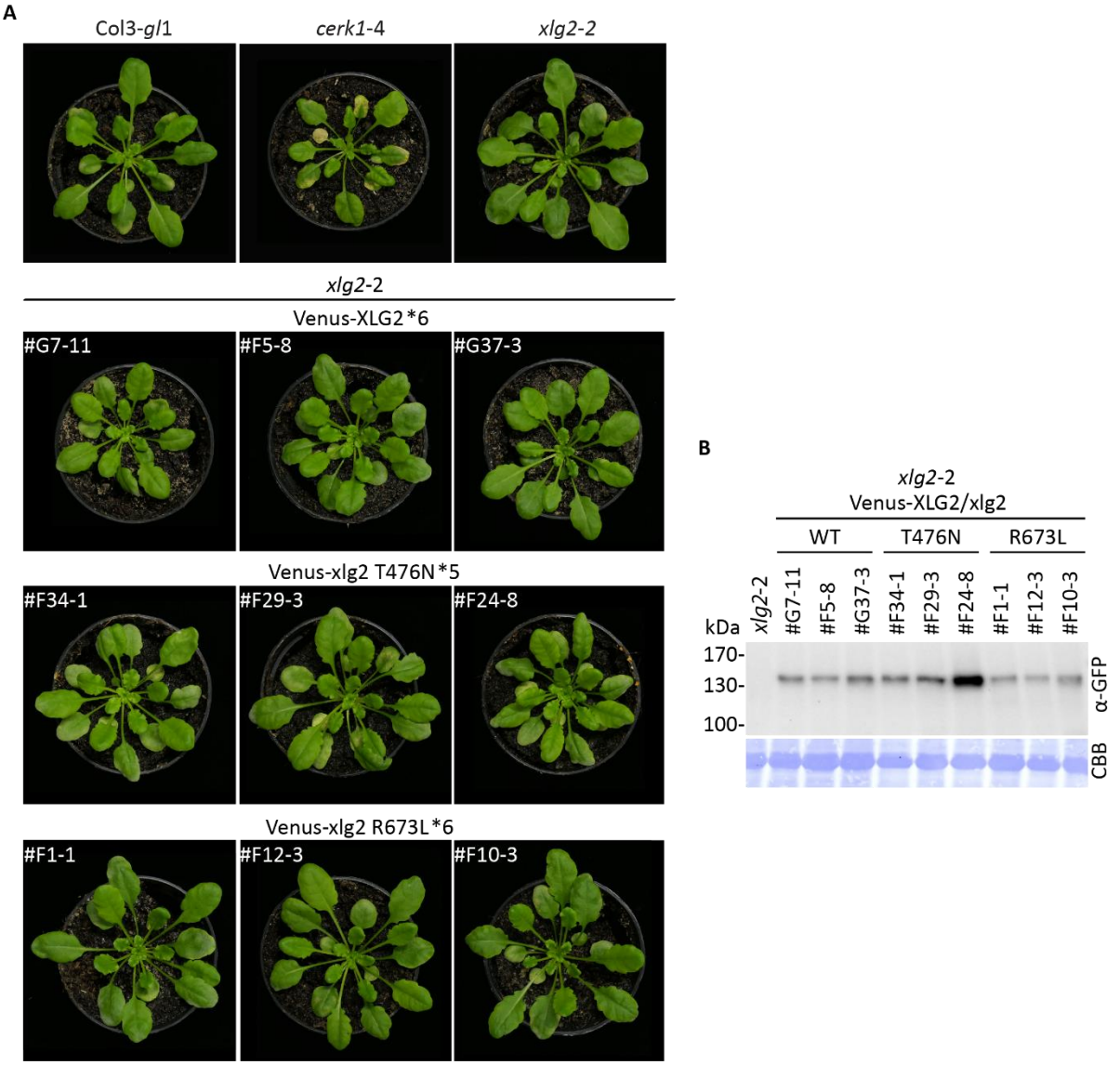

Fig. 42: Expression of Venus-xlg2 T476N/ R673L in *xlg2*-2 results in normal plant growth upon infection.

(A) x*lg2*-2 expressing Venus-XLG2 WT, Venus-xlg2 T476N or Venus-xlg2 R673L and non-transformed controls were evaluated 2wpi with *Ec* for macroscopic cell death and fungal growth. *Indicated number of independent lines per construct were analysed and three representative lines are shown. The plants presented in this Figure were inoculated with *Ec* together with the lines in Fig. 18, 24, 30, 36 and 49. Therefore, the same images for the controls Col-3 *gl*1, *cerk1*-4, *xlg2*-2 and Venus-XLG2 (WT) lines are shown. **(B)** For the lines presented, accumulation of Venus-XLG2 or Venus-xlg2 T476N/ R673L was confirmed by Western blotting after phenotype documentation (3wpi *Ec*) using α-GFP antibody. CBB = Coomassie Brilliant Blue stained membrane.

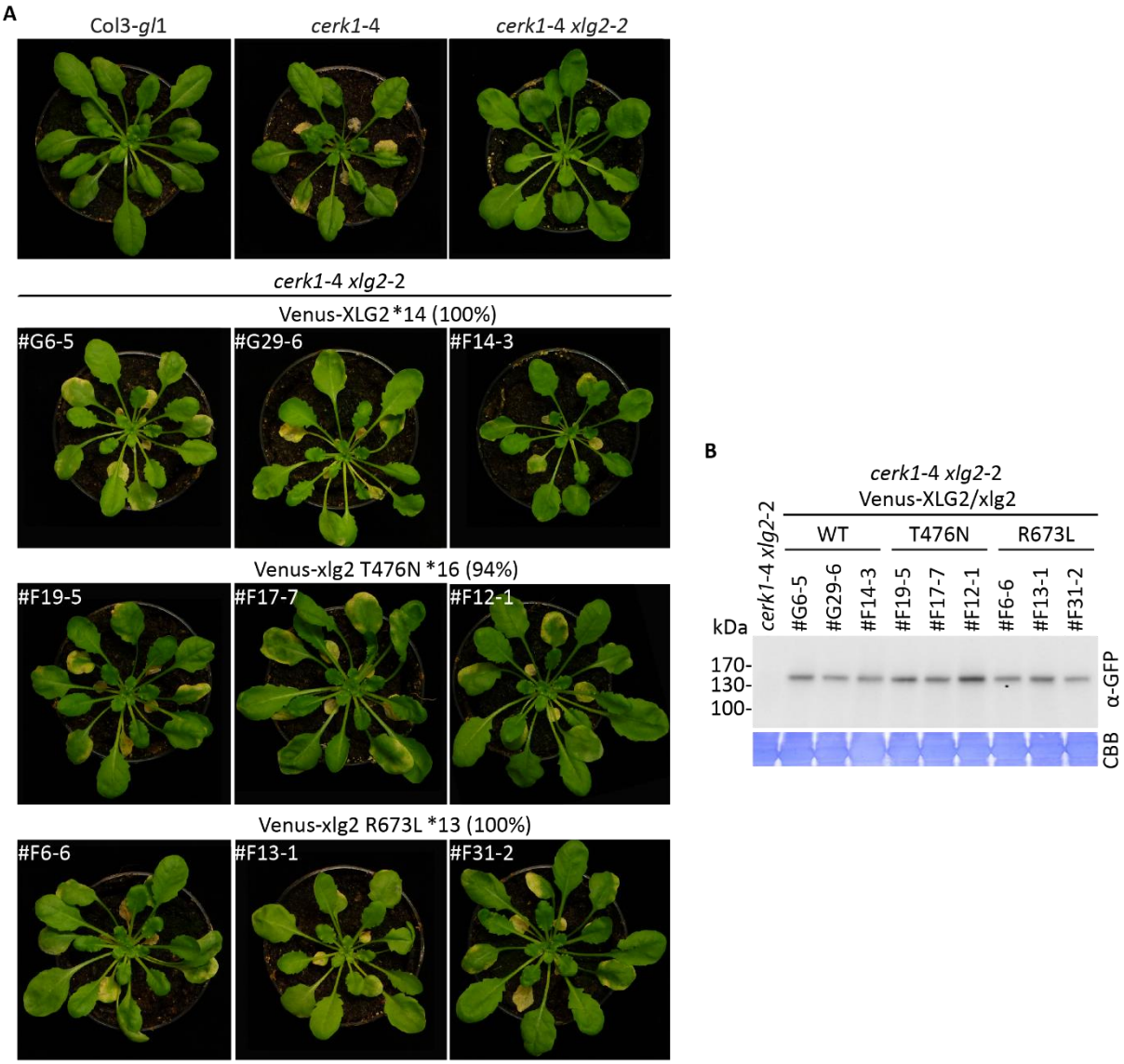

Fig. 43: Expression of Venus-xlg2 T476N and R673L fully complements *cerk1*-4 *xlg2*-2.

(A) *cerk1*-4 *xlg2*-2 expressing Venus-XLG2 WT, Venus-xlg2 T476N or Venus-xlg2 R673L and non-transformed controls were evaluated 2wpi with *Ec* for macroscopic cell death and fungal growth. *Indicated number of independent lines per construct were analysed (complementation rate) and three representative lines are shown. The plants presented in this Figure were inoculated with *Ec* together with the lines in Fig. 25 and Fig. 31. Therefore, the same images for the controls Col-3 *gl*1, *cerk1*-4, *xlg2*-2 and Venus-XLG2 (WT) lines are shown. **(B)** For the lines presented, accumulation of Venus-XLG2 or Venus-xlg2 T476N/ R673L was confirmed by Western blotting after phenotype documentation (3wpi *Ec*) using α-GFP antibody. CBB = Coomassie Brilliant Blue stained membrane.

3.6 Cys-rich region mutations change the localization and functionality of XLG2

XLG cys-rich regions contain eight highly conserved cysteines annotated as degenerate RING-type zinc finger domain (uniprot). RING zinc fingers can have diverse functions including protein-/ DNA-binding or (mostly) E3 ligase activity and characteristically coordinate two zinc ions (Sun et al. 2019). However, with 10 of 477 identified RING domains in *Arabidopsis* only few known plant RING-type proteins belong to the RING-C2 class which is the only class that contains eight conserved cysteines (Stone et al. 2005) including confirmed active E3 ligases (Kabelitz et al. 2016). The closely related FYVE zinc finger domains are known to bind phosphoinositides and also have a conserved spacing pattern of eight cysteines (Wywial and Singh 2010). XLG cys-rich region sequences were, therefore, aligned with known RING-C2/ FYVE domains. The cysteine spacing pattern for several RING/ FYVE domains with eight conserved cysteines matched the cysteine spacing pattern of the potential XLG zinc finger domains (Fig. S 22). In order to analyze the role of the cys-rich region for correct localization of XLG2 and *cerk1*-4 cell death signalling several closely positioned cysteines were exchanged for alanine. Positions of the XLG2 cysteine double or quadruple mutations are indicated in the domain organization of XLG2 (Fig. 44 A). The alignment (Fig. 44 B) shows conservation of XLG1-3 cys-rich regions and the exact positions of the cysteine mutations. The alignment in Fig. 44 C shows the resembling cysteine spacing patterns of XLG2 and a FYVE zinc finger protein (FREE1) and a RING zinc finger protein (CESA1). FREE1 is a ESCRT component involved in regulation of MVB protein sorting and plant growth (Gao et al. 2014), while CESA proteins form a complex that is important for secondary cell wall and cellulose synthesis (Kumar et al. 2020).

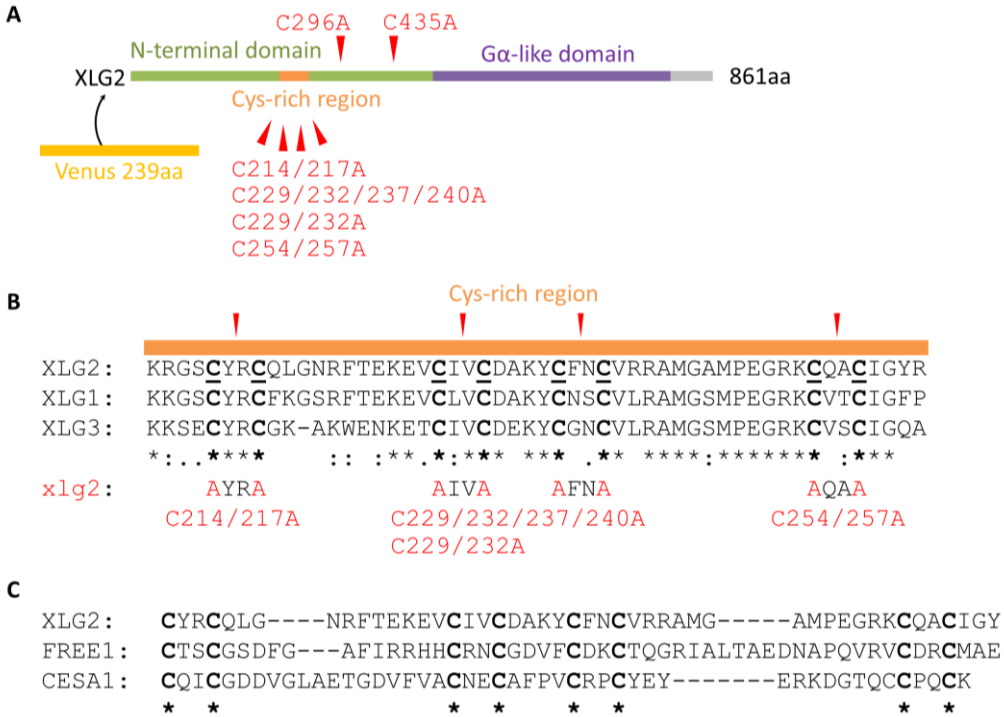

Fig. 44: Conserved XLG2 cysteines were exchanged for alanine.

(A) The cys-rich region is located within the plant-specific N-terminus of XLG2. Four cys-rich region mutant variants were generated in this study. In addition, two conserved cysteines downstream of the cys-rich region (C296, C435) were exchanged for alanine. **(B)** XLG1-3 alignment shows positions of highly conserved XLG cysteines within the cys-rich region. Cysteines were exchanged for alanine as double or quadruple mutations to avoid redundancy effects of neighboring cysteines. **(C)** Alignment of XLG2 and the plant zinc finger protein FREE1 (FYVE domain) and CESA1 (RING) shows overlapping cysteine spacing patterns.

3.6.1 Cys-rich region mutations abolish plasma membrane localization of XLG2

The subcellular localization of Venus-xlg2 cys-mutant variants was initially tested in *N. benthamiana* transiently transformed via *Agrobacterium*-infiltration. Mutating two conserved cysteines downstream of the potential XLG2 RING zinc finger domain and close to the previously analysed E293K (C296A) and nls426 (C435A) positions had no effect on subcellular localization (Fig. 45). Surprisingly, all four tested Venus-xlg2 cys-rich region mutant variants showed strong nuclear signals and drastically reduced cell periphery signals in contrast to XLG2 WT (Fig. 46).

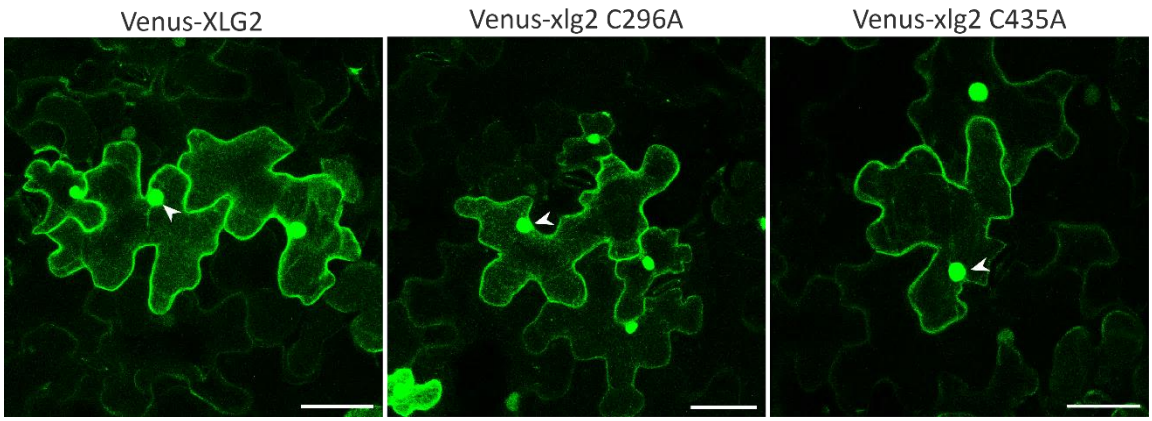

Fig. 45: Mutations of conserved cysteines located between the cys-rich region and the Gα-like domain did not change the localization of XLG2 in *N. benthamiana*.

Venus-XLG2, Venus-xlg2 C296A and Venus-xlg2 C435A were transformed into *N. benthamiana* via *A. tumefaciens* infiltration. CLSM was performed 3dpi. Representative images are maximum projections of 18 single planes recorded 1µm apart. Example nuclei are marked by arrowheads. Scale bar = 50µm.

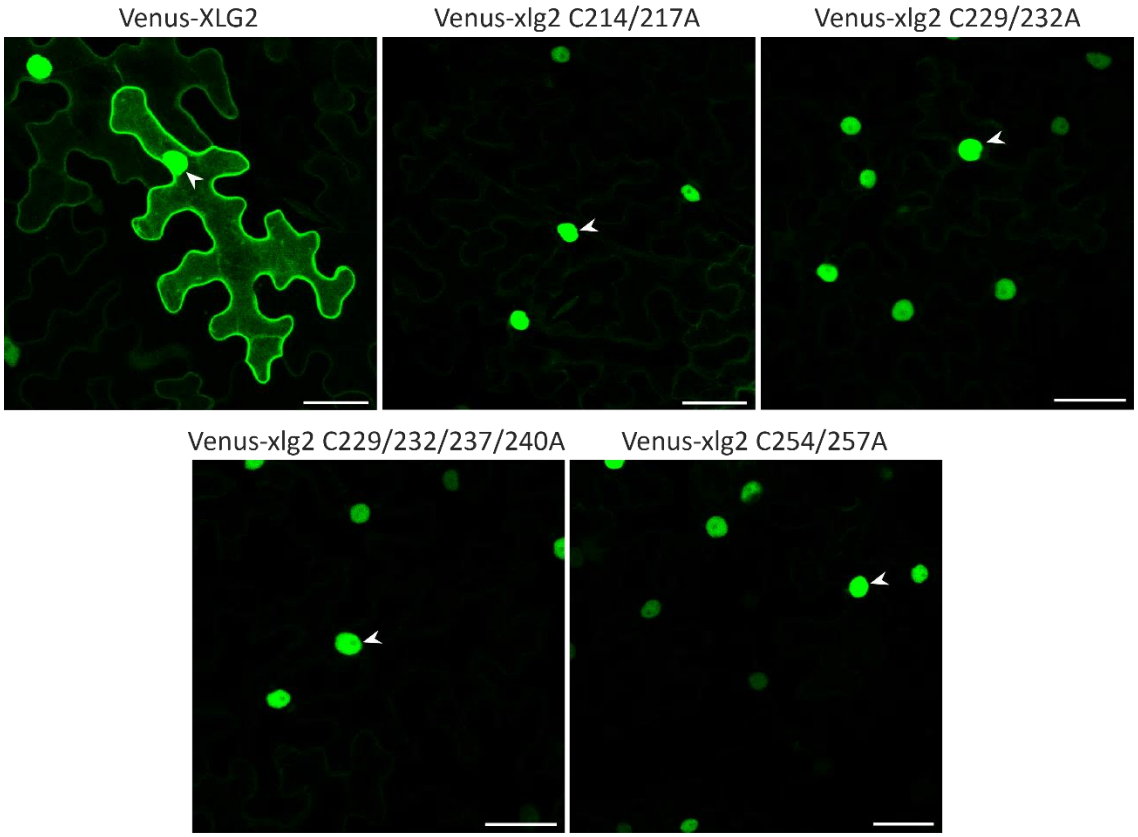

Fig. 46: Cys-rich region C-A mutations abolish plasma membrane localization of XLG2 in *N. benthamiana*.

Venus-XLG2 (WT) and Venus-xlg2 C-A (as indicated) were transformed into *N. benthamiana* via *A. tumefaciens* infiltration. CLSM was performed 3dpi. Representative images of three independent experiments are maximum projections of 20 single planes recorded 1µm apart. Example nuclei are marked by arrowheads. Scale bar = 50µm.

In order to further characterize subcellular localization of Venus-xlg2 cys-mutant proteins, stable transformed *Arabidopsis* plants expressing Venus-xlg2 C214/217A (12 independent lines in *xlg2*-2 and 16 lines in *cerk1*-4 *xlg2*-2), Venus-xlg2 C229/232/237/240A (8 *xlg2*-2 lines and 12 *cerk1*-4 *xlg2*-2 lines) and Venus-xlg2 C254/257A (8 *xlg2*-2 lines and 21 *cerk1*-4 *xlg2*-2 lines) were analysed via CLSM. Selected lines were further analysed via CLSM before as well as one day post inoculation with *Ec*. In unchallenged plants, Venus-xlg2 C-A mutant variants (C214/217A, C229/232/237/240A and C254/257A) showed drastically reduced cell periphery signals and constitutively labeled nuclei in *xlg2*-2 (Fig. 47 A, Fig. S 23) and *cerk1*-4 *xlg2*-2 (Fig. 48, Fig. S 24). One day after infection with *Ec*, cell periphery and nuclear signals increased in *xlg2*-2 (Fig. 47 A, B, C; Fig. S 23) and *cerk1*-4 *xlg2*-2 (Fig. 48, Fig. S 24). However, Venus-xlg2 C-A mutant cell periphery signals were significantly reduced compared to WT XLG2 and nuclear accumulation appeared independently from fungal attack similar to Venus-xlg2 E293K (Fig. 47 B, C).

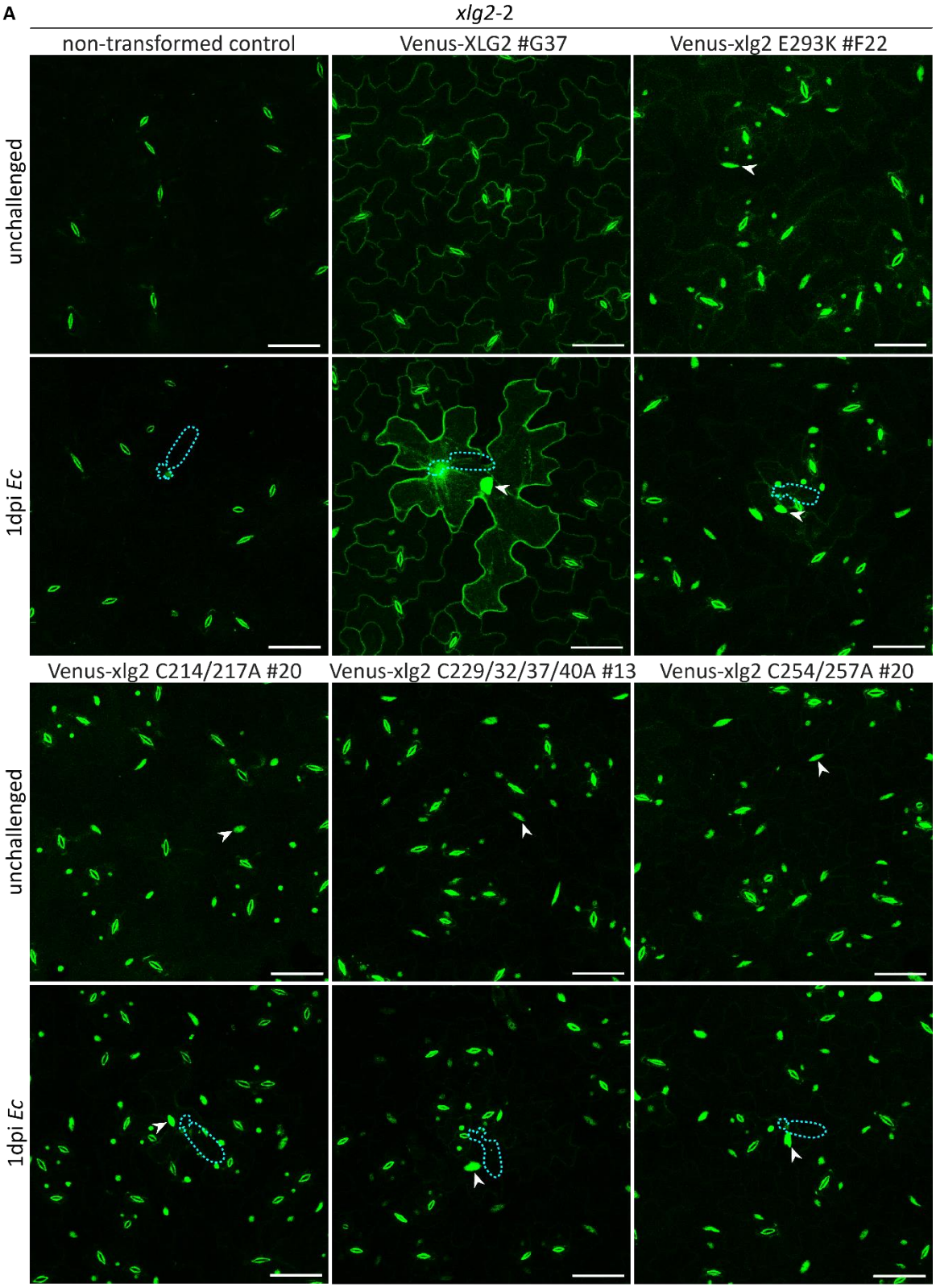
A
xlg2-2
non-transformed control
Venus-XLG2 #G37
Venus-xlg2 E293K #F22
unchallenged
1dpi Ec
Venus-xlg2 C214/217A #20
Venus-xlg2 C229/32/37/40A #13
Venus-xlg2 C254/257A #20
unchallenged
1dpi Ec

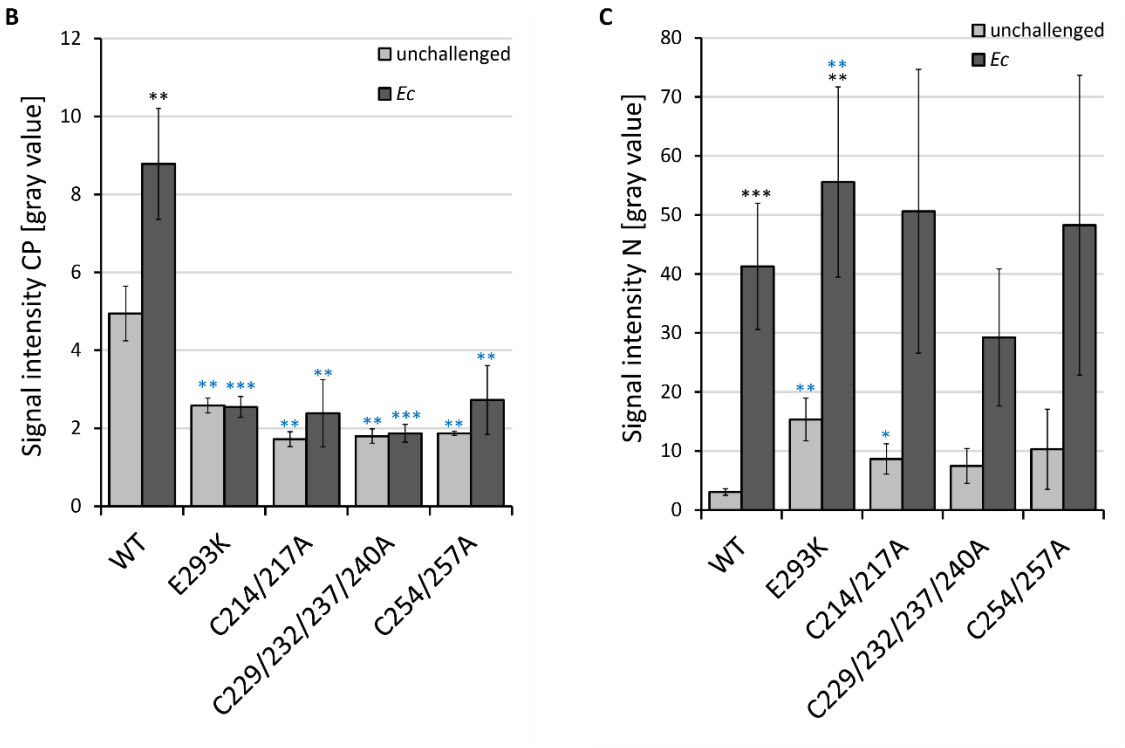

Fig. 47: Cys-rich region C-A mutations abolish plasma membrane localization of XLG2 in *xlg2*-2.

(A) CLSM images of unchallenged vs. infected (1dpi *Ec*) representative *xlg2*-2 lines expressing Venus-XLG2, Venus-xlg2 E293K and Venus-xlg2 C-A (as indicated) are maximum projections of z stacks spanning the epidermal cell layer. Nuclei are marked by arrowheads and the positions of fungal spores at sites of attempted penetration are outlined by dashed blue lines. Scale bar = 50µm. The lines presented in this Figure were analyzed together with the lines in Fig. 18 and 40. Therefore, the same images for Venus-xlg2 E293K (Fig. 18) and Venus-XLG2 WT (Fig. 40) are shown. Quantification of CLSM images of *xlg2*-2 expressing Venus-XLG2, xlg2 E293K and xlg2 C-As (as indicated). Signal intensities at the cell periphery (CP) **(B)** and inside the nucleus (N) **(C)** of unchallenged and infected (1dpi *Ec*) cells were quantified. Data are means ± StDev of three independent lines (1-5 interaction sites of 1-3 plants were analysed per line). Asterisks indicate significance unchallenged vs infected (black) and compared to WT (blue). * P < 0.05, ** P < 0.01, *** P < 0.001

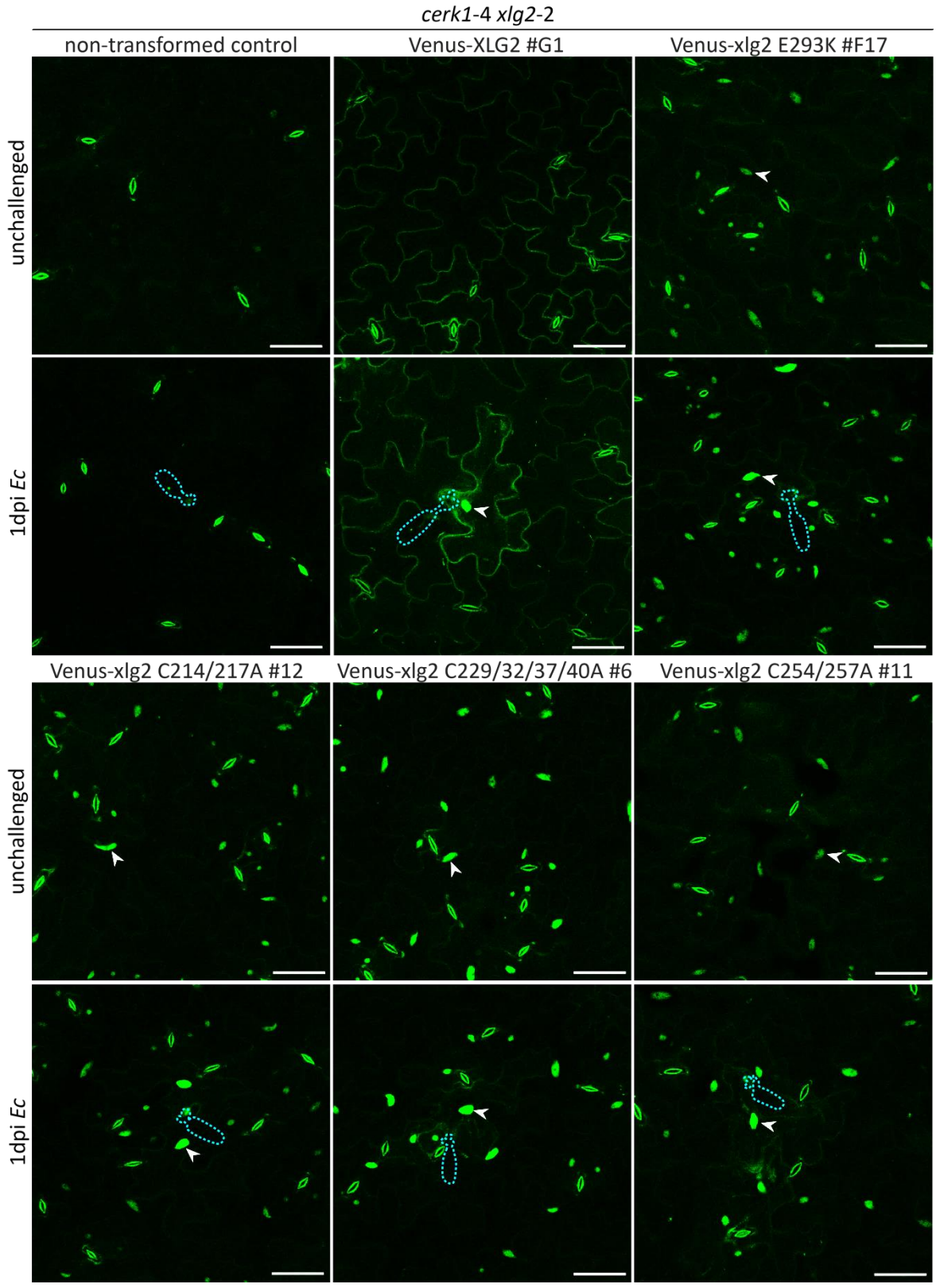

Fig. 48: Cys-rich region C-A mutations abolish plasma membrane localization of XLG2 in *cerk1*-4 *xlg2*-2.

CLSM images of unchallenged vs. infected (1dpi *Ec*) representative *cerk1*-4 *xlg2*-2 lines expressing Venus-XLG2, Venus-xlg2 E293K or Venus-xlg2 C-A (as indicated) are maximum projections of z stacks spanning the epidermal cell layer. Nuclei are marked by arrowheads and the positions of fungal spores at sites of attempted penetration are outlined by dashed blue lines. Scale bar = 50µm.

This study showed that mutations within the XLG2 cys-rich region have tremendous effects on subcellular localization with reduced cell periphery signals and constitutive nuclear accumulation of XLG2 which mimic other analysed mutations (E293K, nes387). The mutation of any two closely positioned highly conserved cysteines within the XLG2 cys-rich region was sufficient to cause the observed dramatic loss of cell periphery localization. This was underlined by the observation that the quadruple mutation C229/232/237/240A had no additional effect concerning subcellular localization compared to the double mutations. For the double cysteine mutations, it is likely that structural changes such as lost disulfide bridges or RING formation cause the observed effects. The drastic effect of cysteine mutations was only observed within the cys-rich region. In contrast, cysteine to alanine exchanges of other highly conserved positions (C296 and C435) did not affect localization of XLG2. Accordingly, the other conserved cysteines at least do not play a major role in subcellular localization of XLG2. Next, it is important to characterize the functionality of the C-A mutant variants that altered the localization of XLG2.

3.6.2 Cys-rich region mutations render XLG2 non-functional

Transgenic *xlg2*-2 and *cerk1*-4 *xlg2*-2 expressing Venus-xlg2 C214/217A, Venus-xlg2 C229/232/237/240A and Venus-xlg2 C225/227A were infected with *Ec* and the (complementation) phenotype was documented two weeks later. Expression of Venus-xlg2 C214/217A, Venus-xlg2 C229/232/237/240A and Venus-xlg2 C225/227A did not change the *xlg2*-2 growth phenotype after *Ec* infection (Fig. 49 A). Expression of Venus-XLG2 WT in *cerk1*-4 *xlg2*-2 complemented *xlg2*-2 as the *cerk1*-4 deregulated cell death phenotype developed upon *Ec* inoculation (Fig. 50 A). In contrast, Venus-xlg2 C214/217A, Venus-xlg2 C229/232/237/240A and Venus-xlg2 C225/227A failed to complement *xlg2*-2 similarly to Venus-xlg2 E293K. Full length expression of fusion proteins was confirmed via Western blotting in *xlg2*-2 (Fig. 49 B) as well as *cerk1*-4 *xlg2*-2 (Fig. 50 B). Venus-xlg2 C-A ran consistently lower than XLG2 WT and to the same apparent molecular size as Venus-xlg2 E293K (Fig. 50 C).

These results underline that there is a strong correlation between non-functional xlg2 mutant variants, which all show drastically reduced cell periphery localization, and a motility difference in Western blotting. According to these results, PM localization is important for XLG2 to be involved in *cerk1*-4 cell death signalling. Further, there might be a role for the RING-like XLG2 domain in PM-tethering.

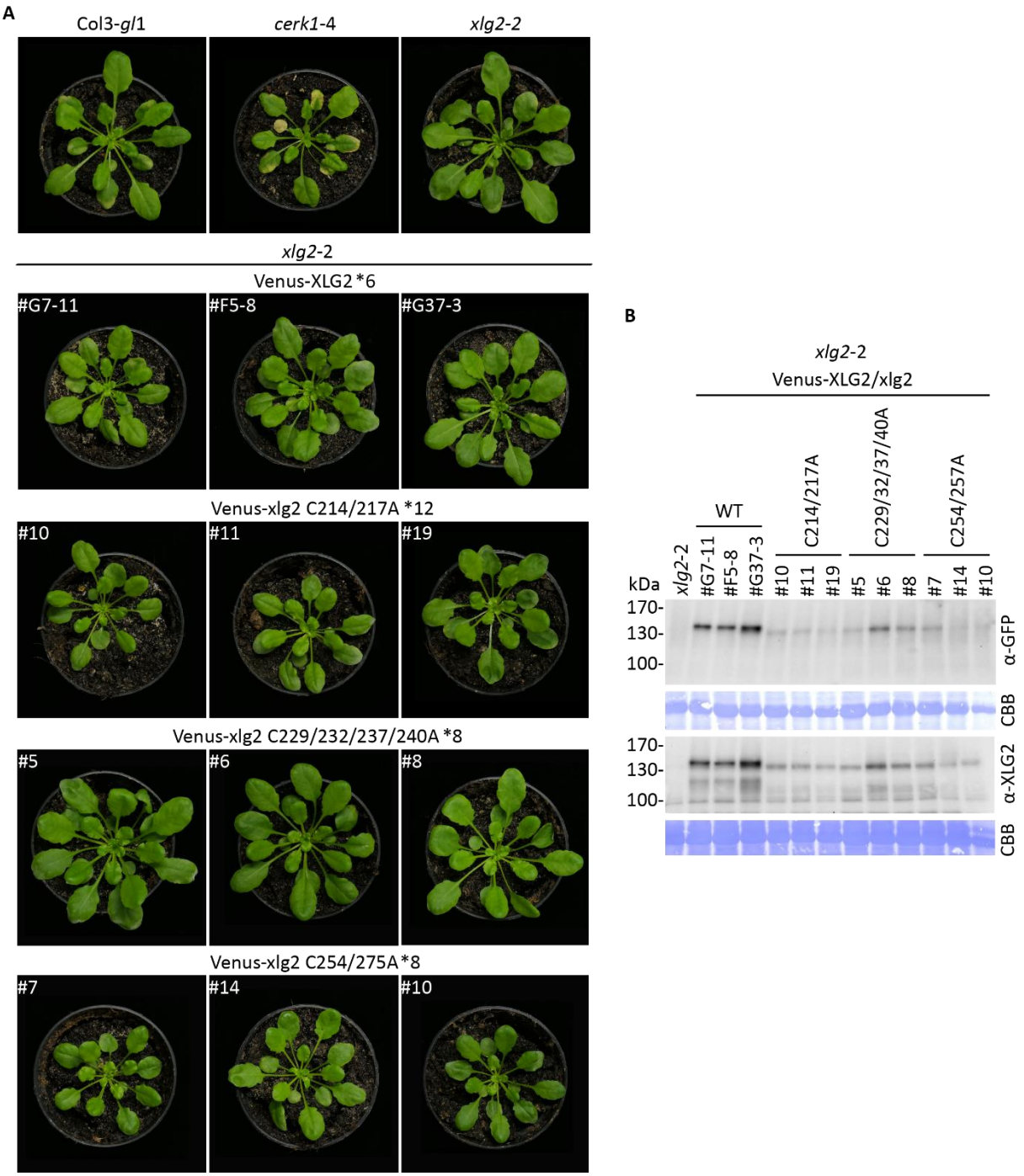

Fig. 49: Expression of XLG2 cys-rich region mutant variants did not change *xlg2*-2 growth upon infection.

(A) *xlg2*-2 expressing Venus-XLG2 WT or Venus-xlg2 C-A (as indicated) and non-transformed controls were evaluated 2wpi with *Ec* for macroscopic cell death and fungal growth. *Indicated number of independent lines per construct were analysed and three representative lines are shown. The plants presented in this Figure were inoculated with *Ec* together with the lines in Fig. 18, 24, 30, 36 and 42. Therefore, the same images for the controls Col-3 *gl*1, *cerk1*-4, *xlg2*-2 and Venus-XLG2 (WT) lines are shown. **(B)** For the lines presented accumulation of Venus-XLG2/ xlg2 was confirmed by Western blotting after phenotype documentation (3wpi *Ec*) using α-GFP/ α-XLG2 antibodies. CBB = Coomassie Brilliant Blue stained membrane.

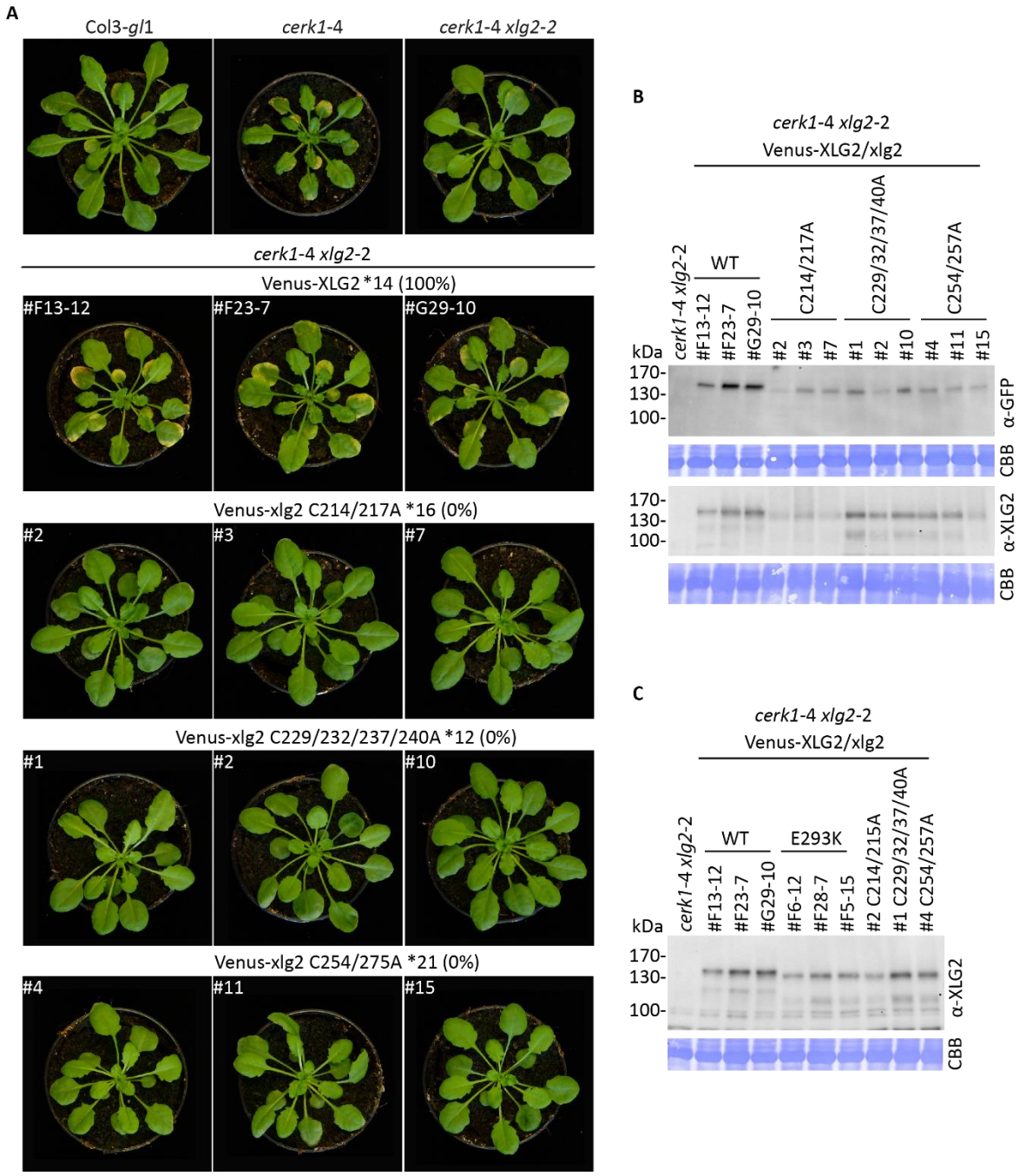

Fig. 50: Mutations within the cys-rich region render XLG2 non-functional.

(A) *cerk1*-4 *xlg2*-2 expressing Venus-XLG2 WT or Venus-xlg2 C-A (as indicated) and non-transformed controls were evaluated 2wpi with *Ec* for macroscopic cell death and fungal growth. *Indicated number of independent lines per construct were analysed (complementation rate) and three representative lines are shown. The plants presented in this Figure were inoculated with *Ec* together with the lines in Fig. 19. Therefore, the same images for the controls Col-3 *gl*1, *cerk1*-4, *xlg2*-2 and Venus-XLG2 (WT) lines are shown. **(B)** For the lines presented accumulation of Venus-XLG2/ xlg2 was confirmed by Western blotting after phenotype documentation (3wpi *Ec*) using GFP-/ XLG2-specific antibodies. **(C)** Western blot showing samples for Venus-XLG2 WT, Venus-xlg2 E293K and Venus-xlg2 C-A (as indicated) as comparison for the apparent molecular mass. CBB = Coomassie brilliant blue stained membrane.

3.7 Absence of the Gβγ-dimer reduces PM localization of XLG2

For the classical GPA1 subunit multiple modifications, including N-myristoylation and reversible S-acylation, are described to be important for PM tethering independently from heterotrimer formation (Adjobo-Hermans et al. 2006). For XLG2 it is still unclear how tethering to the PM is regulated. Similarly to GPA1, XLG2 was shown to interact with the Gβγ-dimer at the PM (Maruta et al. 2015; Chakravorty et al. 2015). This interaction might be relevant for attachment of XLG2 to the PM. In order to further elucidate which factor influences sequestration of XLG2 to the PM, the subcellular localization of Venus-XLG2 in the absence of selected G proteins that are known to form the heterotrimeric complex in *Arabidopsis* was analysed via particle bombardment and subsequent CLSM. Transiently transformed G protein mutants *gpa1*-3, *agb1*-2, and *agg1*-1 *agg2*-1 and as control Col-0 *Arabidopsis* co-expressed Venus-XLG2 with the PM mkate2-Lti6b and nuclear marker mTurquoise2-N7 two days after bombardment. The overlapping signals of Venus-XLG2 and the PM-marker as well as the nuclear marker indicate that XLG2 localized to the PM as well as the nucleus in all tested G protein mutants and the control (Fig. 51 A). The quantification of Venus-XLG2 PM and nuclear signal intensities indicates no difference between Col-0 and the *gpa1* mutant. For *agb1* as well as *agg1 agg2* higher nucleus to PM ratios for transiently expressed Venus-XLG2 were calculated (Fig. 51 B). This difference was also represented by the tendency of weaker PM signals and stronger nuclear signal intensity. This experiment was repeated three times and not all replicates show significant differences. However, all replicates share the same tendency that nuclear signals of Venus-XLG2 are slightly stronger in *agb1* and *agg1 agg2* backgrounds while PM signals are slightly weaker compared to Col-0 (Fig. S 25, Fig. S 26). Conclusive from this study is that absence of either AGB1 or both AGG1 and AGG2 results in slightly reduced tethering of XLG2 to the PM. Further, only a slightly larger fraction of the XLG2 pool accumulates in the nucleus in the absence of the Gβγ-dimer.

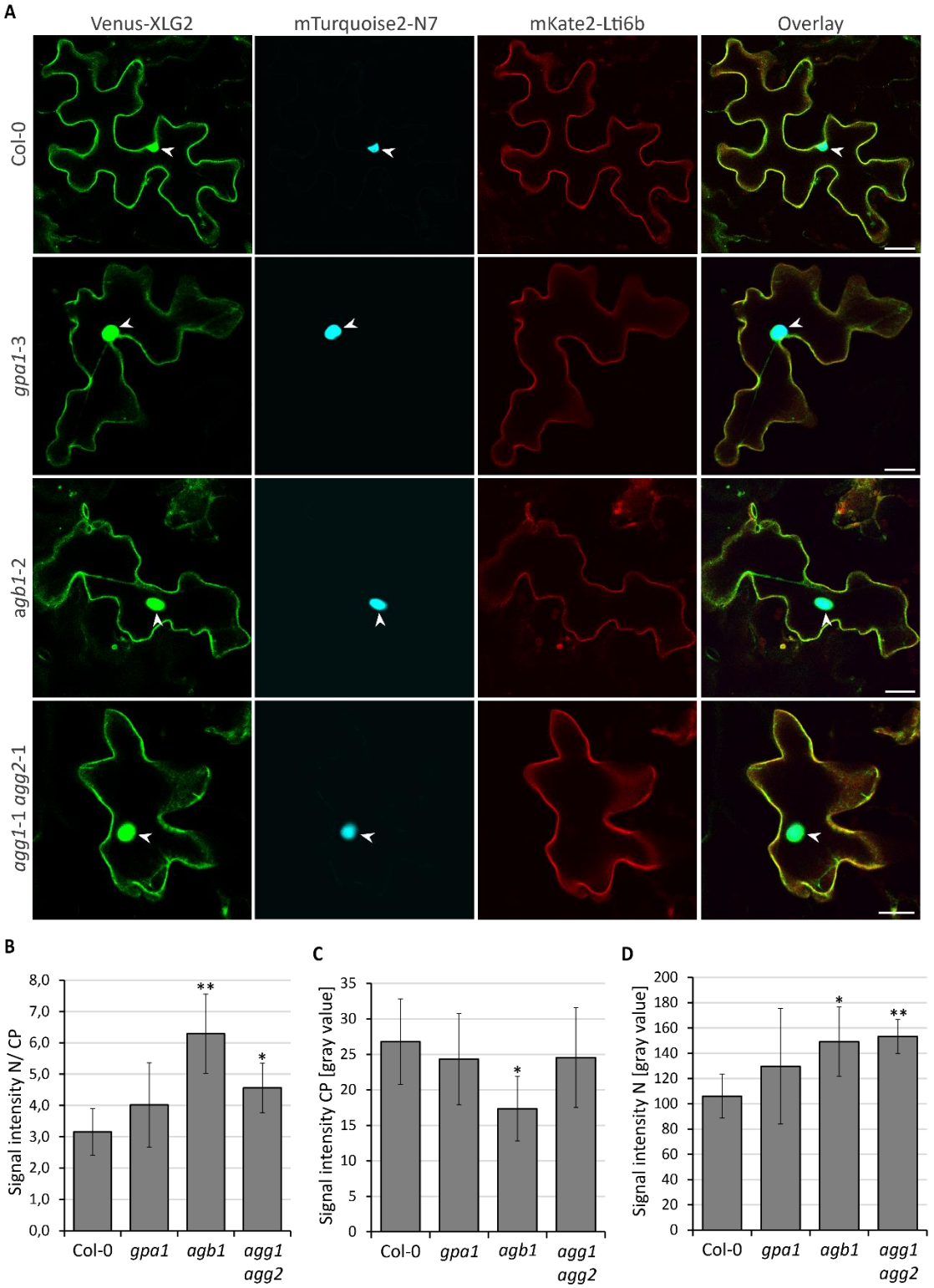

Fig. 51: Transiently expressed Venus-XLG2 localizes to PM and nucleus in G protein mutant *Arabidopsis* plants.

Venus-XLG2 was co-transformed with mTurquoise2-N7 (nuclear marker) and mKate2-LTI6b (PM marker) in Col-0 as well as *gpa1*-3, *agb1*-2, and *agg1*-1 *agg2*-1. **(A)** Representative single plane CLSM images of three independent experiments 1d after bombardment. Nuclei are marked by arrowheads. Scale bar = 50µm.

Quantification of Venus-XLG2 localization in particle bombardment experiments: Signal intensities for **(B)** N/ CP, **(C)** CP, and **(D)** N. Venus intensity was measured in N (= nuclear) and CP (= cell periphery) regions defined by mTurquoise2 and mKate2 channels. Data are means ± StDev of n ≥ 5 cells. * P <0.05 ** P<0.001

3.8 XLG2 associates with the haustorial periphery

Strong local accumulation of Venus-XLG2 at late infection time points with *Ec* was observed in this study and, earlier, a role of XLG2 in pre-invasive resistance against *E. pisi* (*Ep*) was described (Humphry et al. 2010). Inoculation of *Arabidopsis* with the adapted powdery mildews *Ec* or *Ep* results in a compatible interaction with more frequent formation of haustoria. When the fungal feeding structure grows, the plant synthesizes the extrahaustorial membrane (EHM) and also tries to encase the haustorium (Bozkurt and Kamoun 2020). Extrahaustorial encasements (EHC) are defense related cell wall appositions similar to papillae that contain not only cell wall material but also membrane lipid materials and MVBs (Underwood 2012). Partial or complete encasements surrounded only mature haustoria of several tested powdery mildews including *G. orontii* (*Go*), *Bgh* and *Ep* (Meyer et al. 2009). The number of mature *Go* haustoria increased one day after infection onwards (Meyer et al. 2009). In order to characterize the accumulation of XLG2 at the *Ec* haustorial periphery a CLSM-based analysis of these sites was included in this study. Transgenic plants expressing a selection of the previously characterized Venus-XLG2/ xlg2 variants (3.1 - 3.6) were infected with *Ec* and analysed after seven days when fungal growth was more advanced due to the formation of secondary hyphae and, accordingly, a considerable number of successfully formed haustoria was present. An overview of the infected leaf epidermis and the predominant localization pattern of the fusion proteins are presented in Fig. 52. Venus-XLG2 WT/ -NES and Venus-xlg2 nls426 strongly label the cell periphery of infected cells, while Venus-XLG2-NLS and Venus-xlg2 E293K/ nes387 predominantly label nuclei. Further, Venus-XLG2-NES and Venus-xlg2 nls426 showed reduced nuclear labeling compared to Venus-XLG2 WT. This agrees with the previously described subcellular changes of these XLG2 variants. In addition to the previous observations, Venus-xlg2 nls426 occasionally showed weak nuclear accumulation at these very strong expression rates. Other N-terminal XLG2 NLSs were perhaps sufficient to drive a small pool of xlg2 nls426 into the nucleus which became visible only at strong expression rates. In contrast, the C-terminally attached NES was more sufficient to drive XLG2 outside the nucleus even at strong expression levels. Propidium iodide was used to stain fungal hyphae and haustoria as well as the plant PM, stomata, and nuclei. Venus-XLG2 WT as well as Venus-XLG2-NES and Venus-xlg2 nls426 accumulated at the haustorial periphery (HP) at haustorial formation sites presented in Fig. 53, Fig. S 27, and Fig. S 28. The EHC became visible by PI staining and in the bright field channel. Venus-XLG2 WT/ -NES and Venus-xlg2 nls426 seemed to accumulate within the EHC. In contrast, Venus-XLG2-NLS as well as Venus-xlg2 E293K/ nes387 accumulated less efficiently at the HP. Previously, Venus-XLG2-NLS showed cell periphery localization at basal abundance which did not increase upon infection. Accordingly, all XLG2 variants which showed inducible cell periphery abundance were able to label *Ec* haustoria.

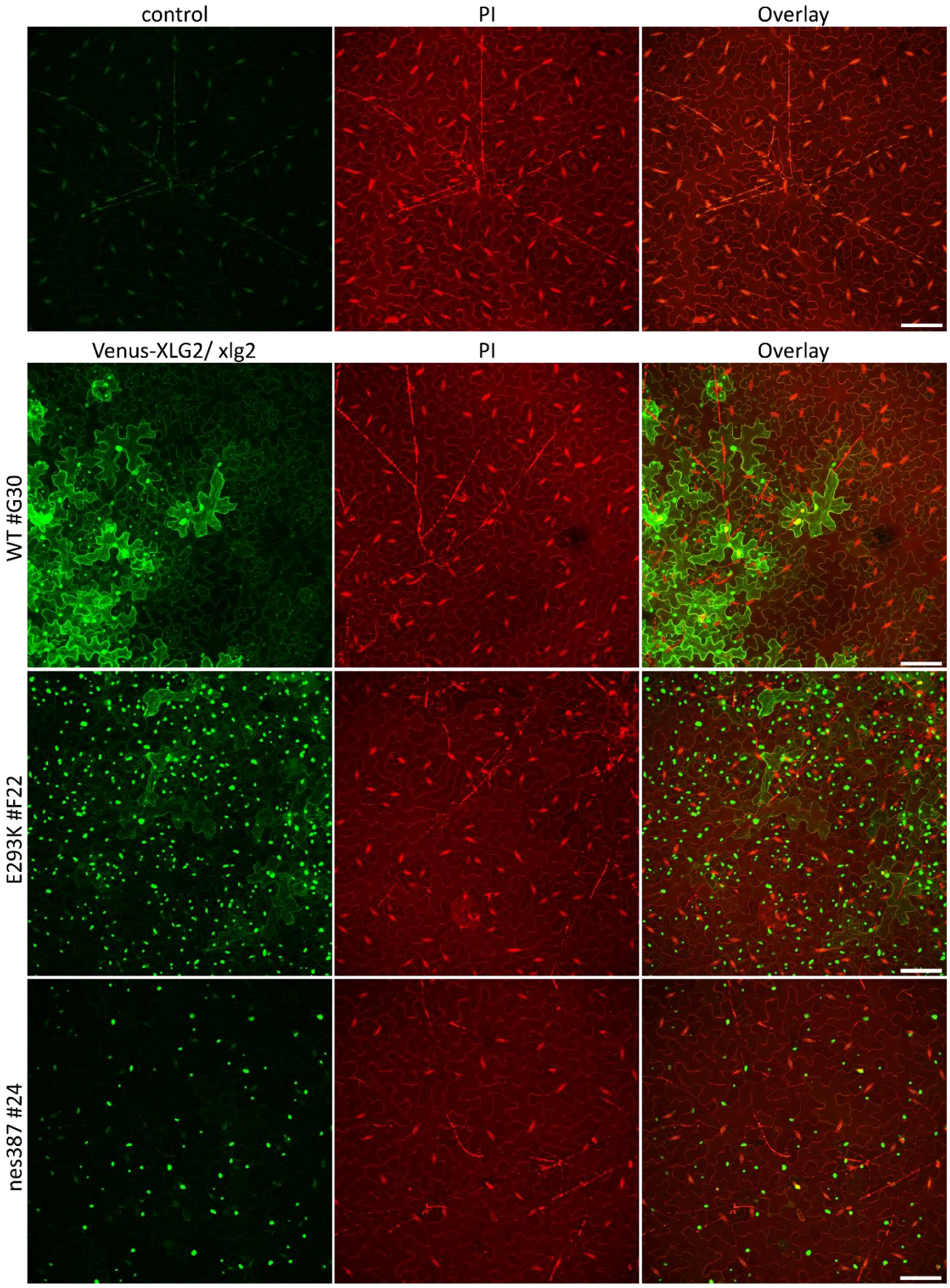
control
PI
Overlay
Venus-XLG2/ xlg2
PI
Overlay
WT #G30
E293K #F22
nes387 #24

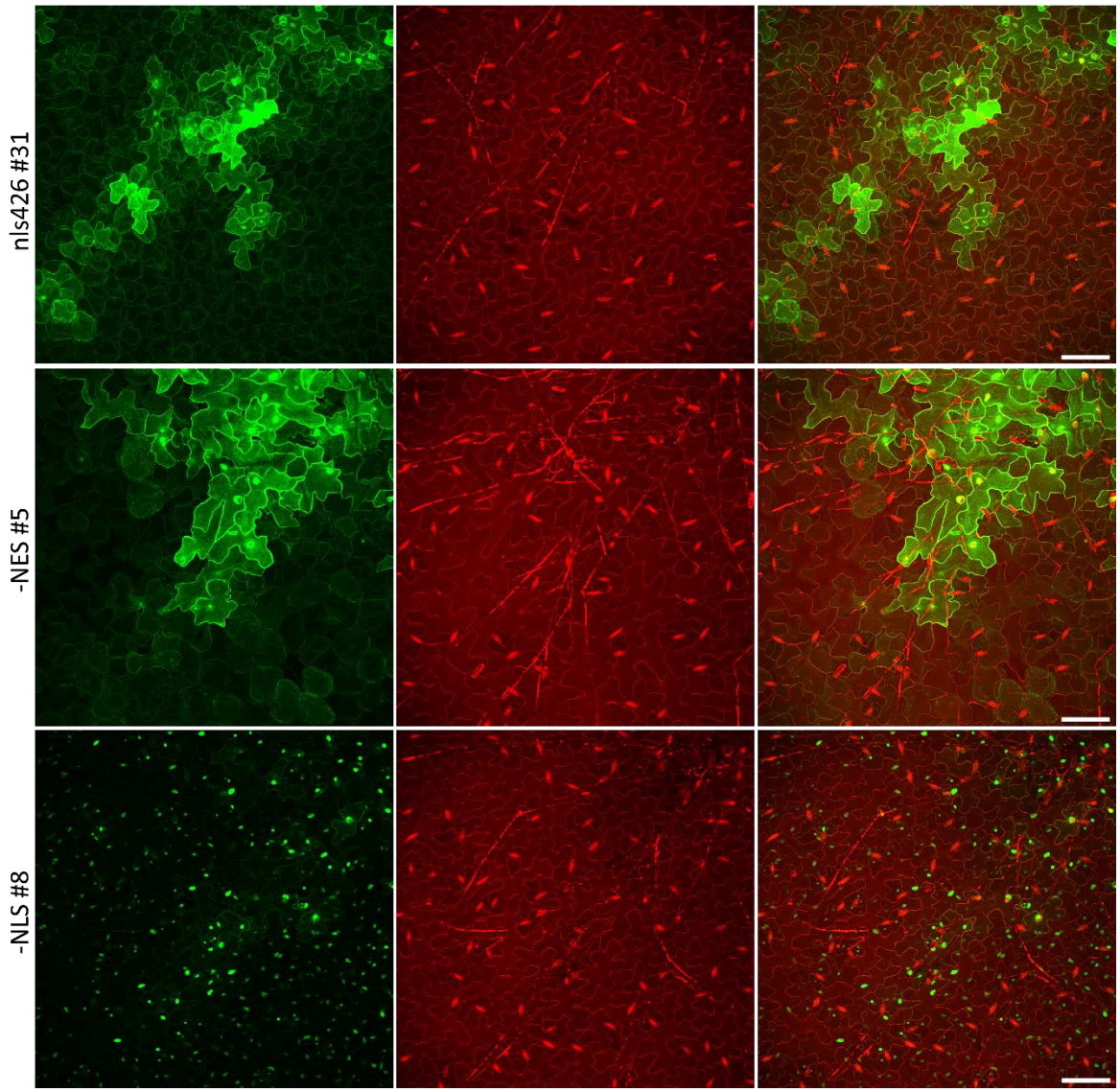

Fig. 52: Local accumulation of XLG2 beneath *Ec* secondary hyphae growth in *xlg2*-2.

CLSM images are maximum projections of 32 - 40 focal planes. Transgenic *xlg2*-2 expressing Venus-XLG2, Venus-xlg2 E293K, Venus-xlg2 nes387, Venus-xlg2 nls426, Venus-XLG2-NES, Venus-XLG2-NLS and a non-transformed control at 7dpi *Ec*. PI stained plant membrane/ stomata/ nuclei and fungal hyphae/ haustoria. Scale bar = 100µm. PI = propidium iodide.

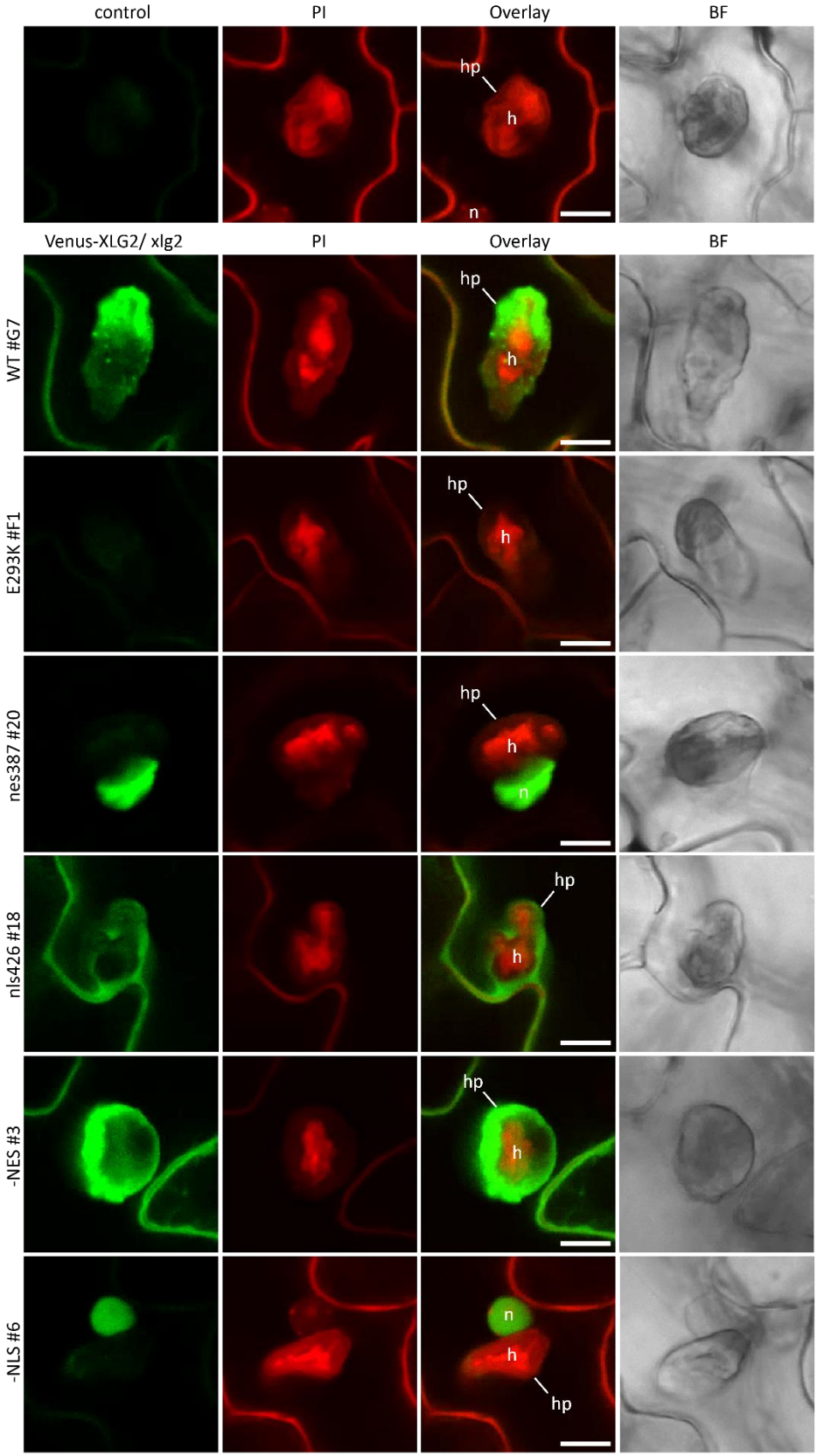

Fig. 53: Mainly nuclear localized mutant variants abolish association of XLG2 with haustorial periphery in *xlg2*-2.

CLSM images are representative single planes of transgenic *xlg2*-2 expressing Venus-XLG2, Venus-xlg2 E293K, Venus-xlg2 nes387, Venus-xlg2 nls426, Venus-XLG2-NES, Venus-XLG2-NLS and a non-transformed control with fully developed *Ec* haustoria recorded at 7dpi. PI stained plant membrane/ stomata/ nuclei and fungal hyphae/ haustoria. Scale bar = 10µm. n = nuclei, h = haustoria, hp = haustorial periphery, PI = propidium iodide, BF = bright field.

Next, Venus-labeled and only PI-stained haustoria were counted and the percentage of labeled haustoria was calculated (Fig. 54). Venus-XLG2-NLS and Venus-xlg2 E293K/ nes387 barely labeled haustoria with a significant difference compared to Venus-XLG2 WT. For Venus-XLG2-NLS slightly more labeled haustoria were counted compared to Venus-xlg2 E293K/ nes387 likely due to the remaining PM-localization at basal levels.

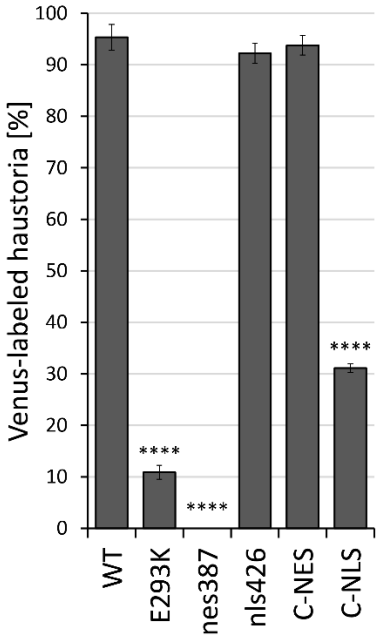

Fig. 54: Mainly cell periphery localized XLG2 variants label haustoria.

Venus-labeled haustoria were counted in Venus-XLG2 WT, Venus-XLG2-NES/ -NLS and Venus-xlg2 E293K/ nes387/ nls426 expressing *xlg2*-2 and presented as percentage of labeled haustoria at 7dpi *Ec*. Data are means ± StDev of 50 haustoria of 3 plants (n = 150) from three independent lines. **** $P < 0.0001$

This study indicates that Venus-XLG2 likely accumulates inside the EHC. XLG2 variants that did not accumulate within the nucleus (nls426, XLG2-NES) still labeled *Ec* haustoria comparable to XLG2 WT. In contrast, XLG2 variants with reduced (-NLS) or lost (E293K, nes387) PM-localization showed significantly reduced labeling of haustoria compared to XLG2 WT. This observation indicates that the PM-localization of XLG2 is necessary for trafficking towards the HP.

4 Discussion

4.1 XLG2 shows dynamic abundance and localization in dependence to stress signals

In this study, different approaches were used to analyze the subcellular localization of XLG2. Transiently expressed Venus-tagged constructs under endogenous promoter control including the 5' UTR were analysed in *A. tumefaciens* infiltrated *N. benthamiana*. In agreement with previous findings, XLG2 WT strongly labeled the plasma membrane, nuclei and cytoplasmic strands (Meusel 2016; Maruta et al. 2015; Chakravorty et al. 2015). Transient expression of Venus-XLG2 WT was also analysed in particle bombarded *xlg2*-2 *Arabidopsis* plants, which resembled the observations made in *N. benthamiana*. In contrast, the analysed E293K mutation, which was identified in the *cerk1*-4 suppressor screen (Meusel 2016), caused a significant loss of plasma membrane localization in *N. benthamiana* as well as in particle bombarded *xlg2*-2 *Arabidopsis* plants. Plasma membrane localization was indicated by sharp fluorescent signals that overlapped with the plasma membrane marker signal, while mainly cytoplasmic signals were visible as diffuse and much weaker signal at the cell periphery. Accordingly, the term cell periphery used in this study refers to the plasma membrane as well as peripheric cytoplasmic signals. In contrast to transient systems, stably transformed *Arabidopsis* plants showed few Venus-XLG2-labeled nuclei. Instead, a weak but continuous cell periphery signal was observed from young age (4-weeks-old) to older plants (7-weeks-old). One possible explanation for this discrepancy could be the lack of homology between *Arabidopsis* and *N. benthamiana* heterotrimeric G proteins. On the other hand, particle bombarded plants also showed strong nuclear signals. Accordingly, a more likely explanation is stress induced nuclear accumulation of XLG2. The native XLG2 promoter including complete 5' UTR was found to contain many stress-responsive cis-acting elements (Humphry et al. 2010) and the mRNA level of XLG2 was increased upon infection (Zhu et al. 2009). In this work, evidence was collected that Venus-XLG2 is mainly found at the cell periphery in unchallenged transgenic *xlg2*-2 and *cerk1*-4 *xlg2*-2. In contrast, xlg2 E293K was found mainly inside the nucleus in unchallenged transgenic *xlg2*-2 and *cerk1*-4 *xlg2*-2. Upon powdery mildew infection Venus-XLG2-derived signals were enhanced, and nuclei were labeled. The abundance of XLG2 and xlg2 E293K was significantly induced upon infection, which was characterized using CLSM as well as Western blotting analysis. These findings agree to previous expression data and observed elicitor/ wounding inducibility of XLG2 (Zhu et al. 2009; Humphry et al. 2010; Meusel 2016). XLG2 showed a significantly stronger increase in protein abundance upon pathogen inoculation compared to xlg2 E293K, while both were significantly induced in *xlg2*-2 as well as *cerk1*-4 *xlg2*-2. Conclusive from this data is that xlg2 E293K might lack a potential feed forward regulation or has a reduced stability. This

effect was slightly weaker when the α-XLG2 antibody was used instead of the α-GFP antibody. The reason for this difference is unclear. One possibility is a difference in affinity of the antibodies to the epitope. Concerning the GFP antibody, no obvious indication for any affinity difference between Venus-XLG2 and Venus-xlg2 E293K is present. In contrast, the XLG2-specific antibody recognizes a region at the N-terminus of XLG2, which is known to be heavily phosphorylated (Chakravorty and Assmann 2018; Liang et al. 2016). It is possible that, due to the E293K (nes387, C-As) mutation, the phosphorylation pattern within the XLG2 N-terminus is changed, which would explain the observed motility difference. The polyclonal antibody against the XLG2 N-terminus (1-200 amino acids), which was expressed in *E. coli*, potentially labeled xlg2 E293K better than XLG2 WT, due to the changed phosphorylation pattern. *Vice versa*, it is possible that XLG2 WT phosphorylations at the antibody recognition site reduce the strength of interaction with the antibody and, thus, the XLG2-specific antibody might give weaker signals for XLG2 WT. However, even when using the α-XLG2 antibody, the same difference in protein abundance between XLG2 WT and xlg2 E293K was observed, only less pronounced. To further characterize a potential role of XLG2 WT in feed forward regulation using Western blotting it would be possible to analyze native XLG2 abundance in non-transformed *xlg2*-3 which naturally harbor the E293K mutation (Meusel 2016) in comparison to Col-3 *gl*1 and *cerk1*-4 before and after infection with *Ec* (best 3 - 5dpi) using the XLG2-specific antibody. The other possible explanation for the observed protein abundance difference, reduced stability of xlg2 E293K, could be further analysed by XLG2 WT and xlg2 E293K mRNA expression profiling via RT-PCR before and after infection in parallel to the Western Blot approach. Protein stability could be further analysed via a pulse-chase assay, which is based on radioactive metabolic labeling, or via a ubiquitin-protein-reference (UPR)-assay. The UPR-assay is based on a reporter fusion (e.g. luciferase and chlor-amphenicol acetyl transferase, LUC/ CAT) that allows direct quantification from crude cell lysates (Planchais et al. 2016). The activity of LUC/ CAT was described to reflect the degradation of the analysed protein or protein variants (Planchais et al. 2016; Chenon et al. 2012). Protein abundance could be further analysed using mass spectrometry perhaps also in combination with isotope labeling (e.g. stable isotope labelling by amino acids in cell culture, SILAC) (Lewandowska et al. 2013) or by measuring the protein half-life (Guo and Yin 2019) of XLG2 WT vs. xlg2 E293K. For the last-mentioned approach, the protein translation inhibitor Cycloheximide is usually used. Due to the low basal protein abundance of XLG2 in the absence of any stress signal, it might be useful to treat plants with MG132 overnight before Cycloheximide treatment. Regarding the observed changes in subcellular localization of XLG2, it would be interesting to further characterize whether plasma membrane localized XLG2 moves to the nucleus upon a stress signal or newly synthesized protein accumulated within the nucleus. A fluorescence recovery after photobleaching (FRAP) approach could be used to further analyze protein mobility within living cells (Bancaud et al. 2010). A protein synthesis-inhibitor (e.g.

cycloheximide) could be used to block XLG2 synthesis and test whether PM-derived XLG2 accumulates in the nucleus. MG132 treatment alone might result in nuclear accumulation of XLG2, in case of primarily interaction-dependent XLG2 PM-tethering, which could potentially reach a saturation point. Previously, PM association of XLG2 was confirmed based on CLSM analysis (Meusel 2016; Maruta et al. 2015; Chakravorty et al. 2015). Microsomal preparation from *Arabidopsis* plants stably expressing XLG2 revealed contradictory results, with either detectability of XLG2 only in the soluble fraction (Meusel 2016), while Maruta et al. detected XLG2 in the microsomal fraction. The used protocols differ in some details. Maruta et al. used a higher initial spin for separating nuclei from the extract and both used a final ultracentrifugation step, while Meusel performed an additional ultracentrifugation step. Further, the used promoters for transgene expression differed. Meusel used the endogenous XLG2 promoter, which results in low basal abundance of XLG2, while Maruta et al. used the 35S promoter, which might explain the contradictory results. Optimized microsomal preparations could help to further identify XLG2-interacting proteins at the plasma membrane via subsequent proteomics analysis. Microsomal preparations could also be used to further characterize the XLG2 mutant variants with changed subcellular localization described in this study. It was shown that XLG2 accumulates when proteasome inhibitors (e.g. MG132) are used, indicating that XLG2 is subject to proteasome-dependent degradation (Zhu et al. 2009). Proteasome inhibitors could be used to trigger accumulation of XLG2 in unchallenged tissue, while infected or elicitor-treated plant material could be included in this analysis in order to identify defense signalling-dependent changes of XLG2-protein interactions. Currently, it is not clear how exactly XLG2 is tethered to the plasma membrane. Protein-interactions and/ or S-acylations are possibly involved. For the small GTPase ROP6 (Rho of plants) cycling between soluble and insoluble membrane fractions in response to in-/activation as well as de/-acylation was described (Hemsley 2009). For XLG2 it is unclear if nucleotide-dependent conformation changes occur *in vivo* (Lou et al. 2019). It is tempting to speculate, that the subcellular localization of heterotrimeric Gα subunits, including GPA1 and XLGs, during nucleotide-dependent and independent functions (Maruta et al. 2019), could be regulated by reversible S-acylation as well as phosphorylation. Further, reversible S-acylation was found to stabilize proteins such as RIN4 (RPM1 interacting protein), which is a guarded inhibitor of defense signalling (Kim et al. 2005). In this study, frequently weaker protein bands in Western blotting were detected for the mainly nuclear localized XLG2 variants (nes387; C-As: C214/217A, C229/232/237/240A, C254/257A). Changes in stability or potential loss of feed forward regulation remain to be analysed for these XLG2 variants similarly to xlg2 E293K. One indication for a possible decrease in stability was the observed stronger signal for xlg2 E293K compared to XLG2 WT, when using a ubiquitin-specific antibody in Western Blot analysis, which could be interpreted as indication for a stronger polyubiquitination of the mutant variant (Hacke, unpublished).

4.2 PM-associated XLG2 mediates *cerk1*-4 cell death signalling

XLG2 mutant variants with changed subcellular localization were obtained in this study, including E293K which was initially identified as suppressor mutation of *cerk1*-4 (Meusel 2016). XLG2 nuclear localization and export signals were mutated and analysed. The XLG2 NES387 was identified based on homology to a previously described XLG3 NES (Chakravorty et al. 2015) and confirmed to be functional by the data presented here. The XLG2 NLS426 was also found to be functional, which agrees to previous results (Chakravorty et al. 2015). Strikingly, the results obtained in this study indicate, that plasma membrane association is a major necessity for *cerk1*-4 cell death signalling, as several mutant variants with lost plasma membrane localization (E293K, nes387, C-As) failed to complement *xlg2*-2 in *cerk1*-4 *xlg2*-2. The loss of plasma membrane localization was indicated by absence of a continuous sharp plasma membrane signal, while instead a weak, diffuse cell periphery signal (likely mainly cytoplasmic) was visible. In addition, viral localization signals (NLS/ NES) and the respective controls (mutated, non-functional nls/nes) (Heidrich et al. 2011) were fused to the C-terminus of XLG2 resulting in changed subcellular localization. The data presented here shows that nuclear accumulation of XLG2 is dispensable for *cerk1*-4 cell death signalling as two nuclear exclusion variants (nls426, XLG2-NES) fully complemented *xlg2*-2. XLG2-responsive genes might be relevant for *cerk1*-4 cell death signalling even though this study shows that nuclear localization of XLG2 is dispensable. Cytoplasmic or PM-localized XLG2 could indirectly be involved in gene expression regulation. Nuclear exclusion variants could be used for co-immunoprecipitation and subsequent proteomics in order to identify XLG2-interacting proteins specifically important at the plasma membrane. C-terminal fusion of a viral NLS did not result in complete loss of PM association and only nuclear signals significantly increased upon infection. Accordingly, a sharp and continuous signal was observed for XLG2-NLS at the cell periphery which did not resemble the xlg2 E293K variant but XLG2 WT. It is important to underline that the PM signals for Venus-XLG2-NLS did not significantly increase upon infection in contrast to Venus-XLG2 WT, Venus-xlg2 nls426 and Venus-XLG2-NES. As the XLG2-NLS variant fully complemented *xlg2*-2, constitutive PM association at basal expression levels is likely most important for *cerk1*-4 cell death signalling. Moreover, over-accumulation of nuclear XLG2 does not abolish *cerk1*-4 cell death signalling.

Further aspects of XLG2 localization-specific function could be analysed by expressing mainly nuclear localized or nuclear exclusion variants of XLG2 in the *xlg1/2/3* triple mutant in order to analyze complementation of the developmental growth phenotype (Wang et al. 2017). The potential XLG2 NLS275 was predicted to be enhanced by the E293K mutation. However, it was not possible to show a causative connection between the predicted enhanced NLS275 and nuclear localization of the XLG2 E293K variant. The combined mutations KR-AA+E293K, with decreased probability of NLS275-dependent nuclear accumulation, did not alter the constitutive nuclear accumulation of XLG2 caused

by the E293K mutation. The potential NLS275 might be involved in supporting nuclear accumulation, while other NLSs (e.g. NLS426) are mainly responsible for directing XLG2 towards the nucleus. Accordingly, the KR-AA mutation might not have a detectable impact on XLG2 localization. In the future, the C-terminal NES could be combined with the nes387 mutation in order to reverse the observed nuclear accumulation of XLG2 harboring the nes387 mutation. This study showed that the C-terminal NES fusion very efficiently excludes XLG2 from the nucleus. Expression of Venus-xlg2(nes387)-NES might result in WT-like localization and functionality of XLG2 in *cerk1*-4 cell death signalling. This potential complementation would be a stronger indication for localization-specific changes in functionality of XLG2. If the nes387 mutation cannot be complemented by adding a functional NES, the lost nuclear export signal would not likely be causative for the nuclear accumulation and loss of functionality of this XLG2 variant. In this case, other effects such as changed protein interaction sites or post-translational modifications could be more relevant for PM-association and functionality than nuclear export of XLG2. According to the results obtained in this work, PM-association of XLG2 is highly important, while nuclear localization is dispensable for *cerk1*-4 cell death signalling. The nuclear pore complex component MOS7 was identified as suppressor of *cerk1*-4 (Genenncher et al. 2017). MOS7 was found to be involved in transporting conserved immune signalling components through the nuclear pore complex including EDS1 and NPR1, which are essential for SA-signalling (Wiermer et al. 2010) and the *cerk1*-4 phenotype depends on SA-accumulation (Petutschnig et al. 2014). The *mos7* mutation results in reduced nuclear accumulation of EDS1, causing major defects in plant immunity (Wiermer et al. 2010). EDS1 together with PAD4 were also identified as suppressors of *cerk1*-4 (Petutschnig et al. 2014). Cytoplasmic EDS1-PAD4 heterodimers and SA-signalling positively regulate each other and induce defense genes to robustly counteract biotrophic pathogens (Straus et al. 2010; Cui et al. 2017). Accordingly, the role of MOS7, EDS1 and PAD4 in *cerk1*-4 cell death signalling is likely linked to SA-signalling.

4.3 Post-translational modification of XLG2 might be important for *cerk1*-4 cell death signalling

The current idea of the plant heterotrimeric G protein complex during immune signalling is defined by presence of all involved components (XLG2-AGB1-AGG1/2-RGS1) at the PM needed for BIK1-dependent phosphorylation and downstream involvement in ROS-burst (Liang et al. 2016; Liang et al. 2018; Maruta et al. 2019; Lou et al. 2019). Loss of these interactions potentially not only cause changed localization dynamics in the absence of the Gβγ-dimer (this work) but also potentially profound side effects regarding post-translational modifications. In this study, several mainly nuclear localized xlg2 mutant variants (E293K, nes387 and C-A) were generated and characterized. The drastically reduced cell periphery signal and absence of sharp, continuous signal in all these mutants indicates a loss of

plasma membrane attachment, which could be further analysed by microsomal fractionation. These mainly nuclear localized XLG2 variants share the loss of functionality regarding *cerk1*-4 cell death signalling. *cerk1*-4-specificity of these loss of function mutations could be further tested by starting a *xlg1/2/3* triple mutant developmental growth phenotype complementation analysis. These mutations share a lower apparent molecular mass compared to XLG2 WT in Western Blots, which indicates that post-translational modifications are lost either as a side effect from lost PM-association or causative and potentially involved in loss of PM association. A diverse repertoire of reversible post-translational modifications is known to play a role in plant immune signalling including phosphorylation, single-/ poly-ubiquitination, S-nitrosylation (refers to binding of a NO to the thiol group of a cysteine residue) and S-acylation (Zheng et al. 2019; Zhang and Zeng 2020). Regarding S-nitrosylation it is worth to mention that RbohD was found to be S-nitrosylated and this modification was found to downregulate ROS production as well as the subsequent HR response (Yun et al. 2011). Recently, phosphoproteomics data revealed that the phosphorylation pattern at the N-terminus of XLG2 harboring the E293K mutation is changed in comparison to XLG2 WT (Petutschnig, unpublished). These phosphorylation changes potentially influence the protein conformation und, thus, can cause changes in motility in Western blotting. Mutational analysis of these phosphorylation sites could help to further understand the reasons for the observed motility difference. BIK1 was found to phosphorylate XLG2 (Liang et al. 2016) and four N-terminal XLG2 phosphorylation sites (S141/148/150/151) were analysed concerning potential involvement in *cerk1*-4 cell death signalling (Petutschnig, Hacke and Anders, unpublished). Phosphomimic and phosphodead mutant variants both complemented *cerk1*-4 *xlg2*-2. Accordingly, these BIK1-specific phosphorylation sites did not affect *cerk1*-4 cell death signalling. Interestingly, BIK1-targeted phosphorylation sites were found to be even stronger phosphorylated in the presence of the E293K mutation (Petutschnig, unpublished). These findings agree with the previously shown independence of the *cerk1*-4 cell death phenotype from chitin signalling (Petutschnig *et al.* 2014) and ROS burst (Trippel, 2020). Importantly, XLG2 WT apparent molecular mass was changed by phosphatase treatment resembling the xlg2 E293K variant (Petutschnig, unpublished). Many phosphorylation sites were found for XLG2 especially at the N-terminus, as recently reviewed (Chakravorty and Assmann 2018). How exactly the changed phosphorylation pattern in xlg2 E293K affects *cerk1*-4 cell death signalling remains to be shown. A selection of phosphorylation sites could be mutated into phosphodead (S into A) or phosphomimic (S into D) variants and analysed regarding complementation of *cerk1*-4 *xlg2*-2. Interestingly, native XLG2 showed a motility difference in Western Blot samples from *agb1* compared to Col-0, which might be explained by changes in post-translational modifications (E. Petutschnig, unpublished). Further, stably transformed *agb1* expressing Venus-XLG2 WT were analysed and showed more frequent nuclear accumulation and retained PM localization

compared to Col-0 (Petutschnig, unpublished) which agrees to the particle bombardment data presented in this work.

One XLG2 variant harboring a KR-AA mutation within the potential NLS at position 275 was analysed in this study. The KR-AA XLG2 variant did show the same motility difference as observed for XLG2 harboring the E293K, nes387 or C-As mutations. E293K, nes387 and C-As XLG2 variants predominantly localized to the nucleus and were non-functional regarding *cerk1*-4 cell death signalling. In contrast, expression of Venus-xlg2 KR-AA complemented *cerk1*-4 *xlg2*-2 and WT-like subcellular localization was observed. Accordingly, the KR-AA mutation did not change the localization of XLG2 but the apparent molecular mass. One explanation would be that protein-protein interactions are affected by the KR-AA mutation which may be needed for post-translational modifications. Post-translational modifications could be changed which might result in the changed apparent molecular mass. Changes in the interactome could be investigated by GFP-pull down and subsequent co-immunoprecipitation or proteomics analysis. Modifications such as phosphorylations could be further analysed using the proteomics data. It would be interesting if the observed motility difference in E293K and KR-AA as well as nes387 and C-As is caused by similar changes of the phosphorylation pattern or other post-translational modifications. The E293K mutation resulted in mainly nuclear localization and was predicted to enhance the potential NLS275. The combined KR-AA+E293K mutation was predicted to localize WT-like, in contrast to the single E293K mutation. However, the KR-AA+E293K XLG2 variant showed mainly nuclear localization. This observation indicates that the E293K mutation might not enhance a potential NLS at position 275 or that the KR-AA mutation had no effect on localization. It would be interesting to analyze whether the Venus-xlg KR-AA expression would be enough to complement the growth phenotype or ROS-burst defects of *xlg1/2/3*. In addition to the mainly nuclear-localized variants, these results indicate that the PM localization is primarily important in *cerk1*-4 cell death signalling.

4.4 The XLG2 cys-rich region is important for PM localization and *cerk1*-4 cell death signalling

The cys-rich region is in proximity to the analysed E293K mutation, which had tremendous impact on functionality, subcellular localization, and the apparent molecular mass of XLG2. The cys-rich region of XLGs is annotated as degenerate RING zinc finger domain (Lee and Assmann 1999). Most RING zinc finger proteins likely have E3 ligase activity (Sun et al. 2019; Jiménez-López et al. 2018). While most of the 508 *Arabidopsis* RING finger domain proteins use a histidine at one of the conserved zinc coordinating positions the eight cysteine containing RING fingers (RING-C2) represent a minor group in plants with only 16 genes (Jiménez-López et al. 2018). Unfortunately, XLGs were not included in this study albeit their annotation as degenerate RING-containing proteins (Jiménez-López et al. 2018).

Accordingly, it is still unclear whether the eight conserved cysteines in the XLG cys-rich region form a RING structure and if so, whether they perform E3 ligase activity or not. The eight RING domain cysteines of two JUMONJI-domain containing proteins JMJ24 and JMJ25 aligned with the eight XLG cysteines (Fig. S 22). JMJ24 was found to have E3 ligase activity (Kabelitz et al. 2016), while JMJ25 (IBM1) showed demethylase activity (Miura et al. 2009). Conclusive from these known degenerate RING domains is that the XLG potential degenerate RING domains could perhaps function as E3 ligases or DNA-binding elements. However, cellulose synthase A catalytic subunit (CESA) proteins also have annotated degenerate RING domains (Kumar et al. 2020) and similarly to XLGs a conserved eight cysteine spacing pattern which aligns with the eight XLG cysteines (Fig. S 22). Further, several CESA proteins were shown to be S-acylated at multiple positions along the sequence. Recently, S-acylation within the potential RING domain of two CESA proteins was identified, which is surprising as S-acylations would contradict RING formation (Kumar et al. 2020). For the S-acylated sites found in cys-rich regions of CESA proteins it was concluded that zinc coordination is rather unlikely, while non-acylated cys-rich regions could still form a RING structure (Kumar et al. 2020). Kumar et al. concluded that CESA proteins might fulfil different functions based on these striking differences. No consensus region is known for plant S-acylation sites but cysteines surrounded by basic and hydrophobic amino acids are more likely S-acylated (Li and Qi 2017). The conserved cysteines within the cys-rich region of XLGs could, therefore, potentially be targeted for dynamic S-acylation instead of forming RING structures. Further, heterotrimeric G proteins such as GPA1 and AGG2 are known to be S-acylated and this S-acylation was shown to be important for PM localization (Adjobo-Hermans et al. 2006; Hemsley et al. 2008; Hemsley et al. 2013). The acylome data published by Kumar et al. (2020) indicated that S-acylation of potential RING domains is rare (Kumar et al. 2020). Kumar et al. might have not been able to identify S-acylation in any XLG protein due to low protein abundance (Zhu et al. 2009). They did find GPA1 S-acylations, while they did not find AGG2 S-acylations (Kumar et al. 2020). S-acylation can be dynamically regulated and is difficult to analyze (Zheng et al. 2019; Li and Qi 2017). Loss of S-acylation due to cysteine to serine/ alanine mutations is typically associated with loss of membrane tethering (Hemsley 2009) as first indication for potential S-acylation. The results obtained in this study concerning subcellular localization of Venus-tagged xlg2 cys-rich region mutant variants, namely xlg2 C214/217A, C229/232A, C229/232/237/240A and C254/257A (C-As), revealed that the cys-rich region is important for PM-localization. Any exchange of a conserved cysteine for alanine within the cys-rich region caused an overall loss of XLG2 PM-tethering. This finding would support the idea of potential S-acylation within the XLG2 cys-rich region. Presence or absence of S-acylations usually do not simply cause a motility difference in Western blotting. Potential S-acylation of XLG2 (with AGG2 as positive control) vs. xlg2 C-A mutant variants could be analysed by using a biotin switch assay (Hemsley et al. 2008). Another approach could be a resin assisted capture (acyl-RAC) assay (Forrester et al. 2011;

Tewari et al. 2020). E3 ligase activity is widespread among RING proteins and due to the alignment of the eight conserved cysteines of XLGs to known RING proteins with confirmed E3 ligase activity, this issue might be worthy of answering by expressing and purifying only the potential XLG2 RING domain in order to perform an *in vitro* auto-ubiquitination and Zn-binding assay. The idea that XLGs might be tethered to the PM by S-acylation is supported by the observation that absence of *agb1* or *agg1 agg2* did not result in loss of PM localization of XLG2, which was analysed via particle bombardment in this work. In addition to the potential RING-formation or S-acylation, the XLG cysteines within the cys-rich regions could be involved in disulfide bond formation useful as structural element for stabilization and redox (ROS) responsiveness (Waszczak et al. 2015). The disulfide bond prediction for XLG2 using the DISULFIND bonds prediction tool (Ceroni et al. 2006) indicates that the eight cysteines within the cys-rich region could theoretically form disulfide bonds but are not likely bonded based on internal distance considerations. One possible approach to experimentally confirm presence of disulfide bonds would be extraction of the protein with and without reducing agent (e.g. DTT). Subsequent treatment with the oxidizing agent PEG-maleimide results in coupling to free thiol groups and slower migration in SDS-gel, while a final DTT-treatment step quenches this labeling reaction (Braakman et al. 2017). If disulfide bridges are present in the non-reduced sample, the non-reduced PEG-maleimide-treated sample should migrate faster. If many cysteines are present, that potentially form disulfide bridges, the effect should be strong enough to be visualized. In the case of the XLG2 cys-rich region this might be, therefore, a suitable approach due to the presence of many cysteines. Independent from any domain similarity it is worth to mention that the cys-rich region of the heterotrimeric G protein AGG3 C-terminal extension was confirmed to be mainly important for PM tethering (Wolfenstetter et al. 2015). The results obtained in this study show that loss-of-function regarding *cerk1*-4 cell death heavily correlates with loss of PM localization of XLG2 as several XLG2 variants with lost PM localization (E293K, nes387, C-As) were identified that no longer complement *cerk1*-4 *xlg2*-2.

4.5 Nucleotide-independent function of XLG2 in *cerk1*-4 cell death signalling

In this study, the XLG2 Gα-like domain was mutated to lose potential *in vivo* nucleotide-binding capacity (T476N) (Heo et al. 2012) or GTP-hydrolysis activity (R673L) resulting in a presumed constitutive active variant (Maruta et al. 2019). These two mutant variants were characterized concerning subcellular localization using an N-terminal Venus-tag and stably transformed plants. The analysed GTP-binding/ -hydrolysis deficient xlg2 mutant variants had no effect on subcellular localization of XLG2 in unchallenged and *Ec* infected plants compared to XLG2 WT. Further, the potential defects in the Gα-like domain did not render XLG2 non-functional regarding *cerk1*-4 signalling as both constructs fully complemented *cerk1*-4 *xlg2*-2. These findings agree with the suggestion that XLGs might lack nucleotide-binding capacity *in vivo* (Lou et al. 2019) while retaining interaction with

other G proteins and RGS1, probably fulfilling mostly nucleotide-independent functions (Maruta et al. 2019; Lou et al. 2019). XLGs might be, therefore, mainly regulated by phosphorylation (Liang et al. 2018; Chakravorty and Assmann 2018). Interestingly, the dominant negative mutation S52C caused slightly reduced stability but retained PM localization of GPA1 (Maruta et al. 2019). Due to the lack of homology of key-residues for GTP-binding and GTPase activity it was suggested that the main function of XLG2 is to act as decoy Gα that rather blocks G protein signalling (Lou et al. 2019). However, Gα subunits with nucleotide-independent functions are known to exist in plants as GPA1 nucleotide-dependent as well as independent functions were described (Maruta et al. 2019). Further, XLG2 was found to play a major role in plant immunity together with AGB1-AGG1/ AGG2 as positive regulator of pathogen induced ROS-burst and cell death (Lorek et al. 2013; Liang et al. 2016; Maruta et al. 2015). GPA1 was described to play a role in stomatal opening and ROS-burst (Zhang et al. 2008a; Zhang et al. 2011). Accordingly, these Gα proteins could act cooperatively or independently in immune signalling (Liang et al. 2018; Xue et al. 2020) rather than antagonistic. These observations do not support the idea of a decoy Gα subunit. The results obtained in this study highlight a XLG2 function in *cerk1*-4 cell death signalling that does not depend on potential GTP-binding or GTPase activity, thus, presenting a nucleotide-independent function of this Gα-like protein. Another experimental approach in which only the N-terminal or C-terminal part of XLG2 is expressed in *Arabidopsis* plants would give insight whether the Gα-like domain is completely dispensable for *cerk1*-4 cell death signalling or might show that it is needed for important protein interactions. Since AGB1 and AGG1/ 2 were found to be involved in *cerk1*-4 cell death signalling (Petutschnig, unpublished) the XLG2 Gα-like domain might be required for protein interactions. Interestingly, over-expression of AGB1-AGG1/2 dimers was found to sequester XLG3 completely to the PM in *N. benthamiana* (Chakravorty et al. 2015) indicating an impact of these protein interactions on the localization of XLGs. Particle bombarded *Arabidopsis* G protein mutants were analysed here in order to characterize the impact of absence of known heterotrimeric G proteins on the subcellular localization of XLG2. Importantly, the AGB1 Gβ-subunit was found to be highly instable in absence of the main γ-subunits AGG1/2 (Adjobo-Hermans et al. 2006). Accordingly, G protein mutants *agb1* and *agg1 agg2* should resemble each other concerning their effects on XLG2 localization. For the classical Gα-subunit GPA1 Gβγ-independent localization to the PM was observed and GPA1 is known to be dually lipidated, which is needed for PM localization (Adjobo-Hermans et al. 2006). The CLSM data of transiently transformed *gpa1*, *agb1*, *agg1 agg2* and control Col-0 plants shows that XLG2 retains a PM-localized pool in all cases. However, in *agb1* and *agg1 agg2* the nuclear pool was found to be slightly increased while the PM-signals were slightly decreased. XLG2 seems to be influenced, at least partially, by the presence or absence of the Gβγ-dimer. Nevertheless, XLG2 retains PM localization similarly to GPA1 in the absence of the Gβγ-dimer (Adjobo-Hermans et al. 2006). The presence of the AGG3 subunit could be responsible for successful sequestration of XLG2 to

the PM (Maruta et al. 2015) in the *agg1 agg2* double mutant background but absence of AGB1 did not cause loss of PM localization of XLG2 either. Unknown protein interactions might be involved in PM-tethering of XLG2. Another idea is that XLG2 might be S-acylated, which would support PM tethering, and was discussed in more detail in 4.3. PUB2, AGB1 and RGS1 association seems to be mostly mediated by the C-terminus of XLG2 which contains the Gα-like domain (Liang et al. 2016; Liang et al. 2018; Wang et al. 2017). However, the N-terminus is also important for certain protein-protein interactions, as recently shown for the xlg2 E293K mutant variant which showed reduced interaction with AGB1 (Much, unpublished). Independent roles of AGB1 and XLG2 in immunity were described against *P. syringae* (Liang et al. 2016) while they showed no additive phenotypic effects against *F. oxysporum* and *A. brassicicola*, which was indirectly investigated using the *xlg2 xlg3 agg1 agg2* quadruple mutant (Maruta et al. 2015). Both were shown to act in similar ways and independently of SOBIR1 in *bir1*-1 cell death signalling (Maruta et al. 2015). In contrast to GPA1 S52C (Maruta et al. 2019), decreased stability of XLG2 T476N was not observed in this study (GPA S52 theoretically resembles XLG2 T476). XLG2 was found to be subject to proteasome-dependent degradation (Zhu et al. 2009). Constitutive interaction of PUB2 and PUB4 with XLGs was described before (Wang et al. 2017; Derkacheva et al. 2020). Further, PUB4 was found to interact with CERK1 and to positively regulate chitin signalling as well as BIK1 stability (Desaki et al. 2019a). It would be interesting to investigate XLG2 and CERK1 abundance in *pub2 pub4*.

In summary, potential nucleotide-binding and -hydrolysis was found to be irrelevant for *cerk1*-4 cell death signalling, providing evidence that cell death signalling is a nucleotide-independent function of XLG2. This finding agrees to the prediction that XLG2 is likely nucleotide-free *in vivo* (Lou et al. 2019), in contrast to the observed *in vitro* GTP-binding capacity (Heo et al. 2012), and is further supported by the commonly observed nucleotide-independent functions of GPA1 (Maruta et al. 2019).

4.6 Working model for *cerk1*-4 cell death signalling and outlook

In the following, the potential role of XLG2 in *cerk1*-4 cell death signalling will be discussed with an overview of other so far identified components relevant for this cell death pathway. The presented working model (Fig. 55) shows a conceivable crosstalk between these components and a potential mechanism behind the *cerk1*-4 cell death phenotype.

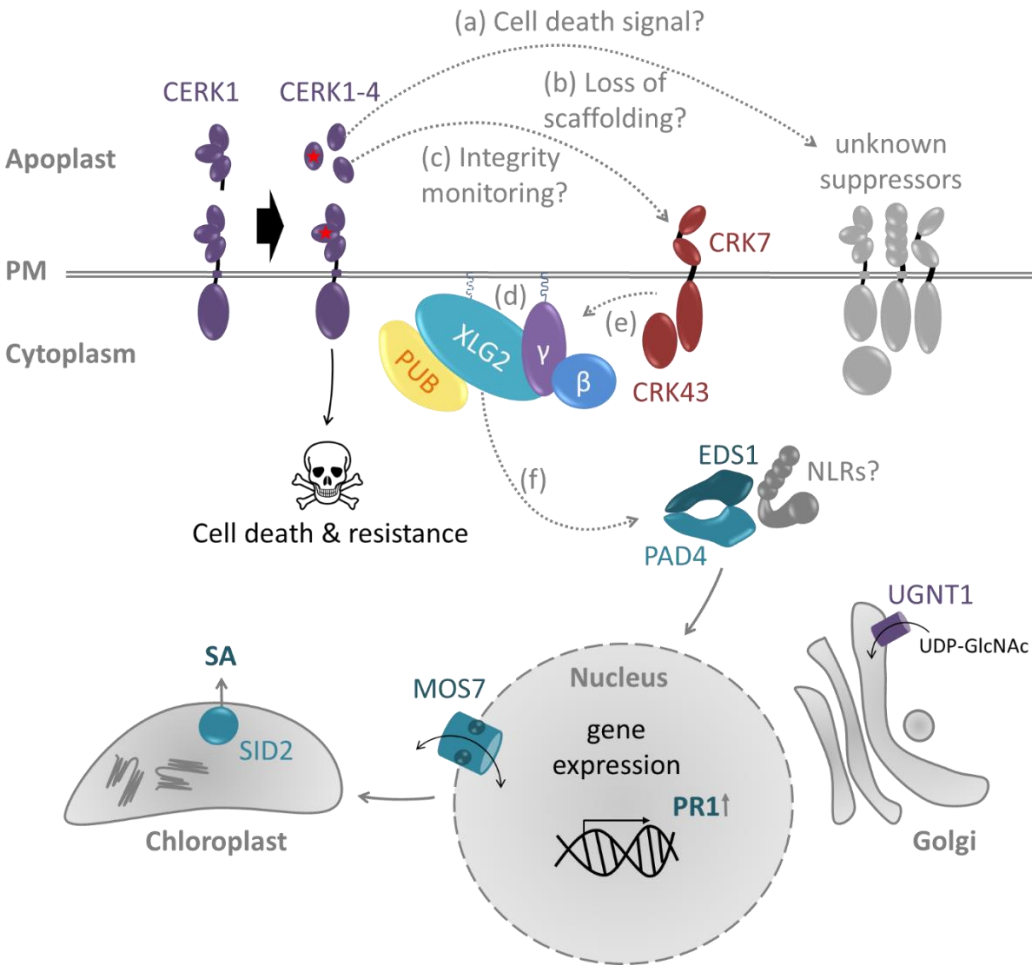

Fig. 55: Working model for the role of XLG2 in *cerk1*-4 cell death signalling.

The modified CERK1-4 ectodomain could potentially result in gain of a pro cell death signal (a), loss of scaffolding (b) or integrity monitoring (c). Basal levels of PM-localized XLG2 constitutively bound to PUB2/4 are required for the *cerk1*-4 cell death and resistance phenotype (d), while the nuclear pool is dispensable. SA-signalling components including MOS7, SID2, EDS1 and PAD4 are required. UGNT1 is required for correct complex N-glycosylations of e.g. CERK1/ CRKs. It is conceivable that PM-localized CRK7 perceives a signal that is transmitted to CRK43 and the PM-localized XLG2 (potentially S-acylated) (e). XLG2 then might transduce a signal to (NLRs?) EDS1-PAD4 (f) to induce BAK1/ SOBIR1-independent cell death. ROS-burst via RBOHD/F as well as potential nucleotide-binding/ -hydrolysis of the XLG2 Gα-like domain are dispensable for this pathway, while XLG2 is supported by AGB1-AGG1/2 likely via enhanced sequestration to the PM. ED = ectodomain

CERK1 undergoes recycling alongside with ectodomain shedding, while the activated CERK1 kinase domain remains at the PM (Erwig et al. 2017; Petutschnig et al. 2014) and is likely subjected to constitutive degradation via PUB12 (Yamaguchi et al. 2017). The CERK1 ectodomain is found in apoplastic wash fluids as well as the soluble fraction of microsomal preparations (Petutschnig et al. 2014). Importantly, expression of only the soluble CERK1-4 ectodomain had no effect on the phenotype, while expression of the CERK1-4 ectodomain with the transmembrane domain caused cell death (Meusel 2016). Accordingly, the CERK1-4 ectodomain might represent a positive cell death signal when attached to the PM. It was speculated that the membrane-bound CERK1 ectodomain could act

as RLP (Petutschnig et al. 2014). Elevated expression levels of NLR proteins were observed for the *bak1 bkk1* autoimmunity mutant and helped to identify the role of ADR1s in cell death signalling (Wu et al. 2020). Accordingly, expression profiles might help to identify potential participation of a certain NLR protein group in *cerk1*-4. The inducibility of the gain-of-function mutation *cerk1*-4, with SA over-accumulation and PR1 expression upon infection (Petutschnig et al. 2014), slightly differs to the stronger loss-of-function autoimmunity phenotype of *bir1*-1 and *bak1-1 bkk1-1*, which are caused by either absence of the inhibitor resulting in autoactivation (*bir1*-1) or by absence of the potentially guarded RLK (*bak1*-1 *bkk1*-1) which in turn likely triggers ADR1-NLR-mediated immunity (Wu et al. 2020). Absence of BAK1, which could potentially activate guarding NLRs (Wu et al. 2020), becomes only visible when also the closest homologue BKK1 is absent. ADR1 was recently found to constitutively interact with a SOBIR1-RLP complex and activates EDS1-PAD4 signalling (Pruitt et al. 2020). SOBIR1 as well as XLG2-AGB1-AGG1/2 are known to be involved in cell death signalling (Maruta et al. 2015). Importantly, BAK1 and SOBIR1 were found to be dispensable for *cerk1*-4 cell death signalling (Petutschnig, unpublished). The *cerk1*-4 phenotype depends on SA accumulation, which can be concluded from the fact that *sid2* as well as *eds1* and *pad4* were identified as suppressors (Petutschnig et al. 2014). Further, heterotrimeric G proteins were identified as suppressors of *cerk1*-4 with a specific function of XLG2 supported by AGB1 and AGG1/2, while *gpa1* as well as *xlg1*/*3* did not suppress *cerk1*-4 (Petutschnig, unpublished). One can consider XLG2 a key positive regulator of cell death and basal immunity due to the findings that *xlg2* does not only suppress *cerk1*-4 cell death signalling (Stolze, unpublished; Meusel, 2016) but also *bir1*-1 (Maruta et al. 2015). Further, XLG2 contributes to PAMP-triggered immunity involving RLKs and RLPs (Liang et al. 2016; Liang et al. 2018; Maruta et al. 2015; Humphry et al. 2010; Wan et al. 2019b; Zhu et al. 2009). The specificity of XLG2 concerning *bir1*-1 cell death signalling is unclear as no data is available concerning the effect of *xlg3* on *bir1*-1 (Maruta et al. 2015). A detailed analysis of the XLG2 interactome before and after infection would provide useful information for these signalling pathways. It is tempting to speculate that NLRs might be involved in *cerk1*-4 cell death signalling and could be activated by XLG2. Further, the commonly used *cerk1*-2 mutant is not a complete knock-out and, due to presence of the soluble ectodomain, might not activate a potential guardee (Petutschnig et al. 2014). Accordingly, a clean knock-out of CERK1 is needed to provide important information regarding the guarding hypothesis. Crossing multiple NLR-mutants with *cerk1*-4 would help to test whether absence of a certain NLR group can suppress the cell death phenotype.

BIK1 is a key component in plant immunity and cell death and was shown to regulate XLG2 and *vice versa* during basal immunity (Wang et al. 2018; Derkacheva et al. 2020; Liu et al. 2017; Liang et al. 2016). BIK1 was found to interact with XLG2 and phosphorylate N-terminal several residues (Liang et al. 2016; Liang et al. 2018). Further, XLG2 was found to regulate BIK1 abundance together with PUB25

and CPK28 (Derkacheva et al. 2020; Zhang and Zeng 2020). Crossing *bik1* and *cerk1*-4 would help to find out whether BIK1 is involved in the *cerk1*-4 cell death pathway, however, due to strong PR1 induction in *bik1* (Liu et al. 2017) this approach might be problematic. It is likely that the role of XLG2 in *cerk1*-4 cell death signalling is uncoupled from its functions in basal immunity and development. This idea is supported by the observation that *xlg3* does not suppress *cerk1*-4 (Petutschnig, unpublished) but was found to act redundantly in many currently known pathways involving XLG2 as main contributor (Liang et al. 2017; Maruta et al. 2015; Liang et al. 2016; Choudhury et al. 2020). Analysis of CERK1-4 loss-of-function (LOF), which has no kinase activity, showed that *cerk1*-4 cell death signalling does not depend on CERK1 kinase activity (Petutschnig et al. 2014). Further, independence of *cerk1*-4 cell death signalling from RBOHD/F-dependent ROS-burst was confirmed via the identification of ROS-burst deficient *rbohd* and *rbohf* mutants as non-suppressors of *cerk1*-4 (Hacke, unpublished). In addition, the BIK1-dependent and ROS-promoting XLG2 phosphorylation sites (S141/148/150/151) (Liang et al. 2016) were found to be irrelevant for *cerk1*-4 cell death signalling (Petutschnig, Anders and Hacke, unpublished) as discussed in 4.3.

Two CRKs, namely CRK7 and CRK43, were identified as suppressors of *cerk1*-4 signalling (Trippel 2020). CRK genes are commonly found to be upregulated upon a variety of stress signals including cell wall integrity, elicitors and pathogen inoculation (Acharya et al. 2007; Vanholme et al. 2014; Liu et al. 2017; Chen et al. 2003). Elevated CRK levels can be observed in several autoimmunity mutants including *bik1*, *bik1 bak1, bak1 bkk1* (Liu et al. 2017) and *cerk1*-4 (Trippel, 2020; Petutschnig, unpublished). CRKs are commonly involved in cell death signalling and perhaps act upstream of SA/ NLR signalling (Acharya et al. 2007; Vanholme et al. 2014; Liu et al. 2017; Trippel 2020; Yadeta et al. 2017). Mannose-binding was observed for some DUF26 domain proteins (Miyakawa et al. 2014; Ma et al. 2018). Accordingly, it can be speculated that CRKs potentially bind sugars with their DUF26 domains. The identification of a new suppressor of *cerk1*-4 involved in UDP-GlcNAc transport into the Golgi, *ugnt1* (A. Vasquez, unpublished), indicates that Golgi-dependent complex N-glycosylations are important for development of the *cerk1*-4 cell death phenotype. The CERK1 ectodomain is found to be heavily N-glycosylated as many PRRs are (Häweker et al. 2010) including CRKs (Oliveira et al. 2016). Whether CRK7/43 and XLG2 directly interact with each other is currently unknown. Interaction studies (FLIM/FRET CLSM and co-immunoprecipitation) for XLG2, PUB2/4, CRK7/43, PAD4, EDS1 and CERK1 might help to further characterize the relationship between these components.

Plasma membrane localized XLG2 is important for *cerk1*-4 cell death signalling, while nuclear localization as well as potential GTP-hydrolysis/ -binding are dispensable (this work, as discussed in 4.1-4.5). The XLG2 N-terminus might serve mainly as hub for post-translational modifications as it was found to be heavily phosphorylated (Liang et al. 2016; Chakravorty and Assmann 2018) and regulation of subcellular trafficking due to the presence of nuclear import and export signals (Ding et al. 2008).

The differential involvement of the XLG2 N- and C-terminus regarding *cerk1*-4 cell death signalling could be analysed by expressing either the N-terminal or the C-terminal part of XLG2 in *cerk1*-4 *xlg2*-2. The molecular mechanism that sequesters XLG2 to the plasma membrane remains to be further analysed. A tempting speculation is that S-acylation might be involved in membrane tethering of XLG2 as discussed in 4.4. Interestingly, CERK1 was found to be S-acylated at the juxtamembrane domain which potentially influences the formation of microdomains but does not impair basal immunity signalling (Chen et al. 2019; Hurst et al. 2019). This finding could motivate an approach to mutate potential S-acylation sites in CERK1 as well as the *cerk1*-4 mutant variant in order to investigate if microdomain formation might influence the *cerk1*-4 cell death phenotype. Phosphorylations potentially enhance certain interactions or trigger dissociation of XLG2 e.g. from the Gβγ-dimer. Co-immunoprecipitation and proteomics analysis using unchallenged plant material could provide candidates that constitutively sequester XLG2 to the PM and, therefore, might be especially important for *cerk1*-4 cell death signalling. A XLG2 variant with reduced PM tethering could be used as control for this approach.

XLG2 was found to be upregulated in heavy metal tolerance against cadmium (Weber 2005) and powdery mildew non-host resistance (Humphry et al. 2010; Pajonk 2007). Interestingly, these stress-responsive pathways share important components such as XLG2, PEN2/4 and MLOs (an overview is provided in Table 5) (Weber 2005; Humphry et al. 2010; Pajonk 2007). CERK1 was found to play a central role in chitinase-overexpression-mediated heavy metal tolerance (Brotman et al. 2012) and was also genetically linked to non-host resistance (Humphry et al. 2010). Invasion of the fungus was shown to trigger the *cerk1*-4 cell death response (Petutschnig et al. 2014). Whether components involved in pre-/ post-invasive resistance against powdery mildews and heavy metal tolerance could be involved in *cerk1*-4 cell death signalling is speculative. Interaction between AGB1 and a defense responsive NDR1-like protein was observed (Yu et al. 2018), which was also found to be co-regulated with PEN1 (Humphry et al. 2010).

4.7 The role of XLG2 in post-invasive resistance

Pre-/ post-invasive resistance of *Arabidopsis* plants against powdery mildews can be analysed using (non-)compatible inoculations such as *Bgh* or *E. pisi*, and subsequent careful examination of penetration sites or invasion frequency (Lipka et al. 2005; Lipka et al. 2008). Heterotrimeric G proteins including XLG2, AGB1 and AGG1/2 were earlier found to play a role in pre-/ post-invasive resistance against *E. pisi* (Humphry et al. 2010; Lorek et al. 2013).

In this work, the focus was to analyze XLG2 regarding *Ec*-induced *cerk1*-4 cell death signalling. Analysis of *Ec*-infected *Arabidopsis* plants at late infection time-points revealed XLG2-association with *Ec* haustoria. Propidium iodide (PI) is known to stain plant and fungal structures, including extrahaustorial encasements (EHC) (Meyer et al. 2009; Wang et al. 2009; Qin et al. 2020). The Venus-XLG2-derived signal co-localized with EHCs, which were visible in bright field images as well as PI stain. The PM-localized SNARE protein PEN1 (SYP121) forms a ternary-complex with the adaptor SNARE protein SNAP33 and redundantly acting v-SNAREs VAMP721/722 (Lipka et al. 2010; Kwon et al. 2008; Underwood and Somerville 2013). These pre-/ post-invasive resistance proteins are known to accumulate at plasma membrane microdomains beneath fungal penetration sites after PRR-dependent recognition (Underwood and Somerville 2013) and were also found within EHCs (Meyer et al. 2009). PEN3, a pleiotropic drug resistance ABC-transporter, was found to be released into the apoplastic space beneath infection sites (Stein et al. 2006). Further, PEN3 was similarly to the other defense components found to be incorporated into EHCs (Meyer et al. 2009). The Venus-XLG2/ xlg2 haustoria-labeling CLSM data, including nuclear exclusion and mainly nuclear localizing XLG2 variants, indicate that PM-association of XLG2 is essential for accumulation within EHCs. Further, nuclear accumulation of XLG2 was found to be dispensable for EHC incorporation. In contrast, nucleocytoplasmic trafficking of RPW8.2 was found to be important for EHM-targeting and cell death (Huang et al. 2019). Three XLG2 variants, namely Venus-xlg2 E293K, Venus-xlg2 nes387 and Venus-XLG2-NLS, showed significantly less haustoria labeling compared to Venus-XLG2 WT. This finding indicates that strong nuclear accumulation of XLG2 might conflict with trafficking towards haustorial formation sites. Post-translational modifications are likely affected by the E293K/ nes387 mutations as discussed in 4.3, which could potentially also influence trafficking towards haustoria. Venus-XLG2 WT, Venus-xlg2 nls426 and Venus-XLG2-NES plasma membrane signals were visible as sharp lines and were stronger after infection, while Venus-XLG2-NLS plasma membrane signals remained at a basal level. XLG2-NLS occasionally labeled EHCs likely due to the retained basal PM localization. Regarding XLG2-NLS it should be noted that counting of haustoria took much longer due to the repeatedly low number of fully developed haustoria in all replicates. This observation could indicate a higher resistance of *xlg2*-2 expressing Venus-XLG2-NLS. Accordingly, the XLG2-NLS potentially represents a gain-of-function

variant due to potentially increased resistance which remains to be evaluated with quantitative resistance and susceptibility phenotype data. Venus-XLG2-NES drove XLG2 successfully out of the nucleus and plasma membrane signals were especially strong as well as the observed EHC accumulation. The nuclear exclusion and mainly nuclear accumulating variants (XLG2-NES/ NLS) could be used to analyze the role of XLG2 in pre- and post-invasive resistance. Nuclear localized XLG2 might be important for basal defense, though, it was found to be dispensable for *cerk1*-4 cell death signalling. Analyzing the host cell entry rates, frequency of invasive growth and microcolony formation after *Bgh* or *E. pisi* inoculation, would give a quantitative output concerning resistance/ susceptibility phenotypes in dependence to nuclear pools of XLG2. The nls426 mutation resulted in a clear reduction of nuclear localized XLG2 (3.3). However, at late infection time-points some nuclear signals were observed (3.8). The presence of other functional, but weaker NLSs, might be responsible for this observation. The CLSM analysis of younger haustoria in this study revealed potential EHM localization of XLG2 (data not shown), which remains to be further analysed including EHM-markers such as RPW8.2 and cytoplasmic Venus as controls. Two XLG2 sequences KRAK (part of NLS426) and KKLK show similarity to two described RPW8.2 sequences, KRAK and KKFR, which were described to be important for EHM-localization (Berkey et al. 2017). One could speculate that the nls426 (KRAK changed to AGTL) mutation might impair potential EHM-targeting of XLG2, which was not further distinguished from EHC in this work. However, nucleocytoplasmic trafficking was shown to be important for EHM-localization of RPW8.2 (Huang et al. 2019). Accordingly, these sequences might just represent NLSs also in RPW8. Nevertheless, analysis of potential EHM-targeting could be supported by another mutation of the second RPW8.2 EHM-targeting sequence-like motif in XLG2 (KKFR, e.g. to AATG). Interestingly, specific EHM localization of RPW8.2 depends also on SNAREs VAMP721/722-mediated TGN sorting (Kim et al. 2014). In contrast to XLG2, RPW8.2 has a predicted transmembrane or signal peptide (Collier et al. 2011). For XLG2 it is still unclear how membrane tethering is regulated and if reversible S-acylations might be involved is still speculative. Callose staining via aniline blue would further help to characterize the subcellular localization of XLG2 at the haustorial periphery. As discussed earlier (4.4), the XLG2 cys-rich region does not likely represent a degenerate FYVE domain. The *Arabidopsis* FYVE domain motif (R/K)(R/K)HHCR is typically involved in PI3P binding (Wywial and Singh 2010). The cysteines of FREE1 and other FYVE domains align with the conserved XLG cysteines (Fig. S 22). However, the main FYVE motif is absent in the XLG sequence and phosphatidylinositol binding based on a potential FYVE domain is, therefore, rather unlikely. FREE1 was shown to interact with phosphatidylinositol 3-phosphate (PtdIns3P) and it specifically localizes to late endosomes (MVBs) (Jensen et al. 2001; Gao et al. 2014). Therefore, FREE1 can be used as MVB marker. CLSM analysis including this marker could potentially help to characterize whether Venus-XLG2 associates with MVBs. Uncharacterized moving structures (towards haustoria) were observed during CLSM analysis of Venus-

XLG2 variants (data not shown) as speculative indication for MVB labeling by XLG2. It is a conceivable idea that trafficking of XLG2 to EHCs (EHM?) could involve the formation of MVBs, as similarly suggested for other defense components such as PEN1 and SNAP33 (Wang et al. 2016). Interestingly, in mammals a Gα subunit was found to regulate the endosomal sorting process of GPCRs into ILVs of MVBs by interacting with endosomal membrane components and the ESCRT machinery (Rosciglione et al. 2014). Importantly, this novel function of a mammalian Gα subunit was found to not depend on the GTPase activity (Rosciglione et al. 2014).

4.7.1 Working model for pre-/ post-invasive resistance and outlook

During basal immunity XLG2 was identified as main contributor to defense signalling partially in redundancy with XLG3 for positive regulation of ROS burst (Liang et al. 2018; Liang et al. 2016; Maruta et al. 2015; Zhu et al. 2009). As heterotrimeric G proteins including XLG2 are involved in (non-)host plant immunity (Zhong et al. 2019; Liang et al. 2018) as well as developmental processes such as root morphogenesis (Ding et al. 2008; Chen et al. 2006), their potential role in symbiotic interactions should not be overlooked. This becomes especially interesting due to the role of XLG2 in *cerk1*-4 cell death signalling, its interaction with PUB4 (Wang et al. 2017), which also regulates CERK1 (Desaki et al. 2019b), and the role of CERK1 homologues in symbiosis (Antolín-Llovera et al. 2014). In *Arabidopsis*, symbiotic interactions do not occur (Antolín-Llovera et al. 2014). Nevertheless, *Arabidopsis* CERK1 potentially retained an ancient mechanism for inhibition of defense signalling in favor of symbiotic interactions. Haustoria are formed by pathogens as well as endosymbionts and are similarly surrounded by a host-derived *de novo* synthesized EHM (Huisman et al. 2012). Whether XLG2 labels the EHM could be further analysed by including an EHM-marker (e.g. RPW8.2) for CLSM analysis. Earlier infection time points would help to analyze the EHM in the absence of encasements.

The potential involvement of PEN-genes in PCD were described earlier (Johansson et al. 2014) including inhibitory effects on other immune signalling pathways as *pen1* and the double mutation *pen1 syp122* were found to cause autoimmunity (Zhang et al. 2007; Zhang et al. 2008b). Immuno-compromising mutations in the ESCRT component AMSH3 were shown to suppress the autoimmune phenotype of *pen1 syp122* (Schultz-Larsen et al. 2018). This finding indicates that absence of PEN1 and its closest homologue activates a ESCRT-III-associated cell death response, which is likely triggered by guarding of MVB sorting processes via NLRs (Schultz-Larsen et al. 2018). It is interesting that an endosomal sorting process can trigger cell death via NLRs and, therefore, worth mentioning in the context of LMM. Previously, *cerk1*-4 was crossed with *pen2*-1 and invasion success of *Bgh* was found to be important for this cell death phenotype (Petutschnig et al. 2014). Heterotrimeric G proteins are involved in different cell death signalling pathways including *cerk1*-4 (Petutschnig et al. 2014) and *bir1*-1 (Maruta et al. 2015). It would be interesting to analyze whether the LMM phenotype of *pen1 syp122* is similarly

affected by absence of XLG2 or AGB1-AGG1/2. The potential suppression of *pen1 syp122* by *xlg2* would support the hypothesis that the cell death promoting role of XLG2 might be connected to NLRs. Pre-/ post-invasive resistance (Humphry et al. 2010) and heavy metal tolerance against cadmium (Weber 2005) share a high number of genetically linked components including XLG2, PEN2/4 and MLOs (Table S 5). Whether these shared components are relevant for the *cerk1*-4-mediated cell death phenotype is rather speculative.

A working model of a heterotrimeric G protein complex potentially involved in pre-/ post-invasive resistance and cell death signalling is depicted in Fig. 56. To further characterize the role of XLG2 in pre-/ post-invasive resistance, *xlg2*-1/2 crossings with *pen1* or *pen2/3* and subsequent quantitative analysis of resistance/ susceptibility phenotypes after *Bgh*/ *E. pisi*/ *Ec* inoculation (penetration efficiency, callose deposition, invasion success) could be used and would also help to characterize whether XLG2 acts in the same pathways or independently from PEN proteins. Previous analysis of *pen2 xlg2*, *pen2 xlg3* and *pen2 agb1 Arabidopsis* non-host resistance against *P. oryzae*, a rice pathogen, revealed that XLG2 (but not XLG3) positively regulates pre-invasive but not post-invasive resistance in the absence of PEN2 (Takahashi et al. 2018). AGB1 positively regulated pre- and post-invasive resistance in this context (Takahashi et al. 2018). Due to the proximity of *AGB1* and *XLG2* genes, a CRISPR/Cas approach could be used to generate *agb1 xlg2* double mutants in order to investigate their genetic interaction in pre-/ post-invasive resistance. The potential accumulation of XLG2 beneath *Bgh* or *E. pisi* infection sites could be analysed in the future using CLSM in transgenic *xlg2* or *xlg2 pen* lines expressing Venus-XLG2 as well as fluorescently labeled PEN proteins or other components known to be involved in pre-invasive resistance as controls. A time-course experiment using CLSM would help to further characterize the coordinated accumulation of Venus-XLG2 during pre- *(Bgh*/ *E. pisi*) and post- (*Ec*) invasive resistance. Interaction studies, such as co-immunoprecipitation after infection, could reveal information about the relation between XLG2 and known components involved in pre-/ post-invasive resistance e.g. PEN1, PEN2, PEN3, PEN4 or MLOs. Direct interaction studies, such as FLIM/FRET CLSM, could then be used to further analyze identified candidates. Nuclear exclusion and enhanced nuclear pool variants with viral localization signal fusions (XLG2-NES/ NLS) could be useful in order to further understand the role of XLG2 nuclear localization for pre-/ post-invasive resistance against powdery mildews. Defense gene expression profiles of e.g. PR1/ PR2/ CRKs/ EDS1/ PAD4 could be analyzed in *Ec*-infected transgenic *xlg2*-2 expressing XLG2 WT or XLG2-NES/ NLS using quantitative RT-PCR.

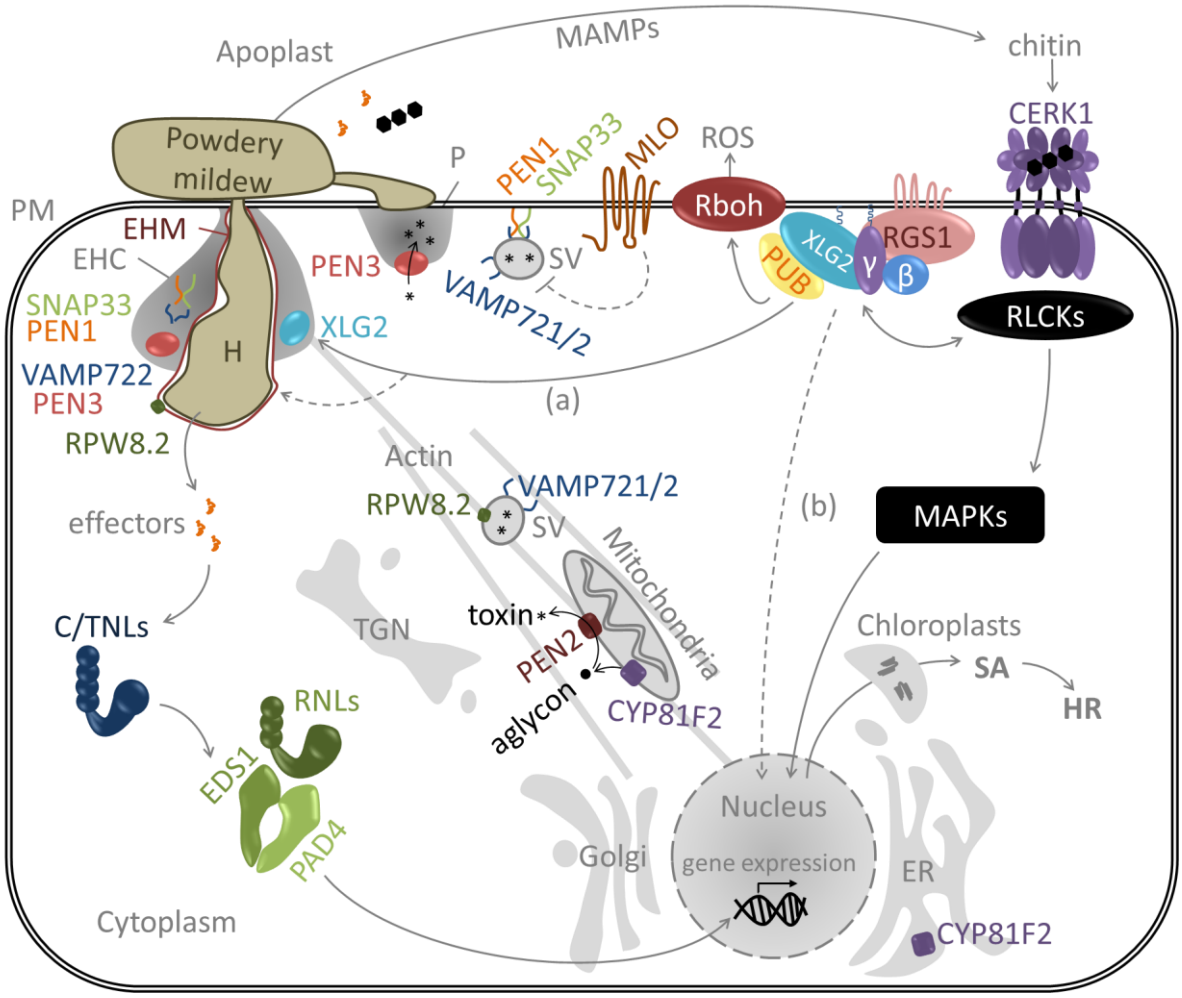

Fig. 56: Potential role of XLG2 in pre-/ post-invasive resistance against powdery mildews.

Known components involved in pre-/ post-invasive resistance are depicted in engaged compartments during cell-autonomous defense against powdery mildew. XLG2 is imbedded in extracellular and intracellular defense signalling (Ngou et al. 2020) with a ROS promoting function (Maruta et al. 2015; Liang et al. 2016) and cell death (Maruta, 2015; Stolze, unpublished, Meusel, 2016). XLG2 associates with haustoria and is likely incorporated into the EHC and perhaps also into the EHM (a). The nuclear pool of XLG2 is dispensable for association with the haustorial periphery, while the role of nuclear localization in pre-/ post-invasive resistance phenotypes is still unclear (b). Information was collected from (Schultz-Larsen et al. 2018; Lorek et al. 2013; Fuchs et al. 2016; Petutschnig et al. 2014; Lipka et al. 2010; Wang et al. 2017; Miller et al. 2019; Palma et al. 2018). P = papilla, EHC = Extrahaustorial encasement, SV = secretory vesicle, TGN = trans-golgi network, ER = endoplasmic reticulum, PM = plasma membrane, CNL = CC-NLR, TNL = TIR-NLR, RNL = RPW8-NLR, HR = hypersensitive response.

5 Supplements

5.1 Supplemental table

Table S 1: Overview of constructs stably transformed into *xlg2*-2. * *Ec*/ *Bgh* infection and senescence phenotype documentation in T1/T2, confirmed Venus expression via CLSM. ** *Ec* infection in T1/T2, confirmed Venus expression via CLSM & Western blotting.

Transgene in *xlg2*-2	Independent lines*	Independent lines (normal growth phenotype)**	Subcellular localization in unchallenged cells	Subcellular localization *Ec* infected cells	Apparent mass in Western Blots
Venus-XLG2 WT	42	6 (yes)	cell periphery, faint nuclei when strongly expressed	nucleus, cell periphery, unknown organelles labeled when strongly expressed	WT ~130kDa
Venus-xlg2 E293K	15	6 (yes)	nucleus, faint cell periphery	nucleus, faint cell periphery	reduced
Venus-XLG2 C-nes	8	6 (yes)	WT-like	WT-like	WT-like
Venus-XLG2 C-NES	10	6 (yes)	cell periphery	cell periphery, faint nuclei and unknown organelles labeled when strongly expressed	WT-like
Venus-XLG2 C-nls	12	4 (yes)	WT-like	WT-like	WT-like
Venus-XLG2 C-NLS	12	5 (yes)	nucleus, cell periphery	nucleus, cell periphery	WT-like
Venus-xlg2 nes387	16	6 (yes)	nucleus, faint cell periphery	nucleus, faint cell periphery	reduced
Venus-xlg2 nls426	15	6 (yes)	cell periphery	cell periphery, faint nuclei and unknown organelles labeled when strongly expressed	WT-like
Venus-xlg2 T476N	16	5 (yes)	WT-like	WT-like	WT-like
Venus-xlg2 R673L	16	6 (yes)	WT-like	WT-like	WT-like
Venus-xlg2 C214/217A	12	12 (yes)	nucleus, faint cell periphery	nucleus, faint cell periphery	reduced
Venus-xlg2 C229/232/237/240A	8	8 (yes)	nucleus, faint cell periphery	nucleus, faint cell periphery	reduced
Venus-xlg2 C254/257A	8	8 (yes)	nucleus, faint cell periphery	nucleus, faint cell periphery	reduced
Venus-xlg2 KR-AA	8	4 (yes)	WT-like	WT-like	reduced
Venus-xlg2 KR-AA + E293K	10	4 (yes)	nucleus, faint cell periphery	nucleus, faint cell periphery	reduced

Table S 2: Overview of constructs stably transformed into *cerk1*-4 *xlg2*-2. * *Ec*/ *Bgh* infection and senescence phenotype documentation in T1/T2, confirmed Venus expression via CLSM. ** *Ec* infection in T1/T2, confirmed Venus expression via CLSM & Western blotting

Transgene in *cerk1*-4 *xlg2*-2	Independent lines*	Independent lines (% with complementation phenotype)**	Subcellular localization in unchallenged cells	Subcellular localization *Ec* infected cells	Apparent mass in Western Blots
Venus-XLG2 WT	46	14 (100%)	cell periphery, faint nuclei when strongly expressed	nucleus, cell periphery, unknown organelles labeled when strongly expressed	WT ~130kDa
Venus-xlg2 E293K	21	11 (0%)	nucleus, faint cell periphery	nucleus, faint cell periphery	reduced
Venus-XLG2 C-nes	31	14 (100%)	WT-like	WT-like	WT-like
Venus-XLG2 C-NES	36	8 (100%)	cell periphery	cell periphery, faint nuclei and unknown organelles labeled when strongly expressed	WT-like
Venus-XLG2 C-nls	41	12 (100%)	WT-like	WT-like	WT-like
Venus-XLG2 C-NLS	27	12 (100%)	nucleus, cell periphery	nucleus, cell periphery	WT-like
Venus-xlg2 nes387	54	25 (0%)	nucleus, faint cell periphery	nucleus, faint cell periphery	reduced
Venus-xlg2 nls426	25	10 (100%)	cell periphery	cell periphery, faint nuclei and unknown organelles labeled when strongly expressed	WT-like
Venus-xlg2 T476N	23	16 (94%)	WT-like	WT-like	WT-like
Venus-xlg2 R673L	24	13 (100%)	WT-like	WT-like	WT-like
Venus-xlg2 C214/217A	16	16 (0%)	nucleus, faint cell periphery	nucleus, faint cell periphery	reduced
Venus-xlg2 C229/232/237/240A	12	12 (0%)	nucleus, faint cell periphery	nucleus, faint cell periphery	reduced
Venus-xlg2 C254/257A	21	21 (0%)	nucleus, faint cell periphery	nucleus, faint cell periphery	reduced
Venus-xlg2 KR-AA	16	5 (100%)	WT-like	WT-like	reduced
Venus-xlg2 KR-AA + E293K	13	6 (0%)	nucleus, faint cell periphery	nucleus, faint cell periphery	reduced

Table S 3: Overview of additional constructs stably transformed into *xlg2*-2. * *Bgh* infection and senescence phenotype documentation in T1, confirmed Venus expression via CLSM. ** *Bgh* infection in T1, confirmed Venus expression via CLSM & Western blotting.

Transgene in *xlg2*-2	Independent lines*	Independent lines (normal growth phenotype)**	Subcellular localization in unchallenged cells	Subcellular localization *Bgh* infected cells	Apparent mass in Western Blots
N-nes-Venus-XLG2	7	5 (yes)	WT-like	WT-like	WT-like
N-NES-Venus-XLG2	16	10 (yes)	cell periphery	cell periphery, faint nuclei when strongly expressed	WT-like
N-nls-Venus-XLG2	10	8 (yes)	WT-like	WT-like	WT-like
N-NLS-Venus-XLG2	9	6 (yes)	nucleus, cell periphery	nucleus, cell periphery	WT-like

Table S 4: Overview of additional constructs stably transformed into *cerk1*-4 *xlg2*-2. * *Bgh* infection and senescence phenotype documentation in T1, confirmed Venus expression via CLSM. ** *Bgh* infection in T1, confirmed Venus expression via CLSM & Western blotting.

Transgene in *cerk1*-4 *xlg2*-2	Independent lines*	Independent lines (% with complementation phenotype)**	Subcellular localization in unchallenged cells	Subcellular localization *Bgh* infected cells	Apparent mass in Western Blots
N-nes-Venus-XLG2	13	8 (15%)	WT-like	WT-like	WT-like
N-NES-Venus-XLG2	17	8 (6%)	cell periphery	cell periphery, faint nuclei when strongly expressed	WT-like
N-nls-Venus-XLG2	10	8 (0%)	WT-like	WT-like	WT-like
N-NLS-Venus-XLG2	12	8 (50%)	nucleus, cell periphery	nucleus, cell periphery	WT-like

Table S 5: XLG2 expression is up-regulated during NHR and heavy metal stress (Pajonk 2007; Humphry et al. 2010; Weber 2005). PEN1/ PEN2/ PEN3 co-regulated genes identified by Humphry et al. 2010. * Gene was upregulated together with PEN1 (Pajonk 2007). ** Gene expression was highly induced under heavy metal stress conditions (cadmium), found via cDNA-AFLP analysis (Weber 2005).

	Present in co-expressed gene list:				
AGI	***MLO2/PEN1/SNAP33***	***PEN1/SNAP33/VAMP722***	***PEN2/ PEN3***	**Gene name**	**Source**
AT3G11820	Yes	Yes		PEN1 (SYP121) *	(Humphry et al. 2010; Pajonk 2007)
AT1G11310	Yes		Yes	MLO2	(Humphry et al. 2010)
AT5G61210	Yes	Yes		SNAP33 * **	(Humphry et al. 2010; Weber 2005; Pajonk 2007)
AT3G52400		Yes	Yes	SYP122 *	(Humphry et al. 2010; Pajonk 2007)
AT2G44490			Yes	PEN2 **	(Humphry et al. 2010; Weber 2005)
AT1G59870	Yes	Yes	Yes	PEN3	(Humphry et al. 2010)
AT5G44070	Yes		Yes	PCS1 (PEN4) **	(Humphry et al. 2010; Weber 2005)

AT2G27660		Yes		DCD	(Humphry et al. 2010)
AT4G34390	Yes	Yes	Yes	XLG2 * **	(Humphry et al. 2010; Pajonk 2007; Weber 2005)
AT4G34460		Yes		AGB1	(Humphry et al. 2010)
AT3G21630	Yes	Yes	Yes	CERK1	(Humphry et al. 2010)
At3g45640	Yes		Yes	MPK3 *	(Humphry et al. 2010; Pajonk 2007)
AT4G23210		Yes		CRK13	(Humphry et al. 2010)
AT3G48090	Yes			EDS1 **	(Humphry et al. 2010; Weber 2005)
AT3G52430	Yes	Yes		PAD4 **	(Humphry et al. 2010; Weber 2005)
AT5G06320	Yes	Yes		NHL3 (NDR1-like) *	(Humphry et al. 2010; Pajonk 2007)
AT1G07000	Yes	Yes	Yes	EXO70B2 *	(Humphry et al. 2010; Pajonk 2007)
AT1G57630		Yes		TIR-NLR	(Humphry et al. 2010)
AT1G57650		Yes		NLR	(Humphry et al. 2010)
AT3G26210	Yes	Yes	Yes	CYP71B23	(Humphry et al. 2010)
AT3G14090	Yes		Yes	EXO70D3	(Humphry et al. 2010)
AT3G29400		Yes		EXO70E1	(Humphry et al. 2010)
AT5G58430		Yes		EXO70B1	(Humphry et al. 2010)
AT2G17290		Yes		CPK6	(Humphry et al. 2010)
AT3G20410		Yes		CPK9	(Humphry et al. 2010)
AT1G18890		Yes		CPK10 **	(Humphry et al. 2010; Weber 2005)
At5g66210	co-expressed with PEN1 (not further specified)			CPK28 *	(Pajonk 2007)
AT1G76040		Yes		CPK29	(Humphry et al. 2010)

Table S 6 Fluorescence intensity quantification with ImageJ. Macros were recorded during a sample quantification process. Subsequently some commands were edited to generate generally applicable protocols. Such placeholder information is shown in italics. * used in Figures 10, 51 and Figure S 25, 26; ** used in Figures 11, 12 and Figure S 5, 6; *** used in Figures 13, 22, 28, 47 and Figure S 7.

a) Intensity quantification in *Arabidopsis* cells transiently transformed by particle bombardment *.

```
open("file path/image.tif");
//setTool("multipoint");
run("ROI Manager...");
//the following steps are iterated for each ROI:
makePoint ( x position, y position, "small gray hybrid") ;
roiManager("Add");
//Measurement of minimum and maximum gray values in each ROI
roiManager("Measure");
//Copying results for export to Excel
String.copyResults();
//Saving image file with ROI annotations
roiManager("Show All");
saveAs("Tiff", "file path/image_ROI.tif ");
```

b) Intensity quantification in stably transformed, unchallenged *Arabidopsis* plants **.

```
open("file path/image.tif");
//setTool("freeline");
run("ROI Manager...");
```

```
//the following steps are iterated for each ROI:
makeLine ;
roiManager("Add");
//Measurement of minimum and maximum gray values in each ROI
roiManager("Measure");
//Copying results for export to Excel
String.copyResults();
//Saving image file with ROI annotations
roiManager("Show All");
saveAs("Tiff", "file path/image_ROI.tif ");
```

c) Intensity quantification in stably transformed *Arabidopsis* lines for comparison of *Ec* infected and control plants***.

```
open("file path/image.tif");
//setTool("line");
run("ROI Manager...");
//the following steps are iterated for each ROI:
makeLine(x position, y position, angle, length);
roiManager("Add");
//Measurement of minimum and maximum gray values in each ROI
roiManager("Measure");
//Copying results for export to Excel
String.copyResults();
//Saving image file with ROI annotations
roiManager("Show All");
saveAs("Tiff", "file path/image_ROI.tif ");
```

5.2 Supplemental figures

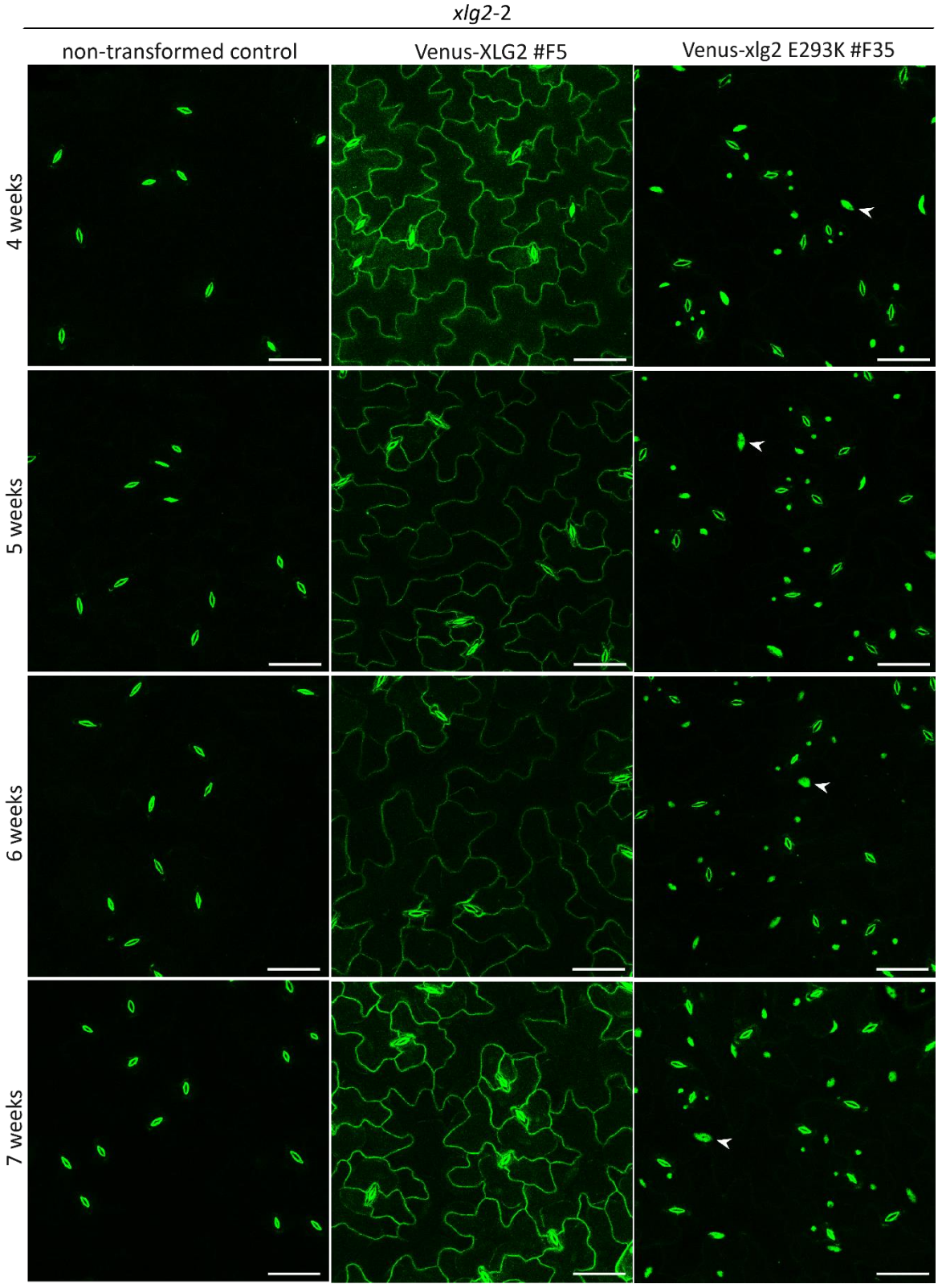

Fig. S 1: Stably expressed Venus-XLG2 was mainly detected at the cell periphery, while Venus-xlg2 E293K accumulated mainly in the nucleus in *xlg2*-2 (more lines).

Images of representative lines expressing either Venus-XLG2 or Venus-xlg2 E293K are maximum projections of z stacks spanning the epidermal cell layer. Scale bar=50µm.

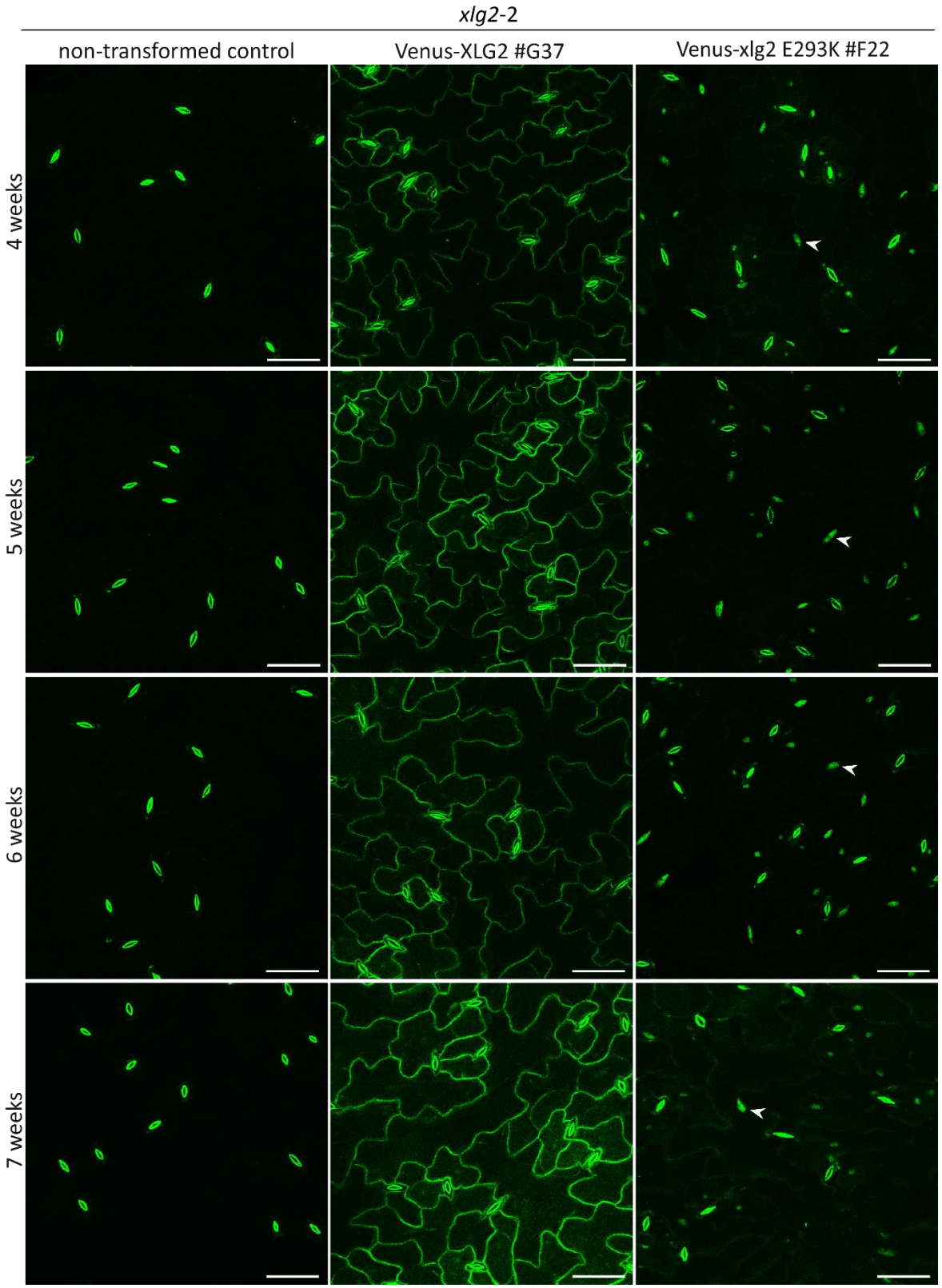

Fig. S 2: Stably expressed Venus-XLG2 was mainly detected at the cell periphery, while Venus-xlg2 E293K accumulated mainly in the nucleus in *xlg2*-2 (more lines).

CLSM images of representative *xlg2*-2 lines expressing either Venus-XLG2 or Venus-xlg2 E293K are maximum projections of z stacks spanning the epidermal cell layer. Scale bar=50µm.

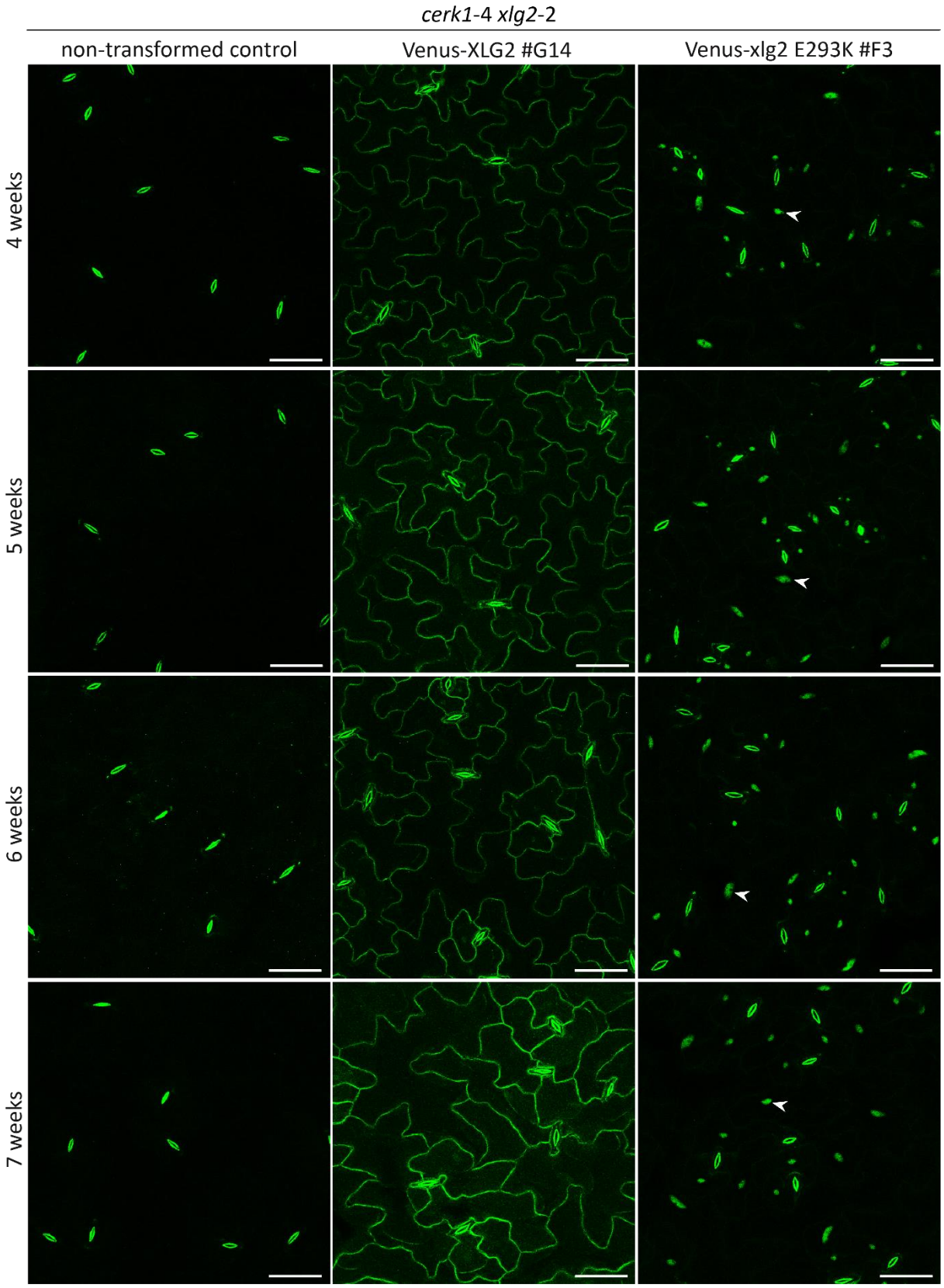

Fig. S 3: Stably expressed Venus-XLG2 was mainly detected at the cell periphery, while Venus-xlg2 E293K accumulated mainly in the nucleus in *cerk1*-4 *xlg2*-2 (more lines).

CLSM images of representative *cerk1*-4 *xlg2*-2 lines expressing either Venus-XLG2 or Venus-xlg2 E293K are maximum projections of z stacks spanning the epidermal cell layer. Scale bar=50µm.

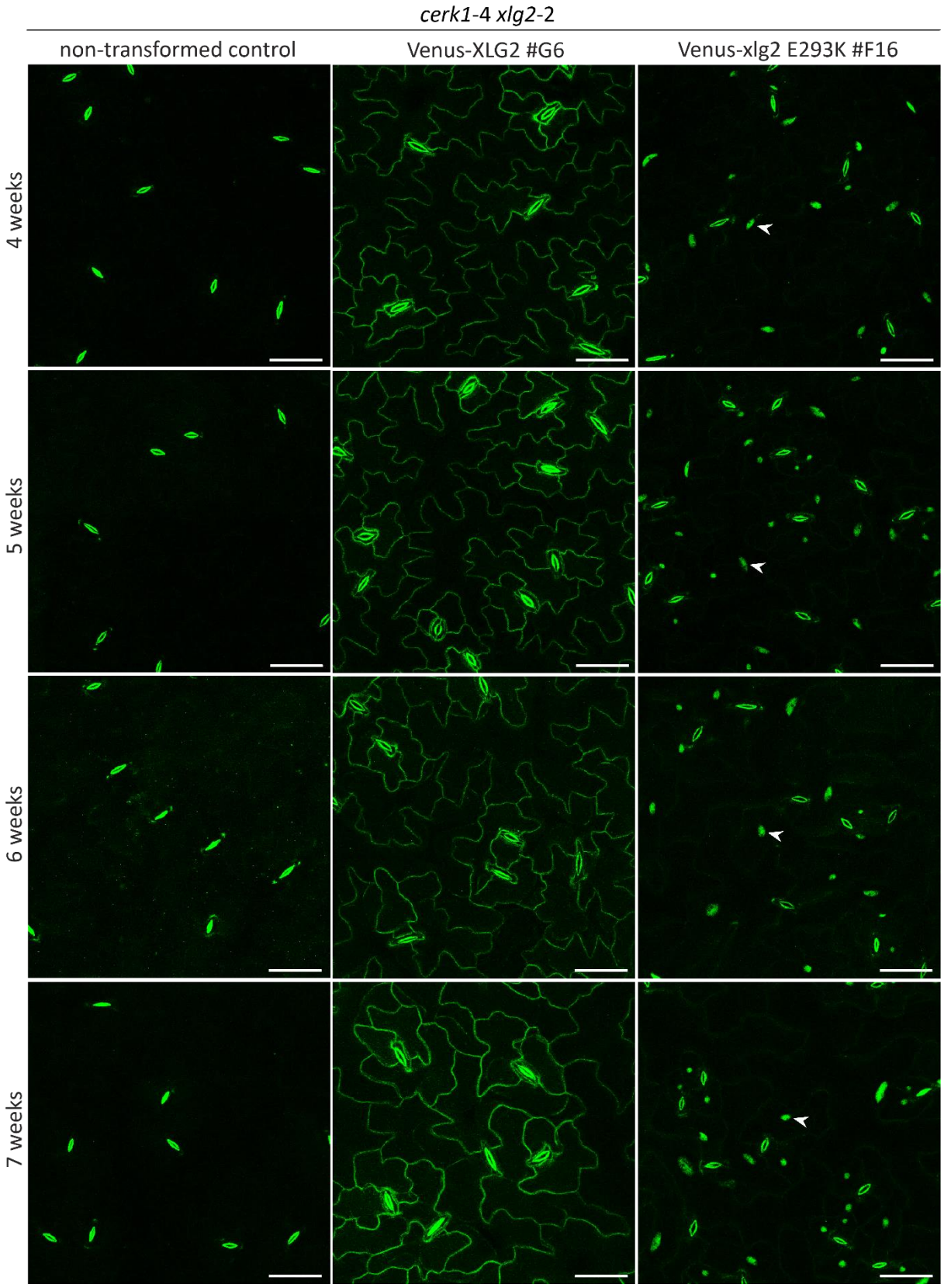

Fig. S 4: Stably expressed Venus-XLG2 was mainly detected at the cell periphery, while Venus-xlg2 E293K accumulated mainly in the nucleus in *cerk1*-4 *xlg2*-2 (more lines).

CLSM images of representative *cerk1*-4 *xlg2*-2 lines expressing either Venus-XLG2 or Venus-xlg2 E293K are maximum projections of z stacks spanning the epidermal cell layer. Scale bar=50µm.

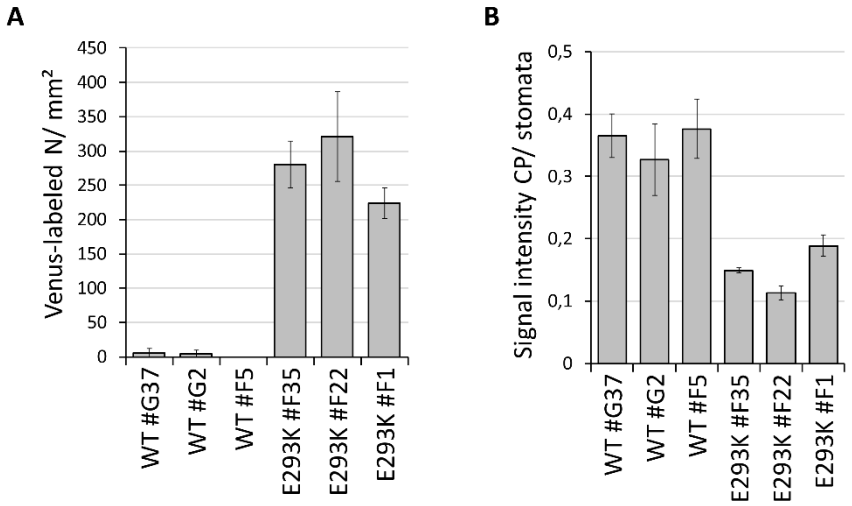

Fig. S 5: Quantification localization/ signal intensities of individual lines stably expressing Venus-XLG2 and Venus-xlg2 E293K in *xlg2*-2.

Quantification of Venus-XLG2 WT and Venus-xlg2 E293K localization/ signal intensities in stably transformed *xlg2*-2: **(A)** Venus-labeled N/ mm²and **(B)** signal intensity CP/ stomata autofluorescence. N = nucleus, CP = cell periphery. Data are means ± StDev of images of 3 plants (≥ 9 images in total).

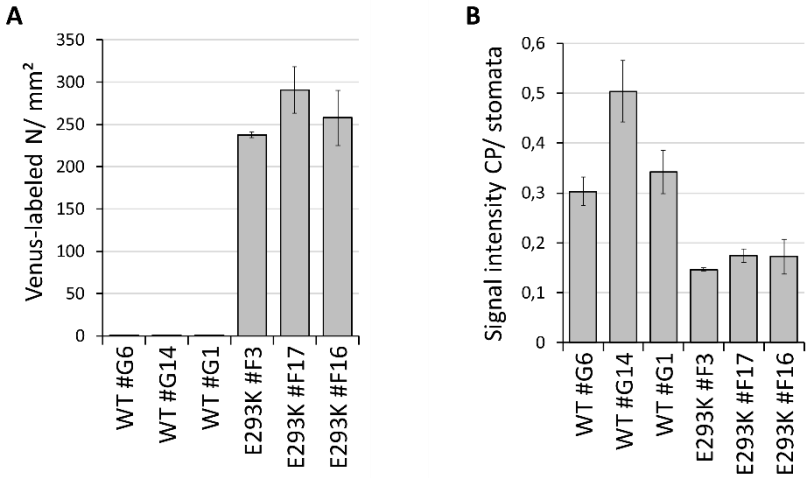

Fig. S 6: Quantification localization/ signal intensities of individual lines stably expressing Venus-XLG2 and Venus-xlg2 E293K in *cerk1*-4 *xlg2*-2.

Quantification of Venus-XLG2 WT and Venus-xlg2 E293K localization/ signal intensities in stably transformed *cerk1*-4 *xlg2*-2: **(A)** Venus-labeled N/ mm² and **(B)** signal intensity CP/ stomata autofluorescence. N = nucleus, CP = cell periphery. Data are means ± StDev of images of 3 plants (≥ 9 images in total).

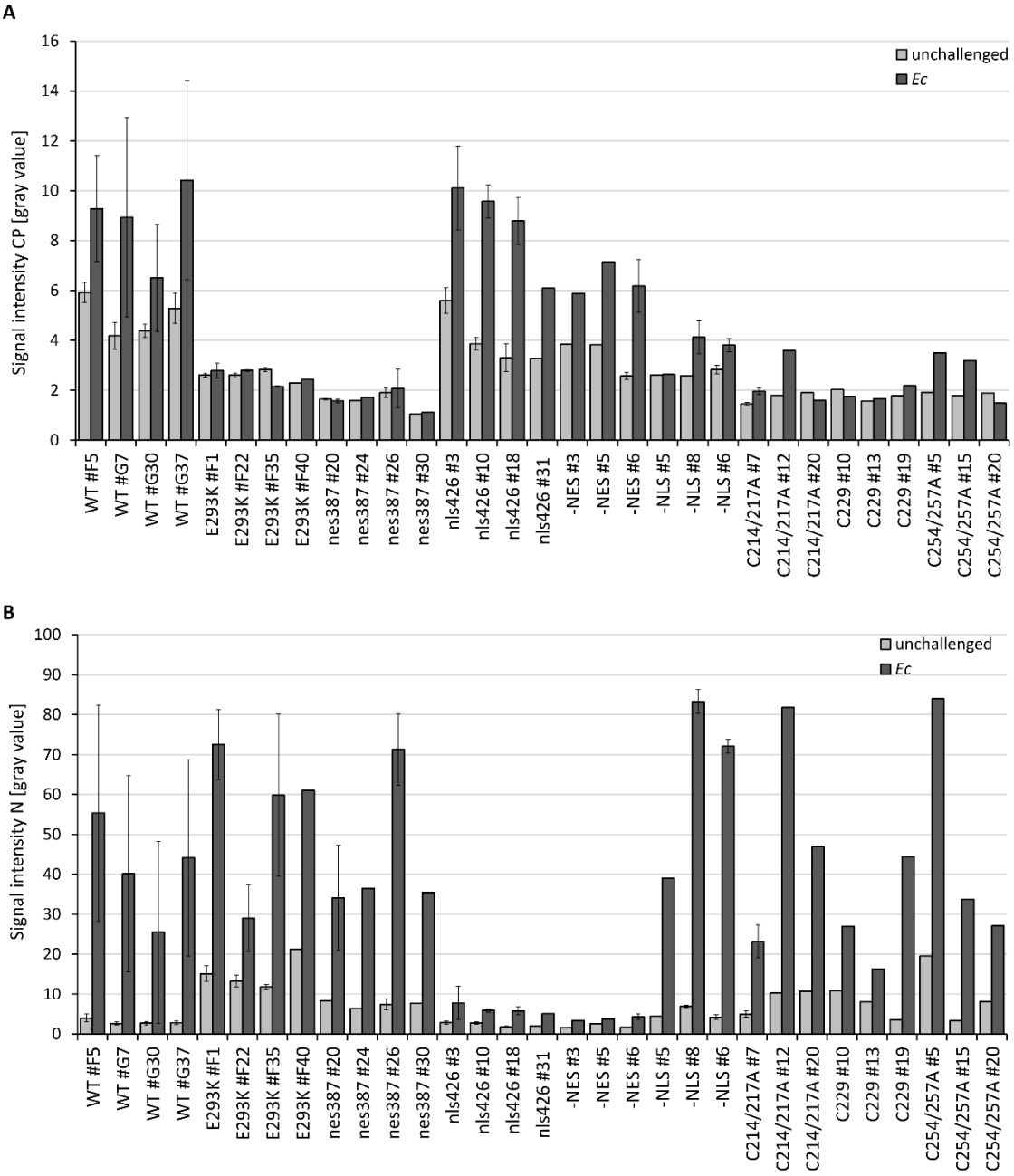

Fig. S 7: Venus-XLG2 signals increased upon pathogen attack.

Quantification of CLSM images of unchallenged vs. infected (1dpi *Ec*) *xlg2*-2 expressing Venus-XLG2/ xlg2 (as indicated). Signal intensities of the cell periphery (CP) **(A)** and the nucleus (N) or background if no nuclei were visible **(B)** are shown. Data are means ± StDev of 1-5 interaction sites (individual cells) analysed per line.

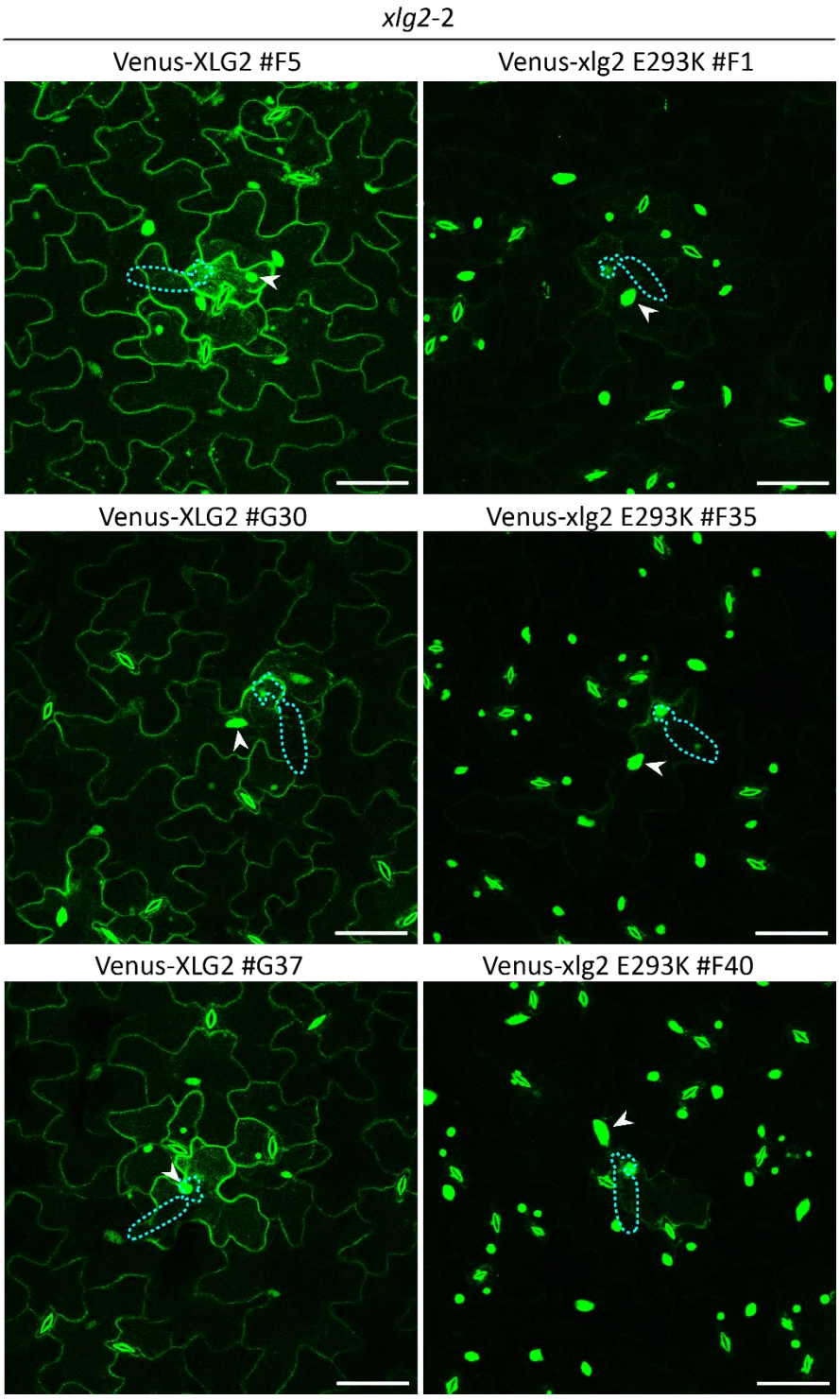

Fig. S 8: Powdery mildew attack increases XLG2 nuclear localization in *xlg2*-2 (more lines).

Images of infected (1dpi *Ec*) lines expressing Venus-XLG2 or Venus-xlg2 E293K in *xlg2*-2 are maximum projections of z stacks spanning the epidermal cell layer. Nuclei are marked by arrowheads and the position of fungal spore and appressorium are outlined by dashed blue lines. Scale bar = 50µm.

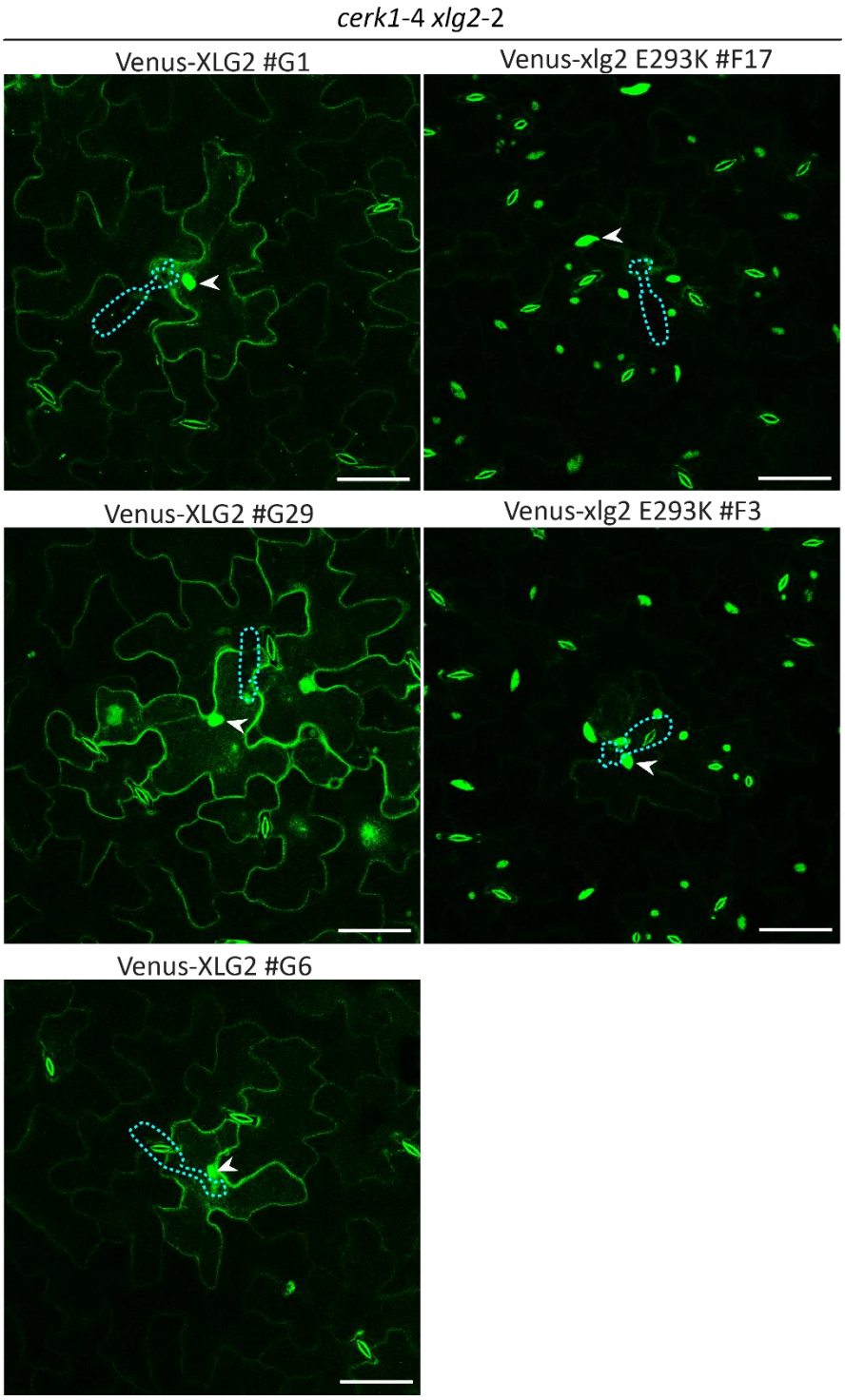

Fig. S 9: Powdery mildew attack increases XLG2 nuclear localization in *cerk1*-4 *xlg2*-2 (more lines).

Images of infected (1dpi *Ec*) lines expressing Venus-XLG2 or Venus-xlg2 E293K in *cerk1*-4 *xlg2*-2 are maximum projections of z stacks spanning the epidermal cell layer. Nuclei are marked by arrowheads and the position of fungal spore and appressorium are outlined by dashed blue lines. Scale bar = 50µm.

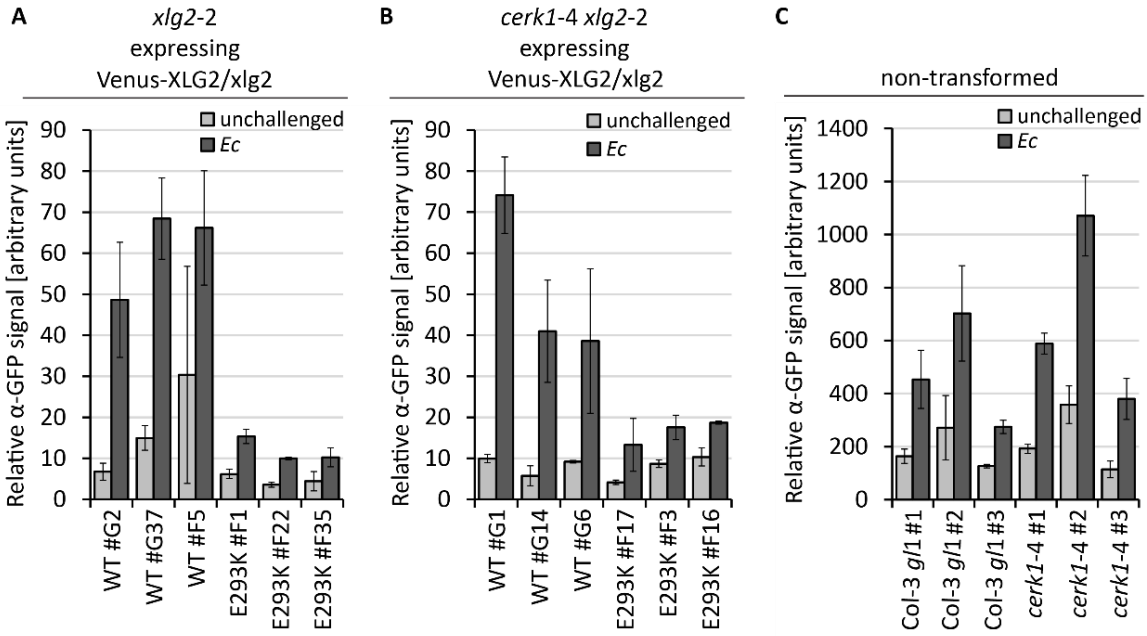

Fig. S 10: XLG2 abundance increased upon pathogen attack.

Relative protein quantification of unchallenged vs. inoculated (3dpi *Ec*) Western Blot samples using α-GFP in *xlg2*-2 **(A)** and in *cerk1*-4 *xlg2*-2 **(B)** expressing Venus-XLG2 or xlg2 E293K as well as α-XLG2 in non-transformed Col-3 *gl*1/ *cerk1*-4 **(C)**. Data are means ± StDev of 3 plants per independent line.

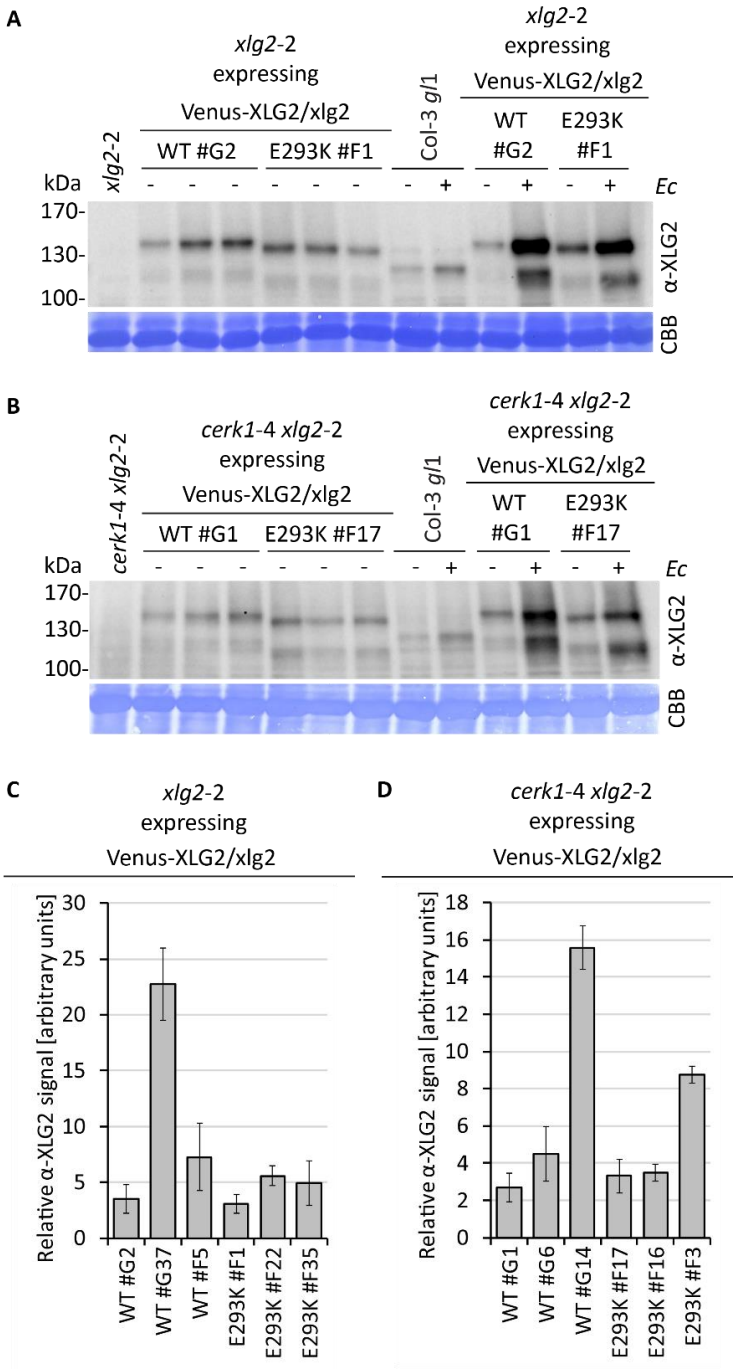

Fig. S 11: Comparison of XLG2 vs. xlg2 E293K abundance using the α-XLG2 antibody.

Unchallenged (-) vs. inoculated (3dpi *Ec*, +) transgenic plants expressing Venus-XLG2 WT or Venus-xlg2 E293K in *xlg2*-2 **(A)**/ *cerk1*-4 *xlg2*-2 **(B)** were analysed via Western blotting. One representative Western blot of three independent experiments is shown. CBB = Coomassie Brilliant Blue stained membrane.

Relative quantification of unchallenged *xlg2*-2 **(C)** and *cerk1*-4 *xlg2*-2 **(D)** expressing (Venus-)XLG2/ xlg2 E293K via α-XLG2 antibody. Signals were normalized to the non-transformed Col-3 *gl*1 (-) control. Data are means ± StDev of 3 plants.

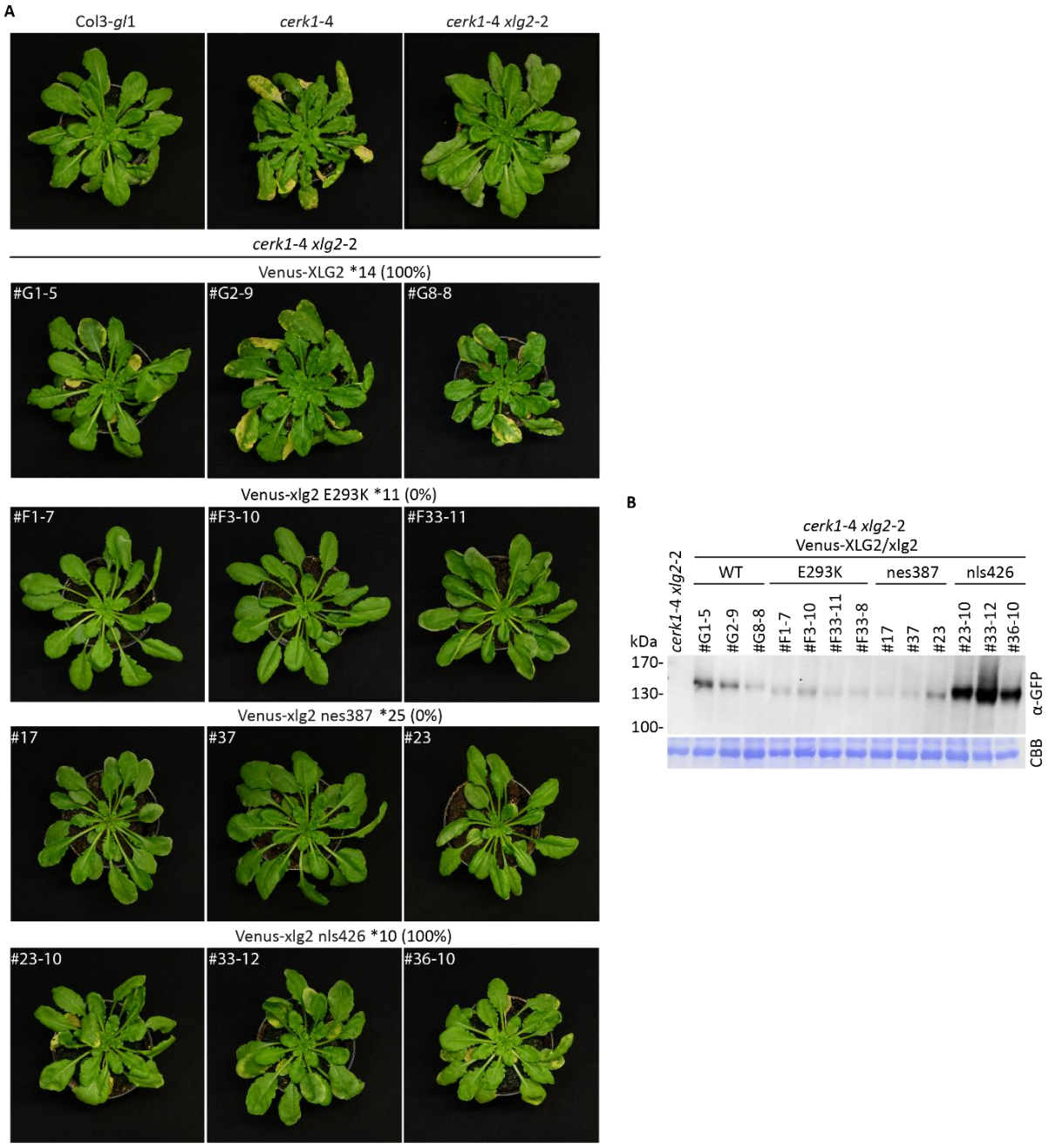

Fig. S 12: Venus-xlg2 E293K and xlg2 nes387 render XLG2 non-functional, while Venus-XLG2 WT and xlg2 nls426 complement *cerk1*-4 *xlg2*-2 (additional phenotypes).

(A) *cerk1*-4 *xlg2*-2 expressing Venus-XLG2 WT, Venus-xlg2 E293K, Venus-xlg2 nes387 or Venus-xlg2 nls426 and non-transformed controls are shown. Macroscopic cell death and fungal growth was evaluated 2wpi with *Ec.* *Indicated number of independent lines per construct were analysed (complementation rate) and three representative lines are shown. 7-week-old plants. **(B)** For the lines presented, accumulation of the Venus-XLG2 or Venus-xlg2 E293K/ nes387/ nls426 fusion proteins was confirmed by Western blotting after phenotype documentation (3wpi *Ec*) using GFP-specific antibody. CBB = Coomassie Brilliant Blue stained membrane.

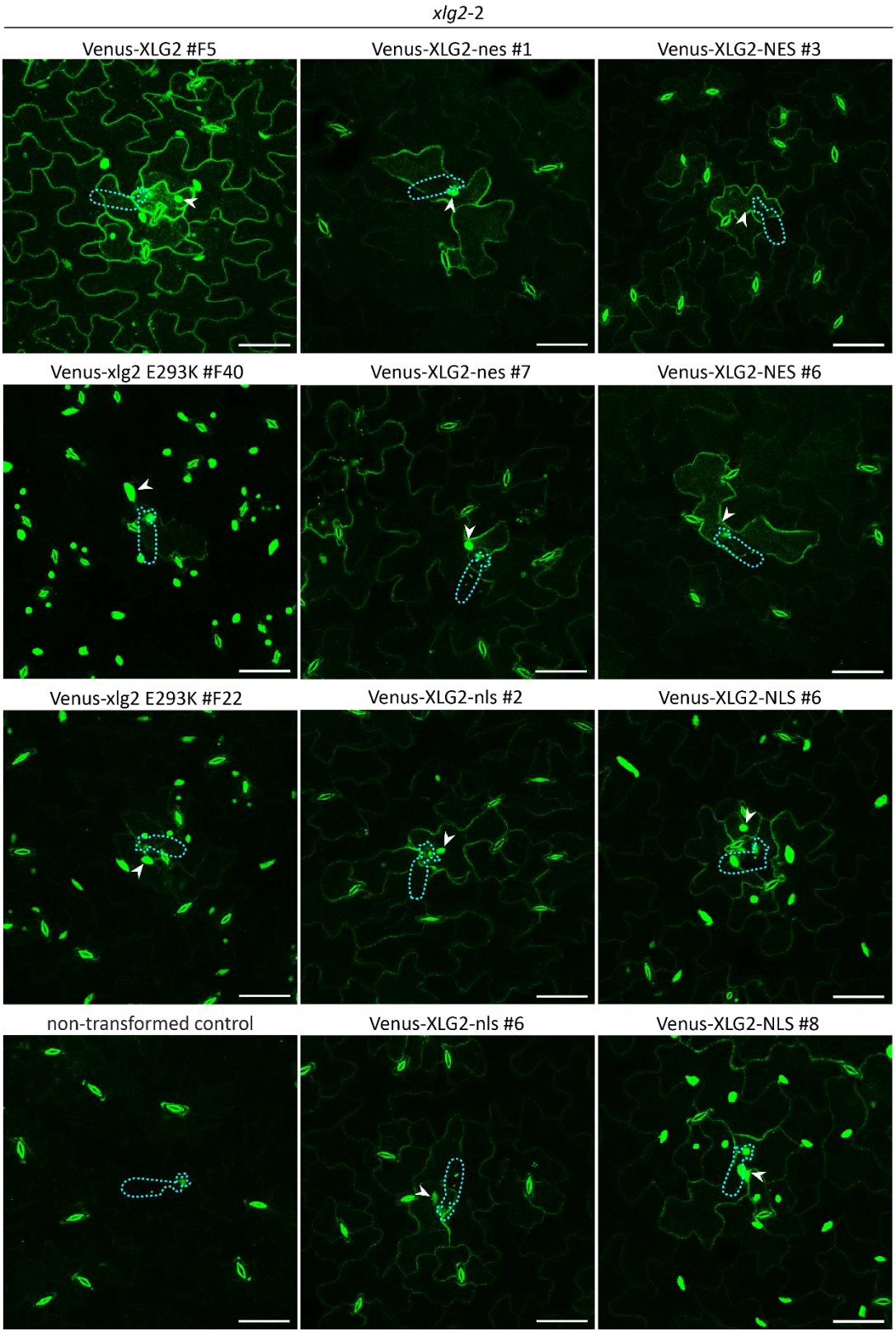

Fig. S 13: C-terminally fused -NES/ -NLS resulted in changed localization of XLG2 in *xlg2*-2 (more lines).

CLSM images of unchallenged vs. infected (1dpi *Ec*) *xlg2*-2 lines expressing Venus-XLG2 or Venus-XLG2-nes/ -NES/ -nls/ -NLS are maximum projections of z stacks spanning the epidermal cell layer. Nuclei are marked by arrowheads and the position of fungal spore and appressorium are outlined by dashed blue lines. Scale bar=50µm.

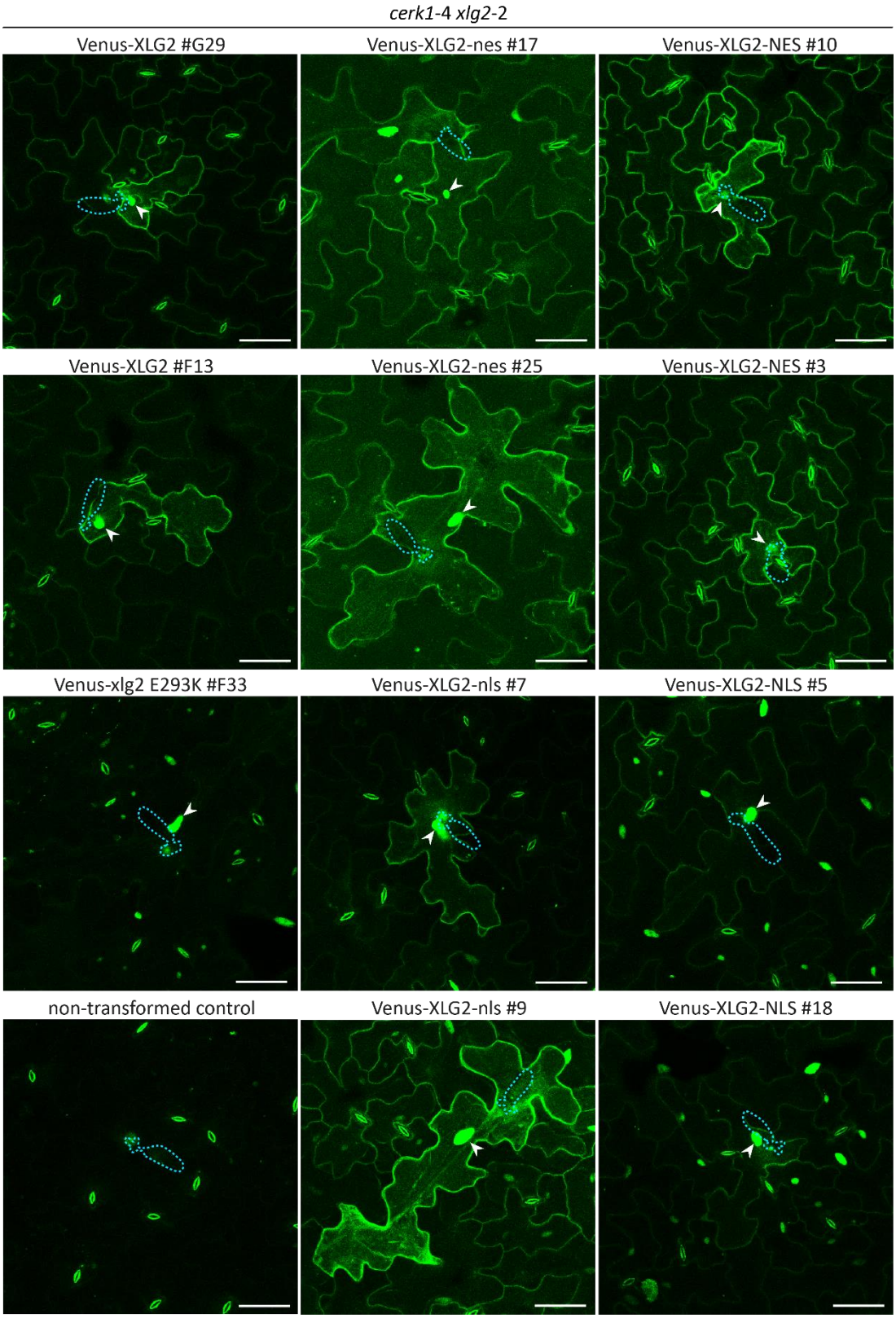

Fig. S 14: C-terminally fused -NES/ -NLS resulted in changed localization of XLG2 in *cerk1*-4 *xlg2*-2 (more lines).

CLSM images of unchallenged vs. infected (1dpi *Ec*) *cerk1*-4 *xlg2*-2 lines expressing Venus-XLG2 or Venus-XLG2-nes/ -NES/ -nls/ -NLS are maximum projections of z stacks spanning the epidermal cell layer. Nuclei are marked by arrowheads and the position of fungal spore and appressorium are outlined by dashed blue lines. Scale bar = 50µm.

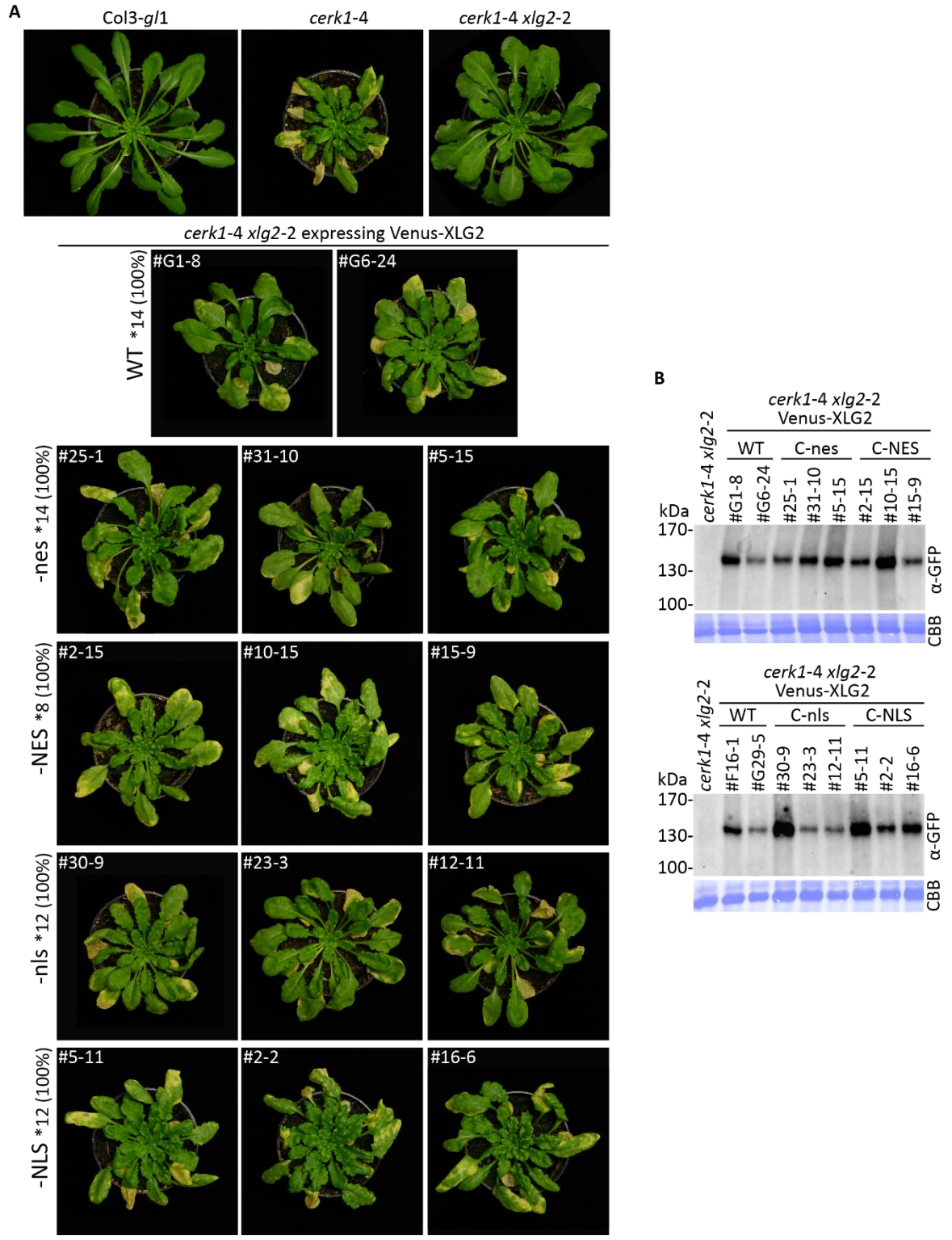

Fig. S 15: C-terminal NES/ nes/ NLS/ nls XLG2 fusion proteins complement *cerk1*-4 *xlg2*-2 (additional phenotypes).

(A) *cerk1*-4 *xlg2*-2 expressing Venus-XLG2 WT or Venus-XLG2-nes/ -NES/ -nls/ -NLS and non-transformed controls were evaluated 2wpi with *Ec* for macroscopic cell death and fungal growth. *Indicated number of independent lines per construct were analysed (complementation rate) and three representative lines are shown. The plants presented in this Figure were inoculated with *Ec* together with the lines in Fig. 37 and Fig S. 21. Therefore, the same images for the controls Col-3 *gl*1, *cerk1*-4, *xlg2*-2 and Venus-XLG2 (WT) lines are shown. **(B)** For the lines presented, accumulation of Venus-XLG2 or Venus-XLG2-nes/ -NES/ -nls/ -NLS fusion proteins was confirmed by Western blotting after phenotype documentation (3wpi *Ec*) using GFP-specific antibody. CBB = Coomassie Brilliant Blue stained membrane.

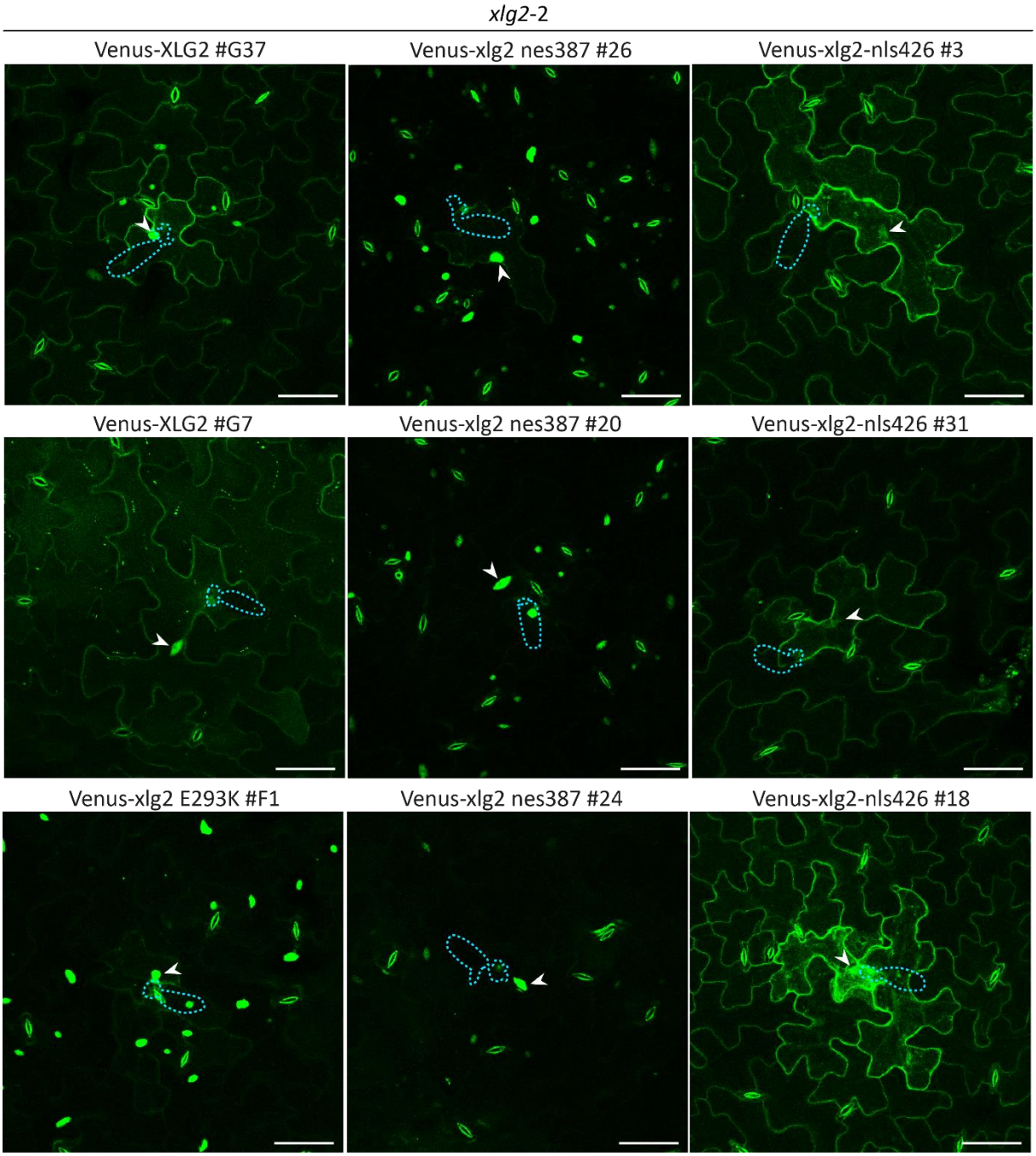

Fig. S 16: The nes387 and nls426 mutations change the localization of XLG2 in *xlg2*-2.

CLSM images of infected (1dpi *Ec*) transgenic lines expressing Venus-XLG2, Venus-xlg2 nes387 and Venus-xlg2 nls426 in *xlg2*-2 are maximum projections of z stacks spanning the epidermal cell layer. Nuclei are marked by arrowheads and the position of fungal spore and appressorium are outlined by dashed blue lines. Scale bar = 50µm.

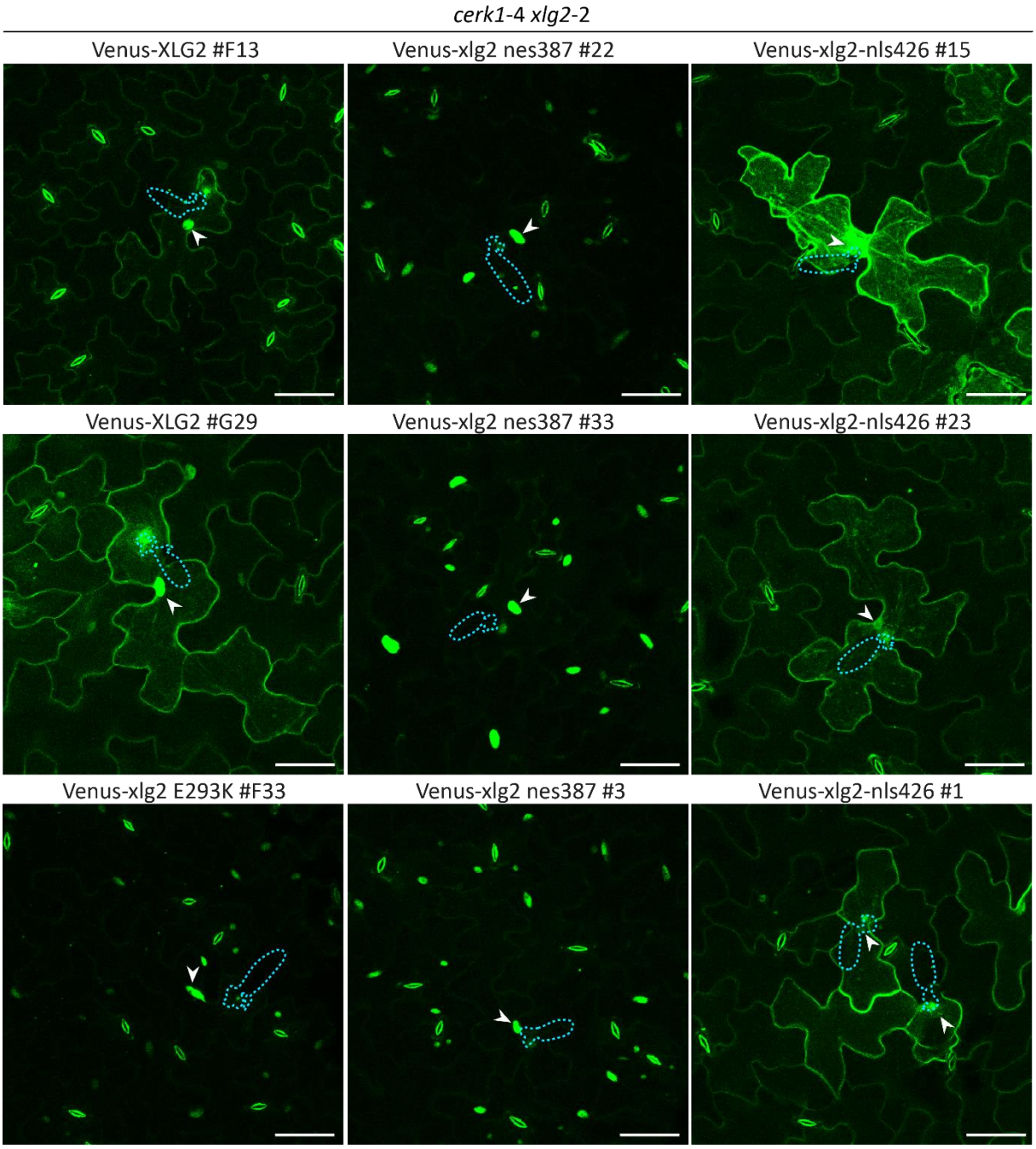

Fig. S 17: The nes387 and nls426 mutations change the localization of XLG2 in *cerk1*-4 *xlg2*-2.

CLSM images of infected (1dpi *Ec*) transgenic lines expressing Venus-XLG2, Venus-xlg2 nes387 and Venus-xlg2 nls426 in *cerk1*-4 *xlg2*-2 are maximum projections of z stacks spanning the epidermal cell layer. Nuclei are marked by arrowheads and the position of fungal spore and appressorium are outlined by dashed blue lines. Scale bar = 50µm.

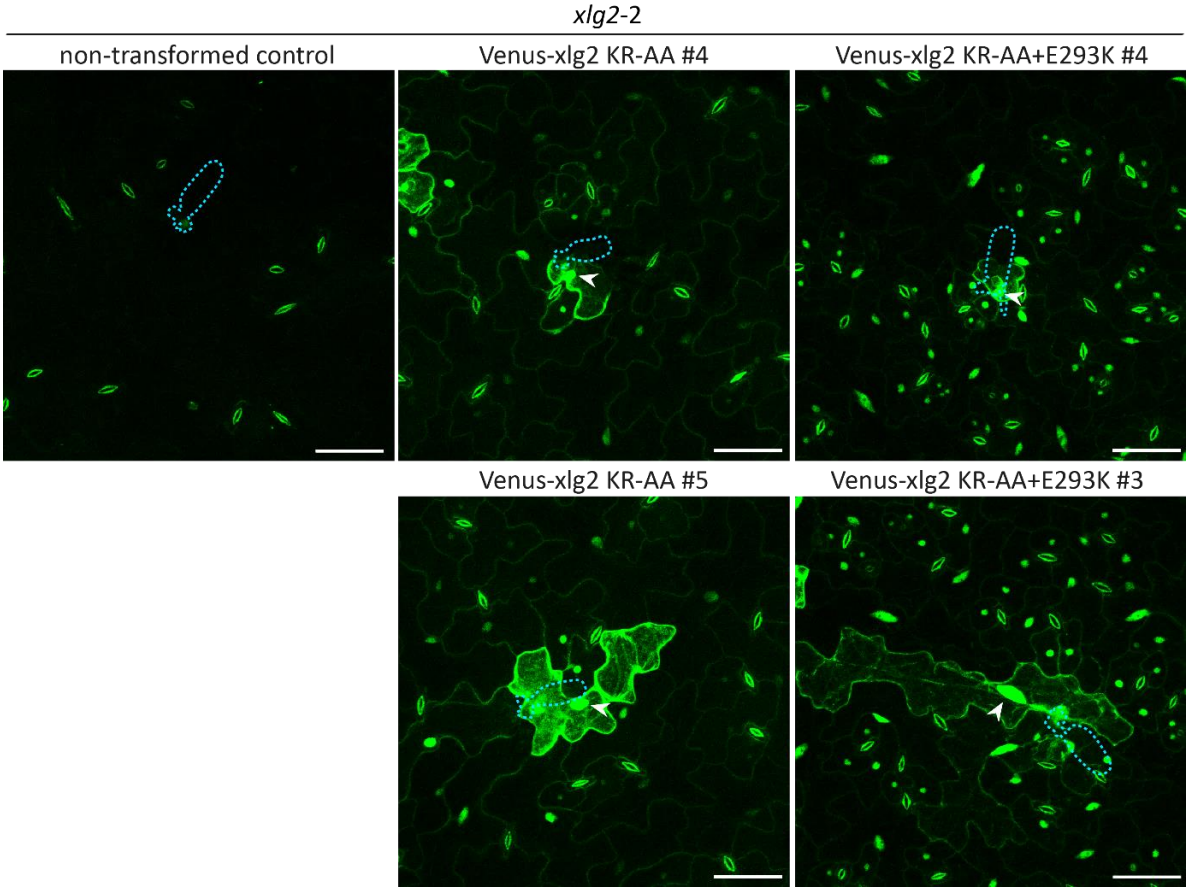

Fig. S 18: The KR-AA mutation did not change the constitutive nuclear localization of xlg2 E293K in *xlg2*-2 (more lines).
CLSM images of unchallenged vs. infected (1dpi *Ec*) representative lines expressing Venus-XLG2, Venus-xlg2 KR-AA or Venus-xlg2 KR-AA+E293K in *xlg2*-2 are maximum projections of z stacks spanning the epidermal cell layer. Nuclei are marked by arrowheads and the position of fungal spore and appressorium are outlined by dashed blue lines. Scale bar = 50µm.

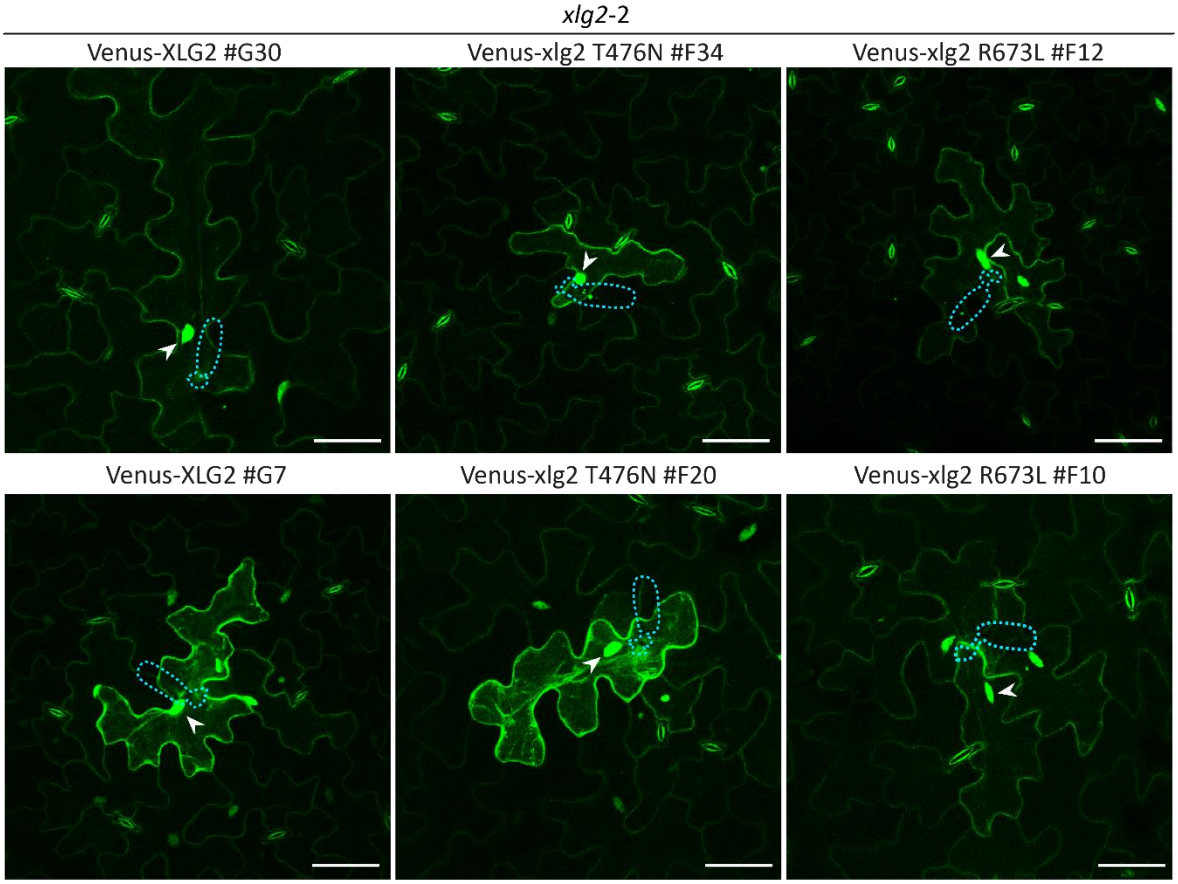

Fig. S 19: Gα-like domain mutations T476N and R673L did not affect localization of XLG2 in *xlg2*-2 (more lines).

CLSM images of unchallenged vs. infected (1dpi *Ec*) representative lines expressing Venus-XLG2 WT and Venus-xlg2 T476N/ R673L in *cerk1*-4 *xlg2*-2 are maximum projections of z stacks spanning the epidermal cell layer. Nuclei are marked by arrowheads and the position of fungal spore and appressorium are outlined by dashed blue lines. Scale bar=50µm.

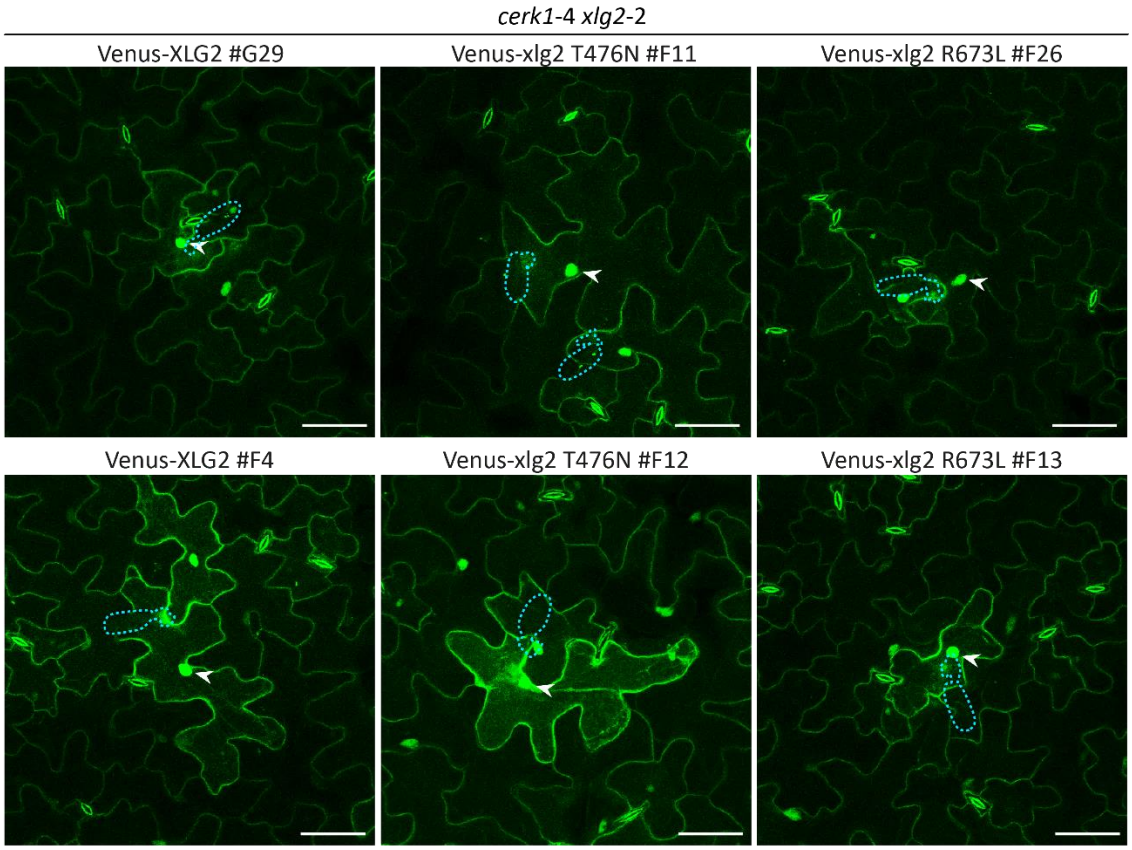

Fig. S 20: Gα-like domain mutations T476N and R673L did not affect localization of XLG2 in *cerk1*-4 *xlg2*-2 (more lines).
CLSM images of unchallenged vs. infected (1dpi *Ec*) representative lines expressing Venus-XLG2 WT and Venus-xlg2 T476N/ R673L in *cerk1*-4 *xlg2*-2 are maximum projections of z stacks spanning the epidermal cell layer. Nuclei are marked by arrowheads and the position of fungal spore and appressorium are outlined by dashed blue lines. Scale bar=50µm.

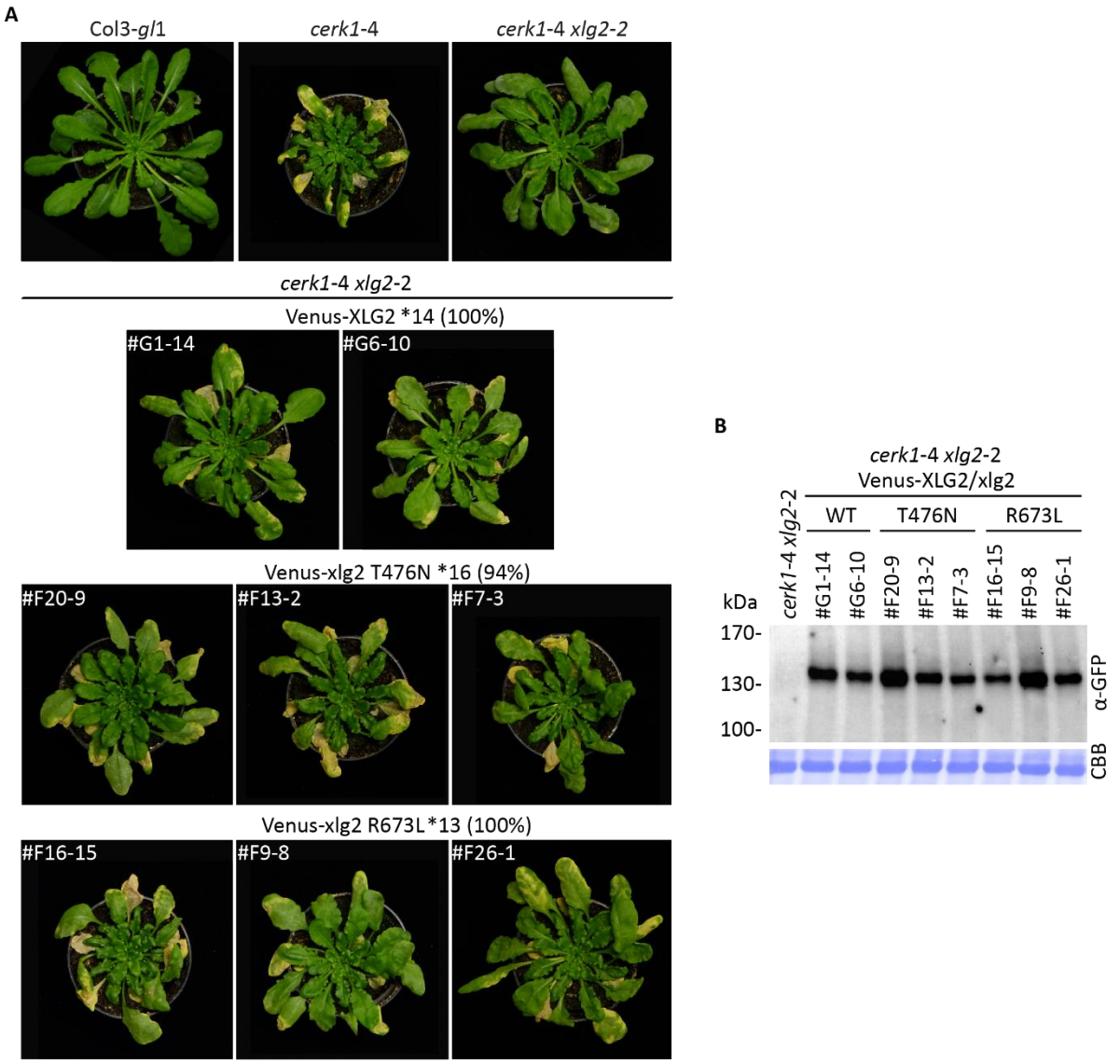

Fig. S 21: xlg2 nucleotide-free (T476N) as well as xlg2 constitutively bound to GTP (R673L) mutants do not suppress *cerk1*-4 (additional phenotypes).

(A) *cerk1*-4 *xlg2*-2 expressing Venus-XLG2 WT or Venus-xlg2 T476N, xlg2 R673L in *cerk1*-4 *xlg2*-2 and non-transformed controls were evaluated 2 weeks post inoculation with *Ec* for macroscopic cell death and fungal growth. 7-week-old plants. *Indicated number of independent lines per construct were analysed (complementation rate) and three representative lines are shown. The plants presented in this Figure were inoculated with *Ec* together with the lines in Fig.37 and Fig. S 15. Therefore, the same images for the controls Col-3 *gl*1, *cerk1*-4, *xlg2*-2 and Venus-XLG2 (WT) lines are shown. **(B)** For the lines presented, accumulation of Venus-XLG2 or Venus-xlg2 T476N/ R673L was confirmed by Western blotting after phenotype documentation (3wpi *Ec*) using α-GFP antibody. CBB = Coomassie Brilliant Blue stained membrane.

A

```
AT4G00990 TF          79-127 CHHCKILT----SESDLIFCSKCNKKCYCFDCIKRSYSERTHEEVRAACPFC-
AT1G09060 TF         220-267 CHQCQRKD----RERI-ISCLKCNQRAFCHNCLSARYSEISLEEVEKVCPACR
AT3G48070 TF         244-286 CPICYEDLDLTDSN--FLPC-PCG-FRLCLFCHK------TICDGDGRCPGCR
At1g11950 TF         194-239 CHQCSKGE----RRYL-FICTFCEVRLYCFPCIKKWYPHLSTDDILEKCPFC-
At1g62310 TF         209-256 CHQCLKGE----RITL-LICSECEKTMFCLQCIRKWYPNLSEDDVVEKCPLCR
AT5G62910 MQB22.3   252-294 CPICYEDLDLTDSN--FLPC-PCG-FRLCLFCHK------TICDGDGRCPGCR
At1g09060 JMJ24     220-267 CHQCQRKD-----RERIISCLKCNQRAFCHNCLSARYSEISLEEVEKVCPACR
AT3G07610 JMJ25     155-201 CHQCQKSD------RIVERCQTCNSKRYCHPCLDTWYPLIAKEDVAKKCMFCS
AT4G32410 CESA1      39-85  CQICGDDVGLAETGDVFVACNECA-FPVCRPCYEY-----ERKDGTQCCPQCK
At4g39350 CESA2      39-85  CQICGDEIELTVSSELFVACNECA-FPVCRPCYEY-----ERREGNQACPQCK
AT5G05170 CESA3      20-66  CQICSDNVGKTVDGDRFVACDICS-FPVCRPCYEY-----ERKDGNQSCPQCK
AT5G44030 CESA4      23-69  CKVCGDEVKDDDNGQTFVACHVCV-YPVCKPCYEY-----ERSNGNKCCPQCN
At5g09870 CESA5      39-85  CQICGDEIELSVDGESFVACNECA-FPVCRPCYEY-----ERREGNQSCPQCK
AT5G64740 CESA6      39-85  CQICRDEIELTVDGEPFVACNECA-FPVCRPCYEY-----ERREGNQACPQCK
AT5G17420 CESA7      37-83  CEICGDQIGLTVEGDLFVACNECG-FPACRPCYEY-----ERREGTQNCPQCK
AT4G18780 CESA8       9-55  CNTCGEEIGVKSNGEFFVACHECS-FPICKACLEY-----EFKEGRRICLRCG
AT2G21770 CESA9      39-85  CKICRDEIELTDNGEPFIACNECA-FPTCRPCYEY-----ERREGNQACPQCG
At2g23460 XLG1      225-268 CYRCFKGS----RFTEKEVCLVCD-AKYCNSCVLRAMGS-MPEG--RKCVTC-
At4g34390 XLG2      214-257 CYRCQLGN----RFTEKEVCIVCD-AKYCFNCVRRAMGA-MPEG--RKCQAC-
At1g31930 XLG3      176-218 CYRCGK-A----KWENKETCIVCD-EKYCGNCVLRAMGS-MPEG--RKCVSC-
                            *  *              *  *     *  *                *  *
```

B

```
                                        (R/K)(R/K)HHCR motif                  RVC motif
AT1G20110 FYVE1   461-510  CTSCGSDFGA-FIRRHHCRNCGDVFCDKCTQGRIA--LTAE----DNAPQVRVCDRC
AT3G43230 FYVE2   181-232  CMQCSTPFTAITCGRHHCRFCGGIFCRNCSKGRCLMPSRF-----RERNPQRVCDSC
At1g29800 FYVE3   191-242  CMLCSVRFHPIMCSRHHCRYCGGIFCRDCSKGKSLVPVKF-----RVSDPQRVCDVC
At1g61690 FYVE4    25-73   CQGCSSQFTF-INRKHHCRRCGGLFCGTCTQQRLSLRG-------QGDSPVRICEPC
At3g14270 FAB1B    45-100  CYECDCQFTL-INRRHHCRHCGRVFCGKCTANSIPFAPSDLRTPREDWERIRVCNYC
At4g33240 FAB1A    42-97   CYECDAQFTV-FNRRHHCRLCGRVFCAKCAANSIPSPSDETKDSHEEPERIRVCNYC
At1G65920 PRAF1   632-695  CSSCKSAFGF-TRRKHNCYNCGLLFCNACSSKKAVNASLAP----NKSKLSRVCDSC
At3g47660 PRAF2   681-732  CSGCRHPFNY-MRKLHNCYNCGSVFCNSCTSKKSLAAAMAP----KTNRPYRVCDDC
At1g69710 PRAF3   657-708  CAGCRNPFNF-RRKRHNCYNCGLVFCKVCSSRKSLRAALAP----DMNKPYRVCYGC
At1G76950 PRAF4   638-689  CSTCRLAFGF-TRKRHNCYNCGLVHCHSCSSKKAFRAALAP----SAGRLYRVCDSC
At3g23270 PRAF6   605-656  CSGCRQAFGF-TRKRHNCYNCGLVHCHACSSKKALKAALAP----TPGKPHRVCDAC
At5g12350 PRAF8   662-713  CSGCRQPFSF-KRKRHNCYNCGLVFCHSCTSKKSLKACMAP----NPNKPYRVCDKC
At5g19420 PRAF9   700-755  CSGCRQPFNF-KRKRHNCYNCGLVFCHSCSNKKSLKACMAP----NPNKPYRVCDRC
At4g14368 PRAF10  625-675  CSGCRQAFGF-TRKRHNCYNCGLVHCHACSSKKALKAALAP----TPGKPHRVCDAC
At2g23460 XLG1    225-268  CYRCFKGSRF--TEKEVCLVCDAKYCNSCVLRAMGS----------MPEGRKCVTC
At4g34390 XLG2    214-257  CYRCQLGNRF--TEKEVCIVCDAKYCFNCVRRAMGA----------MPEGRKCQAC
At1g31930 XLG3    176-218  CYRCGK-AKW--ENKETCIVCDEKYCGNCVLRAMGS----------MPEGRKCVSC
                            *  *           . *  *.  .*  *                    * *  *
```

Fig. S 22: Clustal alignments of RING/ FYVE domains shows conserved cysteine spacing pattern.

Conserved cysteines are highlighted in black**.** CLUSTAL O (version 1.2.4) multiple sequence alignment was used (Madeira et al. 2019). **(A)** Alignment of XLGs with known RING-C2 domains including JMJ24 which is functional E3 ligase (Kabelitz et al. 2016), JMJ25 (IBM1) with demethylase function (Miura et al. 2009) as well as CESA potential RING domains (Kumar et al. 2020; Stone et al. 2005). CESA3, CESA4 and CESA8 were described to be S-acylated within the potential RING domain which would contradict zinc coordination (S-acylated cysteines are labeled in blue) in contrast to CESA1, CESA6 and CESA7 which still potentially form a RING structure (Kumar et al. 2020). **(B)** Alignment of XLGs with FYVE domain proteins. Known amino acids in FYVE domains involved in phosphatidylinositol 3 phosphate binding are highlighted in blue (Wywial and Singh 2010). XLGs lack the main FYVE-motif.

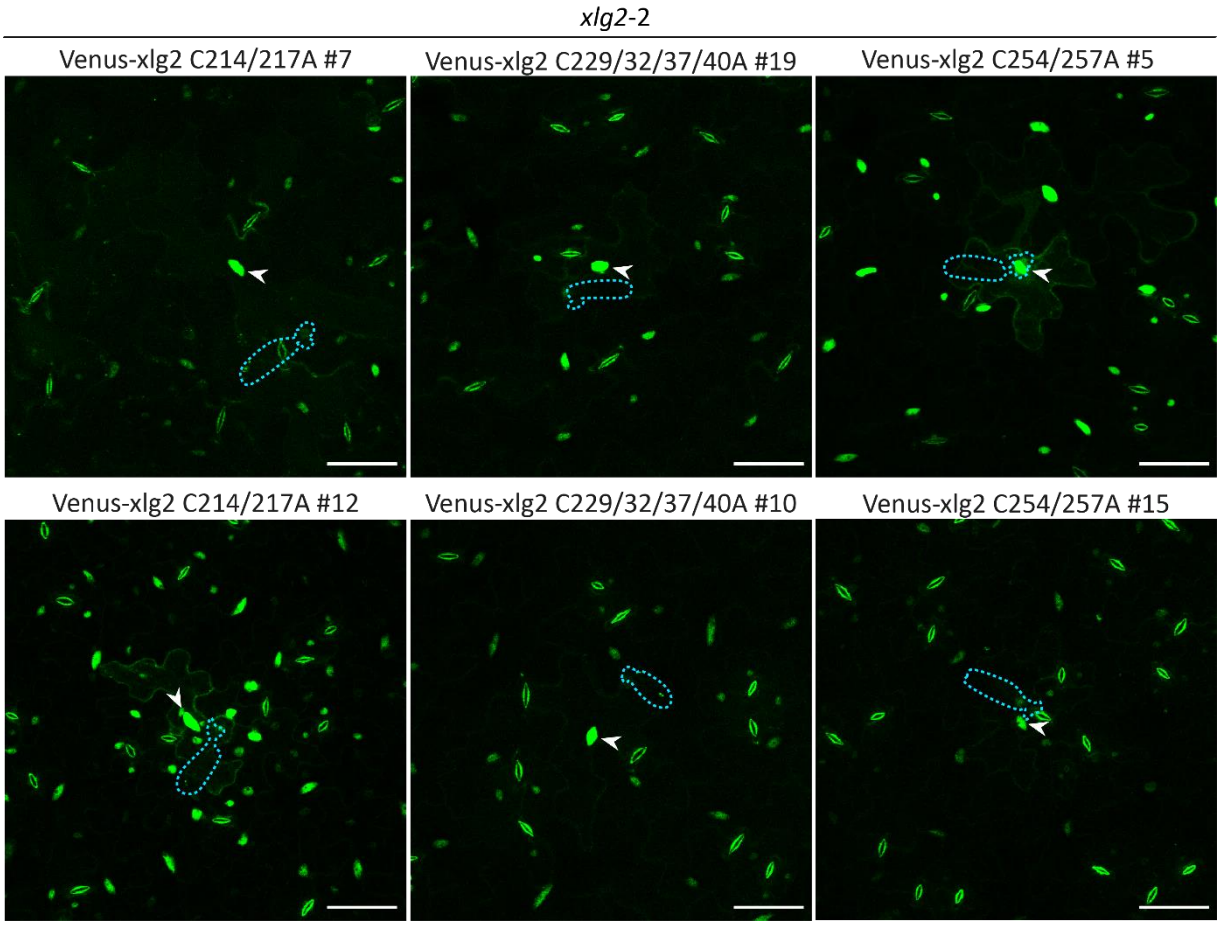

Fig. S 23: Cys-rich region C-A mutations abolish plasma membrane localization of XLG2 in *xlg2*-2 (more lines).

CLSM images of infected (1dpi *Ec*) plants expressing Venus-XLG2 C214/217A, C229/232/237/240A and C254/257A in *xlg2*-2 are maximum projections of z stacks spanning the epidermal cell layer. Nuclei are marked by arrowheads and the position of fungal spore and appressorium are outlined by dashed blue lines. Scale bar=50µm.

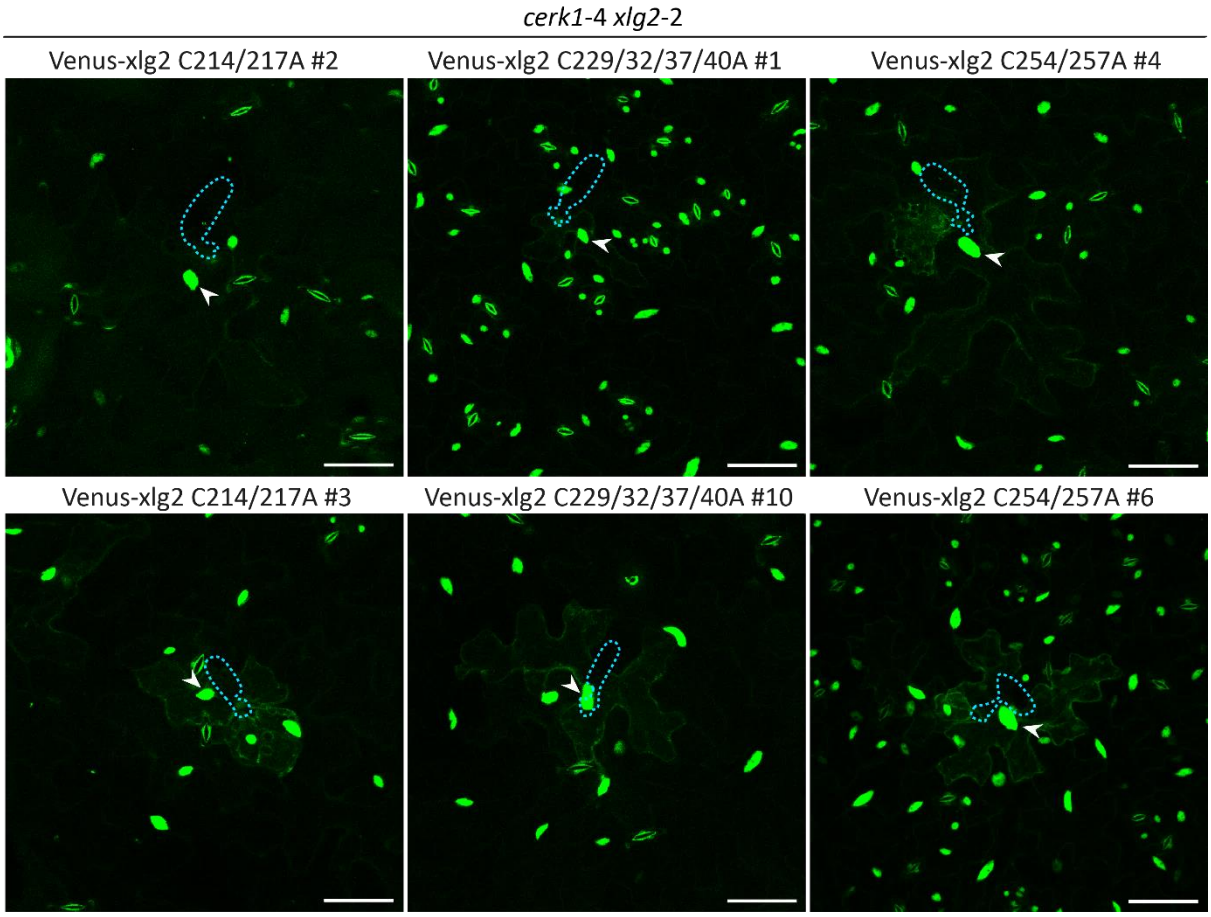

Fig. S 24: Cys-rich region C-A mutations abolish plasma membrane localization of XLG2 in *cerk1*-4 *xlg2*-2 (more lines).
CLSM images of infected (1dpi *Ec*) plants expressing Venus-XLG2 C214/217A, C229/232/237/240A and C254/257A in *cerk1*-4 *xlg2*-2 are maximum projections of z stacks spanning the epidermal cell layer. Nuclei are marked by arrowheads and the position of fungal spore and appressorium are outlined by dashed blue lines. Scale bar=50µm.

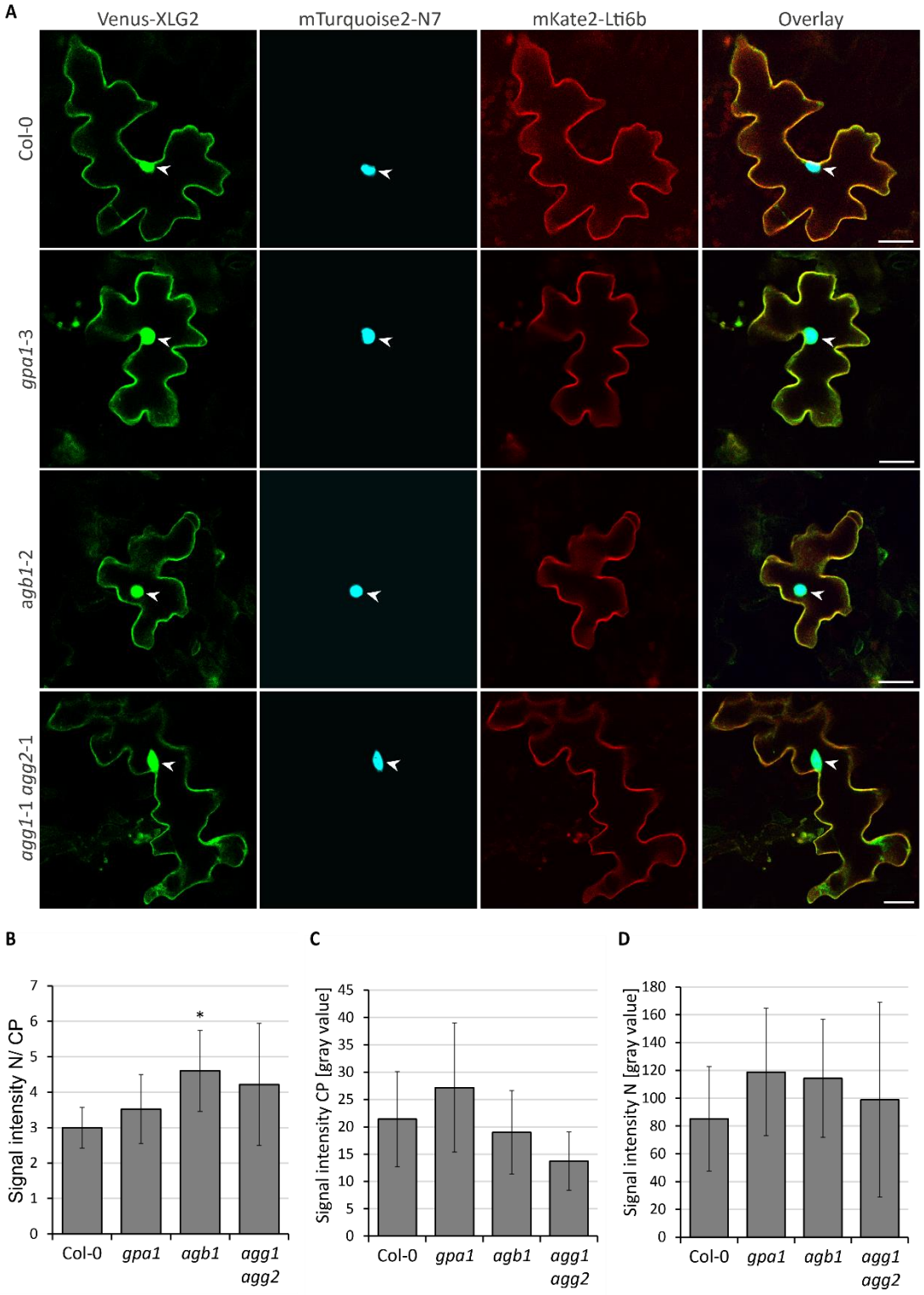

Fig. S 25: Transiently expressed Venus-XLG2 localizes to PM and nucleus in G protein mutant *Arabidopsis* plants (experiment 1).

Venus-XLG2 was co-transformed with mTurquoise2-N7 (nuclear marker) and mKate2-LTI6b (PM marker) in Col-0 as well as *gpa1*-3, *agb1*-2, and *agg1*-1 *agg2*-1. **(A)** Representative single plane CLSM images of three independent experiments 1d after bombardment. Nuclei are marked by arrowheads. Scale bar = 50µm.

Quantification of Venus-XLG2 localization in particle bombardment experiments: Signal intensities for **(B)** N/ CP, **(C)** CP, and **(D)** N. Venus intensity was measured in N (= nuclear) and CP (= cell periphery) regions defined by mTurquoise2 and mKate2 channels. Data are means ± StDev of n ≥ 5 cells. * P <0.05

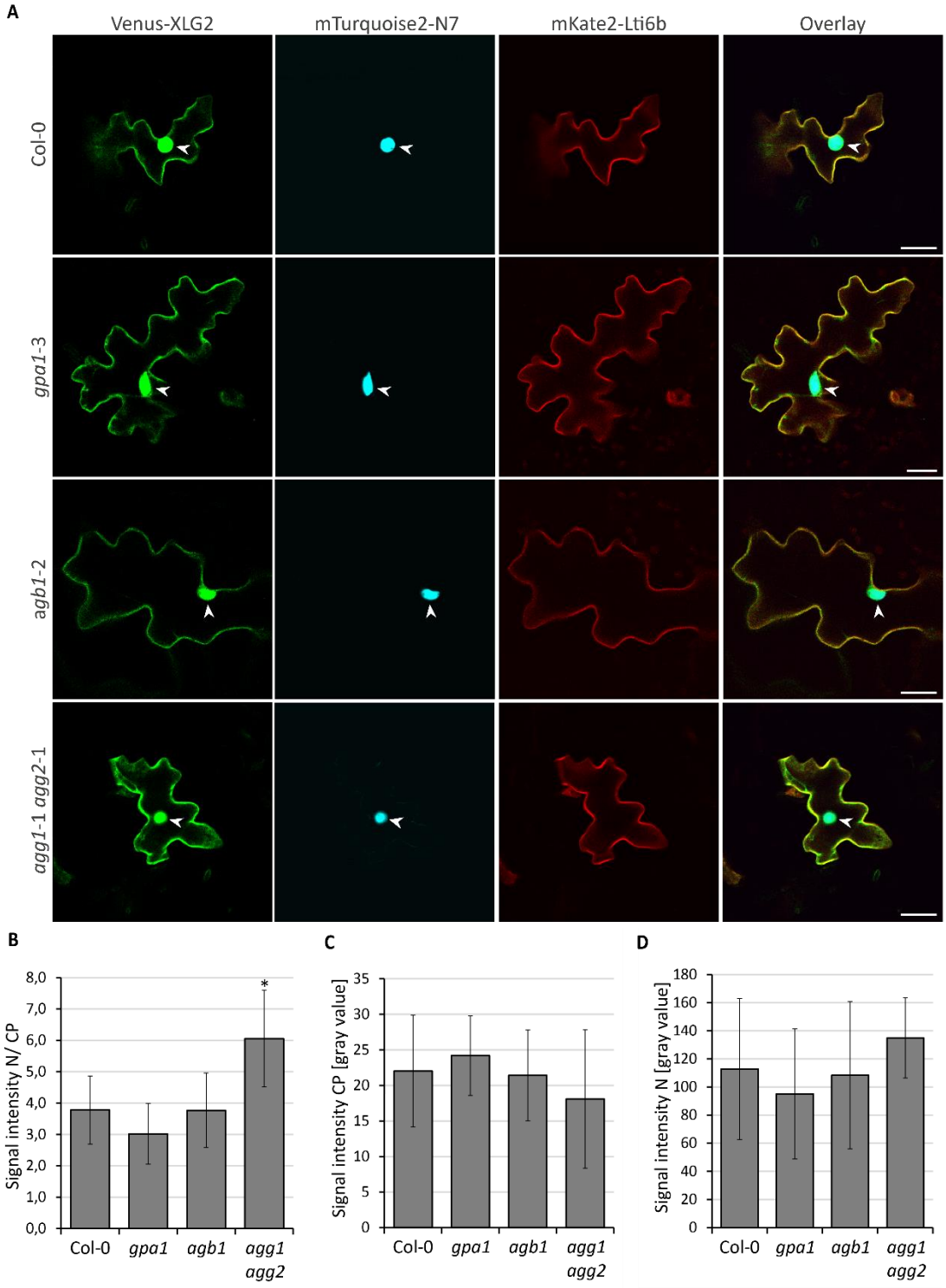

Fig. S 26: Transiently expressed Venus-XLG2 localizes to PM and nucleus in G protein mutant *Arabidopsis* plants (experiment 2).

Venus-XLG2 was co-transformed with mTurquoise2-N7 (nuclear marker) and mKate2-LTI6b (PM marker) in Col-0 as well as *gpa1*-3, *agb1*-2, and *agg1*-1 *agg2*-1. **(A)** Representative single plane CLSM images of three independent experiments 1d after bombardment. Nuclei are marked by arrowheads. Scale bar = 50µm.

Quantification of Venus-XLG2 localization in particle bombardment experiments: Signal intensities for **(B)** N/ CP, **(C)** CP, and **(D)** N. Venus intensity was measured in N (= nuclear) and CP (= cell periphery) regions defined by mTurquoise2 and mKate2 channels. Data are means ± StDev of n ≥ 5 cells. * P <0.05

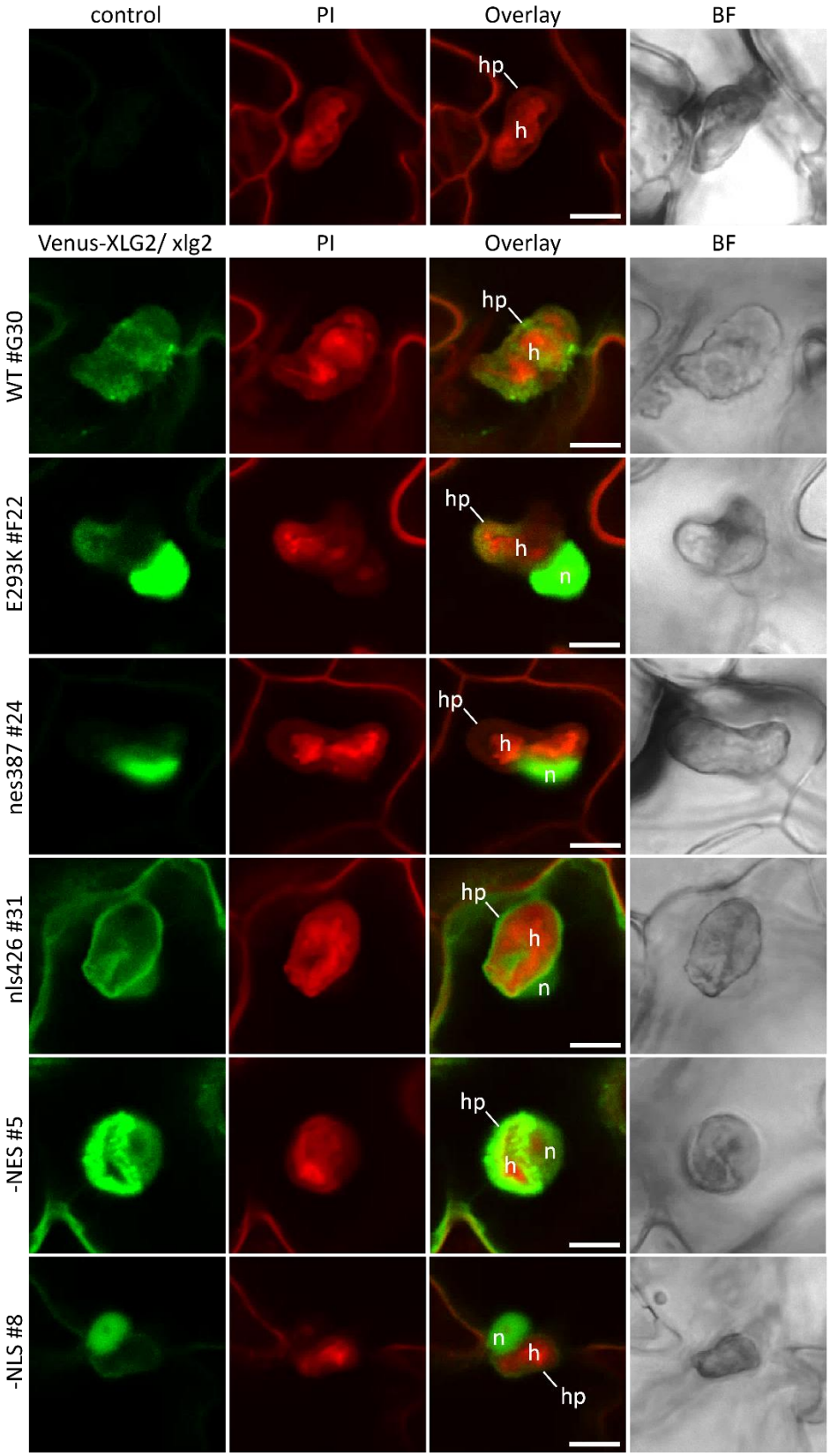

Fig. S 27: XLG2 associates with the haustorial periphery in *xlg2*-2 (more lines).

CLSM images are representative single planes of transgenic *xlg2*-2 expressing Venus-XLG2, Venus-xlg2 E293K, Venus-xlg2 nes387, Venus-xlg2 nls426, Venus-XLG2-NES, Venus-XLG2-NLS and a non-transformed control with fully developed *Ec* haustoria recorded at 7dpi. Scale bar = 10µm. n = nuclei, h = haustoria, hp = haustorial periphery, PI = propidium iodide, BF = bright field.

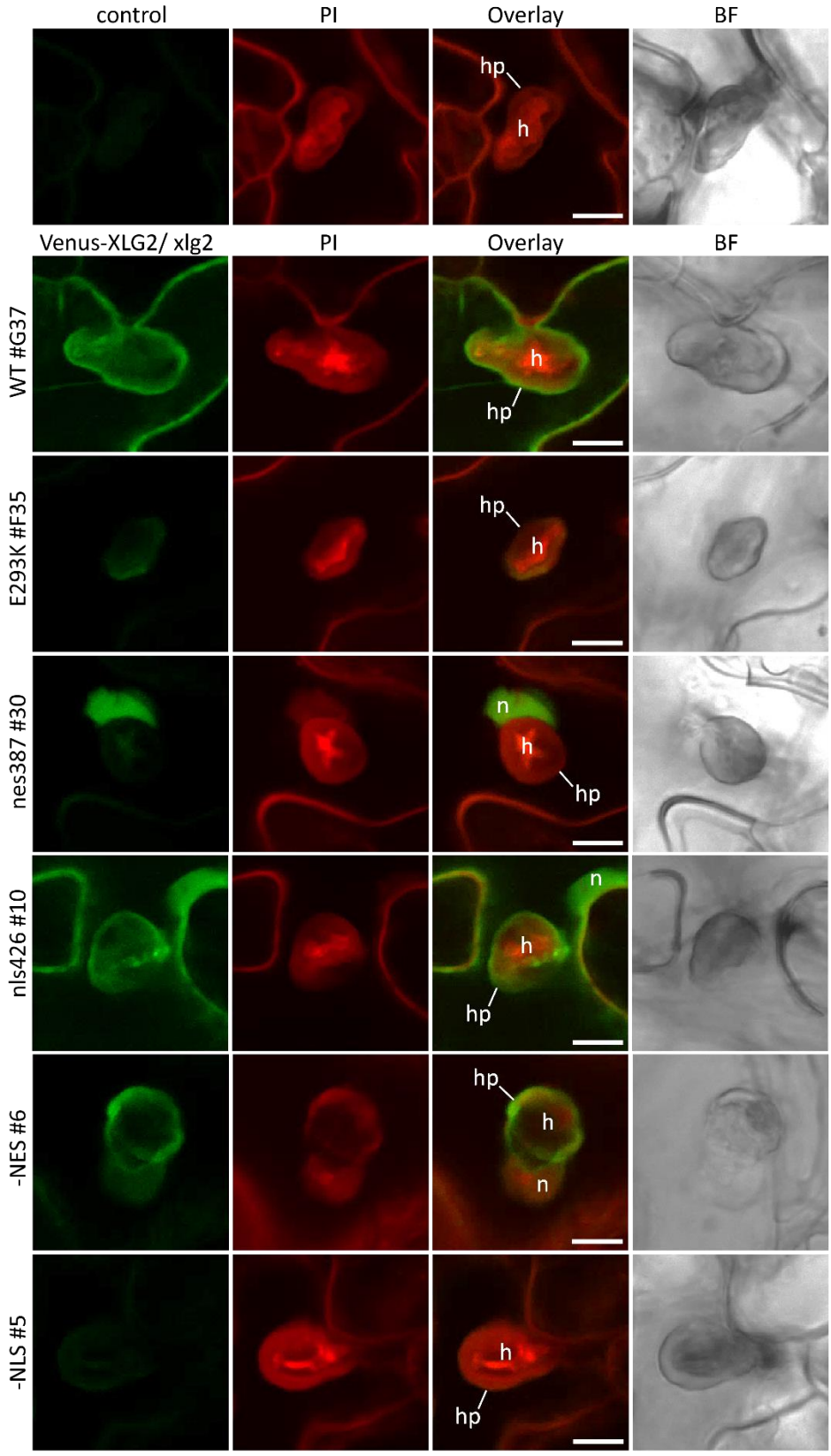

Fig. S 28: XLG2 associates with the haustorial periphery in *xlg2*-2 (more lines).

CLSM images are representative single planes of transgenic *xlg2*-2 expressing Venus-XLG2, Venus-xlg2 E293K, Venus-xlg2 nes387, Venus-xlg2 nls426, Venus-XLG2-NES, Venus-XLG2-NLS and a non-transformed control with fully developed *Ec* haustoria recorded at 7dpi. Scale bar = 10µm. n = nuclei, h = haustoria, hp = haustorial periphery, PI = propidium iodide, BF = bright field.

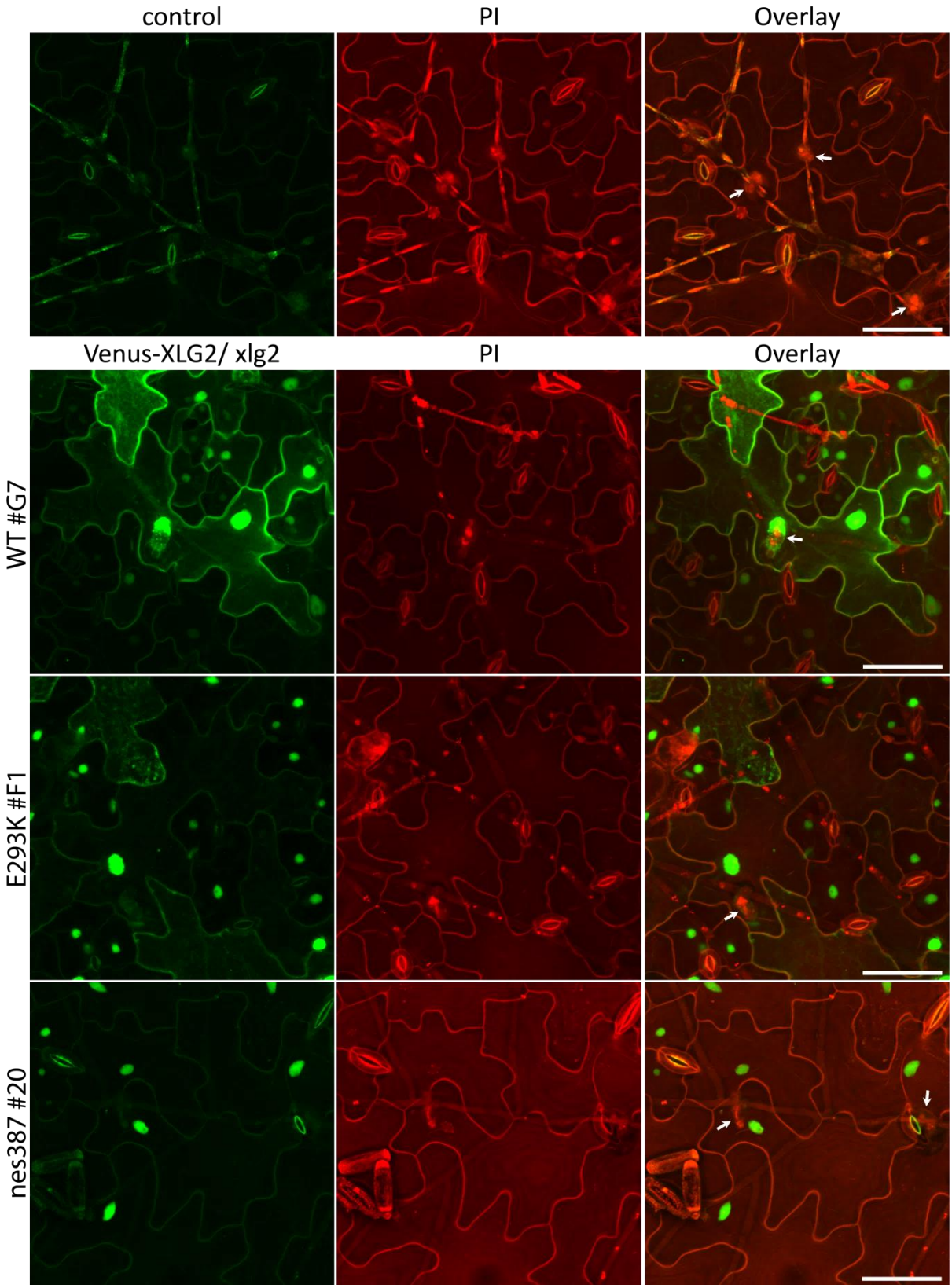
control
PI
Overlay
Venus-XLG2/ xlg2
PI
Overlay
WT #G7
E293K #F1
nes387 #20

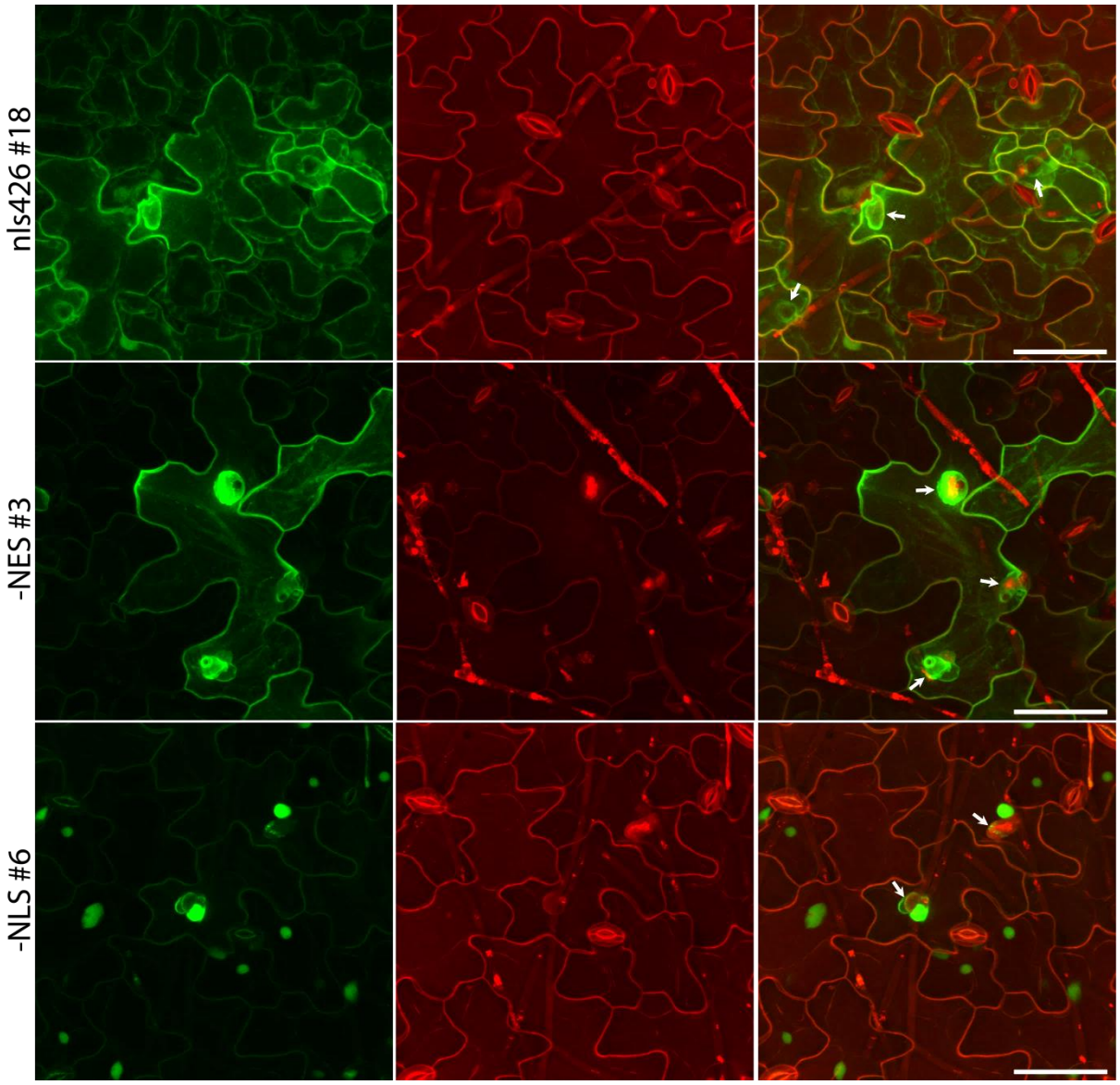

Fig. S 29: XLG2 accumulated at haustorial formation sites in *xlg2*-2.

Representative CLSM images are maximum projections of 32 - 40 focal planes. Transgenic *xlg2*-2 expressing Venus-XLG2, Venus-xlg2 E293K, Venus-xlg2 nes387, Venus-xlg2 nls426, Venus-XLG2-NES, Venus-XLG2-NLS and a non-transgenic control at 7dpi *Ec*. Arrows point at haustoria. Scale bar = 50µm. PI = propidium iodide.

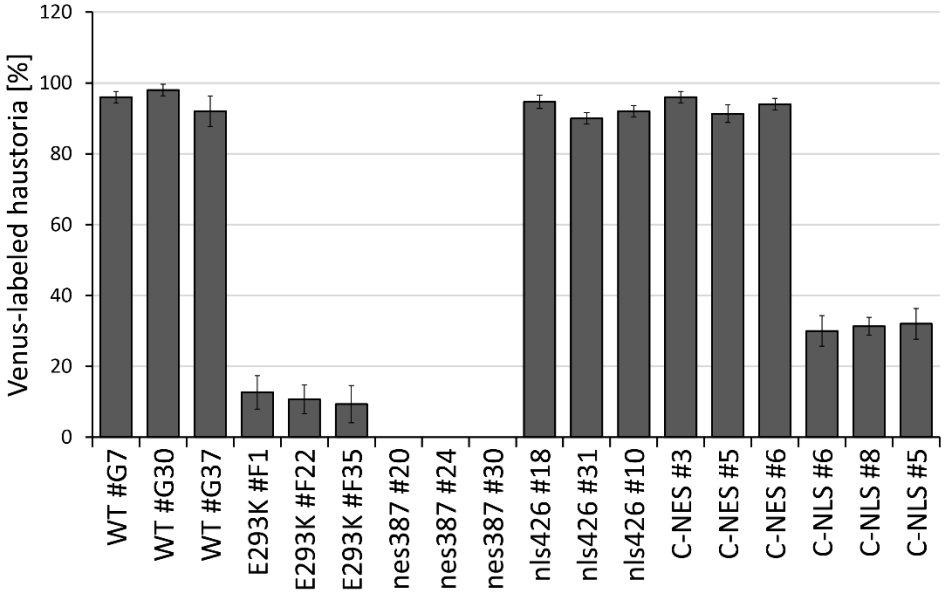

Fig. S 30: Mainly nuclear localized XLG2 variants labeled haustoria significantly less efficient (three independent lines). Venus-labeled haustoria were count in Venus-XLG2 WT, Venus-XLG2-NES/ -NLS and Venus-xlg2 E293K/ nes387/ nls426 expressing *xlg2*-2 and presented as percentage of labeled haustoria at 7dpi *Ec*. Data are means ± StDev of 50 haustoria of 3 plants (n = 150).

6 Danksagung

Ich danke Volker Lipka für seine Entscheidung, mich als Doktorandin in seiner Abteilung willkommen zu heißen. Danke für die auflockernden ornithologischen Bemerkungen, sowie kritischen Anmerkungen während unserer regelmäßigen Meetings und deinem stetigen Einsatz, eine effektive Laborumgebung zu schaffen und zu erhalten. Elena ist die gute Seele des XLG2 Projektes, danke für deinen konstruktiven Input, kritische Anmerkungen und Fragen, die bereicherten, motivierten und für die eine oder andere Überstunde am Mikroskop oder Laptop sorgten. Danke an Thomas und Merlin für Kilometerweise gute Unterhaltungen beim Laufen im Göttinger Umland. Danke für die stets freundlich angebotene Hilfe bei gärtnerischen Tätigkeiten und herzlichen Unterhaltungen an Feli und Susanne. Besonders danken möchte ich Sabine, du hast mich vor allem während meiner Schwangerschaft im Labor sehr unterstützt. Ludmilla, Sina, Chrissi, Mohamed und Lena danke ich für den wunderbaren Wiedereinstieg nach meiner Elternzeit, das schöne Klima im Büro und in den Laboren. Mein Wiedereinstieg wurde auch durch Ronjas hervorragende Arbeit unterstützt, du hast während meiner Pause die schier nicht enden zu wollende Samenliste fortgeführt und inspirierende Beobachtungen zum XLG2 Projekt dokumentiert. Ich möchte mich auch bei allen ungenannten Mitgliedern der Abteilungen Lipka und Wiermer bedanken, die mich unterstützt haben und zu schönen Momenten während dieser Zeit beigetragen haben.

Meinem Partner Fabian danke ich für viele inspirierende Gespräche von der Biologie bis hin zur Physik und für deine stetige Unterstützung Zuhause. Unserer Tochter Mira danke ich für ihre Eigensinnigkeit und Freude. Du hast mir eine wundervolle Perspektive auf das Leben eröffnet. Ich danke meinen Eltern Carsten und Silvie, sowie meiner Schwester Marie, für euren Glauben an mich und in meine Fähigkeiten. Danke für eure Hinweise, dass ich durchhalten kann, aber auch Pausen brauche. Ich danke allen Freunden, die mich und uns als Familie während dieser Zeit unterstützt haben, sei es durch Essen kochen, einfach mal nachfragen wie es uns geht oder das zur Verfügung stellen eines Arbeitszimmers.

Ich bin dankbar für die finanzielle Unterstützung und unkomplizierte Elternzeitregelung durch die Deutsche Forschungsgemeinschaft. Anmerken möchte ich ebenso, dass die finanzielle Unterstützung durch das familienfreundliche Abschluss-Stipendium von GAUSS während meiner Schreibphase und während der Corona-bedingten Schließungen der Betreuungseinrichtungen den Abschluss dieser Arbeit ganz besonders gefördert hat. Ich danke der Deutschen Bahn für meistens pünktliche Schnellzüge zwischen Göttingen und Hannover.

7 Publication bibliography

Aarts, N.; Metz, M.; Holub, E.; Staskawicz, B. J.; Daniels, M. J.; Parker, J. E. (1998): Different requirements for EDS1 and NDR1 by disease resistance genes define at least two R gene-mediated signaling pathways in *Arabidopsis*. In *Proceedings of the National Academy of Sciences of the United States of America* 95 (17), pp. 10306–10311. DOI: 10.1073/pnas.95.17.10306.

Acharya, Biswa R.; Raina, Surabhi; Maqbool, Shahina B.; Jagadeeswaran, Guru; Mosher, Stephen L.; Appel, Heidi M. et al. (2007): Overexpression of CRK13, an *Arabidopsis* cysteine-rich receptor-like kinase, results in enhanced resistance to Pseudomonas syringae. In *The Plant journal : for cell and molecular biology* 50 (3), pp. 488–499. DOI: 10.1111/j.1365-313X.2007.03064.x.

Adachi, Hiroaki; Derevnina, Lida; Kamoun, Sophien (2019): NLR singletons, pairs, and networks: evolution, assembly, and regulation of the intracellular immunoreceptor circuitry of plants. In *Current opinion in plant biology* 50, pp. 121–131. DOI: 10.1016/j.pbi.2019.04.007.

Adjobo-Hermans, Merel J. W.; Goedhart, Joachim; Gadella, Theodorus W. J. (2006): Plant G protein heterotrimers require dual lipidation motifs of Galpha and Ggamma and do not dissociate upon activation. In *Journal of cell science* 119 (Pt 24), pp. 5087–5097. DOI: 10.1242/jcs.03284.

Albert, Isabell; Böhm, Hannah; Albert, Markus; Feiler, Christina E.; Imkampe, Julia; Wallmeroth, Niklas et al. (2015): An RLP23-SOBIR1-BAK1 complex mediates NLP-triggered immunity. In *Nature plants* 1, p. 15140. DOI: 10.1038/nplants.2015.140.

Alvarez, M. E. (2000): Salicylic acid in the machinery of hypersensitive cell death and disease resistance. In *Plant molecular biology* 44 (3), pp. 429–442. DOI: 10.1023/a:1026561029533.

Ambastha, Vivek; Tripathy, Baishnab C.; Tiwari, Budhi Sagar (2015): Programmed cell death in plants: A chloroplastic connection. In *Plant signaling & behavior* 10 (2), e989752. DOI: 10.4161/15592324.2014.989752.

An, Qianli; Hückelhoven, Ralph; Kogel, Karl-Heinz; van Bel, Aart J. E. (2006): Multivesicular bodies participate in a cell wall-associated defence response in barley leaves attacked by the pathogenic powdery mildew fungus. In *Cellular microbiology* 8 (6), pp. 1009–1019. DOI: 10.1111/j.1462-5822.2006.00683.x.

Antolín-Llovera, Meritxell; Petutsching, Elena Kristin; Ried, Martina Katharina; Lipka, Volker; Nürnberger, Thorsten; Robatzek, Silke; Parniske, Martin (2014): Knowing your friends and foes--plant receptor-like kinases as initiators of symbiosis or defence. In *The New phytologist* 204 (4), pp. 791–802. DOI: 10.1111/nph.13117.

Asai, Tsuneaki; Tena, Guillaume; Plotnikova, Joulia; Willmann, Matthew R.; Chiu, Wan-Ling; Gomez-Gomez, Lourdes et al. (2002): MAP kinase signalling cascade in *Arabidopsis* innate immunity. In *Nature* 415 (6875), pp. 977–983. DOI: 10.1038/415977a.

Bacete, Laura; Mélida, Hugo; Miedes, Eva; Molina, Antonio (2018): Plant cell wall-mediated immunity: cell wall changes trigger disease resistance responses. In *The Plant journal : for cell and molecular biology* 93 (4), pp. 614–636. DOI: 10.1111/tpj.13807.

Bancaud, Aurélien; Huet, Sébastien; Rabut, Gwénaël; Ellenberg, Jan (2010): Fluorescence perturbation techniques to study mobility and molecular dynamics of proteins in live cells: FRAP, photoactivation, photoconversion, and FLIP. In *Cold Spring Harbor protocols* 2010 (12), pdb.top90. DOI: 10.1101/pdb.top90.

Bednarek, Pawel; Pislewska-Bednarek, Mariola; Svatos, Ales; Schneider, Bernd; Doubsky, Jan; Mansurova, Madina et al. (2009): A glucosinolate metabolism pathway in living plant cells mediates broad-spectrum antifungal defense. In *Science (New York, N.Y.)* 323 (5910), pp. 101–106. DOI: 10.1126/science.1163732.

Berkey, Robert; Zhang, Yi; Ma, Xianfeng; King, Harlan; Zhang, Qiong; Wang, Wenming; Xiao, Shunyuan (2017): Homologues of the RPW8 Resistance Protein Are Localized to the Extrahaustorial Membrane that Is Likely Synthesized De Novo. In *Plant physiology* 173 (1), pp. 600–613. DOI: 10.1104/pp.16.01539.

Bi, Guozhi; Liebrand, Thomas W. H.; Cordewener, Jan H. G.; America, Antoine H. P.; Xu, Xiangyang; Joosten, Matthieu H. A. J. (2014): *Arabidopsis thaliana* receptor-like protein AtRLP23 associates with the receptor-like kinase AtSOBIR1. In *Plant signaling & behavior* 9 (2), e27937. DOI: 10.4161/psb.27937.

Binder, Andreas; Parniske, Martin (2018): The Nuclear Pore Complex in Symbiosis and Pathogen Defence. In Jeremy A. Roberts (Ed.): Annual Plant Reviews online. Chichester, UK: John Wiley & Sons, Ltd, pp. 229–254.

Bonardi, Vera; Tang, Saijun; Stallmann, Anna; Roberts, Melinda; Cherkis, Karen; Dangl, Jeffery L. (2011): Expanded functions for a family of plant intracellular immune receptors beyond specific recognition of pathogen effectors. In *PNAS* 108 (39), pp. 16463–16468. DOI: 10.1073/pnas.1113726108.

Bozkurt, Tolga O.; Kamoun, Sophien (2020): The plant-pathogen haustorial interface at a glance. In *Journal of cell science* 133 (5). DOI: 10.1242/jcs.237958.

Braakman, Ineke; Lamriben, Lydia; van Zadelhoff, Guus; Hebert, Daniel N. (2017): Analysis of Disulfide Bond Formation. In *Current protocols in protein science* 90, 14.1.1-14.1.21. DOI: 10.1002/cpps.43.

Brenya, Eric; Trusov, Yuri; Dietzgen, Ralf Georg; Botella, José Ramón (2016): Heterotrimeric G-proteins facilitate resistance to plant pathogenic viruses in *Arabidopsis thaliana* (L.) Heynh. In *Plant signaling & behavior* 11 (8), e1212798. DOI: 10.1080/15592324.2016.1212798.

Brotman, Yariv; Landau, Udi; Pnini, Smadar; Lisec, Jan; Balazadeh, Salma; Mueller-Roeber, Bernd et al. (2012): The LysM receptor-like kinase LysM RLK1 is required to activate defense and abiotic-stress responses induced by overexpression of fungal chitinases in *Arabidopsis* plants. In *Molecular plant* 5 (5), pp. 1113–1124. DOI: 10.1093/mp/sss021.

Bruggeman, Quentin; Raynaud, Cécile; Benhamed, Moussa; Delarue, Marianne (2015): To die or not to die? Lessons from lesion mimic mutants. In *Frontiers in plant science* 6, p. 24. DOI: 10.3389/fpls.2015.00024.

Cao, Yangrong; Liang, Yan; Tanaka, Kiwamu; Nguyen, Cuong T.; Jedrzejczak, Robert P.; Joachimiak, Andrzej; Stacey, Gary (2014): The kinase LYK5 is a major chitin receptor in *Arabidopsis* and forms a chitin-induced complex with related kinase CERK1. In *Elife* 3. DOI: 10.7554/eLife.03766.

Ceroni, Alessio; Passerini, Andrea; Vullo, Alessandro; Frasconi, Paolo (2006): DISULFIND: a disulfide bonding state and cysteine connectivity prediction server. In *Nucleic acids research* 34 (Web Server issue), W177-81. DOI: 10.1093/nar/gkl266.

Chakraborty, Navjyoti; Kanyuka, Kostya; Jaiswal, Dinesh Kumar; Kumar, Abhineet; Arora, Vivek; Malik, Aakansha et al. (2019): GCR1 and GPA1 coupling regulates nitrate, cell wall, immunity and light responses in *Arabidopsis*. In *Scientific reports* 9 (1), p. 5838. DOI: 10.1038/s41598-019-42084-2.

Chakravorty, David; Assmann, Sarah M. (2018): G protein subunit phosphorylation as a regulatory mechanism in heterotrimeric G protein signaling in mammals, yeast, and plants. In *The Biochemical journal* 475 (21), pp. 3331–3357. DOI: 10.1042/BCJ20160819.

Chakravorty, David; Gookin, Timothy E.; Milner, Matthew J.; Yu, Yunqing; Assmann, Sarah M. (2015): Extra-Large G Proteins Expand the Repertoire of Subunits in *Arabidopsis* Heterotrimeric G Protein Signaling. In *Plant physiology* 169 (1), pp. 512–529. DOI: 10.1104/pp.15.00251.

Chakravorty, David; Trusov, Yuri; Zhang, Wei; Acharya, Biswa R.; Sheahan, Michael B.; McCurdy, David W. et al. (2011): An atypical heterotrimeric G-protein γ-subunit is involved in guard cell K^+-channel regulation and morphological development in *Arabidopsis thaliana*. In *The Plant journal : for cell and molecular biology* 67 (5), pp. 840–851. DOI: 10.1111/j.1365-313X.2011.04638.x.

Chen, Dongqin; Ahsan, Nagib; Thelen, Jay J.; Stacey, Gary (2019): S -Acylation of plant immune receptors mediates immune signaling in plasma membrane nanodomains.

Chen, Jin-Gui; Gao, Yajun; Jones, Alan M. (2006): Differential roles of *Arabidopsis* heterotrimeric G-protein subunits in modulating cell division in roots. In *Plant Physiol.* 141 (3), pp. 887–897. DOI: 10.1104/pp.106.079202.

Chen, Jin-Gui; Jones, Alan M. (2004): AtRGS1 Function in *Arabidopsis thaliana*. In : Methods in Enzymology : Regulators of G-Protein Signaling, Part A, vol. 389: Academic Press, pp. 338–350. Available online at http://www.sciencedirect.com/science/article/pii/S0076687904890207.

Chen, Kegui; Du, Liqun; Chen, Zhixiang (2003): Sensitization of defense responses and activation of programmed cell death by a pathogen-induced receptor-like protein kinase in *Arabidopsis*. In *Plant molecular biology* 53 (1-2), pp. 61–74. DOI: 10.1023/B:PLAN.0000009265.72567.58.

Chen, Yani; Brandizzi, Federica (2012): AtIRE1A/AtIRE1B and AGB1 independently control two essential unfolded protein response pathways in *Arabidopsis*. In *The Plant Journal* 69 (2), pp. 266–277. DOI: 10.1111/j.1365-313X.2011.04788.x.

Chen, Zhongying; Noir, Sandra; Kwaaitaal, Mark; Hartmann, H. Andreas; Wu, Ming-Jing; Mudgil, Yashwanti et al. (2009): Two seven-transmembrane domain MILDEW RESISTANCE LOCUS O proteins cofunction in *Arabidopsis* root thigmomorphogenesis. In *Plant Cell* 21 (7), pp. 1972–1991. DOI: 10.1105/tpc.108.062653.

Cheng, Zhenyu; Li, Jian-Feng; Niu, Yajie; Zhang, Xue-Cheng; Woody, Owen Z.; Xiong, Yan et al. (2015): Pathogen-secreted proteases activate a novel plant immune pathway. In *Nature* 521 (7551), pp. 213–216. DOI: 10.1038/nature14243.

Chenon, Mélanie; Camborde, Laurent; Cheminant, Soizic; Jupin, Isabelle (2012): A viral deubiquitylating enzyme targets viral RNA-dependent RNA polymerase and affects viral infectivity. In *The EMBO journal* 31 (3), pp. 741–753. DOI: 10.1038/emboj.2011.424.

Cheval, Cécilia; Samwald, Sebastian; Johnston, Matthew G.; Keijzer, Jeroen de; Breakspear, Andrew; Liu, Xiaokun et al. (2020): Chitin perception in plasmodesmata characterizes submembrane immune-signaling specificity in plants. In *Proceedings of the National Academy of Sciences of the United States of America* 117 (17), pp. 9621–9629. DOI: 10.1073/pnas.1907799117.

Chinchilla, Delphine; Bauer, Zsuzsa; Regenass, Martin; Boller, Thomas; Felix, Georg (2006): The *Arabidopsis* receptor kinase FLS2 binds flg22 and determines the specificity of flagellin perception. In *Plant Cell* 18 (2), pp. 465–476. DOI: 10.1105/tpc.105.036574.

Choudhury, Swarup Roy; Li, Mao; Lee, Veronica; Nandety, Raja Sekhar; Mysore, Kirankumar S.; Pandey, Sona (2020): Flexible functional interactions between G-protein subunits contribute to the specificity of plant responses. In *The Plant journal : for cell and molecular biology* 102 (2), pp. 207–221. DOI: 10.1111/tpj.14714.

Choudhury, Swarup Roy; Pandey, Sona (2016): The role of PLDα1 in providing specificity to signal-response coupling by heterotrimeric G-protein components in *Arabidopsis*. In *The Plant journal : for cell and molecular biology* 86 (1), pp. 50–61. DOI: 10.1111/tpj.13151.

Collier, S. M.; Hamel, L. P.; Moffett, P. (2011): Cell death mediated by the Nterminal domains of a unique and highly conserved class of NB-LRR protein. Mol. Plant Microbe Interact (doi:10.1094/MPMI -03-11-0050), pp. 918–931.

Collins, Nicholas C.; Thordal-Christensen, Hans; Lipka, Volker; Bau, Stephan; Kombrink, Erich; Qiu, Jin-Long et al. (2003): SNARE-protein-mediated disease resistance at the plant cell wall. In *Nature* 425 (6961), pp. 973–977. DOI: 10.1038/nature02076.

Consonni, Chiara; Humphry, Matthew E.; Hartmann, H. Andreas; Livaja, Maren; Durner, Jörg; Westphal, Lore et al. (2006): Conserved requirement for a plant host cell protein in powdery mildew pathogenesis. In *Nature genetics* 38 (6), pp. 716–720. DOI: 10.1038/ng1806.

Couto, Daniel; Zipfel, Cyril (2016): Regulation of pattern recognition receptor signalling in plants. In *Nature reviews. Immunology* 16 (9), pp. 537–552. DOI: 10.1038/nri.2016.77.

Crane, Renee A.; Cardénas Valdez, Marielle; Castaneda, Nelly; Jackson, Charidan L.; Riley, Ciairra J.; Mostafa, Islam et al. (2019): Negative Regulation of Age-Related Developmental Leaf Senescence by the IAOx Pathway, PEN1, and PEN3. In *Frontiers in plant science* 10, p. 1202. DOI: 10.3389/fpls.2019.01202.

Cui, Haitao; Gobbato, Enrico; Kracher, Barbara; Qiu, Jingde; Bautor, Jaqueline; Parker, Jane E. (2017): A core function of EDS1 with PAD4 is to protect the salicylic acid defense sector in *Arabidopsis* immunity. In *The New phytologist* 213 (4), pp. 1802–1817. DOI: 10.1111/nph.14302.

D'Ambrosio, Juan Martín; Couto, Daniel; Fabro, Georgina; Scuffi, Denise; Lamattina, Lorenzo; Munnik, Teun et al. (2017): Phospholipase C2 Affects MAMP-Triggered Immunity by Modulating ROS Production. In *Plant Physiol.* 175 (2), pp. 970–981. DOI: 10.1104/pp.17.00173.

Delgado-Cerezo, Magdalena; Sánchez-Rodríguez, Clara; Escudero, Viviana; Miedes, Eva; Fernández, Paula Virginia; Jordá, Lucía et al. (2012): *Arabidopsis* heterotrimeric G-protein

regulates cell wall defense and resistance to necrotrophic fungi. In *Molecular plant* 5 (1), pp. 98–114. DOI: 10.1093/mp/ssr082.

Derkacheva, Maria; Yu, Gang; Rufian, Jose S.; Jiang, Shushu; Derbyshire, Paul; Morcillo, Rafael J. L. et al. (2020): The *Arabidopsis* E3 ubiquitin ligase PUB4 regulates BIK1 homeostasis and is targeted by a bacterial type-III effector: Cold Spring Harbor Laboratory.

Desaki, Yoshitake; Kohari, Masaki; Shibuya, Naoto; Kaku, Hanae (2019a): MAMP-triggered plant immunity mediated by the LysM-receptor kinase CERK1. In *J Gen Plant Pathol* 85 (1), pp. 1–11. DOI: 10.1007/s10327-018-0828-x.

Desaki, Yoshitake; Takahashi, Shohei; Sato, Kenta; Maeda, Kanako; Matsui, Saki; Yoshimi, Ikuya et al. (2019b): PUB4, a CERK1-Interacting Ubiquitin Ligase, Positively Regulates MAMP-Triggered Immunity in *Arabidopsis*. In *Plant & cell physiology* 60 (11), pp. 2573–2583. DOI: 10.1093/pcp/pcz151.

Ding, Lei; Pandey, Sona; Assmann, Sarah M. (2008): *Arabidopsis* extra-large G proteins (XLGs) regulate root morphogenesis. In *The Plant journal : for cell and molecular biology* 53 (2), pp. 248–263. DOI: 10.1111/j.1365-313X.2007.03335.x.

Dingwall, Colin; Laskey, Ronald A. (1991): Nuclear targeting sequences — a consensus? In *Trends in Biochemical Sciences* 16, pp. 478–481. DOI: 10.1016/0968-0004(91)90184-W.

Domínguez-Ferreras, Ana; Kiss-Papp, Marta; Jehle, Anna Kristina; Felix, Georg; Chinchilla, Delphine (2015): An Overdose of the *Arabidopsis* Coreceptor BRASSINOSTEROID INSENSITIVE1-ASSOCIATED RECEPTOR KINASE1 or Its Ectodomain Causes Autoimmunity in a SUPPRESSOR OF BIR1-1-Dependent Manner. In *Plant Physiol.* 168 (3), pp. 1106–1121. DOI: 10.1104/pp.15.00537.

Du, Junbo; Gao, Yang; Zhan, Yanyan; Zhang, Shasha; Wu, Yujun; Xiao, Yao et al. (2016): Nucleocytoplasmic trafficking is essential for BAK1- and BKK1-mediated cell-death control. In *The Plant journal : for cell and molecular biology* 85 (4), pp. 520–531. DOI: 10.1111/tpj.13125.

Eichmann, Ruth; Hückelhoven, Ralph (2008): Accommodation of powdery mildew fungi in intact plant cells. In *Journal of plant physiology* 165 (1), pp. 5–18. DOI: 10.1016/j.jplph.2007.05.004.

Erwig, Jan (2016): Analysis of the subcellular behavior of *Arabidopsis thaliana* LysM-proteins and their role in plant innate immunity.

Erwig, Jan; Ghareeb, Hassan; Kopischke, Michaela; Hacke, Ronja; Matei, Alexandra; Petutschnig, Elena; Lipka, Volker (2017): Chitin-induced and CHITIN ELICITOR RECEPTOR KINASE1 (CERK1) phosphorylation-dependent endocytosis of *Arabidopsis thaliana* LYSIN MOTIF-CONTAINING RECEPTOR-LIKE KINASE5 (LYK5). In *The New phytologist* 215 (1), pp. 382–396. DOI: 10.1111/nph.14592.

Faulkner, Christine; Petutschnig, Elena; Benitez-Alfonso, Yoselin; Beck, Martina; Robatzek, Silke; Lipka, Volker; Maule, Andrew J. (2013): LYM2-dependent chitin perception limits molecular flux via plasmodesmata. In *Proceedings of the National Academy of Sciences of the United States of America* 110 (22), pp. 9166–9170. DOI: 10.1073/pnas.1203458110.

Feys, B. J.; Moisan, L. J.; Newman, M. A.; Parker, J. E. (2001): Direct interaction between the *Arabidopsis* disease resistance signaling proteins, EDS1 and PAD4. In *The EMBO journal* 20 (19), pp. 5400–5411. DOI: 10.1093/emboj/20.19.5400.

Forrester, Michael T.; Hess, Douglas T.; Thompson, J. Will; Hultman, Rainbo; Moseley, M. Arthur; Stamler, Jonathan S.; Casey, Patrick J. (2011): Site-specific analysis of protein S-acylation by resin-assisted capture. In *Journal of lipid research* 52 (2), pp. 393–398. DOI: 10.1194/jlr.D011106.

Fuchs, Rene; Kopischke, Michaela; Klapprodt, Christine; Hause, Gerd; Meyer, Andreas J.; Schwarzländer, Markus et al. (2016): Immobilized Subpopulations of Leaf Epidermal Mitochondria Mediate PENETRATION2-Dependent Pathogen Entry Control in *Arabidopsis*. In *The Plant cell* 28 (1), pp. 130–145. DOI: 10.1105/tpc.15.00887.

Furlan, Giulia; Klinkenberg, Jörn; Trujillo, Marco (2012): Regulation of plant immune receptors by ubiquitination. In *Frontiers in plant science* 3, p. 238. DOI: 10.3389/fpls.2012.00238.

Gao, Caiji; Luo, Ming; Zhao, Qiong; Yang, Renzhi; Cui, Yong; Zeng, Yonglun et al. (2014): A unique plant ESCRT component, FREE1, regulates multivesicular body protein sorting and plant growth. In *Current biology : CB* 24 (21), pp. 2556–2563. DOI: 10.1016/j.cub.2014.09.014.

Gao, Minghui; Wang, Xia; Wang, Dongmei; Xu, Fang; Ding, Xiaojun; Zhang, Zhibin et al. (2009): Regulation of cell death and innate immunity by two receptor-like kinases in *Arabidopsis*. In *Cell host & microbe* 6 (1), pp. 34–44. DOI: 10.1016/j.chom.2009.05.019.

García, Ana V.; Blanvillain-Baufumé, Servane; Huibers, Robin P.; Wiermer, Marcel; Li, Guangyong; Gobbato, Enrico et al. (2010): Balanced nuclear and cytoplasmic activities of EDS1 are required for a complete plant innate immune response. In *PLoS pathogens*, e1000970. DOI: 10.1371/journal.ppat.1000970.

Genenncher, Bianca; Lipka, Volker; Petutschnig, Elena K.; Wiermer, Marcel (2017): Nucleoporin NUP88/MOS7 is required for manifestation of phenotypes associated with the *Arabidopsis* CHITIN ELICITOR RECEPTOR KINASE1 mutant *cerk1*-4. In *Plant signaling & behavior* 12 (5), e1313378. DOI: 10.1080/15592324.2017.1313378.

Ghusinga, Khem Raj; Jones, Roger D.; Jones, Alan M.; Elston, Timothy C. (2020): Molecular switch architecture drives response properties.

Gijzen, Mark; Nürnberger, Thorsten (2006): Nep1-like proteins from plant pathogens: recruitment and diversification of the NPP1 domain across taxa. In *Phytochemistry* 67 (16), pp. 1800–1807. DOI: 10.1016/j.phytochem.2005.12.008.

Glazebrook, Jane (2005): Contrasting mechanisms of defense against biotrophic and necrotrophic pathogens. In *Annual review of phytopathology* 43, pp. 205–227. DOI: 10.1146/annurev.phyto.43.040204.135923.

Guo, Hongqing; Yin, Yanhai (2019): Measuring Protein Half-life in *Arabidopsis thaliana*. In *BIO-PROTOCOL* 9 (15). DOI: 10.21769/BioProtoc.3318.

Haasen, D.; Köhler, C.; Neuhaus, G.; Merkle, T. (1999): Nuclear export of proteins in plants: AtXPO1 is the export receptor for leucine-rich nuclear export signals in *Arabidopsis thaliana*. In *The Plant journal : for cell and molecular biology* 20 (6), pp. 695–705. DOI: 10.1046/j.1365-313x.1999.00644.x.

Hackenberg, Dieter; McKain, Michael R.; Lee, Soon Goo; Roy Choudhury, Swarup; McCann, Tyler; Schreier, Spencer et al. (2017): Gα and regulator of G-protein signaling (RGS) protein pairs maintain functional compatibility and conserved interaction interfaces throughout

evolution despite frequent loss of RGS proteins in plants. In *The New phytologist* 216 (2), pp. 562–575. DOI: 10.1111/nph.14180.

Halter, Thierry; Imkampe, Julia; Mazzotta, Sara; Wierzba, Michael; Postel, Sandra; Bücherl, Christoph et al. (2014): The leucine-rich repeat receptor kinase BIR2 is a negative regulator of BAK1 in plant immunity. In *Current biology : CB*, pp. 134–143. DOI: 10.1016/j.cub.2013.11.047.

Hansen, Line Lykke; Nielsen, Mads Eggert (2017): Plant exosomes: using an unconventional exit to prevent pathogen entry? In *Journal of experimental botany* 69 (1), pp. 59–68. DOI: 10.1093/jxb/erx319.

Häweker, Heidrun; Rips, Stephan; Koiwa, Hisashi; Salomon, Susanne; Saijo, Yusuke; Chinchilla, Delphine et al. (2010): Pattern recognition receptors require N-glycosylation to mediate plant immunity. In *The Journal of biological chemistry* 285 (7), pp. 4629–4636. DOI: 10.1074/jbc.M109.063073.

Hayafune, Masahiro; Berisio, Rita; Marchetti, Roberta; Silipo, Alba; Kayama, Miyu; Desaki, Yoshitake et al. (2014): Chitin-induced activation of immune signaling by the rice receptor CEBiP relies on a unique sandwich-type dimerization. In *PNAS* 111 (3), E404-13. DOI: 10.1073/pnas.1312099111.

He, Kai; Gou, Xiaoping; Yuan, Tong; Lin, Honghui; Asami, Tadao; Yoshida, Shigeo et al. (2007): BAK1 and BKK1 regulate brassinosteroid-dependent growth and brassinosteroid-independent cell-death pathways. In *Current biology : CB* 17 (13), pp. 1109–1115. DOI: 10.1016/j.cub.2007.05.036.

Heidrich, Katharina; Wirthmueller, Lennart; Tasset, Céline; Pouzet, Cécile; Deslandes, Laurent; Parker, Jane E. (2011): *Arabidopsis* EDS1 connects pathogen effector recognition to cell compartment-specific immune responses. In *Science (New York, N.Y.)* 334 (6061), pp. 1401–1404. DOI: 10.1126/science.1211641.

Hellens, Roger; Mullineaux, Philip; Klee, Harry (2000): Technical Focus:A guide to *Agrobacterium* binary Ti vectors. In *Trends in plant science* 5 (10), pp. 446–451. DOI: 10.1016/S1360-1385(00)01740-4.

Hématy, Kian; Lim, Melisa; Cherk, Candice; Piślewska-Bednarek, Mariola; Sanchez-Rodriguez, Clara; Stein, Monica et al. (2020): Moonlighting Function of Phytochelatin Synthase1 in Extracellular Defense against Fungal Pathogens. In *Plant physiology* 182 (4), pp. 1920–1932. DOI: 10.1104/pp.19.01393.

Hemsley, Piers A. (2009): Protein S-acylation in plants (Review). In *Molecular membrane biology* 26 (1), pp. 114–125. DOI: 10.1080/09687680802680090.

Hemsley, Piers A.; Taylor, Laura; Grierson, Claire S. (2008): Assaying protein palmitoylation in plants. In *Plant methods* 4, p. 2. DOI: 10.1186/1746-4811-4-2.

Hemsley, Piers A.; Weimar, Thilo; Lilley, Kathryn S.; Dupree, Paul; Grierson, Claire S. (2013): A proteomic approach identifies many novel palmitoylated proteins in *Arabidopsis*. In *The New phytologist* 197 (3), pp. 805–814. DOI: 10.1111/nph.12077.

Heo, Jae Bok; Sung, Sibum; Assmann, Sarah M. (2012): Ca2+-dependent GTPase, extra-large G protein 2 (XLG2), promotes activation of DNA-binding protein related to vernalization 1 (RTV1), leading to activation of floral integrator genes and early flowering in *Arabidopsis*. In *The Journal of biological chemistry* 287 (11), pp. 8242–8253. DOI: 10.1074/jbc.M111.317412.

Hershko, A.; Ciechanover, A. (1998): The ubiquitin system. In *Annual review of biochemistry* 67, pp. 425–479. DOI: 10.1146/annurev.biochem.67.1.425.

Hofius, D.; Munch, D.; Bressendorff, S.; Mundy, J.; Petersen, M. (2011): Role of autophagy in disease resistance and hypersensitive response-associated cell death. In *Cell death and differentiation* 18 (8), pp. 1257–1262. DOI: 10.1038/cdd.2011.43.

Hou, Shuguo; Jamieson, Pierce; He, Ping (2018): The cloak, dagger, and shield: proteases in plant-pathogen interactions. In *The Biochemical journal* 475 (15), pp. 2491–2509. DOI: 10.1042/BCJ20170781.

Huang, Yan-Yan; Zhang, Ling-Li; Ma, Xian-Feng; Zhao, Zhi-Xue; Zhao, Jing-Hao; Zhao, Ji-Qun et al. (2019): Multiple intramolecular trafficking signals in RESISTANCE TO POWDERY MILDEW 8.2 are engaged in activation of cell death and defense. In *The Plant journal : for cell and molecular biology* 98 (1), pp. 55–70. DOI: 10.1111/tpj.14199.

Hückelhoven, Ralph (2005): Powdery mildew susceptibility and biotrophic infection strategies. In *FEMS microbiology letters* 245 (1), pp. 9–17. DOI: 10.1016/j.femsle.2005.03.001.

Huisman, Rik; Ovchinnikova, Evgenia; Bisseling, Ton; Limpens, Erik (2012): Endocytic Accommodation of Microbes in Plants. In Jozef Šamaj (Ed.): Endocytosis in Plants. Berlin, Heidelberg: Springer Berlin Heidelberg, pp. 271–295.

Humphry, Matt; Bednarek, Pawel; Kemmerling, Birgit; Koh, Serry; Stein, Mónica; Göbel, Ulrike et al. (2010): A regulon conserved in monocot and dicot plants defines a functional module in antifungal plant immunity. In *Proceedings of the National Academy of Sciences of the United States of America* 107 (50), pp. 21896–21901. DOI: 10.1073/pnas.1003619107.

Hunziker, Pascal; Ghareeb, Hassan; Wagenknecht, Lena; Crocoll, Christoph; Halkier, Barbara Ann; Lipka, Volker; Schulz, Alexander (2019): De novo indol-3-ylmethyl glucosinolate biosynthesis, and not long-distance transport, contributes to defence of *Arabidopsis* against powdery mildew.

Hurst, Charlotte H.; Wright, Kathryn M.; Turnbull, Dionne; Leslie, Kerry; Jones, Susan; Hemsley, Piers A. (2019): Juxta-membrane S-acylation of plant receptor-like kinases is likely fortuitous and does not necessarily impact upon function. In *Scientific reports* 9 (1), p. 12818. DOI: 10.1038/s41598-019-49302-x.

Huysmans, Marlies; Lema A, Saul; Coll, Nuria S.; Nowack, Moritz K. (2017): Dying two deaths - programmed cell death regulation in development and disease. In *Current opinion in plant biology* 35, pp. 37–44. DOI: 10.1016/j.pbi.2016.11.005.

Isono, Erika; Katsiarimpa, Anthi; Müller, Isabel Karin; Anzenberger, Franziska; Stierhof, York-Dieter; Geldner, Niko et al. (2010): The deubiquitinating enzyme AMSH3 is required for intracellular trafficking and vacuole biogenesis in *Arabidopsis thaliana*. In *Plant Cell* 22 (6), pp. 1826–1837. DOI: 10.1105/tpc.110.075952.

Jensen, R. B.; La Cour, T.; Albrethsen, J.; Nielsen, M.; Skriver, K. (2001): FYVE zinc-finger proteins in the plant model *Arabidopsis thaliana*: identification of PtdIns3P-binding residues by comparison of classic and variant FYVE domains. In *The Biochemical journal* 359 (Pt 1), pp. 165–173. DOI: 10.1042/0264-6021:3590165.

Jeon, Byeong Wook; Acharya, Biswa R.; Assmann, Sarah M. (2019): The *Arabidopsis* heterotrimeric G-protein β subunit, AGB1, is required for guard cell calcium sensing and

calcium-induced calcium release. In *The Plant journal : for cell and molecular biology* 99 (2), pp. 231–244. DOI: 10.1111/tpj.14318.

Jeong, Yu Jeong; Shang, Yun; Kim, Beg Hab; Kim, Sun Young; Song, Jae Hyo; Lee, June Seung et al. (2010): BAK7 displays unequal genetic redundancy with BAK1 in brassinosteroid signaling and early senescence in *Arabidopsis*. In *Molecules and cells*, pp. 259–266. DOI: 10.1007/s10059-010-0024-0.

Jiménez-López, Domingo; Muñóz-Belman, Francisco; González-Prieto, Juan Manuel; Aguilar-Hernández, Victor; Guzmán, Plinio (2018): Repertoire of plant RING E3 ubiquitin ligases revisited: New groups counting gene families and single genes. In *PloS one* 13 (8), e0203442. DOI: 10.1371/journal.pone.0203442.

Johansson, Oskar N.; Fantozzi, Elena; Fahlberg, Per; Nilsson, Anders K.; Buhot, Nathalie; Tör, Mahmut; Andersson, Mats X. (2014): Role of the penetration-resistance genes PEN1, PEN2 and PEN3 in the hypersensitive response and race-specific resistance in *Arabidopsis thaliana*. In *The Plant Journal*, pp. 466–476. DOI: 10.1111/tpj.12571.

Johnston, Christopher A.; Taylor, J. Philip; Gao, Yajun; Kimple, Adam J.; Grigston, Jeffrey C.; Chen, Jin-Gui et al. (2007): GTPase acceleration as the rate-limiting step in *Arabidopsis* G protein-coupled sugar signaling. In *Proceedings of the National Academy of Sciences of the United States of America* 104 (44), pp. 17317–17322. DOI: 10.1073/pnas.0704751104.

Jones, Alan M.; Assmann, Sarah M. (2004): Plants: the latest model system for G-protein research. In *EMBO reports* 5 (6), pp. 572–578. DOI: 10.1038/sj.embor.7400174.

Jones, Alan M.; Ecker, Joseph R.; Chen, Jin-Gui (2003): A reevaluation of the role of the heterotrimeric G protein in coupling light responses in *Arabidopsis*. In *Plant Physiol.* 131 (4), pp. 1623–1627. DOI: 10.1104/pp.102.017624.

Jones, J. C.; Duffy, J. W.; Machius, M.; Temple, B.R.S.; Dohlman, H. G.; Jones, A. M. (2011): Crystal structure of the G alpha protein AtGPA1 from *Arabidopsis thaliana*.

Jones, Jonathan D. G.; Dangl, Jeffery L. (2006): The plant immune system. In *Nature* 444 (7117), pp. 323–329. DOI: 10.1038/nature05286.

Jones, Jonathan D. G.; Vance, Russell E.; Dangl, Jeffery L. (2016): Intracellular innate immune surveillance devices in plants and animals. In *Science (New York, N.Y.)* 354 (6316). DOI: 10.1126/science.aaf6395.

Jubic, Lance M.; Saile, Svenja; Furzer, Oliver J.; El Kasmi, Farid; Dangl, Jeffery L. (2019): Help wanted: helper NLRs and plant immune responses. In *Current opinion in plant biology* 50, pp. 82–94. DOI: 10.1016/j.pbi.2019.03.013.

Kabelitz, Tina; Brzezinka, Krzysztof; Friedrich, Thomas; Górka, Michał; Graf, Alexander; Kappel, Christian; Bäurle, Isabel (2016): A JUMONJI Protein with E3 Ligase and Histone H3 Binding Activities Affects Transposon Silencing in *Arabidopsis*. In *Plant Physiol.* 171 (1), pp. 344–358. DOI: 10.1104/pp.15.01688.

Kadota, Yasuhiro; Liebrand, Thomas W. H.; Goto, Yukihisa; Sklenar, Jan; Derbyshire, Paul; Menke, Frank L. H. et al. (2019): Quantitative phosphoproteomic analysis reveals common regulatory mechanisms between effector- and PAMP-triggered immunity in plants. In *The New phytologist* 221 (4), pp. 2160–2175. DOI: 10.1111/nph.15523.

Kadota, Yasuhiro; Sklenar, Jan; Derbyshire, Paul; Stransfeld, Lena; Asai, Shuta; Ntoukakis, Vardis et al. (2014): Direct regulation of the NADPH oxidase RBOHD by the PRR-associated kinase BIK1 during plant immunity. In *Molecular cell* 54 (1), pp. 43–55. DOI: 10.1016/j.molcel.2014.02.021.

Kelley, Lawrence A.; Mezulis, Stefans; Yates, Christopher M.; Wass, Mark N.; Sternberg, Michael J. E. (2015): The Phyre2 web portal for protein modeling, prediction and analysis. In *Nature protocols* 10 (6), pp. 845–858. DOI: 10.1038/nprot.2015.053.

Kemmerling, Birgit; Schwedt, Anne; Rodriguez, Patricia; Mazzotta, Sara; Frank, Markus; Qamar, Synan Abu et al. (2007): The BRI1-associated kinase 1, BAK1, has a brassinolide-independent role in plant cell-death control. In *Current biology : CB* 17 (13), pp. 1116–1122. DOI: 10.1016/j.cub.2007.05.046.

Kim, Han-Suk; Desveaux, Darrell; Singer, Alex U.; Patel, Priyesh; Sondek, John; Dangl, Jeffery L. (2005): The Pseudomonas syringae effector AvrRpt2 cleaves its C-terminally acylated target, RIN4, from *Arabidopsis* membranes to block RPM1 activation. In *Proceedings of the National Academy of Sciences of the United States of America* 102 (18), pp. 6496–6501. DOI: 10.1073/pnas.0500792102.

Kim, Hyeran; O'Connell, Richard; Maekawa-Yoshikawa, Makoto; Uemura, Tomohiro; Neumann, Ulla; Schulze-Lefert, Paul (2014): The powdery mildew resistance protein RPW8.2 is carried on VAMP721/722 vesicles to the extrahaustorial membrane of haustorial complexes. In *The Plant Journal*, pp. 835–847. DOI: 10.1111/tpj.12591.

Kim, Sun Young; Shang, Yun; Joo, Se-Hwan; Kim, Seong-Ki; Nam, Kyoung Hee (2017): Overexpression of BAK1 causes salicylic acid accumulation and deregulation of cell death control genes. In *Biochemical and biophysical research communications*, pp. 781–786. DOI: 10.1016/j.bbrc.2017.01.166.

Knepper, Caleb; Savory, Elizabeth A.; Day, Brad (2011): *Arabidopsis* NDR1 is an integrin-like protein with a role in fluid loss and plasma membrane-cell wall adhesion. In *Plant Physiol.* 156 (1), pp. 286–300. DOI: 10.1104/pp.110.169656.

Koncz, Csaba; Schell, Jeff (1986): The promoter of TL-DNA gene 5 controls the tissue-specific expression of chimaeric genes carried by a novel type of *Agrobacterium* binary vector. In *Molec Gen Genet* 204 (3), pp. 383–396. DOI: 10.1007/BF00331014.

Kosugi, Shunichi; Hasebe, Masako; Tomita, Masaru; Yanagawa, Hiroshi (2009): Systematic identification of cell cycle-dependent yeast nucleocytoplasmic shuttling proteins by prediction of composite motifs. In *Proceedings of the National Academy of Sciences of the United States of America* 106 (25), pp. 10171–10176. DOI: 10.1073/pnas.0900604106.

Kuhn, Hannah; Kwaaitaal, Mark; Kusch, Stefan; Acevedo-Garcia, Johanna; Wu, Hongpo; Panstruga, Ralph (2016): Biotrophy at Its Best: Novel Findings and Unsolved Mysteries of the *Arabidopsis*-Powdery Mildew Pathosystem. In *The Arabidopsis book* 14, e0184. DOI: 10.1199/tab.0184.

Kuhn, Hannah; Lorek, Justine; Kwaaitaal, Mark; Consonni, Chiara; Becker, Katia; Micali, Cristina et al. (2017): Key Components of Different Plant Defense Pathways Are Dispensable for Powdery Mildew Resistance of the *Arabidopsis mlo2 mlo6 mlo12* Triple Mutant. In *Frontiers in plant science* 8, p. 1006. DOI: 10.3389/fpls.2017.01006.

Kühnlenz, Tanja; Westphal, Lore; Schmidt, Holger; Scheel, Dierk; Clemens, Stephan (2015): Expression of *Caenorhabditis elegans* PCS in the AtPCS1-deficient *Arabidopsis thaliana cad1*-3 mutant separates the metal tolerance and non-host resistance functions of phytochelatin synthases. In *Plant, cell & environment* 38 (11), pp. 2239–2247. DOI: 10.1111/pce.12534.

Kumar, Manoj; Carr, Paul; Turner, Simon (2020): An atlas of *Arabidopsis* protein S-Acylation reveals its widespread role in plant cell organisation of and function.

Kwon, Chian; Neu, Christina; Pajonk, Simone; Yun, Hye Sup; Lipka, Ulrike; Humphry, Matt et al. (2008): Co-option of a default secretory pathway for plant immune responses. In *Nature* 451 (7180), pp. 835–840. DOI: 10.1038/nature06545.

Lapin, Dmitry; Kovacova, Viera; Sun, Xinhua; Dongus, Joram A.; Bhandari, Deepak; Born, Patrick von et al. (2019): A Coevolved EDS1-SAG101-NRG1 Module Mediates Cell Death Signaling by TIR-Domain Immune Receptors. In *The Plant cell* 31 (10), pp. 2430–2455. DOI: 10.1105/tpc.19.00118.

Leary, Alexandre Y.; Sanguankiattichai, Nattapong; Duggan, Cian; Tumtas, Yasin; Pandey, Pooja; Segretin, Maria E. et al. (2018): Modulation of plant autophagy during pathogen attack. In *Journal of experimental botany* 69 (6), pp. 1325–1333. DOI: 10.1093/jxb/erx425.

Lee, Jae-Hoon; Terzaghi, William; Gusmaroli, Giuliana; Charron, Jean-Benoit F.; Yoon, Hye-Jin; Chen, Haodong et al. (2008): Characterization of *Arabidopsis* and rice DWD proteins and their roles as substrate receptors for CUL4-RING E3 ubiquitin ligases. In *Plant Cell* 20 (1), pp. 152–167. DOI: 10.1105/tpc.107.055418.

Lee, Seonghee; Rojas, Clemencia M.; Ishiga, Yasuhiro; Pandey, Sona; Mysore, Kirankumar S. (2013): *Arabidopsis* heterotrimeric G-proteins play a critical role in host and nonhost resistance against *Pseudomonas syringae* pathogens. In *PloS one* 8 (12), e82445. DOI: 10.1371/journal.pone.0082445.

Lee, Y. R.; Assmann, S. M. (1999): *Arabidopsis thaliana* 'extra-large GTP-binding protein' (AtXLG1): a new class of G-protein. In *Plant Mol Biol* 40 (1), pp. 55–64. DOI: 10.1023/A:1026483823176.

Lei, Jiaxin; A Finlayson, Scott; Salzman, Ron A.; Shan, Libo; Zhu-Salzman, Keyan (2014): BOTRYTIS-INDUCED KINASE1 Modulates *Arabidopsis* Resistance to Green Peach Aphids via PHYTOALEXIN DEFICIENT4. In *Plant Physiol.*, pp. 1657–1670. DOI: 10.1104/pp.114.242206.

Levine, Alex (2002): Regulation of stress responses by intracellular vesicle trafficking? In *Plant Physiology and Biochemistry* 40 (6-8), pp. 531–535. DOI: 10.1016/S0981-9428(02)01398-0.

Lewandowska, Dominika; Have, Sara ten; Hodge, Kelly; Tillemans, Vinciane; Lamond, Angus I.; Brown, John W. S. (2013): Plant SILAC: stable-isotope labelling with amino acids of *Arabidopsis* seedlings for quantitative proteomics. In *PloS one* 8 (8), e72207. DOI: 10.1371/journal.pone.0072207.

Li, Bo; Tunc-Ozdemir, Meral; Urano, Daisuke; Jia, Haiyan; Werth, Emily G.; Mowrey, David D. et al. (2018): Tyrosine phosphorylation switching of a G protein. In *The Journal of biological chemistry* 293 (13), pp. 4752–4766. DOI: 10.1074/jbc.RA117.000163.

Li, Lei; Habring, Anette; Wang, Kai; Weigel, Detlef (2020): Atypical Resistance Protein RPW8/HR Triggers Oligomerization of the NLR Immune Receptor RPP7 and Autoimmunity. In *Cell host & microbe* 27 (3), 405-417.e6. DOI: 10.1016/j.chom.2020.01.012.

Li, Yaxiao; Qi, Baoxiu (2017): Progress toward Understanding Protein S-acylation: Prospective in Plants. In *Frontiers in plant science* 8, p. 346. DOI: 10.3389/fpls.2017.00346.

Liang, Xiangxiu; Ding, Pingtao; Lian, Kehui; Jinlong Wang, Miaomiao Ma, Lin Li, Lei Li, Meng Li, Xiaojuan Zhang, She Chen, Yuelin Zhang, Jian-Min Zhou (2016): *Arabidopsis* heterotrimeric G proteins regulate immunity by directly coupling to the FLS2 receptor. In *Elife*. DOI: 10.7554/eLife.13568.001.

Liang, Xiangxiu; Ma, Miaomiao; Zhou, Zhaoyang; Wang, Jinlong; Yang, Xinru; Rao, Shaofei et al. (2018): Ligand-triggered de-repression of *Arabidopsis* heterotrimeric G proteins coupled to immune receptor kinases. In *Cell research* 28 (5), pp. 529–543. DOI: 10.1038/s41422-018-0027-5.

Liang, Xiangxiu; Zhou, Jian-Min (2018): Receptor-Like Cytoplasmic Kinases: Central Players in Plant Receptor Kinase–Mediated Signaling. In *Annu. Rev. Plant Biol.* 69 (1), pp. 267–299. DOI: 10.1146/annurev-arplant-042817-040540.

Liang, Ying; Gao, Yajun; Jones, Alan M. (2017): Extra Large G-Protein Interactome Reveals Multiple Stress Response Function and Partner-Dependent XLG Subcellular Localization. In *Frontiers in plant science* 8, p. 1015. DOI: 10.3389/fpls.2017.01015.

Lichtenthaler, Stefan F.; Lemberg, Marius K.; Fluhrer, Regina (2018): Proteolytic ectodomain shedding of membrane proteins in mammals-hardware, concepts, and recent developments. In *The EMBO journal* 37 (15). DOI: 10.15252/embj.201899456.

Liebrand, Thomas W. H.; van den Berg, Grardy C. M.; Zhang, Zhao; Smit, Patrick; Cordewener, Jan H. G.; America, Antoine H. P. et al. (2013): Receptor-like kinase SOBIR1/EVR interacts with receptor-like proteins in plant immunity against fungal infection. In *PNAS* 110 (24), pp. 10010–10015. DOI: 10.1073/pnas.1220015110.

Liebrand, Thomas W. H.; van den Burg, Harrold A.; Joosten, Matthieu H. A. J. (2014): Two for all: receptor-associated kinases SOBIR1 and BAK1. In *Trends in plant science* 19 (2), pp. 123–132. DOI: 10.1016/j.tplants.2013.10.003.

Lin, Wenwei; Li, Bo; Lu, Dongping; Chen, Sixue; Zhu, Ning; He, Ping; Shan, Libo (2014): Tyrosine phosphorylation of protein kinase complex BAK1/BIK1 mediates *Arabidopsis* innate immunity. In *PNAS* 111 (9), pp. 3632–3637. DOI: 10.1073/pnas.1318817111.

Lipka, Ulrike; Fuchs, Rene; Kuhns, Christine; Petutschnig, Elena; Lipka, Volker (2010): Live and let die - *Arabidopsis* nonhost resistance to powdery mildews. In *European journal of cell biology* 89 (2-3), pp. 194–199. DOI: 10.1016/j.ejcb.2009.11.011.

Lipka, Ulrike; Fuchs, Rene; Lipka, Volker (2008): *Arabidopsis* non-host resistance to powdery mildews. In *Current opinion in plant biology* 11 (4), pp. 404–411. DOI: 10.1016/j.pbi.2008.04.004.

Lipka, Volker; Dittgen, Jan; Bednarek, Pawel; Bhat, Riyaz; Wiermer, Marcel; Stein, Monica et al. (2005): Pre- and postinvasion defenses both contribute to nonhost resistance in *Arabidopsis*. In *Science (New York, N.Y.)* 310 (5751), pp. 1180–1183. DOI: 10.1126/science.1119409.

Liu, Jinman; Ding, Pingtao; Sun, Tongjun; Nitta, Yukino; Dong, Oliver; Huang, Xingchuan et al. (2013): Heterotrimeric G proteins serve as a converging point in plant defense signaling activated by multiple receptor-like kinases. In *Plant physiology* 161 (4), pp. 2146–2158. DOI: 10.1104/pp.112.212431.

Liu, Jun; Chen, Sufen; Chen, Lijuan; Zhou, Qi; Wang, Menglong; Feng, Dongru et al. (2017): BIK1 cooperates with BAK1 to regulate constitutive immunity and cell death in *Arabidopsis*. In *Journal of integrative plant biology* 59 (4), pp. 234–239. DOI: 10.1111/jipb.12529.

Liu, Tingting; Liu, Zixu; Song, Chuanjun; Hu, Yunfei; Han, Zhifu; She, Ji et al. (2012): Chitin-induced dimerization activates a plant immune receptor. In *Science (New York, N.Y.)* 336 (6085), pp. 1160–1164. DOI: 10.1126/science.1218867.

Liu, Yanan; Huang, Xingchuan; Li, Meng; He, Ping; Zhang, Yuelin (2016): Loss-of-function of *Arabidopsis* receptor-like kinase BIR1 activates cell death and defense responses mediated by BAK1 and SOBIR1. In *The New phytologist*, pp. 637–645. DOI: 10.1111/nph.14072.

Liu, Yule; Schiff, Michael; Czymmek, Kirk; Tallóczy, Zsolt; Levine, Beth; Dinesh-Kumar, S. P. (2005): Autophagy regulates programmed cell death during the plant innate immune response. In *Cell* 121 (4), pp. 567–577. DOI: 10.1016/j.cell.2005.03.007.

Lorek, Justine; Griebel, Thomas; Jones, Alan M.; Kuhn, Hannah; Panstruga, Ralph (2013): The role of *Arabidopsis* heterotrimeric G-protein subunits in MLO2 function and MAMP-triggered immunity. In *Molecular plant-microbe interactions : MPMI* 26 (9), pp. 991–1003. DOI: 10.1094/MPMI-03-13-0077-R.

Lou, Fei; Abramyan, Tigran M.; Jia, Haiyan; Tropsha, Alexander; Jones, Alan M. (2019): An atypical heterotrimeric Gα protein has substantially reduced nucleotide binding but retains nucleotide-independent interactions with its cognate RGS protein and Gβγ dimer. In *Journal of biomolecular structure & dynamics*, pp. 1–15. DOI: 10.1080/07391102.2019.1704879.

Lüdke, Daniel; Roth, Charlotte; Kamrad, Sieglinde A.; Messerschmidt, Jana; Hartken, Denise; Appel, Jonas et al. (2020): Functional requirement of the *Arabidopsis* importin-α nuclear transport receptor family in autoimmunity mediated by the NLR protein SNC1.

Ma, Cuiyan; Liu, Yanan; Bai, Bing; Han, Zhifu; Tang, Jiao; Zhang, Heqiao et al. (2017): Structural basis for BIR1-mediated negative regulation of plant immunity. In *Cell research* 27 (12), pp. 1521–1524. DOI: 10.1038/cr.2017.123.

Ma, Jiong; Goryaynov, Alexander; Sarma, Ashapurna; Yang, Weidong (2012): Self-regulated viscous channel in the nuclear pore complex. In *PNAS*, pp. 7326–7331. DOI: 10.1073/pnas.1201724109.

Ma, Lay-Sun; Wang, Lei; Trippel, Christine; Mendoza-Mendoza, Artemio; Ullmann, Steffen; Moretti, Marino et al. (2018): The Ustilago maydis repetitive effector Rsp3 blocks the antifungal activity of mannose-binding maize proteins. In *Nature communications* 9 (1), p. 1711. DOI: 10.1038/s41467-018-04149-0.

Madeira, Fábio; Park, Young mi; Lee, Joon; Buso, Nicola; Gur, Tamer; Madhusoodanan, Nandana et al. (2019): The EMBL-EBI search and sequence analysis tools APIs in 2019. In *Nucleic acids research* 47 (W1), W636-W641. DOI: 10.1093/nar/gkz268.

Maruta, Natsumi; Trusov, Yuri; Brenya, Eric; Parekh, Urvi; Botella, José Ramón (2015): Membrane-localized extra-large G proteins and Gbg of the heterotrimeric G proteins form functional complexes engaged in plant immunity in *Arabidopsis*. In *Plant physiology* 167 (3), pp. 1004–1016. DOI: 10.1104/pp.114.255703.

Maruta, Natsumi; Trusov, Yuri; Chakravorty, David; Urano, Daisuke; Assmann, Sarah M.; Botella, Jose R. (2019): Nucleotide exchange-dependent and nucleotide exchange-

independent functions of plant heterotrimeric GTP-binding proteins. In *Science signaling* 12 (606). DOI: 10.1126/scisignal.aav9526.

Mason, M. G.; Botella, J. R. (2000): Completing the heterotrimer: isolation and characterization of an *Arabidopsis thaliana* G protein gamma-subunit cDNA. In *Proceedings of the National Academy of Sciences of the United States of America* 97 (26), pp. 14784–14788. DOI: 10.1073/pnas.97.26.14784.

Mélida, Hugo; Sopeña-Torres, Sara; Bacete, Laura; Garrido-Arandia, María; Jordá, Lucía; López, Gemma et al. (2018): Non-branched β-1,3-glucan oligosaccharides trigger immune responses in *Arabidopsis*. In *The Plant journal : for cell and molecular biology* 93 (1), pp. 34–49. DOI: 10.1111/tpj.13755.

Meng, Xiangzong; Shan, Libo; He, Ping (2015): Stack Heterotrimeric G Proteins and MAPK Cascades on a RACK. In *Molecular plant* 8 (12), pp. 1691–1693. DOI: 10.1016/j.molp.2015.11.005.

Meusel, Chrisopher (2016): Analysis of CERK1 ectodomain shedding and the role of XLG2 in cerk1-4 cell death execution. Doctoral thesis.

Meyer, Dorit; Pajonk, Simone; Micali, Cristina; O'Connell, Richard; Schulze-Lefert, Paul (2009): Extracellular transport and integration of plant secretory proteins into pathogen-induced cell wall compartments. In *The Plant journal : for cell and molecular biology* 57 (6), pp. 986–999. DOI: 10.1111/j.1365-313X.2008.03743.x.

Micali, Cristina; Göllner, Katharina; Humphry, Matt; Consonni, Chiara; Panstruga, Ralph (2008): The Powdery Mildew Disease of *Arabidopsis*: A Paradigm for the Interaction between Plants and Biotrophic Fungi. In *The Arabidopsis book* 6, e0115. DOI: 10.1199/tab.0115.

Micali, Cristina O.; Neumann, Ulla; Grunewald, Dorit; Panstruga, Ralph; O'Connell, Richard (2011): Biogenesis of a specialized plant-fungal interface during host cell internalization of Golovinomyces orontii haustoria. In *Cellular microbiology* 13 (2), pp. 210–226. DOI: 10.1111/j.1462-5822.2010.01530.x.

Miller, Jimi C.; Barco, Brenden; Clay, Nicole K. (2019): Discovery of novel Defense Regulated WD40-repeat proteins DRW1/2 and their roles in plant immunity.

Miller, Jimi C.; Chezem, William R.; Clay, Nicole K. (2015): Ternary WD40 Repeat-Containing Protein Complexes: Evolution, Composition and Roles in Plant Immunity. In *Frontiers in plant science* 6, p. 1108. DOI: 10.3389/fpls.2015.01108.

Minina, Elena A.; Bozhkov, Peter V.; Hofius, Daniel (2014): Autophagy as initiator or executioner of cell death. In *Trends in plant science* 19 (11), pp. 692–697. DOI: 10.1016/j.tplants.2014.07.007.

Miura, Asuka; Nakamura, Miyuki; Inagaki, Soichi; Kobayashi, Akie; Saze, Hidetoshi; Kakutani, Tetsuji (2009): An *Arabi*dopsis jmjC domain protein protects transcribed genes from DNA methylation at CHG sites. In *The EMBO journal* 28 (8), pp. 1078–1086. DOI: 10.1038/emboj.2009.59.

Miyakawa, Takuya; Hatano, Ken-ichi; Miyauchi, Yumiko; Suwa, You-ichi; Sawano, Yoriko; Tanokura, Masaru (2014): A secreted protein with plant-specific cysteine-rich motif functions as a mannose-binding lectin that exhibits antifungal activity. In *Plant Physiol.* 166 (2), pp. 766–778. DOI: 10.1104/pp.114.242636.

Monaghan, Jacqueline; Germain, Hugo; Weihmann, Tabea; Li, Xin (2010): Dissecting plant defence signal transduction: modifiers of *snc1* in *Arabidopsis*†. In *Canadian Journal of Plant Pathology* 32 (1), pp. 35–42. DOI: 10.1080/07060661003621001.

Monaghan, Jacqueline; Zipfel, Cyril (2012): Plant pattern recognition receptor complexes at the plasma membrane. In *Current opinion in plant biology* 15 (4), pp. 349–357. DOI: 10.1016/j.pbi.2012.05.006.

Mou, Zhonglin; Fan, Weihua; Dong, Xinnian (2003): Inducers of Plant Systemic Acquired Resistance Regulate NPR1 Function through Redox Changes. In *Cell* 113 (7), pp. 935–944. DOI: 10.1016/S0092-8674(03)00429-X.

Nawrath, C.; Métraux, J. P. (1999): Salicylic acid induction-deficient mutants of *Arabidopsis* express PR-2 and PR-5 and accumulate high levels of camalexin after pathogen inoculation. In *Plant Cell* 11 (8), pp. 1393–1404. DOI: 10.1105/tpc.11.8.1393.

New, D. C.; Wong, J. T. (1998): The evidence for G-protein-coupled receptors and heterotrimeric G proteins in protozoa and ancestral metazoa. In *Biological signals and receptors* 7 (2), pp. 98–108. DOI: 10.1159/000014535.

Ngou, Bruno Pok Man; Ahn, Hee-Kyung; Ding, Pingtao; Jones, Jonathan D. G. (2020): Mutual Potentiation of Plant Immunity by Cell-surface and Intracellular Receptors.

Nürnberger, Thorsten; Brunner, Frédéric; Kemmerling, Birgit; Piater, Lizelle (2004): Innate immunity in plants and animals: striking similarities and obvious differences. In *Immunological reviews* 198, pp. 249–266. DOI: 10.1111/j.0105-2896.2004.0119.x.

Olejnik, Kamil; Bucholc, Maria; Anielska-Mazur, Anna; Lipko, Agata; Kujawa, Martyna; Modzelan, Marta et al. (2011): *Arabidopsis thaliana* Nudix hydrolase AtNUDT7 forms complexes with the regulatory RACK1A protein and Ggamma subunits of the signal transducing heterotrimeric G protein. In *Acta biochimica Polonica* 58 (4), pp. 609–616.

Oliveira, Marcos V. V. de; Xu, Guangyuan; Li, Bo; Souza Vespoli, Luciano de; Meng, Xiangzong; Chen, Xin et al. (2016): Specific control of *Arabidopsis* BAK1/SERK4-regulated cell death by protein glycosylation. In *Nature plants*, p. 15218. DOI: 10.1038/nplants.2015.218.

Pajonk, Simone (2007): SNARE-mediated plant immune responses at the cell periphery. Inaugural-Dissertation.

Palma, Kristoffer; Wiermer, Marcel; Li, Xin (2018): Marshalling the Troops: Intracellular Dynamics in Plant Pathogen Defense. In Jeremy A. Roberts (Ed.): Annual Plant Reviews online. Chichester, UK: John Wiley & Sons, Ltd, pp. 177–219.

Pandey, Sona (2020): Plant receptor-like kinase signaling through heterotrimeric G-proteins. In *Journal of experimental botany* 71 (5), pp. 1742–1751. DOI: 10.1093/jxb/eraa016.

Pandey, Sona; Assmann, Sarah M. (2004): The *Arabidopsis* putative G protein-coupled receptor GCR1 interacts with the G protein alpha subunit GPA1 and regulates abscisic acid signaling. In *Plant Cell* 16 (6), pp. 1616–1632. DOI: 10.1105/tpc.020321.

Panstruga, Ralph; Moscou, Matthew James (2020): What is the molecular basis of nonhost resistance? In *Molecular plant-microbe interactions : MPMI*. DOI: 10.1094/MPMI-06-20-0161-CR.

Petutschnig, Elena K.; Jones, Alexandra M. E.; Serazetdinova, Liliya; Lipka, Ulrike; Lipka, Volker (2010): The lysin motif receptor-like kinase (LysM-RLK) CERK1 is a major chitin-binding

protein in *Arabidopsis thaliana* and subject to chitin-induced phosphorylation. In *The Journal of biological chemistry* 285 (37), pp. 28902–28911. DOI: 10.1074/jbc.M110.116657.

Petutschnig, Elena K.; Stolze, Marnie; Lipka, Ulrike; Kopischke, Michaela; Horlacher, Juliane; Valerius, Oliver et al. (2014): A novel *Arabidopsis* CHITIN ELICITOR RECEPTOR KINASE 1 (CERK1) mutant with enhanced pathogen-induced cell death and altered receptor processing. In *The New phytologist* 204 (4), pp. 955–967. DOI: 10.1111/nph.12920.

Pinosa, Francesco; Buhot, Nathalie; Kwaaitaal, Mark; Fahlberg, Per; Thordal-Christensen, Hans; Ellerström, Mats; Andersson, Mats X. (2013): *Arabidopsis* phospholipase dδ is involved in basal defense and nonhost resistance to powdery mildew fungi. In *Plant Physiol.* 163 (2), pp. 896–906. DOI: 10.1104/pp.113.223503.

Planchais, Séverine; Camborde, Laurent; Jupin, Isabelle (2016): Protocols for Studying Protein Stability in an *Arabidopsis* Protoplast Transient Expression System. In *Methods in molecular biology (Clifton, N.J.)* 1450, pp. 175–194. DOI: 10.1007/978-1-4939-3759-2_14.

Postle, Kathleen (2007): TonB System, In Vivo Assays and Characterization. In Melvin I. Simon, Brian R. Crane, Alexandrine Crane (Eds.): Two-component signaling systems, vol. 422. Amsterdam: Academic Press (Methods in Enzymology, 422-423, 471), pp. 245–269, checked on 2007.

Pruitt, Rory N.; Zhang, Lisha; Saile, Svenja C.; Karelina, Darya; Fröhlich, Katja; Wan, Wei-Lin et al. (2020): *Arabidopsis* cell surface LRR immune receptor signaling through the EDS1-PAD4-ADR1 node.

Qi, Junsheng; Song, Chun-Peng; Wang, Baoshan; Zhou, Jianmin; Kangasjärvi, Jaakko; Zhu, Jian-Kang; Gong, Zhizhong (2018): Reactive oxygen species signaling and stomatal movement in plant responses to drought stress and pathogen attack. In *Journal of integrative plant biology* 60 (9), pp. 805–826. DOI: 10.1111/jipb.12654.

Qin, Li; Zhou, Zhuqing; Li, Qiang; Zhai, Chun; Liu, Lijiang; Quilichini, Teagen D. et al. (2020): Specific Recruitment of Phosphoinositide Species to the Plant-Pathogen Interfacial Membrane Underlies *Arabidopsis* Susceptibility to Fungal Infection. In *The Plant cell* 32 (5), pp. 1665–1688. DOI: 10.1105/tpc.19.00970.

Raffaele, Sylvain; Rivas, Susana; Roby, Dominique (2006): An essential role for salicylic acid in AtMYB30-mediated control of the hypersensitive cell death program in *Arabidopsis*. In *FEBS letters* 580 (14), pp. 3498–3504. DOI: 10.1016/j.febslet.2006.05.027.

Raices, Marcela; D'Angelo, Maximiliano A. (2012): Nuclear pore complex composition: a new regulator of tissue-specific and developmental functions. In *Nature reviews. Molecular cell biology* 13 (11), pp. 687–699. DOI: 10.1038/nrm3461.

Rosciglione, Stéphanie; Thériault, Caroline; Boily, Marc-Olivier; Paquette, Marilène; Lavoie, Christine (2014): Gαs regulates the post-endocytic sorting of G protein-coupled receptors. In *Nature communications* 5, p. 4556. DOI: 10.1038/ncomms5556.

Rueden, Curtis T.; Schindelin, Johannes; Hiner, Mark C.; DeZonia, Barry E.; Walter, Alison E.; Arena, Ellen T.; Eliceiri, Kevin W. (2017): ImageJ2: ImageJ for the next generation of scientific image data. In *BMC bioinformatics* 18 (1), p. 529. DOI: 10.1186/s12859-017-1934-z.

Rustérucci, C.; Aviv, D. H.; Holt, B. F.; Dangl, J. L.; Parker, J. E. (2001): The disease resistance signaling components EDS1 and PAD4 are essential regulators of the cell death pathway

controlled by LSD1 in *Arabidopsis*. In *Plant Cell* 13 (10), pp. 2211–2224. DOI: 10.1105/tpc.010085.

Rutter, Brian D.; Innes, Roger W. (2017): Extracellular Vesicles Isolated from the Leaf Apoplast Carry Stress-Response Proteins. In *Plant physiology* 173 (1), pp. 728–741. DOI: 10.1104/pp.16.01253.

Schindelin, Johannes; Arganda-Carreras, Ignacio; Frise, Erwin; Kaynig, Verena; Longair, Mark; Pietzsch, Tobias et al. (2012): Fiji: an open-source platform for biological-image analysis. In *Nature methods* 9 (7), pp. 676–682. DOI: 10.1038/nmeth.2019.

Schultz-Larsen, Torsten; Lenk, Andrea; Kalinowska, Kamila; Vestergaard, Lau Kræsing; Pedersen, Carsten; Isono, Erika; Thordal-Christensen, Hans (2018): The AMSH3 ESCRT-III-Associated Deubiquitinase Is Essential for Plant Immunity. In *Cell reports* 25 (9), 2329-2338.e5. DOI: 10.1016/j.celrep.2018.11.011.

Schwessinger, Benjamin; Roux, Milena; Kadota, Yasuhiro; Ntoukakis, Vardis; Sklenar, Jan; Jones, Alexandra; Zipfel, Cyril (2011): Phosphorylation-dependent differential regulation of plant growth, cell death, and innate immunity by the regulatory receptor-like kinase BAK1. In *PLOS Genetics* 7 (4), e1002046. DOI: 10.1371/journal.pgen.1002046.

Shao, Zhu-Qing; Xue, Jia-Yu; Wu, Ping; Zhang, Yan-Mei; Wu, Yue; Hang, Yue-Yu et al. (2016): Large-Scale Analyses of Angiosperm Nucleotide-Binding Site-Leucine-Rich Repeat Genes Reveal Three Anciently Diverged Classes with Distinct Evolutionary Patterns. In *Plant Physiol.* 170 (4), pp. 2095–2109. DOI: 10.1104/pp.15.01487.

Shimizu, Takeo; Nakano, Takuto; Takamizawa, Daisuke; Desaki, Yoshitake; Ishii-Minami, Naoko; Nishizawa, Yoko et al. (2010): Two LysM receptor molecules, CEBiP and OsCERK1, cooperatively regulate chitin elicitor signaling in rice. In *The Plant journal : for cell and molecular biology* 64 (2), pp. 204–214. DOI: 10.1111/j.1365-313X.2010.04324.x.

Shinya, Tomonori; Motoyama, Noriko; Ikeda, Asahi; Wada, Miyuki; Kamiya, Kota; Hayafune, Masahiro et al. (2012): Functional characterization of CEBiP and CERK1 homologs in A*rabidopsis* and rice reveals the presence of different chitin receptor systems in plants. In *Plant & cell physiology* 53 (10), pp. 1696–1706. DOI: 10.1093/pcp/pcs113.

Shiu, S. H.; Bleecker, A. B. (2001): Receptor-like kinases from *Arabidopsis* form a monophyletic gene family related to animal receptor kinases. In *Proceedings of the National Academy of Sciences of the United States of America* 98 (19), pp. 10763–10768. DOI: 10.1073/pnas.181141598.

Shiu, Shin Han; Bleecker, Anthony B. (2003): Expansion of the receptor-like kinase/Pelle gene family and receptor-like proteins in *Arabidopsis*. In *Plant Physiol.* 132 (2), pp. 530–543. DOI: 10.1104/pp.103.021964.

Stein, Mónica; Dittgen, Jan; Sánchez-Rodríguez, Clara; Hou, Bi-Huei; Molina, Antonio; Schulze-Lefert, Paul et al. (2006): *Arabidopsis* PEN3/PDR8, an ATP binding cassette transporter, contributes to nonhost resistance to inappropriate pathogens that enter by direct penetration. In *Plant Cell* 18 (3), pp. 731–746. DOI: 10.1105/tpc.105.038372.

Stone, Sophia L.; Hauksdóttir, Herborg; Troy, Andrew; Herschleb, Jill; Kraft, Edward; Callis, Judy (2005): Functional Analysis of the RING-Type Ubiquitin Ligase Family of *Arabidopsis*. In *Plant Physiol.* 137 (1), pp. 13–30. DOI: 10.1104/pp.104.052423.

Straus, Marco R.; Rietz, Steffen; Ver Loren Themaat, Emiel; Bartsch, Michael; Parker, Jane E. (2010): Salicylic acid antagonism of EDS1-driven cell death is important for immune and oxidative stress responses in *Arabidopsis*. In *The Plant Journal* 62 (4), pp. 628–640. DOI: 10.1111/j.1365-313X.2010.04178.x.

Su, Jianbin; Yang, Liuyi; Zhu, Qiankun; Wu, Hongjiao; He, Yi; Liu, Yidong et al. (2018): Active photosynthetic inhibition mediated by MPK3/MPK6 is critical to effector-triggered immunity. In *PLOS Biology* 16 (5), e2004122. DOI: 10.1371/journal.pbio.2004122.

Sun, Jinhao; Sun, Yuhe; Ahmed, Rana Imtiaz; Ren, Angyan; Xie, And Minmin (2019): Research Progress on Plant RING-Finger Proteins. In *Genes* 10 (12). DOI: 10.3390/genes10120973.

Suntharalingam, Mythili; Wente, Susan R. (2003): Peering through the Pore. In *Developmental Cell* 4 (6), pp. 775–789. DOI: 10.1016/S1534-5807(03)00162-X.

Suzuki, Maruya; Shibuya, Masatoshi; Shimada, Hikaru; Motoyama, Noriko; Nakashima, Masato; Takahashi, Shohei et al. (2016): Autophosphorylation of Specific Threonine and Tyrosine Residues in *Arabidopsis* CERK1 is Essential for the Activation of Chitin-Induced Immune Signaling. In *Plant & cell physiology* 57 (11), pp. 2312–2322. DOI: 10.1093/pcp/pcw150.

Tada, Yasuomi; Spoel, Steven H.; Pajerowska-Mukhtar, Karolina; Mou, Zhonglin; Song, Junqi; Wang, Chun et al. (2008): Plant immunity requires conformational changes corrected of NPR1 via S-nitrosylation and thioredoxins. In *Science (New York, N.Y.)* 321 (5891), pp. 952–956. DOI: 10.1126/science.1156970.

Taddese, Bruck; Upton, Graham J. G.; Bailey, Gregory R.; Jordan, Siân R. D.; Abdulla, Nuradin Y.; Reeves, Philip J.; Reynolds, Christopher A. (2014): Do plants contain g protein-coupled receptors? In *Plant physiology* 164 (1), pp. 287–307. DOI: 10.1104/pp.113.228874.

Takáč, Tomáš; Novák, Dominik; Šamaj, Jozef (2019): Recent Advances in the Cellular and Developmental Biology of Phospholipases in Plants. In *Frontiers in plant science* 10, p. 362. DOI: 10.3389/fpls.2019.00362.

Takahashi, Toshiharu; Murano, Tomoya; Ishikawa, Atsushi (2018): SOBIR1 and AGB1 independently contribute to nonhost resistance to Pyricularia oryzae (syn. Magnaporthe oryzae) in *Arabidopsis thaliana*. In *Bioscience, biotechnology, and biochemistry* 82 (11), pp. 1922–1930. DOI: 10.1080/09168451.2018.1498727.

Takemoto, Daigo; Hardham, Adrienne R. (2004): The cytoskeleton as a regulator and target of biotic interactions in plants. In *Plant physiology* 136 (4), pp. 3864–3876. DOI: 10.1104/pp.104.052159.

Tamura, Kentaro (2020): Nuclear pore complex-mediated gene expression in *Arabidopsis* thaliana. In *Journal of plant research* 133 (4), pp. 449–455. DOI: 10.1007/s10265-020-01177-0.

Tateda, Chika; Zhang, Zhongqin; Greenberg, Jean T. (2015): Linking pattern recognition and salicylic acid responses in *Arabidopsis* through ACCELERATED CELL DEATH6 and receptors. In *Plant signaling & behavior* 10 (10), e1010912. DOI: 10.1080/15592324.2015.1010912.

Tewari, Ritika; West, Savannah J.; Shayahati, Bieerkehazi; Akimzhanov, Askar M. (2020): Detection of Protein S-Acylation using Acyl-Resin Assisted Capture. In *Journal of visualized experiments : JoVE* (158). DOI: 10.3791/61016.

Theriault, G.; Nkongolo, K. K. (2017): Evidence of prokaryote like protein associated with nickel resistance in higher plants: horizontal transfer of TonB-dependent receptor/protein in Betula genus or de novo mechanisms? In *Heredity* 118 (4), pp. 358–365. DOI: 10.1038/hdy.2016.106.

Thomma, Bart P. H. J.; Nürnberger, Thorsten; Joosten, Matthieu H. A. J. (2011): Of PAMPs and effectors: the blurred PTI-ETI dichotomy. In *The Plant cell* 23 (1), pp. 4–15. DOI: 10.1105/tpc.110.082602.

Trippel, Christine (2020): Two cysteine-rich receptor-like protein kinases, CRK7 and CRK43, are required for CERK1-4 dependent cell death responses in *Arabidopsis thaliana*. Doctoral Thesis.

Trusov, Yuri; Botella, José R. (2016): Plant G-Proteins Come of Age: Breaking the Bond with Animal Models. In *Frontiers in chemistry* 4, p. 24. DOI: 10.3389/fchem.2016.00024.

Trusov, Yuri; Rookes, James Edward; Chakravorty, David; Armour, David; Schenk, Peer Martin; Botella, José Ramón (2006): Heterotrimeric G proteins facilitate *Arabidopsis* resistance to necrotrophic pathogens and are involved in jasmonate signaling. In *Plant Physiol.* 140 (1), pp. 210–220. DOI: 10.1104/pp.105.069625.

Trusov, Yuri; Rookes, James Edward; Tilbrook, Kimberley; Chakravorty, David; Mason, Michael Glenn; Anderson, David et al. (2007): Heterotrimeric G protein gamma subunits provide functional selectivity in Gbetagamma dimer signaling in *Arabidopsis*. In *Plant Cell* 19 (4), pp. 1235–1250. DOI: 10.1105/tpc.107.050096.

Trusov, Yuri; Sewelam, Nasser; Rookes, James Edward; Kunkel, Matt; Nowak, Ekaterina; Schenk, Peer Martin; Botella, José Ramón (2009): Heterotrimeric G proteins-mediated resistance to necrotrophic pathogens includes mechanisms independent of salicylic acid-, jasmonic acid/ethylene- and abscisic acid-mediated defense signaling. In *The Plant journal : for cell and molecular biology* 58 (1), pp. 69–81. DOI: 10.1111/j.1365-313X.2008.03755.x.

Tunc-Ozdemir, Meral; Jones, Alan M. (2017): Ligand-induced dynamics of heterotrimeric G protein-coupled receptor-like kinase complexes. In *PloS one* 12 (2), e0171854. DOI: 10.1371/journal.pone.0171854.

Tunc-Ozdemir, Meral; Urano, Daisuke; Jaiswal, Dinesh Kumar; Clouse, Steven D.; Jones, Alan M. (2016): Direct Modulation of Heterotrimeric G Protein-coupled Signaling by a Receptor Kinase Complex. In *The Journal of biological chemistry* 291 (27), pp. 13918–13925. DOI: 10.1074/jbc.C116.736702.

Ullah, Hemayet; Chen, Jin-Gui; Temple, Brenda; Boyes, Douglas C.; Alonso, José M.; Davis, Keith R. et al. (2003): The beta-subunit of the *Arabidopsis* G protein negatively regulates auxin-induced cell division and affects multiple developmental processes. In *The Plant cell* 15 (2), pp. 393–409. DOI: 10.1105/tpc.006148.

Underwood, William (2012): The plant cell wall: a dynamic barrier against pathogen invasion. In *Frontiers in plant science* 3, p. 85. DOI: 10.3389/fpls.2012.00085.

Underwood, William; Somerville, Shauna C. (2013): Perception of conserved pathogen elicitors at the plasma membrane leads to relocalization of the *Arabidopsis* PEN3 transporter. In *PNAS* 110 (30), pp. 12492–12497. DOI: 10.1073/pnas.1218701110.

Underwood, William; Somerville, Shauna C. (2017): Phosphorylation is required for the pathogen defense function of the *Arabidopsis* PEN3 ABC transporter. In *Plant signaling & behavior* 12 (10), e1379644. DOI: 10.1080/15592324.2017.1379644.

Urano, Daisuke; Chen, Jin-Gui; Botella, José Ramón; Jones, Alan M. (2013): Heterotrimeric G protein signalling in the plant kingdom. In *Open biology* 3 (3), p. 120186. DOI: 10.1098/rsob.120186.

Urano, Daisuke; Maruta, Natsumi; Trusov, Yuri; Stoian, Richard; Wu, Qingyu; Liang, Ying et al. (2016): Saltational evolution of the heterotrimeric G protein signaling mechanisms in the plant kingdom. In *Science signaling* 9 (446), ra93. DOI: 10.1126/scisignal.aaf9558.

Urano, Daisuke; Phan, Nguyen; Jones, Janice C.; Yang, Jing; Huang, Jirong; Grigston, Jeffrey et al. (2012): Endocytosis of the seven-transmembrane RGS1 protein activates G-protein-coupled signalling in *Arabidopsis*. In *Nature cell biology* 14 (10), pp. 1079–1088. DOI: 10.1038/ncb2568.

van der Burgh, Aranka M.; Postma, Jelle; Robatzek, Silke; Joosten, Matthieu H. A. J. (2019): Kinase activity of SOBIR1 and BAK1 is required for immune signalling. In *Molecular plant pathology* 20 (3), pp. 410–422. DOI: 10.1111/mpp.12767.

van Durme, Matthias; Nowack, Moritz K. (2016): Mechanisms of developmentally controlled cell death in plants. In *Current opinion in plant biology* 29, pp. 29–37. DOI: 10.1016/j.pbi.2015.10.013.

van Niel, Guillaume; Porto-Carreiro, Isabel; Simoes, Sabrina; Raposo, Graça (2006): Exosomes: a common pathway for a specialized function. In *Journal of biochemistry* 140 (1), pp. 13–21. DOI: 10.1093/jb/mvj128.

van Wersch, Rowan; Li, Xin; Zhang, Yuelin (2016): Mighty Dwarfs: *Arabidopsis* Autoimmune Mutants and Their Usages in Genetic Dissection of Plant Immunity. In *Frontiers in plant science* 7, p. 1717. DOI: 10.3389/fpls.2016.01717.

van Wersch, Solveig; Tian, Lei; Hoy, Ryan; Li, Xin (2020): Plant NLRs: The Whistleblowers of Plant Immunity. In *Plant Communications* 1 (1), p. 100016. DOI: 10.1016/j.xplc.2019.100016.

Vanholme, Bartel; Vanholme, Ruben; Turumtay, Halbay; Goeminne, Geert; Cesarino, Igor; Goubet, Florence et al. (2014): Accumulation of N-acetylglucosamine oligomers in the plant cell wall affects plant architecture in a dose-dependent and conditional manner. In *Plant physiology* 165 (1), pp. 290–308. DOI: 10.1104/pp.113.233742.

Wan, Jinrong; Tanaka, Kiwamu; Zhang, Xue-Cheng; Son, Geon Hui; Brechenmacher, Laurent; Nguyen, Tran Hong Nha; Stacey, Gary (2012): LYK4, a lysin motif receptor-like kinase, is important for chitin signaling and plant innate immunity in *Arabidopsis*. In *Plant Physiol.* 160 (1), pp. 396–406. DOI: 10.1104/pp.112.201699.

Wan, Li; Essuman, Kow; Anderson, Ryan G.; Sasaki, Yo; Monteiro, Freddy; Chung, Eui-Hwan et al. (2019a): TIR domains of plant immune receptors are NAD+-cleaving enzymes that promote cell death. In *Science (New York, N.Y.)* 365 (6455), pp. 799–803. DOI: 10.1126/science.aax1771.

Wan, Wei-Lin; Zhang, Lisha; Pruitt, Rory; Zaidem, Maricris; Brugman, Rik; Ma, Xiyu et al. (2019b): Comparing *Arabidopsis* receptor kinase and receptor protein-mediated immune signaling reveals BIK1-dependent differences. In *The New phytologist* 221 (4), pp. 2080–2095. DOI: 10.1111/nph.15497.

Wang, Fei; Shang, Yifen; Fan, Baofang; Yu, Jing-Quan; Chen, Zhixiang (2014): Arabidopsis LIP5, a positive regulator of multivesicular body biogenesis, is a critical target of pathogen-responsive MAPK cascade in plant basal defense. In *PLoS pathogens* 10 (7), e1004243. DOI: 10.1371/journal.ppat.1004243.

Wang, Jinlong; Grubb, Lauren E.; Wang, Jiayu; Liang, Xiangxiu; Li, Lin; Gao, Chulei et al. (2018): A Regulatory Module Controlling Homeostasis of a Plant Immune Kinase. In *Molecular cell* 69 (3), 493-504.e6. DOI: 10.1016/j.molcel.2017.12.026.

Wang, Jizong; Hu, Meijuan; Wang, Jia; Qi, Jinfeng; Han, Zhifu; Wang, Guoxun et al. (2019): Reconstitution and structure of a plant NLR resistosome conferring immunity. In *Science (New York, N.Y.)* 364 (6435). DOI: 10.1126/science.aav5870.

Wang, Shiyu; Narendra, Savitha; Fedoroff, Nina (2007): Heterotrimeric G protein signaling in the Arabidopsis unfolded protein response. In *Proceedings of the National Academy of Sciences of the United States of America* 104 (10), pp. 3817–3822. DOI: 10.1073/pnas.0611735104.

Wang, Wei; Feng, Baomin; Zhou, Jian-Min; Tang, Dingzhong (2020): Plant immune signaling: Advancing on two frontiers. In *Journal of integrative plant biology* 62 (1), pp. 2–24. DOI: 10.1111/jipb.12898.

Wang, Wenming; Wen, Yingqiang; Berkey, Robert; Xiao, Shunyuan (2009): Specific targeting of the Arabidopsis resistance protein RPW8.2 to the interfacial membrane encasing the fungal Haustorium renders broad-spectrum resistance to powdery mildew. In *Plant Cell* 21 (9), pp. 2898–2913. DOI: 10.1105/tpc.109.067587.

Wang, Wen-Ming; Liu, Peng-Qiang; Xu, Yong-Ju; Xiao, Shunyuan (2016): Protein trafficking during plant innate immunity. In *Journal of integrative plant biology* 58 (4), pp. 284–298. DOI: 10.1111/jipb.12426.

Wang, Yiping; Wu, Yingying; Yu, Boying; Yin, Zhao; Xia, Yiji (2017): EXTRA-LARGE G PROTEINs Interact with E3 Ligases PUB4 and PUB2 and Function in Cytokinin and Developmental Processes. In *Plant physiology* 173 (2), pp. 1235–1246. DOI: 10.1104/pp.16.00816.

Waszczak, Cezary; Akter, Salma; Jacques, Silke; Huang, Jingjing; Messens, Joris; van Breusegem, Frank (2015): Oxidative post-translational modifications of cysteine residues in plant signal transduction. In *Journal of experimental botany* 66 (10), pp. 2923–2934. DOI: 10.1093/jxb/erv084.

Weber, Michael (2005): Identifizierung und Charakterisierung von Hyperakkumulationsfaktoren bzw. schwermetallregulierten Genen in Arabidopsis *halleri* und *Arabidopsis thaliana*. Doctoral Thesis.

Wettschureck, Nina; Offermanns, Stefan (2005): Mammalian G proteins and their cell type specific functions. In *Physiological reviews* 85 (4), pp. 1159–1204. DOI: 10.1152/physrev.00003.2005.

Wiermer, Marcel; Cheng, Yu Ti; Imkampe, Julia; Li, Meilan; Wang, Dongmei; Lipka, Volker; Li, Xin (2012): Putative members of the *Arabidopsis* Nup107-160 nuclear pore sub-complex contribute to pathogen defense. In *The Plant journal : for cell and molecular biology* 70 (5), pp. 796–808. DOI: 10.1111/j.1365-313X.2012.04928.x.

Wiermer, Marcel; Germain, Hugo; Cheng, Yu Ti; García, Ana V.; Parker, Jane E.; Li, Xin (2010): Nucleoporin MOS7/Nup88 contributes to plant immunity and nuclear accumulation of

defense regulators. In *Nucleus (Austin, Tex.)* 1 (4), pp. 332–336. DOI: 10.4161/nucl.1.4.12109.

Willmann, Roland; Lajunen, Heini M.; Erbs, Gitte; Newman, Mari-Anne; Kolb, Dagmar; Tsuda, Kenichi et al. (2011): *Arabidopsis* lysin-motif proteins LYM1 LYM3 CERK1 mediate bacterial peptidoglycan sensing and immunity to bacterial infection. In *Proceedings of the National Academy of Sciences of the United States of America* 108 (49), pp. 19824–19829. DOI: 10.1073/pnas.1112862108.

Wolfenstetter, Susanne; Chakravorty, David; Kula, Ryan; Urano, Daisuke; Trusov, Yuri; Sheahan, Michael B. et al. (2015): Evidence for an unusual transmembrane configuration of AGG3, a class C Gγ subunit of *Arabidopsis*. In *The Plant journal : for cell and molecular biology* 81 (3), pp. 388–398. DOI: 10.1111/tpj.12732.

Wu, Chih-Hang; Abd-El-Haliem, Ahmed; Bozkurt, Tolga O.; Belhaj, Khaoula; Terauchi, Ryohei; Vossen, Jack H.; Kamoun, Sophien (2017): NLR network mediates immunity to diverse plant pathogens. In *Proceedings of the National Academy of Sciences of the United States of America* 114 (30), pp. 8113–8118. DOI: 10.1073/pnas.1702041114.

Wu, Hongpo (2018): Genetic and chemical suppressors of mlo mediated powdery mildew resistance. Dissertation.

Wu, Yujun; Gao, Yang; Zhan, Yanyan; Kui, Hong; Liu, Hongyan; Yan, Li et al. (2020): Loss of the common immune coreceptor BAK1 leads to NLR-dependent cell death. In *PNAS* 117 (43), pp. 27044–27053. DOI: 10.1073/pnas.1915339117.

Wu, Zhongshou; Li, Meng; Dong, Oliver Xiaoou; Xia, Shitou; Liang, Wanwan; Bao, Yongkang et al. (2019): Differential regulation of TNL-mediated immune signaling by redundant helper CNLs. In *The New phytologist* 222 (2), pp. 938–953. DOI: 10.1111/nph.15665.

Wywial, Ewa; Singh, Shaneen M. (2010): Identification and structural characterization of FYVE domain-containing proteins of *Arabidopsis thaliana*. In *BMC Plant Biol* 10 (1). DOI: 10.1186/1471-2229-10-157.

Xiao, S.; Ellwood, S.; Calis, O.; Patrick, E.; Li, T.; Coleman, M.; Turner, J. G. (2001): Broad-spectrum mildew resistance in *Arabidopsis thaliana* mediated by RPW8. In *Science (New York, N.Y.)* 291 (5501), pp. 118–120. DOI: 10.1126/science.291.5501.118.

Xing, Jingjing; Li, Xiaojuan; Wang, Xiaohua; Lv, Xueqin; Wang, Li; Zhang, Liang et al. (2019): Secretion of Phospholipase Dδ Functions as a Regulatory Mechanism in Plant Innate Immunity. In *Plant Cell* 31 (12), pp. 3015–3032. DOI: 10.1105/tpc.19.00534.

Xu, Darui; Marquis, Kara; Pei, Jimin; Fu, Szu-Chin; Cağatay, Tolga; Grishin, Nick V.; Chook, Yuh Min (2015): LocNES: a computational tool for locating classical NESs in CRM1 cargo proteins. In *Bioinformatics (Oxford, England)* 31 (9), pp. 1357–1365. DOI: 10.1093/bioinformatics/btu826.

Xue, De-Xing; Li, Chun-Lian; Xie, Zhi-Ping; Staehelin, Christian (2019): LYK4 is a component of a tripartite chitin receptor complex in *Arabidopsis thaliana*. In *Journal of experimental botany* 70 (19), pp. 5507–5516. DOI: 10.1093/jxb/erz313.

Xue, Jiao; Gong, Ben-Qiang; Yao, Xinran; Huang, Xiangjuan; Li, Jian-Feng (2020): BAK1-mediated phosphorylation of canonical G protein alpha during flagellin signaling in *Arabidopsis*. In *Journal of integrative plant biology* 62 (5), pp. 690–701. DOI: 10.1111/jipb.12824.

Yadeta, Koste A.; Elmore, James M.; Creer, Athena Y.; Feng, Baomin; Franco, Jessica Y.; Rufian, Jose Sebastian et al. (2017): A Cysteine-Rich Protein Kinase Associates with a Membrane Immune Complex and the Cysteine Residues Are Required for Cell Death. In *Plant Physiol.* 173 (1), pp. 771–787. DOI: 10.1104/pp.16.01404.

Yamada, Kenta; Yamaguchi, Koji; Shirakawa, Tomomi; Nakagami, Hirofumi; Mine, Akira; Ishikawa, Kazuya et al. (2016): The *Arabidopsis* CERK1-associated kinase PBL27 connects chitin perception to MAPK activation. In *The EMBO journal* 35 (22), pp. 2468–2483. DOI: 10.15252/embj.201694248.

Yamaguchi, Koji; Mezaki, Hirohisa; Fujiwara, Masayuki; Hara, Yuki; Kawasaki, Tsutomu (2017): *Arabidopsis* ubiquitin ligase PUB12 interacts with and negatively regulates Chitin Elicitor Receptor Kinase 1 (CERK1). In *PloS one* 12 (11), e0188886. DOI: 10.1371/journal.pone.0188886.

Yu, Yunqing; Chakravorty, David; Assmann, Sarah M. (2018): The G Protein β-Subunit, AGB1, Interacts with FERONIA in RALF1-Regulated Stomatal Movement. In *Plant Physiol.* 176 (3), pp. 2426–2440. DOI: 10.1104/pp.17.01277.

Yuan, Guo-Liang; Li, Hong-Ju; Yang, Wei-Cai (2017): The integration of Gβ and MAPK signaling cascade in zygote development. In *Scientific reports* 7 (1), p. 8732. DOI: 10.1038/s41598-017-08230-4.

Yuan, Minhang; Jiang, Zeyu; Bi, Guozhi; Nomura, Kinya; Liu, Menghui; He, Sheng Yang et al. (2020): Pattern-recognition receptors are required for NLR-mediated plant immunity: Cold Spring Harbor Laboratory.

Yun, Byung-Wook; Atkinson, Helen A.; Gaborit, Charlotte; Greenland, Andy; Read, Nick D.; Pallas, Jacqueline A.; Loake, Gary J. (2003): Loss of actin cytoskeletal function and EDS1 activity, in combination, severely compromises non-host resistance in *Arabidopsis* against wheat powdery mildew. In *The Plant journal : for cell and molecular biology* 34 (6), pp. 768–777. DOI: 10.1046/j.1365-313x.2003.01773.x.

Yun, Byung-Wook; Feechan, Angela; Yin, Minghui; Saidi, Noor B. B.; Le Bihan, Thierry; Yu, Manda et al. (2011): S-nitrosylation of NADPH oxidase regulates cell death in plant immunity. In *Nature* 478 (7368), pp. 264–268. DOI: 10.1038/nature10427.

Zavaliev, Raul; Mohan, Rajinikanth; Chen, Tianyuan; Dong, Xinnian (2020): Formation of NPR1 Condensates Promotes Cell Survival during the Plant Immune Response. In *Cell* 182 (5), 1093-1108.e18. DOI: 10.1016/j.cell.2020.07.016.

Zeng, Qin; Wang, Xuejun; Running, Mark P. (2007): Dual lipid modification of *Arabidopsis* Ggamma-subunits is required for efficient plasma membrane targeting. In *Plant Physiol.* 143 (3), pp. 1119–1131. DOI: 10.1104/pp.106.093583.

Zhang, Qian; Sun, Tongjun; Zhang, Yuelin (2015): ER quality control components UGGT and STT3a are required for activation of defense responses in bir1-1. In *PloS one*, e0120245. DOI: 10.1371/journal.pone.0120245.

Zhang, Wei; He, Sheng Yang; Assmann, Sarah M. (2008a): The plant innate immunity response in stomatal guard cells invokes G-protein-dependent ion channel regulation. In *The Plant journal : for cell and molecular biology* 56 (6), pp. 984–996. DOI: 10.1111/j.1365-313X.2008.03657.x.

Zhang, Wei; Jeon, Byeong Wook; Assmann, Sarah M. (2011): Heterotrimeric G-protein regulation of ROS signalling and calcium currents in *Arabidopsis* guard cells. In *Journal of experimental botany* 62 (7), pp. 2371–2379. DOI: 10.1093/jxb/erq424.

Zhang, Xiaoxiao; Bernoux, Maud; Bentham, Adam R.; Newman, Toby E.; Ve, Thomas; Casey, Lachlan W. et al. (2017): Multiple functional self-association interfaces in plant TIR domains. In *Proceedings of the National Academy of Sciences of the United States of America* 114 (10), E2046-E2052. DOI: 10.1073/pnas.1621248114.

Zhang, Yi; Zeng, Lirong (2020): Crosstalk between Ubiquitination and Other Post-translational Protein Modifications in Plant Immunity. In *Plant Communications* 1 (4), p. 100041. DOI: 10.1016/j.xplc.2020.100041.

Zhang, Yuelin; Goritschnig, Sandra; Dong, Xinnian; Li, Xin (2003): A gain-of-function mutation in a plant disease resistance gene leads to constitutive activation of downstream signal transduction pathways in suppressor of npr1-1, constitutive 1. In *Plant Cell* 15 (11), pp. 2636–2646. DOI: 10.1105/tpc.015842.

Zhang, Yuelin; Li, Xin (2005): A putative nucleoporin 96 Is required for both basal defense and constitutive resistance responses mediated by suppressor of npr1-1,constitutive 1. In *Plant Cell*, pp. 1306–1316. DOI: 10.1105/tpc.104.029926.

Zhang, Ziguo; Feechan, Angela; Pedersen, Carsten; Newman, Mari-Anne; Qiu, Jin-Long; Olesen, Karen L.; Thordal-Christensen, Hans (2007): A SNARE-protein has opposing functions in penetration resistance and defence signalling pathways. In *The Plant journal : for cell and molecular biology* 49 (2), pp. 302–312. DOI: 10.1111/j.1365-313X.2006.02961.x.

Zhang, Ziguo; Lenk, Andrea; Andersson, Mats X.; Gjetting, Torben; Pedersen, Carsten; Nielsen, Mads E. et al. (2008b): A lesion-mimic syntaxin double mutant in *Arabidopsis* reveals novel complexity of pathogen defense signaling. In *Molecular plant* 1 (3), pp. 510–527. DOI: 10.1093/mp/ssn011.

Zhao, Jian; Wang, Xuemin (2004): *Arabidopsis* phospholipase Dalpha1 interacts with the heterotrimeric G-protein alpha-subunit through a motif analogous to the DRY motif in G-protein-coupled receptors. In *The Journal of biological chemistry* 279 (3), pp. 1794–1800. DOI: 10.1074/jbc.M309529200.

Zheng, Lihua; Liu, Peng; Liu, Qianwen; Wang, Tao; Dong, Jiangli (2019): Dynamic Protein S-Acylation in Plants. In *International journal of molecular sciences* 20 (3). DOI: 10.3390/ijms20030560.

Zhong, Chen-Li; Zhang, Chi; Liu, Jian-Zhong (2019): Heterotrimeric G protein signaling in plant immunity. In *Journal of experimental botany* 70 (4), pp. 1109–1118. DOI: 10.1093/jxb/ery426.

Zhou, Jinggeng; Wang, Ping; Claus, Lucas A. N.; Savatin, Daniel V.; Xu, Guangyuan; Wu, Shujing et al. (2019): Proteolytic Processing of SERK3/BAK1 Regulates Plant Immunity, Development, and Cell Death. In *Plant Physiol.* 180 (1), pp. 543–558. DOI: 10.1104/pp.18.01503.

Zhu, Huifen; Li, Guo-Jing; Ding, Lei; Cui, Xiangqin; Berg, Howard; Assmann, Sarah M.; Xia, Yiji (2009): *Arabidopsis* extra large G-protein 2 (XLG2) interacts with the Gbeta subunit of heterotrimeric G protein and functions in disease resistance. In *Molecular plant* 2 (3), pp. 513–525. DOI: 10.1093/mp/ssp001.